ANALYSIS OF FAULT-SLIP MECHANISMS

IN HARD ROCK MINING

By

Richard Simon

Department of Mining and Metallurgical Engineering

McGill University, Montréal, Canada

January 1999

A thesis submitted to the Faculty of Graduate Studies and Research in partial fulfilment of the requirements of the degree of Doctor of Philosophy

0-612-50263-5

To my parents,

You are not wrong, who deem
That my days have been a dream;
Yet if hope has flown away
In a night, or in a day,
In a vision, or in none,
Is it therefore the less gone?
All that we see or seem
Is but a dream within a dream.

Edgar A. Poe, 1827

ABSTRACT

Rockbursts may cause damages to underground openings and to equipment, and constitute a major hazard to the safety of mine workers. One method that can be used to evaluate if there is a rockburst potential is to compare the stiffness of the failed rock with that of the surrounding rock mass. This method has been applied successfully in the past to rockbursts involving fracturing of the rock mass.

This thesis deals with the development of a similar approach for rockbursts involving a violent slip along major geological discontinuities. To evaluate the post-peak shear stiffness of a discontinuity, a new non-linear constitutive model for rock joint was developed. This model is based on two exponential formulations expressing the two phenomena taking part in the shearing process: friction resistance along surfaces and shearing of asperities. Compared with test results, the model showed a correlation factor (R^2) of 0.90. The model was then implemented in an existing boundary element code to evaluate the interaction between underground openings and nearby geological discontinuities. Verification of the implementation was done by reproducing direct shear tests on a discontinuity. Parametric analyses were performed on the new model that highlighted the most important parameters. Methods to obtain the different stiffnesses involved in the violent slip process were developed. Examples of applications were given to illustrate the proposed methods.

Finally, an alternative method to evaluate the fault-slip rockburst potential was developed. This new method relies on a linear analysis and the calculation of a new index called the Out-of-Balance Index or OBI. The OBI showed some agreement with the stiffness approach.

RÉSUMÉ

Les coups de terrain causent des dommages aux excavations souterraines et aux équipements, en plus de représenter une grave menace pour la sécurité des travailleurs. Une méthode pouvant être utilisée pour évaluer s'il existe un potentiel de coups de terrain est de comparer la rigidité post-pic du massif instable avec celle du massif rocheux autour de l'instabilité. Par le passé, cette approche a été utilisée avec succès pour des coups de terrain impliquant la rupture du massif rocheux.

Cette thèse traite du développement d'une approche similaire pour les coups de terrain impliquant un glissement violent le long d'une discontinuité géologique. Pour évaluer la rigidité post-pic d'une discontinuité, un nouveau modèle constitutif non-linéaire pour les discontinuités structurales a été développé. Ce modèle repose sur deux formulations exponentielles représentant les deux processus agissant lors du cisaillement: la résistance en friction et le cisaillement des aspérités. Comparé à plusieurs essais de laboratoire, le modèle proposé a montré un facteur de corrélation (R^2) de 0.90. Le nouveau modèle a ensuite été intégré dans un code d'éléments frontières existant afin d'évaluer l'interaction entre des excavations souterraines près de discontinuités géologiques. Une vérification de l'intégration a été effectuée en reproduisant des essais de cisaillement direct sur des discontinuités. Des analyses paramétriques ont ensuite été réalisées à l'aide du modèle, ce qui a permis d'identifier les paramètres les plus importants. Des méthodes pour obtenir les différentes rigidités impliquées à l'aide des outils créés ont été détaillées. Des exemples d'application ont permis d'illustrer l'utilisation des méthodes proposées.

Finalement, une autre méthode pour évaluer le potentiel de glissements violents le long de discontinuités a également été développée. Cette nouvelle approche est basée sur l'utilisation d'un nouvel index appelé OBI (pour "Out-of-Balance Index") lors d'une

analyse linéaire. Cette approche a mené à des résultats concordant avec l'approche basée sur la comparaison des rigidités.

ACKNOWLEDGEMENTS

I would like to thank my supervisor Prof. Hani. S. Mitri for his guidance throughout this research project and his financial contribution. I also whish to express my most sincere gratitude to Prof. Michel Aubertin of École Polytechnique de Montréal for his help in this project and for his financial support; without this support, this thesis wouldn't have been a reality. A good portion of this work was financed through grants from the Institut de recherche en santé et en sécurité du travail du Québec (IRSST) and their contribution is greatfully acknowledged.

I also thank the comprehensive examination committee composed of Profs. Hani Mitri, Ferri Hassani, and Mr. Wilfrid Comeau of McGill University, Prof. Michel Aubertin of École Polytechnique, and Dr Luc Vandamme of Noranda Technology Center. Their comments and suggestions have been extremely helpful.

Finally, I wish to thank my family for their incessant encouragement and kindness, my friends and colleagues, and Mr. Jérémie Wizzard for his moral support.

TABLE OF CONTENTS

LIST OF FIGURES

LIST OF TABLES

LIST OF SYMBOLS

A	Area of pillar
[A]	Boundary coefficients matrix
$\overset{ij}{A}_{ss}$	Boundary stress influence coefficient
A_1	Elastic area at peak strength
A_2	Total area under the curve
a_j	Initial joint aperture
a_s	Shear area ratio
B	Pillar width
{B}	Known vector
BEM	Boundary element method
B_{er}	Burst-efficiency ratio
$\overset{ij}{B}_{ss}$	Boundary displacement influence coefficient
BIM	Brittleness Index Modified
BPR	Bursting potential ratio
BPR_j	Bursting potential ratio for rock joints
B_0	Ratio of residual to peak strength
B_1, B_2	Brittleness
C_0	Uniaxial compressive strength
c	Cohesion
DDE	Displacement discontinuity element
DDM	Displacement discontinuity method
DEM	Discrete element method
D_i	Differential displacement between sides of a joint segment
$\overset{j}{D}_n$	Normal displacement discontinuity of the j^{th} element
$\overset{j}{D}_s$	Shear displacement discontinuity of the j^{th} element
Dt	Failure duration index
d_n^0	Peak dilation angle
E	Young's modulus or deformation modulus
E_D	Energy dissipated
E_D	Energy generated by the tremor in the rock mass
E_K	Energy accumulated in the rock mass
E_K^o	Energy necessary for initiating rockbursting
E_m	Deformation modulus of the rock mass
E'_m	Post-peak deformation modulus of the rock mass
E_R	Elastic energy recovered
ERR	Energy release rate
ESS	Excess shear stress
e_c	Critical strain energy

e_4	Induced strain energy calculated at the boundary
FEM	Finite element method
F_i	Force acting in the *i* direction
FSM	Fictitious stress method
G	Shear modulus
H	Pillar height
h	Thickness of joint
i	Angle of asperities
i_0	Initial angle of asperities
JCS	Joint wall compressive strength
JRC	Joint roughness coefficient
JRC_m	Mobilized joint roughness coefficient
K	Applied stiffness
k	Stiffness of a spring
k_e	Local mine stiffness or surrounding rock mass stiffness
k_{ls}	Loading system stiffness
k_n,k_{nn}	Normal stiffness
k_{ni}	Initial normal stiffness
k_p	Pre-peak stiffness of a discontinuity
k'_p	Post-peak stiffness of a discontinuity
k_{pr}	Pre-peak stiffness of a pillar
k'_{pr}	Post-peak stiffness of a pillar
k_r	Rock pre-peak stiffness
k'_r	Rock post-peak stiffness
k_s,k_{ss}	Shear stiffness
k_{sn},k_{ns}	Stiffness matrix coefficients
k_1,k_2	Joint strength constants (namely 1.5 and 4)
L_n	Natural block size
L_0	Laboratory joint size (100 mm)
L_{ZN}	Work used for breaking and crushing rock mass volume
N	Ratio of compressive over tensile strength
n_j	Cosine director vector
OBI	Out-of-Balance Index
$\overset{j}{P}_n$	Fictitious normal stress applied to the j^{th} element on the boundary
$\overset{j}{P}_s$	Fictitious shear stress applied to the j^{th} element on the boundary
p_z	Initial vertical stress in the elementary volume
RMR	Rock mass rating
R	Schmidt rebound on dry surfaces
r	Schmidt rebound on wet surfaces
S_0	Cohesion of intact rock
s_r	Shear strength of intact rock
T_e	Energetic rockburst indicator
t_i	Traction in the *i* direction

t'_i	Induced traction	W_{et}	Index of rockburst potential
$(t_i)_0$	Initial traction	W_k	Kinetic energy
U_c	Stored strain energy in the rock mass	W_r	Released energy
		W_s	Work on support
U_m	Stored strain energy in the mined rock	$\{X\}$	Unknown vector
		α	Coefficient of vertical stress concentration
u	Shear displacement		
u_i	Displacement in the *i* direction	β	Coefficient of energy concentration
u'_i	Induced displacement	β_i	Body force acting in the *i* direction
$(u_i)_0$	Initial displacement	Δ	Convergence of walls
u_o	Displacement in front of the spring	δ_{ij}	Kronecker delta
u_p	Peak displacement	ε	Deformation
u_r	Residual displacement	ε_f	Deformation at failure (uniaxial)
V_C	Elastic energy accumulated in the broken rock mass during rockburst	ϕ	Shear angle
		ϕ_b	Basic friction angle
V_c	Strain energy of the rock mass in the elementary volume	ϕ_p	Peak friction angle
		ϕ_r	Residual friction angle
V_c^i	Initial strain energy of the rock mass in the elementary volume	ϕ_s	Static friction angle
		ϕ_u	Angle of friction
V_m	Maximum normal closure	ϕ_l	Energy of particles ejected at failure
V_o	Strain energy of volume change	ϕ_0	Maximum energy stored in loading cycle
V_p	Strain energy of distortion		
v	Normal displacement		
$\dot{v}$	Rate of dilation at peak strength	ϕ_0	Angle of friction of intact rock
W	Work	μ_s	Static friction factor
W_b	Ratio of effective stress to rock strength	ν	Poisson's ration

v_o	Average velocity of broken rock mass
ρ_{sr}	Average density of broken rock mass
σ	Stress
σ_c	Uniaxial compressive strength
σ_{ii}	Normal stress
σ_{ij}	Shear stress
σ'_{ij}	Induced stresses
$(\sigma_{ij})_0$	Initial stresses
$(\sigma'_{ij})_0$	Initial induced stresses
$(\sigma_{ij})_0^\infty$	Far field stresses
σ_n	Normal stress
σ_{n0}	Initial normal stress
σ_o	Mean applied stress
σ_p	Applied stress
σ_s	Shear stress
σ_T	Transitional stress
σ_t	Uniaxial tensile strength
σ_z	Vertical stress in the elementary volume
σ_1	Major principal stress
σ_2	Intermediate principal stress
σ_3	Minor principal stress
τ	Shear stress
τ_d	Dynamic shear resistance
τ_p	Peak shear strength
τ_r	Residual shear strength
τ_s	Static shear resistance
ξ	Length of element

CHAPTER 1
INTRODUCTION

The rockburst problem in underground mines has been around since the beginning of the century. As technology allows for the exploitation of deeper orebodies mined with higher extraction ratios, the mining engineer will most probably have to deal with this problem more often. Moreover, mines in Canada are most likely to operate at greater depth in the near future. Due to the "unpredictability" and the recurrence nature of the phenomenon, rockbursts might just be the biggest challenge facing rock mechanics engineers in hard rock mines.

Although rockbursts can occur in every types of rock and at any depth (Blake, 1972), they constitute a problem mainly for deep underground hard rock mines where the extraction ratio is large (Blake, 1984).

The first reports about rockbursts seem to have emerged from the Kolar Gold Field in India at the end of the 19th century, when the mining depth was still below 500 m (Morrison, 1942; Blake, 1972). A few years later, the problem appeared in the Witwatersrand mines in South Africa (Cook et al., 1966). Russia and other East European countries also had to deal with the problem (Petukhov, 1987, 1990), and so did China (Tan, 1986; Mei and Lu, 1987a, 1987b).

In the United States, the first rockburst seems to have occurred in 1904 at the Atlantic mine in the copper district in Michigan (Bolstad, 1990). In Canada, Morrison (1942) reported that the problem existed in Ontario at the end of the 1920's, in the Kirkland Lake region, and then, in the Sudbury region some years later. More recently, large rockbursts have occurred in the Elliot Lake region, Ontario, in the potash mines in Saskatchewan, in Bathurst, New Brunswick, and at the Springhill Colliery in Nova Scotia (Hedley, 1992).

The history of rockburst in the Québec province is not well documented. However, the problem exists (at least) since the 1960's (Gill and Aubertin, 1988). The East Malartic mine in the NorthWest part of the province, which closed in 1979 because of serious rockburst problems, is a good example. In recent years, several Québec mines had to face this problem, especially in the Abitibi region (Roctest, 1980; AMMQ, 1988; Falmagne, 1991; Hedley, 1992; Mottahed, 1992; Gill et al., 1993; Plouffe et al., 1993; Harvey et al., 1996). Table 1.1 lists mines where rockbursts have occurred in Canada.

Table 1.1: Canadian mines where rockbursts or large seismic events have occurred

Québec	Ontario		Rest of Canada
Agnico-Eagle Mine	Campbell	Kidd Creek	Brunswick Mining, NB
Ansil	Copper Cliff	Lake Shore	Central Canada Potash, Sask.
Camflo	Creighton	Levack	Elk River, BC
Chimo	Denison	Lockerby	K1 & K2 Mines, Sask.
Copper Rand	Dickenson	Macassa	McGillivray, Al.
East-Malartic	Falconbridge	Onaping	Patience Lake Mine, Sask.
Lac Shortt	Fraser	Quirke	PCS Mining Cory, Sask.
Normétal	Frood-Stobie	Stobie	Springhill #2, NS
Opemiska	Garson	Strathcona	
Sigma	Golden Giant	Wright-Hargreaves	
	Kerr Addison		

With the persistence and (sometimes) growth of the problem, research efforts were made worldwide and principally in the region touched by rockbursts. Gill and Aubertin (1988) noted that before the 1960's, the approaches used were mostly empirical or phenomenological. Canada was amongst the pioneers in this field with the work of

Morrison (1942, 1976), of Hodgson and Jouhgin (1967) and of Coates and Dickout (1970).

However, it is the analytical studies from South Africa that set the pace on subsequent rockburst research. The post-failure studies on rocks, and the energy approach in the unstable equilibrium analysis (Cook, 1965a; Diest, 1965; Cook et al., 1966; Salamon 1970, 1974) are important notions still used in present research works.

Many countries are presently working on this problem. Canada in particular has put a lot of effort over the last few years to better comprehend the problem (Roctest, 1980; Hedley et al., 1984, 1985; Whiteway, 1985; Udd and Hedley, 1985; Singh, 1986, 1987, 1989; Musial, 1987; Scoble et al., 1987; Gill and Aubertin, 1988; Mitri et al., 1988, 1993; Hedley, 1991, 1992; Gill et al., 1993; Kaiser, 1993; Chen et al., 1995; Vasak and Kaiser, 1995; Kaiser et al., 1996; Simon et al., 1998).

Although rockbursts do not occur in the majority of Québec underground mines, it is a problem that presents a high risk of fatalities in mines where the problem exists. Even if research in this field has not been a major priority in Québec, as it has been in South Africa or even in Ontario, some efforts have been initiated over the last decade (e.g., Gill et Aubertin, 1988; Mitri et al., 1988, 1993; McCreary et al., 1993; Plouffe et al., 1993a,b; Mitri, 1996a; Aubertin et al., 1997; Simon et al., 1998) to provide tools to help rock mechanics engineers to assess the rockburst potential of their openings.

On that matter, Gill and Aubertin (1988; see also Aubertin et al., 1992; Gill et al., 1993; Simon et al., 1998) proposed a methodology that makes use of standard rock mechanics tools, which attempts to evaluate rockburst potential of rock structures. This methodology, called the ERP method, is based on the stiffness comparison between the failed rock and the surrounding rock mass, as was proposed initially by Cook (1965b). However, this comparison could only be established for instabilities involving the fracturing of the rock mass. Thus it was not possible to distinguish between gradual and violent failure for instabilities involving slip on pre-existing discontinuities (the second type of rockbursts). This research project focuses on this type of rockburst and aims at developing a method to evaluate the stiffness in question, to make comparisons possible. This method uses numerical modeling tools such as the boundary element method (and in particular a modified version of the software SATURN originally created by Fotoohi, 1993) and a new constitutive model for joint behavior partially based on the one proposed by Saeb and Amadei (1989, 1990, 1992).

This brief introduction is followed by a chapter on the rockburst problem and a review of existing methods for the evaluation of the rockburst potential. Chapter 3 presents a literature review on the behavior of joints and describes in details Saeb and Amadei's constitutive model. Chapter 4 reviews the foundation of the boundary element method (BEM) for rock mechanics. Chapter 5 describes the development and implementation of a new constitutive model for rock joint into the SATURN software. Chapter 6 presents analyses of parametric cases and analysis of an actual mine situation. Then follow a discussion and conclusions.

CHAPTER 2
EVALUATION OF ROCKBURST POTENTIAL

2.1 ROCKBURST PHENOMENA

Rockbursts may cause damage to underground openings and to equipment, and constitute a major hazard to the safety of mine workers. This results in a cost increase and a loss of productivity for the operator. Bláha (1990) reported that the production costs in coal mines in the Ostrava-Karviná region in Poland increased by 100% when the mined area became burst-prone. On the safety level, Salamon (1983) noted that in 1979, 62% of fatalities in South African mines could be attributed to rockburst and rockfalls. He also reported that even though the total number of fatalities has drastically decreased in the last fifty years, the number of fatalities per year associated with rockbursts has not changed. In the first half of 1996 only, there were more than 35 fatalities associated with rockbursts in South African mines (Ryman-Lipinsky and Bakker, 1997). Rockburst is a worldwide problem that is not expected to decrease, since the depth and size of openings seem to keep on increasing.

This chapter starts with a definition of the rockburst phenomenon. The problem is then classified according to the mechanism involved. Finally, existing methods for the evaluation of rockburst potential are presented.

2.1.1 Definition

A rockburst is generally defined as a sudden rock failure characterized by the breaking up and expulsion of rock from its surroundings, accompanied by a violent release of energy (Blake, 1972). Although the definition of rockburst differs from one author to another, the common ground of these definitions is the sudden release of energy in the form of a violent expulsion of rock (McMahon, 1988). Brown (1984) suggests that a rockburst should be considered as a particular manifestation of seismic events that are induced by mining activities. In fact, the sudden failure that characterizes a rockburst can be, in itself, the source of the seismic event, or may have been triggered by a distant seismic event or from a load transfer due to the latter (Gill and Aubertin, 1988).

The released seismic energy during a rockburst can range in magnitude from 0.5 to over 5.0 on the Richter scale (Jaeger and Cook, 1979). Usually, damages (or rockbursts) occur when the magnitude of the seismic event is larger than 0.5 (McMahon, 1988). It is important to note that although every rockburst is a seismic event, not all seismic events are rockbursts. In this document, a seismic event is considered a rockburst when damage reaches the mine openings.

The necessary conditions to produce a seismic event are (Salamon, 1983):

- A region in the rock mass must be on the brink of unstable equilibrium either because of:
    - a) the presence of an appropriately loaded pre-existing geological weakness such as a joint, fault, dyke or bedding plane; or because
    - b) the changing stresses are driving a volume of rock towards sudden failure; or because

c) some support system approaches a state in which its unstable collapse is imminent.

- Some induced stresses must affect the region in question and the magnitude of these stress changes, however small, must be sufficiently large to trigger off the instability.
- Sudden stress change of sizable amplitude must take place at the locus of instability to initiate the propagation of seismic waves.
- Substantial amount of energy must be stored in the rock around the instability to provide the source of kinetic or seismic energy. The origin of this stored strain energy is work done by:
  a) gravitational forces and/or
  b) tectonic forces and/or
  c) stresses induced by mining.

Three sources can produce these energy releases:

- the stored strain energy in the rock mass;
- the changes in the potential energy of the rock mass;
- the slip along a weakness plane.

The changes in potential energy occur during mining and a portion of this energy can be stored in the surrounding rock mass. These changes brought by mining may trigger latent seismic events that derive mainly from the strain energy produced by geological differences in the state of stress (Cook, 1983).

2.1.2 Classification of rockbursts

Rockbursts and other seismic events that may occur within rock masses influenced by mining and other activities are associated with unstable equilibrium states that may involve (Brown, 1984):

- slip on pre-existing discontinuities; or
- fracturing of intact rock.

This leads to the definition of two broad categories of rockbursts:

i) Fault-slip rockbursts resulting from the first unstable equilibrium state mentioned above;

ii) Strain rockbursts (including pillar burst) resulting from the second unstable equilibrium state mentioned above.

It is important to note that several case studies (Morrison and Coates, 1957; Ortlepp, 1984) seem to demonstrate that a non-violent failure of a portion of the rock mass can trigger a fault-slip, and vice versa. Figure 2.1 shows the different situations that may induce either strainbursts or fault-slip.

2.1.3 Rockburst mechanism

Rockburst is essentially a failure phenomenon, and the largest step to understand its mechanism is to study the failure mechanism. Rockbursts can then be explained by using classical rock mechanics principles.

Creating a new underground opening modifies the in situ stresses in the rock mass and induces a new stress field. Usually, the modification in the pre-mining stress field is limited to a region known as zone of influence. Figure 2.2 shows a schematic representation of a typical zone of influence for a drift. When the drift face advances, the zone of influence, where the stress field has changed, moves with the drift. This zone of influence can pass through a geological discontinuity and can provoke a violent slip along the discontinuity (events S_1 and S_2). In the same manner, if this zone passes through a weak zone, a failure process can be induced (event S_3) creating a new fracture in the rock mass. Also, a portion of the rock mass can fail violently (events C_1 and C_2), when the opening crosses the discontinuity f-f', a dyke in the Figure 2.2.

It was proposed in the USSR by Petukhov (1957) - and later in South Africa by Cook (1965b) and Diest (1965) - that the violent failure of a rock sample under uniaxial compression in a low stiffness loading system represents, on a smaller scale, the dynamic fracturation of rock during a rockburst. In this context, the rock mass that is brought to failure around the opening is associated with the rock sample, and the rock mass surrounding the failed rock represents the loading system.

Figure 2.3 presents schematically this analogy using the load-displacement curve. In this figure, k_r represents the stiffness of the rock in its pre-failure state (elastic behavior), and k_{ls} represents the loading system stiffness. On Figure 2.3a, point A represents the start of microcracking; point B represents the peak resistance; and point C can be identified as the limit of the stable equilibrium of the system (Salamon, 1970, 1974). Figure 2.3b shows the evolution of the rock stiffness with the displacement.

As we can see on Figure 2.4a, when the loading system stiffness is smaller (in absolute values) than k'_r (the rock post-peak stiffness), the amount of stored strain energy in the system (rock and loading system) exceeds the work that the rock can do in its post-peak phase, and the failure will be violent. Otherwise, if k_{ls} is larger than k'_r (in absolute values), then the failure will be gradual and can be controlled (Figure 2.4b).

Pininska and Lukaszewski (1991) observed that laboratory results seem to indicate that rocks with a lesser strength show greater post-peak strains and vice-versa: the greater the strength, the fastest is its final failure. This phenomenon, although not being an absolute law, has been confirmed by a compilation of test results made by Aubertin et al. (1994a, 1994b).

Even if the analogy described above is simple, it remains nonetheless true for the rock mass (Gill and Aubertin, 1988). The strength and the deformability of a rock sample are controlled by the intragranular bonds while the essential forces in a rock mass act principally on the surfaces of geomechanical discontinuities (Pininska and Lukaszewski, 1991). The transposition to the rock mass of this analogy must however consider the fact that the stress field in rock structures is not necessarily uniaxial. With this end in view, Gill and Aubertin (1988) proposed the notion of equivalent stiffness that will be detailed in section 2.3.

Salamon (1974) extended this analogy to explain fault-slip rockbursts. Figure 2.5 shows two diagrams shear stress-tangential displacement obtained from direct shear tests on a structural plane with a low normal stress. In this figure, k_p is the pre-peak stiffness of the plane and k_{ls} is the loading system stiffness. Point A on Figure 2.5b represents the ultimate (peak) shear strength of the plane, and loading beyond this point leads to the residual strength. A comparison between the stiffness of the loading system k_{ls} and the post-peak stiffness of the plane k'_p shows that the equilibrium of the system loading-structural plane is stable and the evolution of the post-peak behavior is gradual since

$|k_{ls}|>|k'_p|$. However, on Figure 2.5a, the evolution toward the residual strength is violent for $|k_{ls}| < |k'_p|$ since the stored energy can not be totally dissipated through straining.

Of course, the transposition of this model to the rock mass must also consider that the normal stress to the discontinuities is not necessarily low nor constant.

2.2 Methods for the evaluation of rockburst potential

The techniques or methods to evaluate the rockburst potential in underground mines are numerous. However, due to the complex nature of the phenomenon, no technique can yet predict each and every single event. Existing techniques can be divided into two broad categories:

i) Methods based on indices derived from rock properties;
ii) Methods based on in situ conditions.

The goal of this literature review is not to present an exhaustive list of every technique available but rather to provide a brief summary of the different tools available for the evaluation of rockburst potential in underground mines.

2.2.1 Methods based on indices derived from rock properties

Usually, these techniques are used the same way. First, the index is calibrated for the mine or the mine district by linking the value of the index with the number of events. The index can then be used to evaluate the potential of a new zone by calculating its index value.

Most of these indices are closely related to the behavior of rock under uniaxial compression. Hence, a brief review of this behavior is useful.

2.2.1.1 Behavior of hard rocks under uniaxial compression

Figure 2.6 shows schematically a typical stress-strain relationship for a rock specimen submitted to uniaxial compression. Some phase boundaries are also added. The first phase (phase 1), curved upward, is associated with the reversible closure of microcracks; in dense rocks with very low porosity, this first phase is almost non-existent. Then follows a linear phase (phase 2) due to the elastic response of the rock, which extends up to the microfracturing threshold where stable crack propagation starts. The onset of microcrack growth (phase 3), which precedes the peak strength, commonly begins above about 50% of the ultimate load, as shown by studies on volumetric measurements, acoustic emissions, wave velocity, etc. (e.g., Paterson, 1978; Hakami, 1988; Cox and Meredith, 1993). When approaching the peak strength, the size and density of cracks increase, and cracks interaction becomes more important, and unstable crack propagation can be initiated (phase 4).

Damage accumulation during crack propagation (phase 4) leads to a rapid increase in dilation and eventually to strain localisation. It is known that, for brittle materials such as rocks, localisation associated with a loss of homogeneity of the strain field, usually occurs in the vicinity of the peak load (e.g., Wawersik et al., 1990). In the post-peak phase (phase 5), localisation phenomena become more important, and usually produce a gradual reduction of the sample cohesion with increasing inelastic strain. This causes a pronounced softening of the material, which is a progressive decrease of strength as strain accumulates.

One important aspect of the rock behavior, used with several indices, is that inelastic strain can develop in the pre-peak regime and can dissipate energy by microcracking.

2.2.1.2 Indices based on energy

A) Relative violence at failure

Proposed by Denkhaus et al. (1958), this index measures the rebound of the loading system at failure during a uniaxial compression test with a non-stiff loading system. The hypothesis of this index is that the rebound is proportional to the violence (seismic energy released, volume of rock fragments, etc.) at failure.

B) Indices based on stored elastic strain

Several indices are based on the elastic energy recovered in a loading-unloading test. Among these is the Bursting Liability Index or W_{et} Index proposed by Neyman et al. (1972) for coal mines. This index is determined with a uniaxial compression test by:

$$W_{et} = \frac{E_R}{E_D} \tag{2.1}$$

where E_R is the elastic energy recovered during unloading which can be calculated by the area under the unloading curve, and E_D is the energy dissipated in the cycle which can be calculated by the area between the loading and unloading curves (Figure 2.7). The load during the test must attain between 80% and 90% of the uniaxial compressive strength. The larger the value of the index, the less the rock can dissipate energy via stable propagation and the larger is the rockburst potential. Stewarski (1987) also proposed the Rock Dynamic Index that is determined by the same ratio but for a loading test on a Hopkin's bar.

However, to achieve 80% to 90% of the strength with the W_{et} index is a problem since this strength can be known, a priori, only in a probabilistic manner. Moreover, the size of the hysterisis and the value of the index are directly influenced by the relative value of the load attained (Hueckel, 1987). To eliminate this problem, Aubertin and Gill (1988) proposed the Brittleness Index Modified (BIM). To calculate the value of this index, a uniaxial compression test is carried out up to failure. The area under the loading curve (A_2) is easy to evaluate (Figure 2.8). A_2 is then compared to the area under the curve corresponding to the deformation modulus of the rock (A_1) taken at 50% of the peak strength. The value of this index is then determined by (Aubertin and Gill, 1988):

$$BIM = \frac{A_2}{A_1} \geq 1.0 \qquad (2.2)$$

The smaller the value of the BIM, the higher is the rockburst potential. Aubertin et al. (1994a, 1994b) also proposed a classification of the proneness of the rock for rockbursting:

Table 2.1 Indicative values of BIM as related to bursting liabilities (after Aubertin et al., 1994a, 1994b).

BIM	Bursting liabilities
between 1.00 and 1.20	high
between 1.20 and 1.50	moderate
above 1.50	low

The BIM has also been related to the ratio of pre-peak modulus to the post-peak modulus and can be used to find the post-peak modulus when it was not determined in laboratory testing.

One last index based on a somewhat similar principle is the Burst-efficiency Ratio proposed by Motyczha (see Kidybinski, 1981) given by:

$$B_{er} = \frac{\phi_1}{\phi_0} \tag{2.3}$$

where ϕ_1 is the energy of particle ejected at failure in a uniaxial compression test, and ϕ_0 is the maximum energy stored in loading and given by (also, Mitri, 1996b):

$$\phi_0 \approx \frac{\sigma_c \varepsilon_r}{2} \tag{2.4}$$

where σ_c is the uniaxial compressive strength, and ε_r is the deformation at failure.

C) Index of released energy

Proposed by Singh (1988a), this index measures, with a seismograph, the sum of maximum speeds of vibrations produced in the loading system during a uniaxial compression test. This sum would be a measure of the released energy at failure.

D) Failure duration index (Dt)

Wu and Zhang (1997) proposed to monitor the time of failure (Dt) of coal samples during a uniaxial compression test (stress rate between 0.5 to 1.0 MPa/s). The Dt index is the time between peak strength and complete break down. The authors proposed the following values of proneness:

Table 2.2 Indicative values for the Dt index (after Wu and Zhang, 1997)

Dt value	Bursting proneness
lower than 50 ms	strong
between 50 and 500 ms	medium
larger than 500 ms	no

2.2.1.3 Brittleness

The brittleness of rocks is sometimes evaluated from two different empirical (and more or less arbitrary) concepts such as (Hucka and Das, 1974):

$$B_1 = \frac{\sigma_c - \sigma_t}{\sigma_c + \sigma_t} \tag{2.5}$$

$$B_2 = \sin\phi \tag{2.6}$$

where σ_c is the uniaxial compressive strength, σ_t is the uniaxial tensile strength, and ϕ is the shear angle taken from the failure surface in Mohr's diagram. Rockburst potential seems to increase with larger brittleness values.

2.2.1.4 Decrease Modulus Index

This index is obtained from the ratio of the pre-peak deformation modulus over the post-peak deformation modulus (Homand et al., 1990). The pre-peak modulus corresponds to the slope of the linear part of the pre-peak curve and the post-peak modulus is given by the slope of the post-peak portion of the curve. The rockburst potential increases with a lower value of the index.

2.2.1.5 Elastic strain energy factor

Hou and Jia (1988) presented this factor that combines drilling observations with in situ stresses. The mean length of drilling core is associated to the in situ stress and then classified. The rockburst potential is evaluated from this class.

2.2.1.6 Energy-Band failure index (criterion)

Mitri (1996b) suggested the calculation of pillar skin strainburst using an index based on strain energy which is given by:

$$\text{S.L.} = \frac{e_4}{e_c} \qquad (2.7)$$

where e_4 is the mining-induced strain energy calculated at the boundary of the opening (pillar skin) and e_c is the critical strain energy given by equation 2.4.

2.2.1.7 Concluding remarks

Using indices presented in this section implies that a mine or a mining zone had already a certain number of rockbursts to establish the different zone boundaries as to: no risk; moderate risk; high risk. Altough these indices can easily be obtained, they only indicate the proneness of the rock to fail violently, and they do not provide a tool that can be easily integrated into routine mine design. They can, however, indicate mine zones where rock structure might be at higher risk.

2.2.2 Methods based on in situ conditions

Due to the problems of integrating the use of indices based on rock properties into routine mining engineering, many researchers turned to an in situ approach to predict, a priori, the rockburst potential of openings. These methods emerged principally with a better understanding of the rockburst phenomenon.

2.2.2.1 Rock mass electric resistance

The continuous monitoring of the electric resistance changes in the rock mass has been used to predict the frequency of rockbursting (Stopinski and Dmowska, 1984). This monitoring facilitates the observation of the effects of tectonic stresses and mining induced stresses. These observations can also indicate the location and necessity for applying a destressing technique to the rock mass (Singh, 1989).

2.2.2.2 Seismic velocities

Krawiec and Stanislaw (1977) showed that the seismic velocities could be related to the stress level in the rock mass, the velocity value being proportional to the stress level. Changes in velocity values can then be used to monitor stress changes in the rock mass and then prevent failure and rockburst situations.

2.2.2.3 Energy balance

This approach is essentially the elaboration of the balance of stored energy in a rock mass and the energy that can be dissipated when a change (geometrical and/or in stress level) occurs in the rock mass. This balance is used to calculate the energy available for rockbursting. This approach was reviewed in detail by Salamon (1970, 1974, 1983, 1984), Walsh (1977), Budavari (1983), Brady and Brown (1985), McMahon (1988), and Hedley (1992).

Since 1960, many measurements of rock displacement have been performed and they suggest that the rock mass mechanical behavior in rockburst situations is essentially of elastic nature (Ortlepp, 1983). Then, the energy balance is usually performed using elastic laws. It could also be shown that using elastic laws to evaluate the energy available for rockbursting is a conservative approach since the energy dissipated by fracturing is neglected, hence, the stress concentration around opening is overestimated.

When an opening is created or modified, the stored strain energy equilibrium is changed (Cook et al., 1966). Let stage I be the initial situation before the creation of the opening; the stage following the creation (or modification) of the opening will be called stage II. The energy balance is concerned with the transition between stage I and stage II.

When an opening is created, energy becomes available and is provided from two sources. The first one is the work W (or the variation of potential energy in the system) done by the shifting of external and gravitational forces working on the convergence and deformation of the rock mass. The second source is the stored strain energy U_m in the mined rock. The sum of these energies ($W + U_m$) is the total energy available when passing from stage I to stage II.

This energy can be dissipated in two ways. A portion of this energy will be dissipated with an increase in the strain energy U_c stored in the rock mass surrounding the excavation. It is also possible that the pressure on support elements surrounding the opening increases; this work W_s is the second way of energy dissipation.

If the rock mass is considered as an ideal elastic continuum, then no energy is dissipated through fracturing or inelastic deformation of the rock. With this simplification in mind, the sum ($U_c + W_s$) is the total energy dissipated during the mining of the opening.

It is obvious that the total energy dissipated cannot be larger than the energy available ($W+U_m$). Considering that the stored strain energy in stage I in the mined rock (U_m) is not available anymore, then:

$$W \geq U_c + W_s \tag{2.8}$$

and since $U_m > 0$, then

$$W + U_m > U_c + W_s \tag{2.9}$$

This inequality implies the existence of an excess of energy that must be dissipated when passing from stage I to stage II. This energy is referred to as the released energy W_r. Then, one can write:

$$W_r = (W + U_m) - (U_c + W_s) > 0 \tag{2.10}$$

and $$W_r \geq U_m > 0 \tag{2.11}$$

The amount of released energy W_r, when larger than the stored strain energy in the mined rock (U_m) in stage I, produces a wave (kinetic energy) that propagates from the new limits of the opening. The vibrations produced by the wave will be damped by minor flaws in the rock mass (the latter not being perfectly elastic). This kinetic energy W_k will be dissipated by the damping process.

Since there is no other way to dissipate the energy, then:

$$W_r = U_m + W_k \tag{2.12}$$

and $$W_k = W - (U_c + W_s) \geq 0 \tag{2.13}$$

Then the final equation of the energy balance is given by:

$$W_r = W - [(U_c - U_m) + W_s] \tag{2.14}$$

The evaluation of the released energy of an opening is relatively easy for any geometry (Gill and Aubertin, 1988) and the Boundary Element Method (BEM) is well adapted to make such evaluation (Brady and Brown, 1981).

It is obvious that the amount of released energy is proportional to the depth of the excavation (or the pre-mining stress) and its dimensions (Gill and Aubertin, 1988).

2.2.2.4 Energy Release Rate (ERR)

Based on the energy balance, an incremental approach can be used to follow the changes due to mining. The mining of an underground orebody usually implies the widening of excavations by increments. This leads to an energy release rate by unit surface (dW_r/dS), used when the opening geometry is regular, or a volumetric energy release rate (dW_r/dV), used for irregular geometry openings.

Stacey and Page (1986) provide a way to evaluate, in a preliminary manner, this energy release rate (the symbol ERR is commonly used in the literature) with the equation:

$$ERR_{V=1} = \tfrac{1}{2}\sigma\varepsilon \qquad (2.15)$$

where σ is the stress on the unit volume before mining, and ε is the convergence resulting from the opening.

This ERR has become a rockburst prediction tool in South African mines. Spottiswoode (1990) notes that ERR is one of the most used parameters for stope design in deep underground South African mines. A correlation between the ERR and rockburst hazards was established for longwall mining (Cook, 1978) as seen on Figure 2.9.

2.2.2.5 Strain energy approach

Based also on the energy balance concept, Mitri and Suriyachat (1990; see also Mitri et al., 1993; Momoh et al., 1996) developed a 2D finite element program that can calculate mining induced strain densities around mine openings. The idea is based on the assumption that rockburst can be attributed to total strain energy stored at this moment as well as the energy release rate (same as the ERR) caused by the past mining steps.

Figure 2.10 explains the calculation of energy. From the initial mining step (before the excavation) to mining step 1, where we go from $(0, \sigma_0)$ to $(\varepsilon_1, \sigma_1)$ the total stored strain energy is given by area ABCD. The mining induced strain energy density is given by area ABE and the energy stored or lost by the pre-mining stresses is the area AECD. When portion 2 of the excavation is mined, the total stored strain energy is given by area AHGD, the mining induced strain energy density is given by area BHJ and the energy stored or lost by the pre-mining stresses is the area BIGC. These energy densities are calculated, using linear elasticity, at every integration point within each element in the mesh of the finite element model.

This software can be a useful tool to help determine the less burst-prone mining sequence of openings. However, it requires calibrating with actual rockburst case histories in order to give values for the strain energy level to assess the risk of rockbursting in Canadian underground mines.

2.2.2.6 Excess Shear Stress (ESS)

The South African experience showed that the notion of energy release rate (ERR) was very limited for fault-slip type rockbursts. Ryder (1987) proposed a similar criterion, the excess shear stress criterion (ESS), that could be applied to this type of rockbursts. This criterion is based on the energy available when passing from static resistance (before slip movement) to the dynamic resistance (during the slip).

The static resistance τ_s of the discontinuity can be estimated with a Mohr-Coulomb type criterion such as:

$$\tau_s = c + \mu_s \sigma_n \tag{2.16}$$

with $$\mu_s = \tan\phi_s \tag{2.17}$$

where c is the cohesion, μ_s is the static friction factor, σ_n is the normal stress at the slipping point, and ϕ_s is the static friction angle. Once the motion has started, the value of the ESS is given by:

$$ESS = \tau_e = |\tau| - \tau_d \tag{2.18}$$

where τ_e is the net shear stress available to produce a seismic event once failure has started, τ is the shear stress at the initiation point, and τ_d is the dynamic resistance at this point and given by:

$$\tau_d = \mu \sigma_n \tag{2.19}$$

with $$\mu = \tan\phi \tag{2.20}$$

where μ is the dynamic friction factor, and ϕ is the dynamic friction angle. Ryder (1987) has suggested these average values of τ_e to produce significative seismic events:

$\tau_e \approx 5$ - 10 MPa	for an unstable movement along a pre-existing discontinuity;
$\tau_e \approx 20$ MPa	for a shear failure of intact rock.

In theory, the larger ESS value brought by the progression of the opening towards the discontinuity, the larger surface of the discontinuity would be involved, and the larger would be the seismic event produced. In practice however, back analyses performed showed that not all positive ESS situation yielded seismic events. This could be due to lack of accuracy on the data and/or stress involved (Ryder, 1987). Gill and Aubertin (1988) note that this absence of rockbursts for positive ESS confirms the fact that the discontinuity post-peak stiffness and the rock mass stiffness on both sides of the discontinuity may play a major role in the process, or maybe τ_e should not be assumed; rather it should be assessed by laboratory testing.

2.2.2.7 Activity index

Tao (1988) proposed an index that considers the uniaxial compressive strength σ_c and the major principal stress σ_1 in the region of the opening. His experience in Chinese mines led to the following class of risk:

Table 2.3: Rockburst potential classes (after Tao, 1988)

Class	σ_c/σ_1	Bursting activity	Comments
1	> 13.5	no activity	no acoustic emission
2	13.5 - 5.5	low activity	weak acoustic emissions
3	5.5 - 2.5	average activity	loud acoustic emissions
4	< 2.5	high activity	very loud acoustic emissions

2.2.2.8 Microseismic activity

Rockburst research has focused basically on two fields - prediction and control. The first studies on prediction focused on acoustic and microseismic emission monitoring. Relation between microseismic emission rate and stress state was first verified in 1938 in the United States (Bolstad, 1990). However, it is with the work of Obert and Duvall in the 1940's (see Obert and Duvall, 1967) that this technique really started.

In a stable elastic homogeneous and isotropic domain, no acoustic or microseismic emission should theoretically occur. Daihua and Miller (1987) note that there is little acoustic emission in a uniaxial compression test until the load reaches a certain level, that is 75% to 80% of the peak strength (50% for Paterson, 1978), which shows that the rock specimen has an elastic behavior. However, heterogeneities and anisotropy in rock masses will create some local instabilities (Salamon, 1974; Jaeger and Cook, 1979).

Mine microseismicity is highly influenced by local geology and tectonic - i.e., by heterogeneities and discontinuities, and the interaction between gravitational, tectonic and induced stresses at a local and regional scale (Gibowicz, 1990). It is usually assumed (see for example Blake, 1982) that at the scale of rock masses, one finds the same phenomena as in laboratory tests.

Microseismic events can be recorded by sensors strategically located in a mining region and connected to a computer. During an event, the computer locates its position and its amplitude by analyzing arrival times at each sensor. It is then possible to locate regions where there is microseismic activity. These regions are then considered as burst-prone regions (Blake, 1972).

Microseismic monitoring can also be used for other purposes than localization. Experience showed that microseismic activity could be related to the ERR and bursting activity; an increase in ERR will usually produce an increase in microseismic activity (Gay et al., 1982), and in periods preceding rockbursts, there is often a high increase of the number of seismic events (Jaeger and Cook, 1979). For example, a 17 month experiment in a South African mine where a warning was issued for an increased in seismic activity showed a 80% success in predicting rockbursts (Glazer, 1997). However, half of these rockbursts occurred more than 4 days after the warning was issued (only 27% occurred within 24 hours).

Microseismic monitoring in the mining industry has been used widely in Canada and worldwide. Canada in particular has spent a lot of efforts in that field (e.g., Roctest, 1980; Calder et al., 1986; Daihua and Miller, 1987; Hedley and Udd, 1987; Hasegawa et al., 1989, 1990; Young et al., 1989, 1990; Hedley, 1991, 1992; Plouffe et al, 1993; Beghoul et al., 1996).

Nevertheless, the relative high cost for the purchase, installation, maintenance and use of this technique makes it a tool that is not easily available for small mines including several mines in the province of Québec. Moreover, it is hardly a predictive method but rather a monitoring tool.

2.2.2.9 Rockburst hazard based on 3D stress field analysis

Tajdus et al. (1997) proposed several rockbursts indicators for the evaluation of the rockburst potential for Polish underground coal mines:

- Coefficient of vertical stress concentration:

$$\alpha = \frac{\sigma_z(x,y,z)}{p_z} \qquad (2.21)$$

where σ_z (x,y,z) is the vertical stress in the elementary volume, p_z is the initial vertical stress in the elementary volume.

- Coefficient of energy concentration:

$$\beta = \frac{V_c}{V_c^i} \qquad (2.22)$$

where V_c is the strain energy of the rock mass in the elementary volume and V_c^i is the initial strain energy of the rock mass in the elementary volume, with:

$$V_c = V_o + V_p \tag{2.23}$$

where V_o is the strain energy of volume change given by:

$$V_o = \frac{1-2\nu}{6\,E}\left[\sigma_x^2 + \sigma_y^2 + \sigma_z^2 + 2\left(\sigma_x\sigma_y + \sigma_y\sigma_z + \sigma_z\sigma_x\right)\right] \tag{2.24}$$

and V_p is the strain energy of distortion given by:

$$V_p = \frac{1+\nu}{6\,E}\left[\left(\sigma_x - \sigma_y\right)^2 + \left(\sigma_y - \sigma_z\right)^2 + \left(\sigma_z - \sigma_x\right)^2 + 6\left(\tau_{xy}^2 + \tau_{yz}^2 + \tau_{zx}^2\right)\right] \tag{2.25}$$

The initial elementary strain energy of the rock mass can be obtained by:

$$V_c^i = \frac{p_z^2\left(1-\nu-2\nu^2\right)}{2\,E\left(1-\nu\right)} \tag{2.26}$$

where E is the elastic modulus and ν is the Poisson's ratio.

- Ratio of effective stress to rock strength

$$W_b = \frac{\sigma_0}{\sigma_c \text{ or } \sigma_t} \tag{2.27}$$

where σ_0 is the mean applied stress, σ_c is the uniaxial compressive strength and σ_t is the uniaxial tensile strength.

- Energetic rockburst indicator

$$T_e = \frac{E_K}{E_K^o} \tag{2.28}$$

where E_K is the energy accumulated in the rock mass and E_K^o is the energy necessary for initiating rockbursting. Based on the energy balance, E_K is given by:

$$E_K = V_C + E_D - L_{ZN} \tag{2.29}$$

where V_C is the elastic energy accumulated in the broken rock mass during rockburst, which is a sum of initial and induced stresses, E_D is the energy generated by the tremor in the rock mass and L_{ZN} is the work used for breaking and crushing rock mass volume discharged to an opening. The minimum energy necessary for initiating a rockburst E_K^o can be estimated by:

$$E_K^o = \tfrac{1}{2}\rho_{sr}\, v_o^2 \tag{2.30}$$

where ρ_{sr} is the average density of broken rock mass (assumed to be 2,5 t/m^3) and v_o is the average velocity of broken rock mass ejected to an opening during rockburst (estimated at 10 m/s by Filcek, 1980). Thus, $E_K^o = 1{,}25 \cdot 10^5$ J/m^3. Then, the energetic rockburst indicator is given by:

$$T_e = \frac{V_C + E_D - L_{ZN}}{E_K^o} \tag{2.31}$$

If $T_e < 1$, then the rock mass is not capable of rockbursting; if $T_e \geq 1$, then a rockburst is possible (the probability of occurrence increases with the value of T_e). From their experience in polish coal mines, Tajdus et al. (1997) have combined the preceding indices to provide the following limits:

> when in a given region the following conditions are fulfilled: $\alpha \geq 1{,}5$; $\beta \geq 1{,}5$; rock mass is close to failure $W_b \approx 1$ and $T_e < 1$, then the probability of rock tremors occurrence is very high.
>
> If the following conditions are fulfilled: $\alpha \geq 2$; $\beta \geq 3$; rock mass is close to failure $W_b \approx 1$ and $T_e \geq 1$, then there is a probability of rockburst occurrence.

2.2.2.10 Analytical bump criteria

Kleczek and Zorycha (1991, 1993) developed a criterion for Polish coal mines to evaluate if a rockburst can occur at the roof of a large excavation. Based on the bending conditions, the condition for fracturing (W) is given by:

$$W = \frac{1.325\left[\frac{R_g}{p_z}\right]^2 \frac{F}{E_s}}{\frac{h}{E_g} + \frac{h_i}{E_i}} \tag{2.32}$$

2.3 THE STIFFNESS APPROACH

An analogy based on stiffness difference between the rock and the loading system was presented in section 2.1.3 to explain the rockburst mechanism. This analogy has been integrated in the local mine stiffness coefficient approach for predicting stability of mine pillars (e.g., Starfield and Fairhurst, 1968; Starfield and Wawersik, 1968; Salamon, 1970; Zipf, 1996).

It has also been used to develop a methodology to evaluate the rockburst potential of underground excavations, starting from routine mining and ground control engineering. Convinced that proper engineering design of rock structures should include the evaluation of its rockburst potential, Gill and Aubertin (1988) - see also Aubertin et al. (1992) and Gill et al. (1993) - have extended a methodology presented in Gill's (1982) lecture notes. As shown in the diagram of Figure 2.11, it includes up to four steps: zoning, identification of vulnerable rock structures, stability analysis and a stiffness comparison when a strain or pillar burst is expected. This methodology is briefly described in the following.

2.3.1 Zoning

It consists in dividing the rock mass into different sectors in which a specific mechanical behaviour is foreseen (rock mass deformability, strength, etc.). It includes the determination of the location, boundaries and general properties of the different zones. The initial zoning is usually based on geological data. It should be thereafter confirmed by geomechanical classifications. The RMR system (Bieniawski, 1973, 1984) or the Q system (Barton et al., 1974) are the most commonly used in the northwestern Québec underground mines. All the major geological discontinuities (that are frequently delineating the different zones) must also be identified and located at this stage.

2.3.2 Identification of vulnerable rock structures

The methodology considers three broad categories of potentially vulnerable rock structures, namely:

i) An excavation that approaches a major geological discontinuity, as shown in Figure 2.12a. Here, the stress changes induced by the excavation can increase the shear stress and/or reduce the normal stress along the discontinuity. Any of these can provoke a type I (fault-slip) rockburst;
ii) An excavation that goes through a major geological discontinuity or through a zone boundary; this case is illustrated in Figure 2.12b. If part of the rock mass, located close to both the zone and the excavation boundaries in one of the zones, is brought to its failure state, a sudden and violent failure is possible depending on the deformational properties of the rock mass of the other zone. This can then lead to a type II (strain burst) rockburst;
iii) An excavation that follows a major geological discontinuity or a zone boundary. A typical example of this case is a mine pillar, as shown in Figure 2.12c. If the pillar

(zone C) fails, its failure can be violent (type II rockburst) if the deformation properties of zones A and/or B satisfy certain requirements. This category includes any isolated structure that may present some differences in mechanical properties due to local heterogeneities in the rock mass; it also includes isolated structures that may show pronounced geometrical irregularities.

2.3.3 Stability analysis

In routine mining engineering, stress analyses are usually performed using an elastic constitutive model for the rock mass; this has been proven to be an adequate approach for rockburst situation (e.g., Ortlepp, 1983). Rock properties are generally obtained through standard laboratory tests conducted on specimens prepared from appropriate rock samples. Rock mass properties are extrapolated from rock properties by using various relationships that take into account the mechanical effects of geological discontinuities; relationships based on geomechanical classification ratings are often used for that purpose (Hoek and Brown, 1980; Bieniawski, 1984). The knowledge of the pre-mining state of stress results from in situ measurements or from empirical relationships such as those proposed by Herget (1987; Arjang and Herget, 1997) for the Canadian Shield underground mines or Arjang (1996) or Corthésy et al. (1997) for the Abitibi mining district.

A) Fault-slip type rockburst

This type of rockburst has been defined as a sudden slip on a pre-existing discontinuity. Unfortunately, up until now, very little information on post-peak behavior of geological discontinuities was available. In addition, there seemed to be no recognized method to evaluate the equivalent local stiffness of the rock mass on both sides of the discontinuity.

This was why the proposed methodology recommended (at this stage of its development) that if the stress conditions are such that a slip on the discontinuity is possible, then it should be considered that the equilibrium state is unstable and that there is a potential for rockbursting. However, it should also be considered that if the normal stress is approaching the uniaxial compressive strength of either one of the rock masses bordering the discontinuity, the failure should be gradual.

To model the peak shear strength of the discontinuity, Gill and Aubertin (1988) suggested using Barton's equation (Barton and Choubey, 1977; Bandis et al., 1983), for its relative simplicity and broad applicability.

B) Strain and pillar burst type rockburst

This type of rockburst has been defined as the brittle failure of a certain volume of rock. Unlike the situation described above, it is possible, here, to be more specific about whether the failure is violent or gradual.

If, while performing the stability analysis, expressing the rock mass strength through its uniaxial compressive strength is not adequate, the authors suggested using the well-known Hoek and Brown (1980, 1988) failure criterion.

With mine pillars, both size and shape effects should be considered; these affect the peak strength as well as the pre-peak and the post-peak parts of the stress-strain relationship. Such effects can be introduced into the stress-strain relationship through geomechanical classification ratings (e.g., Särkkä, 1984), empirical formulas (e.g., Bieniawski, 1975; Barron and Yang, 1992) or confined core concept (e.g., Wilson, 1972).

2.3.4 Stiffness comparison

Before the results that will be presented in the following chapters, this final step only applied to strain and pillar burst type rockbursts. Two different situations are dealt with here: (i) mine pillars; (ii) other rock structures.

i) Mine pillars: Let us consider a mine pillar which is axially loaded, as it is postulated with the tributary area theory (Brady and Brown, 1985) or with the pillar loading theory proposed by Coates (1965). It can be shown that the pre-peak stiffness coefficient, k_{pr}, for a "long" pillar (plane strain conditions), considering a unit thickness and idealizing the stress-strain relationship, is given for a unit length of pillar by:

$$k_{pr} = \frac{E_m\ B}{H(1-v^2)} \tag{2.33}$$

where E_m is the pre-peak rock mass elastic modulus, v is the Poisson ratio, B is the pillar width, and H is the pillar height. The post-peak stiffness coefficient, k'_{pr} is obtained by substituting E'_m, the post-peak rock mass elastic modulus, into equation (2.33). It should be noted that stiffness coefficients are expressed here as a force per unit length (e.g., pounds per inch or meganewtons per metre) as it is the case in most publications.

If the post-peak modulus of the rock mass involved is unknown, empirical relationships that have been proposed for rocks can be used, such as the relationship proposed by Brady et Brown (1981) for instance or by using the BIM described in section 2.2.1.2. To account for scale effects, it was proposed by Gill and Aubertin (1988; see also Aubertin et al., 1997; Simon et al., 1998) to use similar relationships as the ones used for estimating the elastic modulus of the rock mass (using geomechanical classification for instance).

On the other hand, the stiffness coefficient of the country rock mass, k_c, can be determined in a number of ways. The analytical models proposed by Starfield and Wawersik (1968) and by Salamon (1970) could be used as such or implemented into a variety of numerical stress analysis methods. Gill and Aubertin (1988) rather favor a simpler approach that is easier to incorporate into routine engineering. It consists in performing numerical stress analyses following the process described by Hoek and Brown (1980) for obtaining ground characteristic lines with the convergence-confinement method as applied to pillar design. To illustrate this approach, let us consider the schematic single symmetrical pillar model shown in Figure 2.13a. A uniformly distributed stress σ_p is applied at the pillar location over a strip of width B and the relative displacement Δ of points A and A' along the pillar axis (or the relative average displacement along the pillar-country rock interfaces) is computed using any two-dimensional numerical code. This analysis is repeated for different values of σ_p and the results are plotted on a $B\sigma_p$ (load) versus Δ (displacement) diagram (Figure 2.13b). It can be shown that the slope of the line so obtained is the local mine stiffness coefficient k_c for the pillar under investigation, as defined by Starfield and Fairhurst (1968) for instance.

For pillars with finite cross-sectional dimensions, plane stress conditions have to be assumed and it can be demonstrated, for an idealized stress-strain relationship, that their pre-peak stiffness coefficient, k_{pr}, is:

$$k_{pr} = \frac{EA}{H} \tag{2.34}$$

In this equation, E is the pre-peak rock mass modulus and A, the cross-sectional area of the pillar. Again, the post-peak stiffness coefficient k'_{pr} can be obtained by substituting E', the post-peak rock mass elastic modulus, into equation (2.34).

The determination of local mine stiffness coefficients (k_e) can be done as suggested above (Figure 2.13a), using instead a three-dimensional stress analysis code. For a given pillar, the results are plotted on a $A\sigma_p$ vs Δ diagram; the slope of the line so obtained is the local mine stiffness coefficient for that pillar. If no 3D code is available, a correction factor can be applied to a 2D analysis (Simon et al., 1998) to obtain k_e.

It is recalled that if the pillar should fail, and if k'_{pr} is larger than k_e (in absolute values), then the failure would be sudden and violent, leading to a pillar burst type rockburst. This comparison is usually done on what has been called force-convergence diagram by Starfield and Fairhurst (1968). These diagrams can be used to evaluate the rockburst potential as illustrated in Figure 2.13b. Curve (i) in this figure is an idealized reaction curve for a pillar which should fail and potentially burst while in the case of the pillar with reaction curve (ii), the failure should be gradual; curve (iii) stands for a pillar that should not fail.

ii) Other rock structures: An approach similar to that described for mine pillars is suggested for other rock structures. The local mine stiffness of the surrounding rock mass can be estimated by replacing the failed rock by fictitious forces P_i applied to the surfaces as shown on Figure 2.14a, and then by measuring the convergence Δ between points A-A'. The analysis is repeated for different values of P_i, and the local mine stiffness is given by the slope of the graph $B*P_i$ vs Δ.

It has been recognized, when the rock mass is assumed to be linear elastic and homogeneous, that the stresses known to trigger the failure of any unsupported underground excavation are those at the boundary of the opening. In routine mining engineering work, failure criteria generally used, when performing stability analyses, involve only the two extreme principal stresses (σ_1 and σ_3); it is then postulated that the average principal stress (σ_2) has no effect on the failure process. At the boundary of the excavation the value of the minor principal stress σ_3 is nil; at the limits of the failure zone, it is sufficiently low (in first approximation) to be neglected. With these simplifications in mind, the portion of the rock mass near the excavation that is brought to its failure state can be considered as a structural element submitted to a uniaxial state of stress (Figure 2.14). Then, the post-peak stiffness of the failed rock mass can be estimated with equation (2.33).

As usual, if it is found that failure can occur and if the value of $|k'_{pr}|$ is larger than $|k_e|$ then a type II rockburst can occur.

Several back-analysis of actual rockburst cases have been presented, using this methodology, in Simon (1992); Aubertin et al. (1992, 1997), Simon et al. (1993), Gill et al. (1993), Simon et al. (1995), and Simon et al. (1998).

On the other hand, because several uncertainties exist when estimating the different stiffnesses, it might be useful to compare them in a relative manner. Then a Bursting Potential Ratio (BPR) can be defined as the post-peak stiffness of the failed zone over the local mine stiffness (Simon et al., 1995):

$$BPR = \left|\frac{k'_{pr}}{k_e}\right| \tag{2.35}$$

If the value of BPR in a first analysis is much larger than unity (1.0), this would indicate a clear rockburst potential, but a value near 1.0 might require further investigation (like the determination in laboratory of the post-peak modulus, or a better approximation of the dimensions of the failed zone for example).

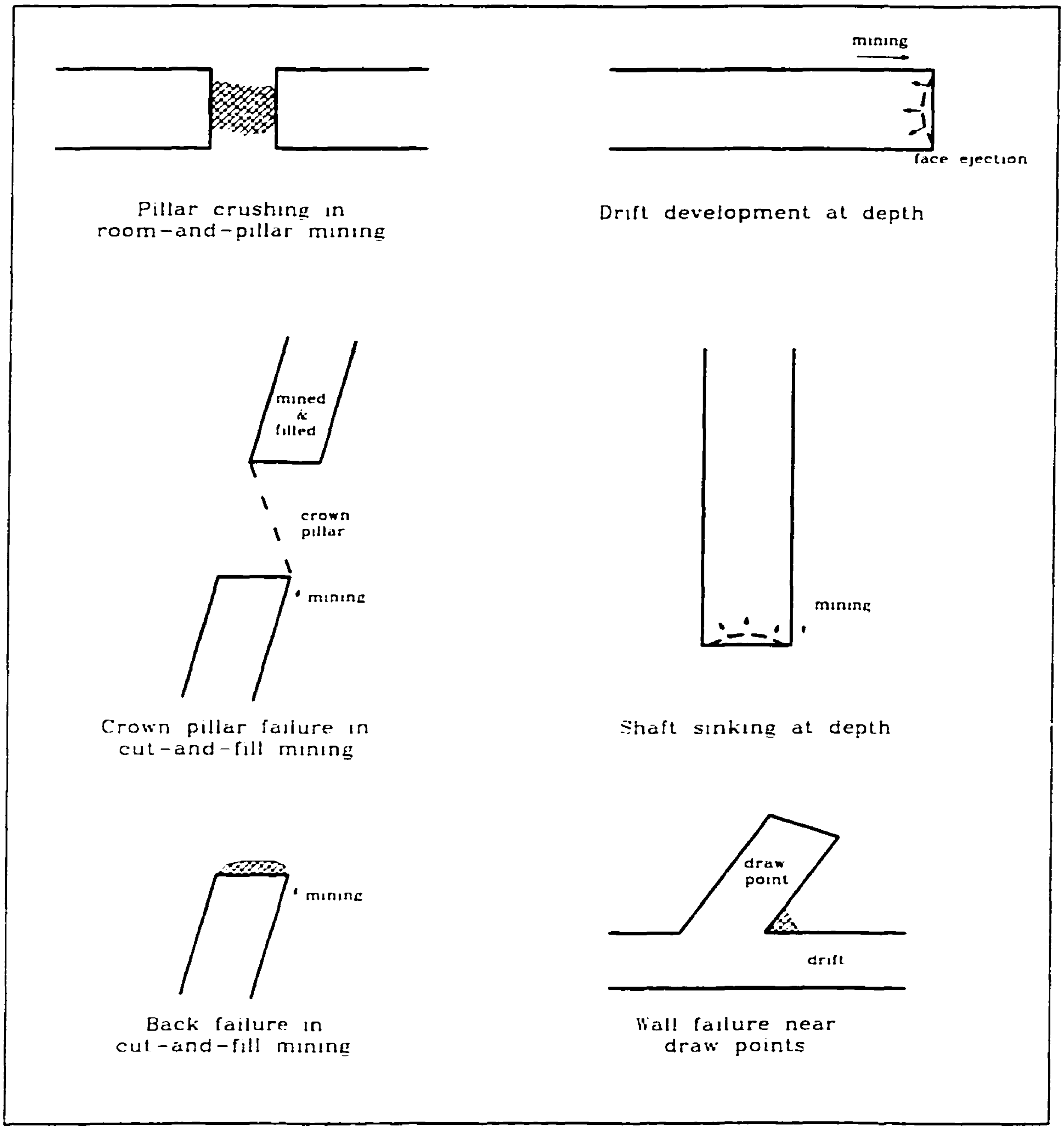

Figure 2.1a: Typical situations that may lead to strainburst type of rockbursts.

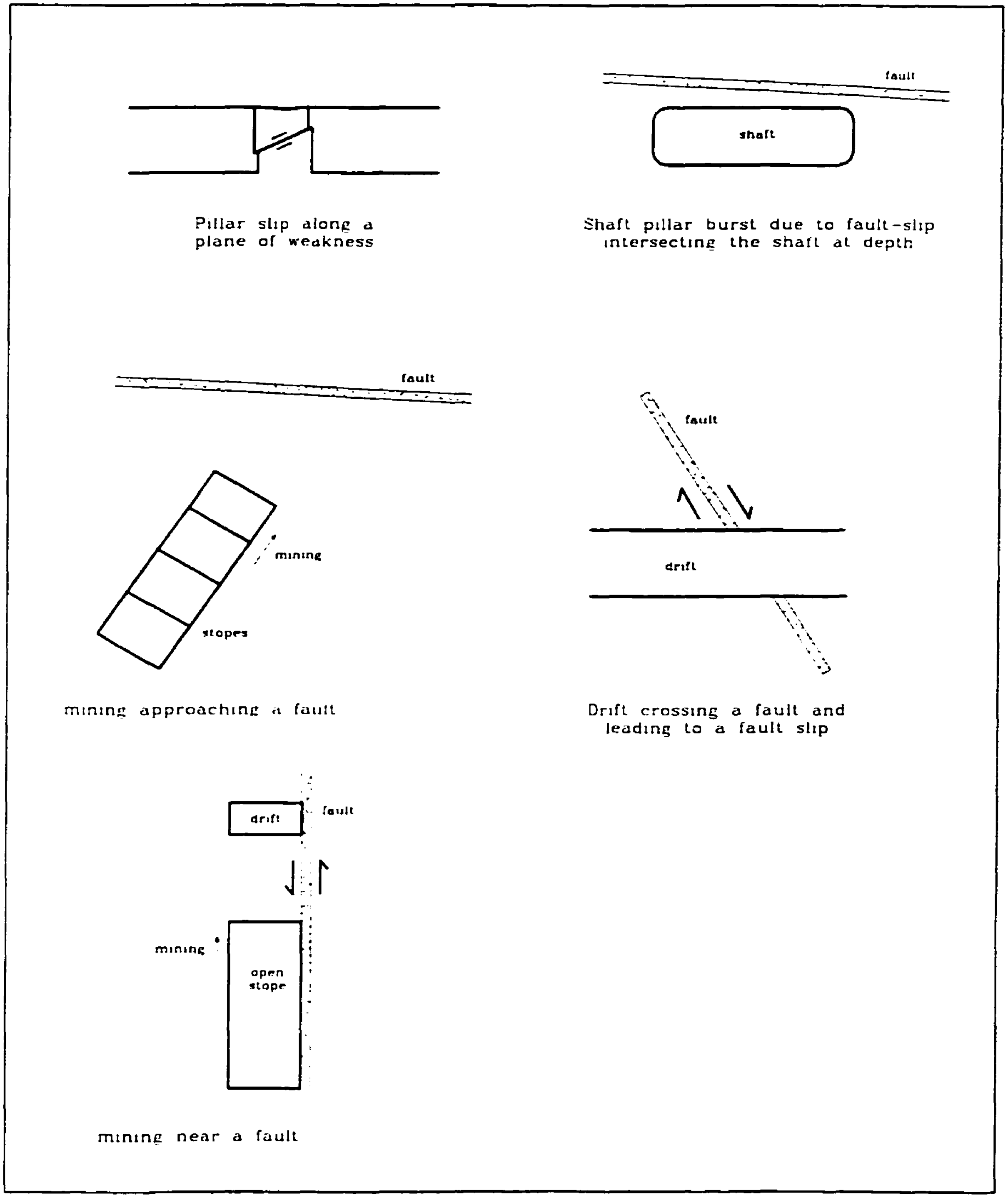

Figure 2.1b: Typical situations that may lead to fault-slip type of rockbursts.

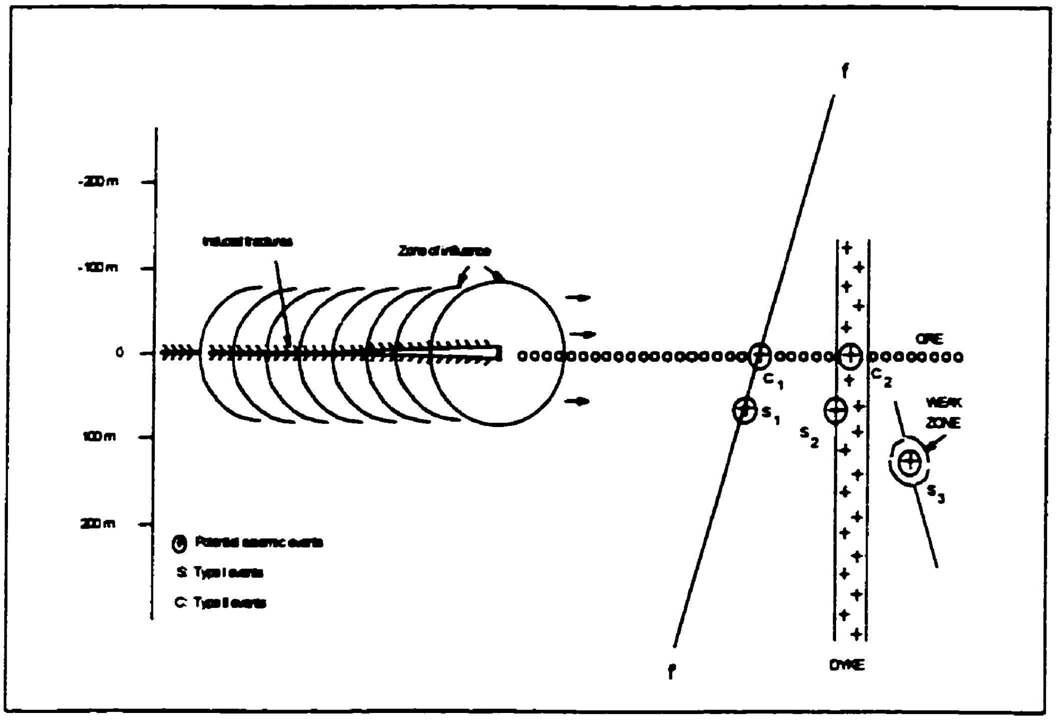

Figure 2.2: Schematic representation of the zone of influence of a drift and localization of potential seismic events (after Ryder, 1987, 1988).

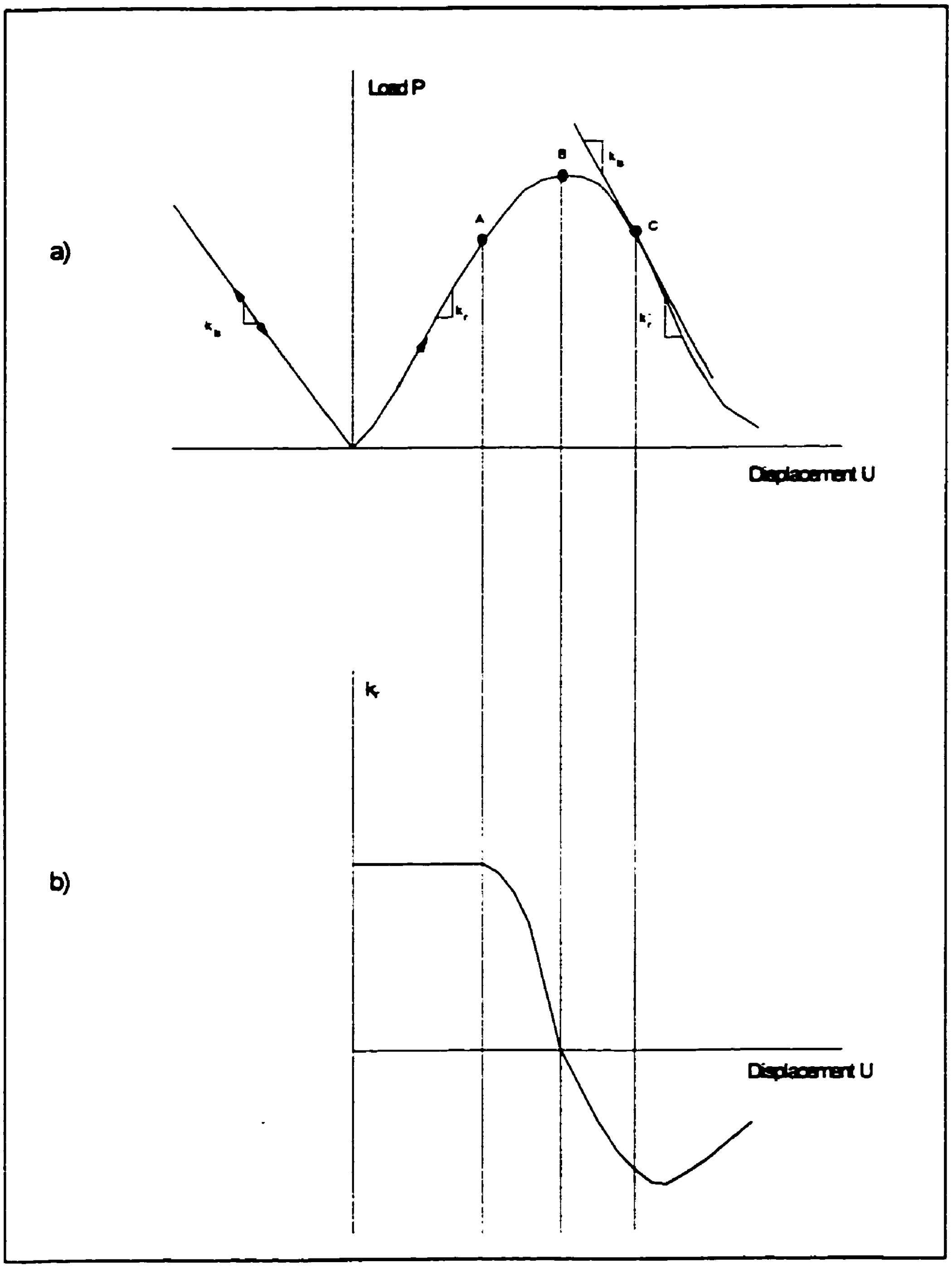

Figure 2.3: a) Schematic load-displacement curve of a rock sample in a uniaxial compression test. b) Evolution of the rock stiffness with the displacement (after Salamon, 1974).

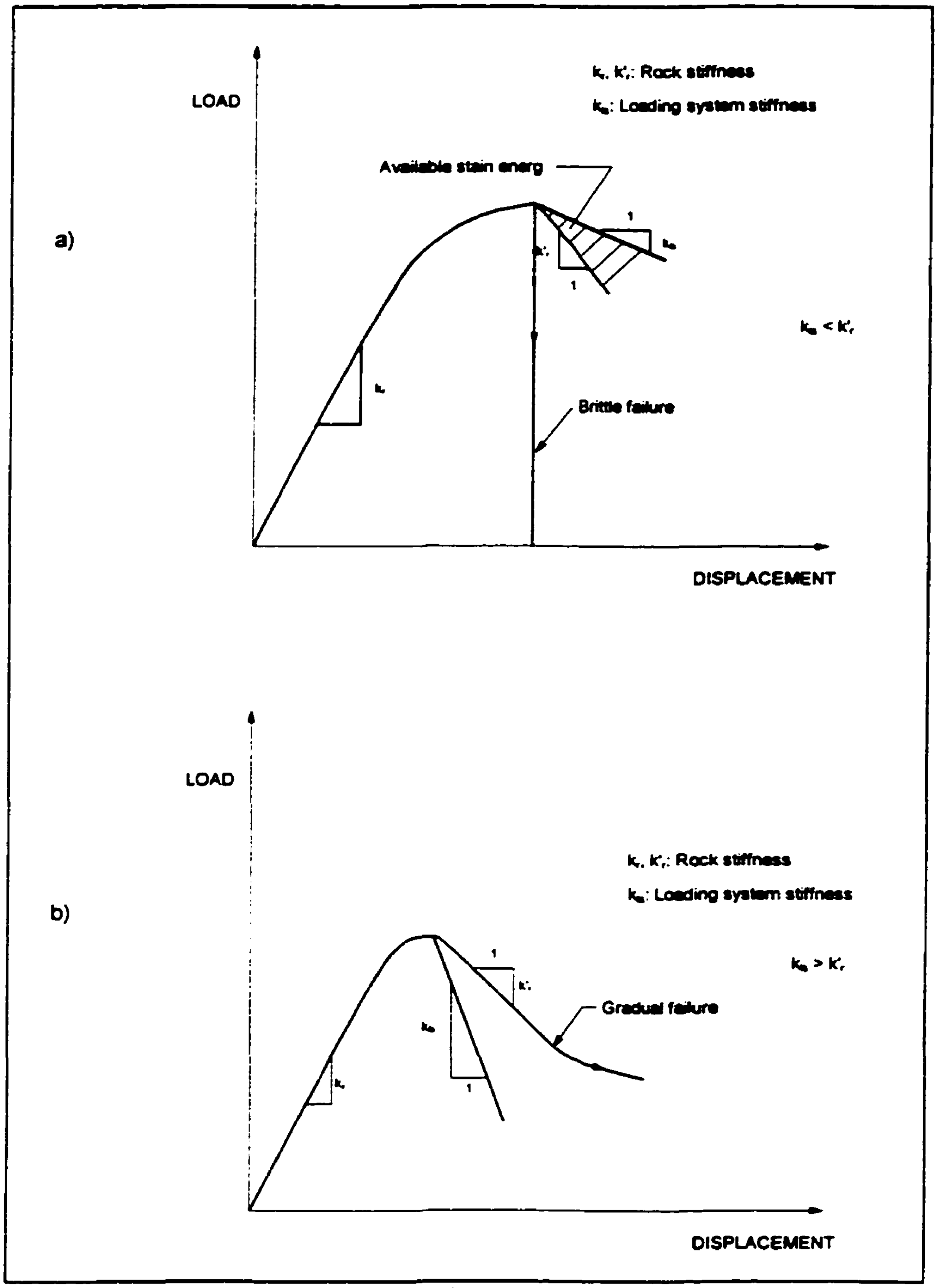

Figure 2.4: Influence of the relative stiffness of the loading system and the loaded material. a) Unstable and violent failure. b) Stable and controlled failure (after Cook, 1965b).

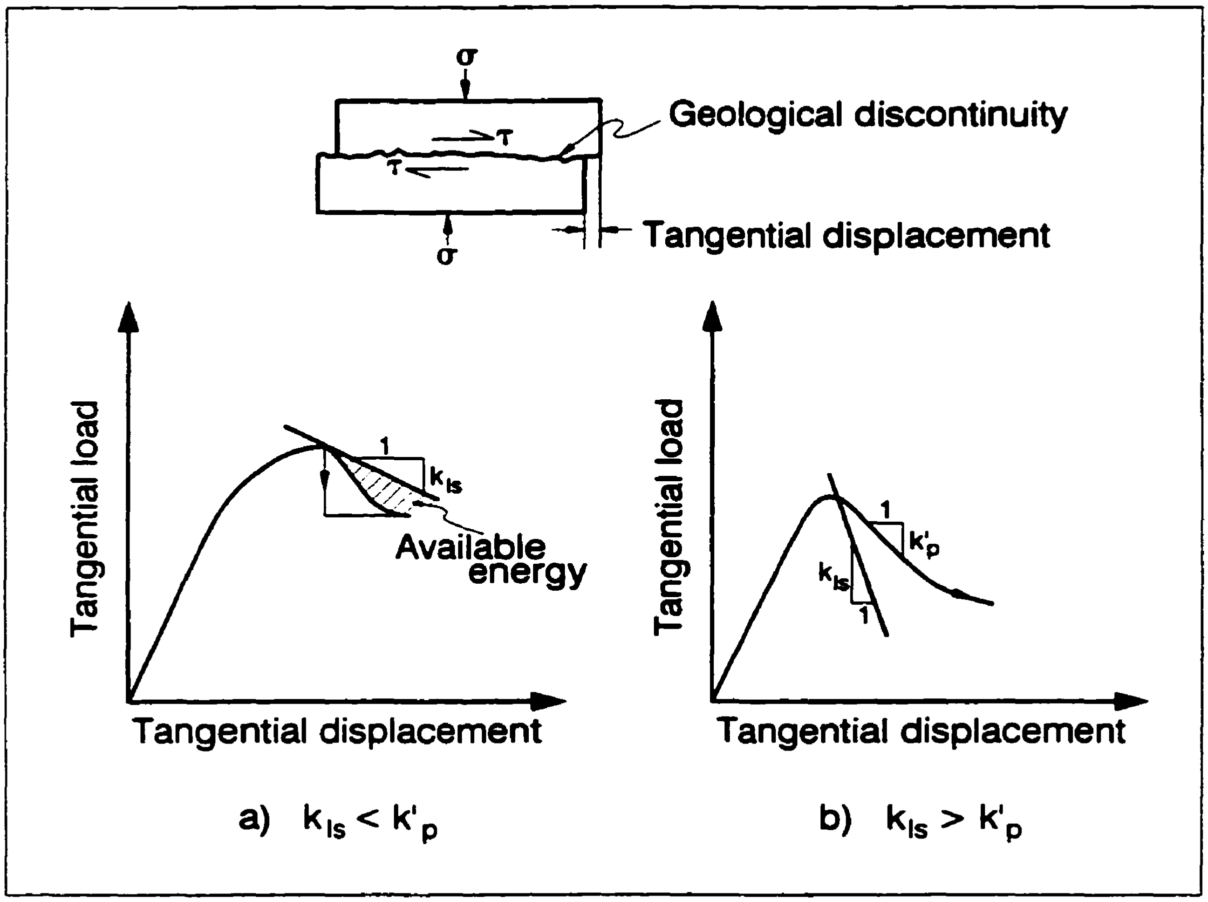

Figure 2.5 Influence of the relative stiffness of the loading system and of the discontinuity in a direct shear test. a) Violent failure. b) Gradual failure (after Salamon, 1974).

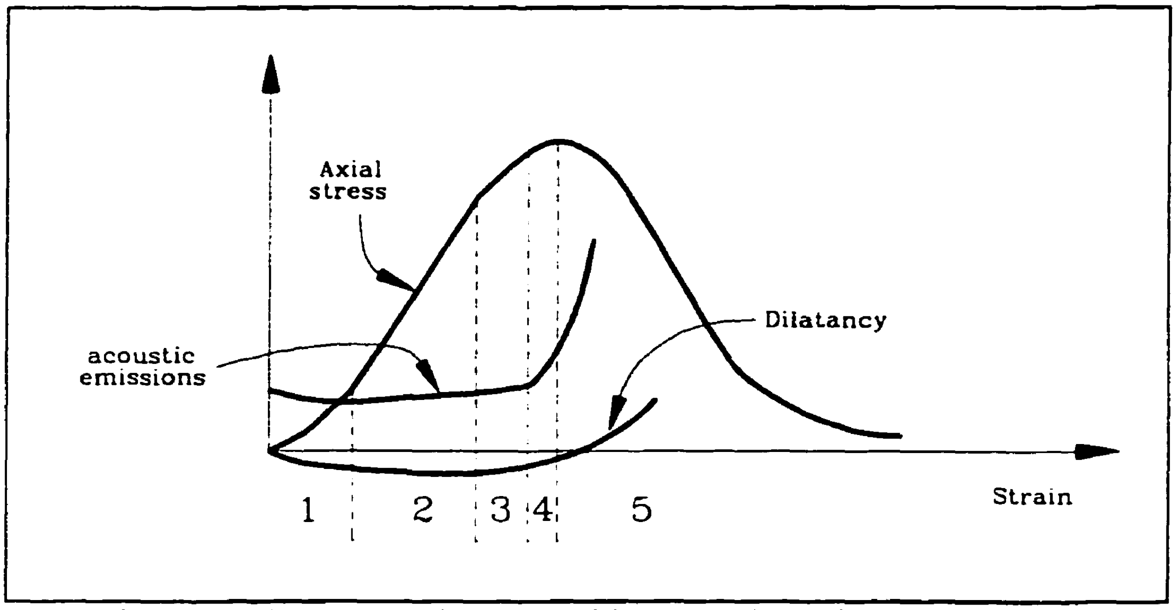

Figure 2.6: Schematic stress-strain curve of low porosity, brittle rocks under uniaxial compression (after Bieniawski, 1967, and Paterson, 1978).

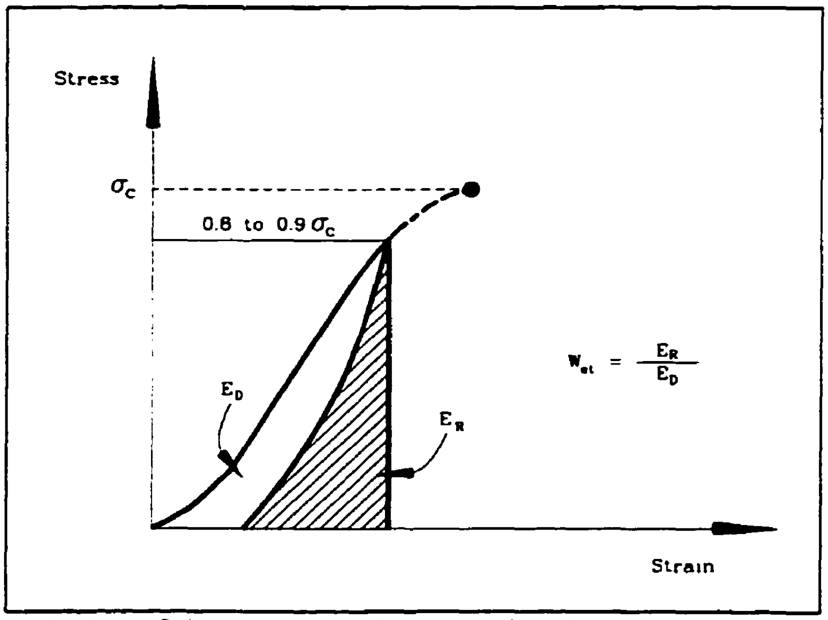

Figure 2.7: Calculation of the W_{et} index from a uniaxial compression stress-strain curve (after Kidibinski, 1981).

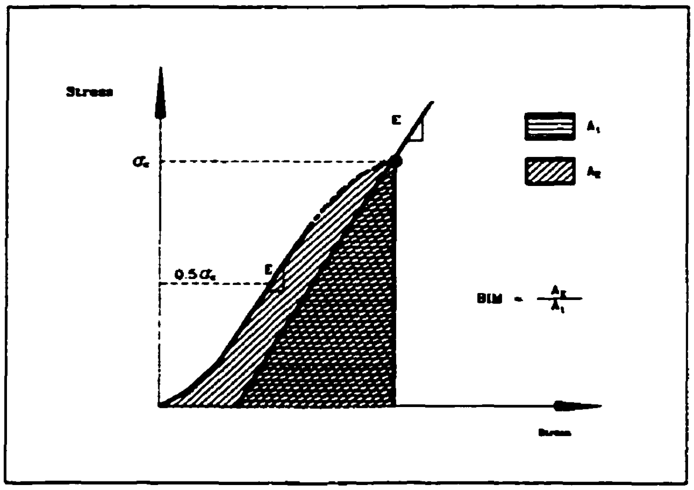

Figure 2.8: A schematical representation of the BIM value determination from a uniaxial compression test result (after Aubertin and Gill, 1988).

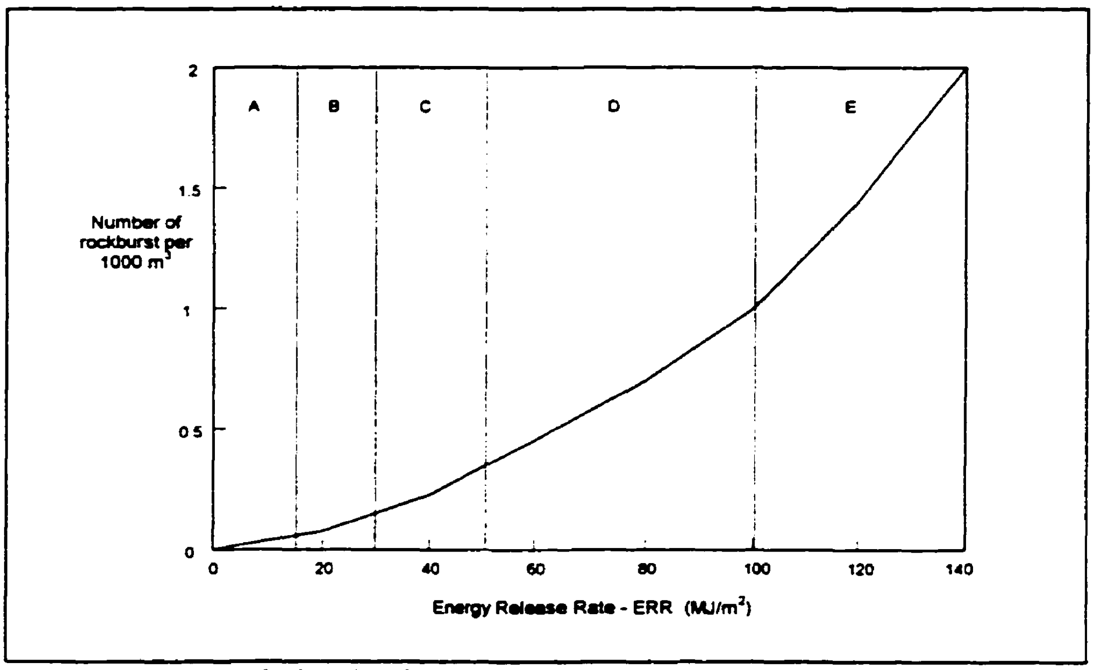

Figure 2.9: Empirical relationship between the energy release rate (ERR), the incidence of rockbursts and the risk level. A: negligible; B: slight; C: moderate; D: severe; E: extreme (after Cook, 1978).

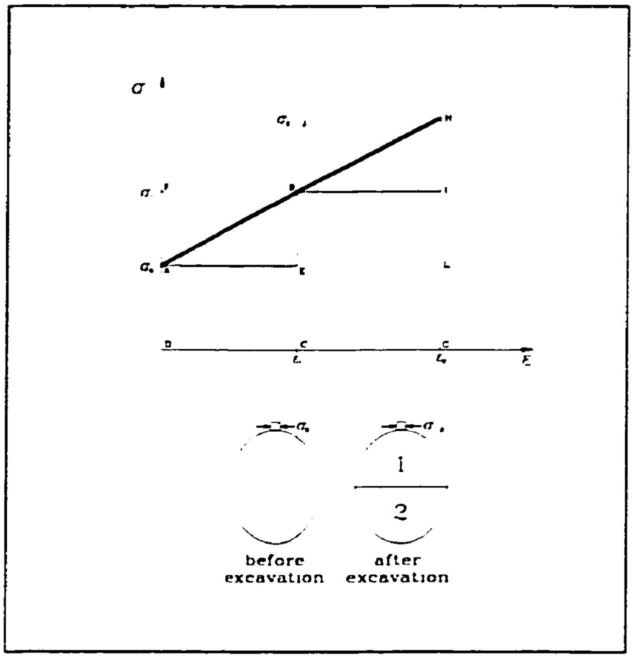

Figure 2.10: The energy densities calculation as a result of mining sequence (after Mitri and Rizkalla, 1995).

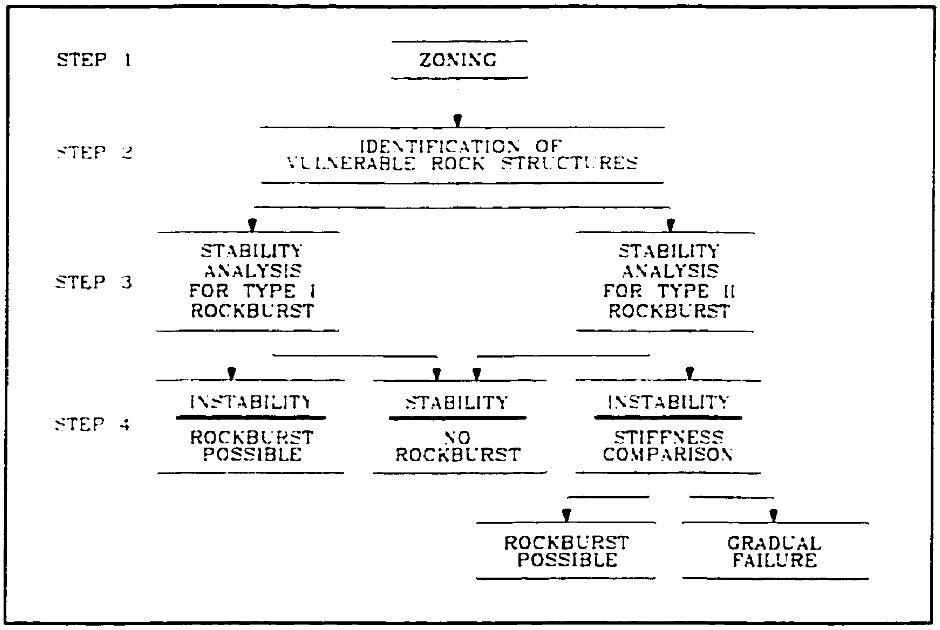

Figure 2.11: Diagram showing the methodology to evaluate the rockburst potential (after Gill and Aubertin, 1988).

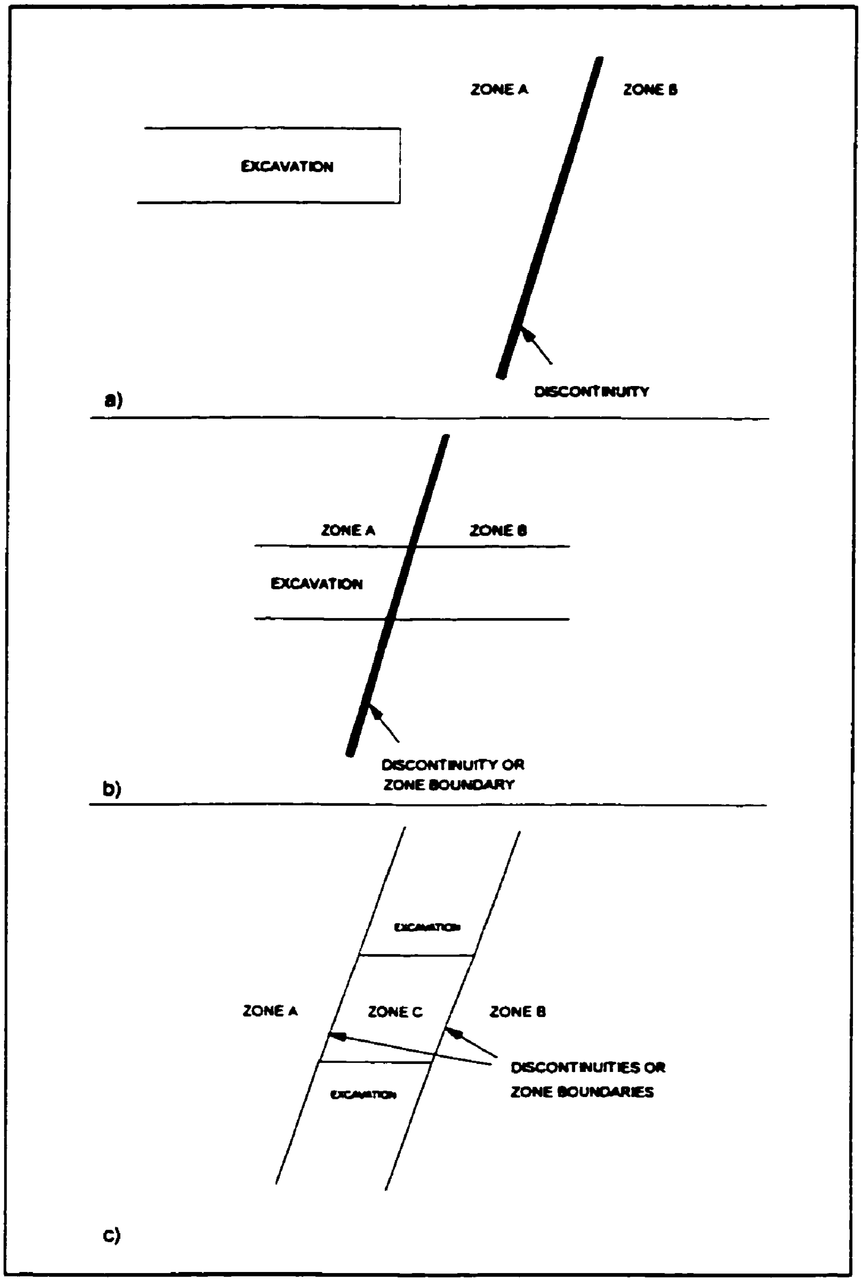

Figure 2.12: Vulnerable rock structures: a) Excavation that comes near a major geological discontinuity - potential for a type I rockburst; b) Excavation that goes through a major geological discontinuity or zone boundary - potential for a type II rockburst; c) Excavation that follows major geological discontinuities or zone boundaries - potential for a type II rockburst (after Gill and Aubertin, 1988).

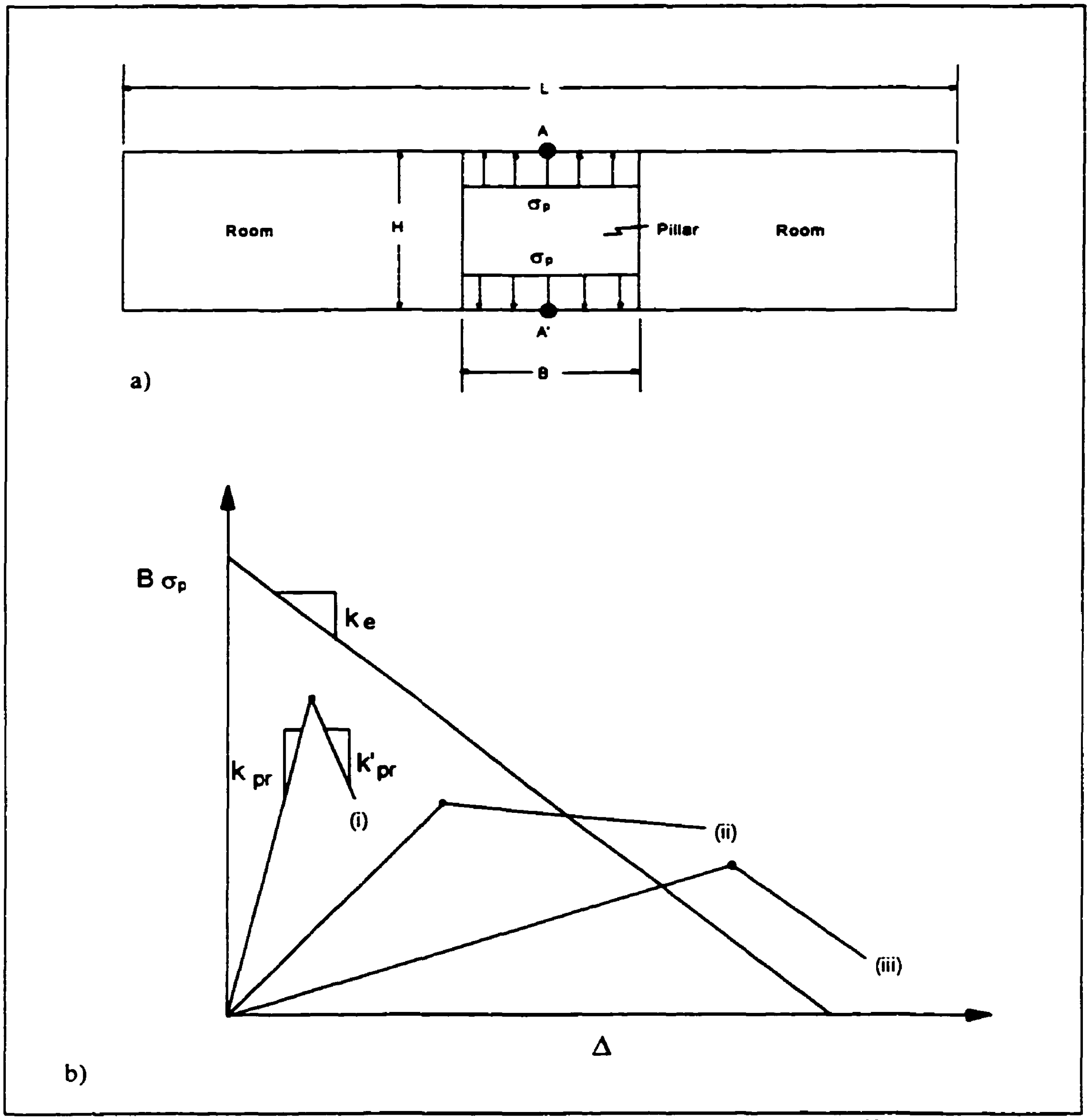

Figure 2.13: a) Model used to evaluate the equivalent local mine stiffness of the rock mass surrounding a pillar (after Hoek and Brown, 1980; b) Force - convergence diagram usually used to state on the nature of pillar failure; (i): violent failure; (ii): gradual failure; (iii): no failure (after Starfield and Fairhurst, 1968).

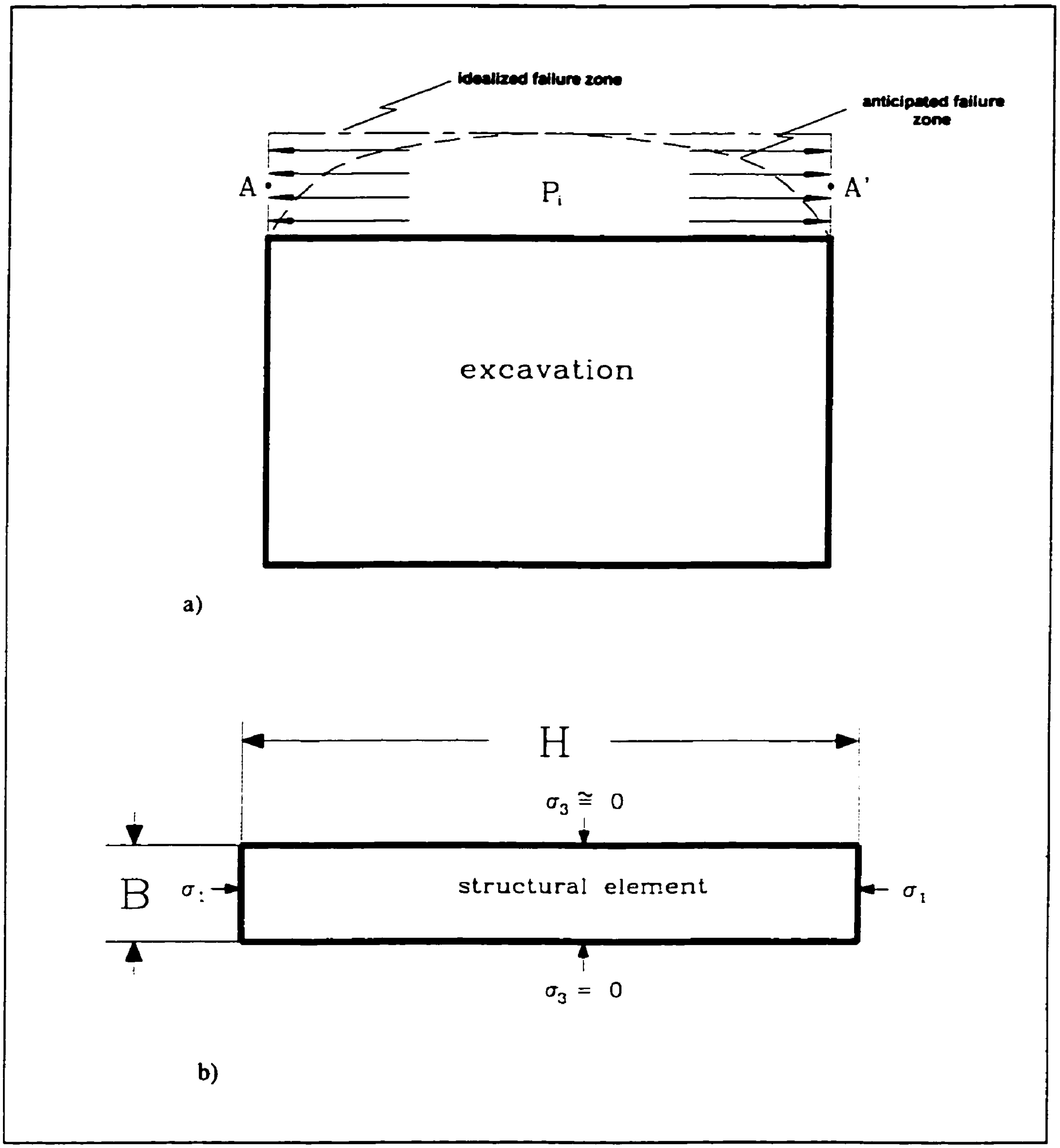

Figure 2.14: a) Model used to estimate the local mine stiffness of the surrounding rock mass (after Aubertin et al., 1997). b) Structural element in a uniaxial state of stress (after Simon et al., 1995).

CHAPTER 3
MECHANICAL BEHAVIOR OF JOINTS

3.1 INTRODUCTION

To better understand the fault-slip rockburst mechanism, one must first understand the behavior of geological discontinuities. The term discontinuity is widely used in rock engineering to describe any measurable interruption of a rock mass (Farmer, 1983). Figure 3.1 shows different types of discontinuities encountered in rock masses. These discontinuities can either be persistent or interrupted by rock bridging; opened, closed or filled. Systematic discontinuities in rock masses are usually referred to as joints. A joint is a break of geological origin in the continuity of a body of rock along which there has been no visible displacement (Brown, 1993). They frequently form parallel to bedding planes, foliation and cleavage (Brown, 1981). Some joints are assumed to be formed by tensile stresses caused by contraction resulting from cooling of magma and of lava flows (Jumikis, 1979). In the following, the geomechanical behavior of joints is presented in some detail.

3.2 JOINT BEHAVIOR

One important aspect of joint behavior is its deformability (or its stress-displacement relationship). Joint deformability can be better explained with its stress-displacement curves. On these curves, the normal stiffness of the joint (k_{nn}) is described as the rate of change of normal stress (σ_n) with respect to normal displacements (v), and the shear stiffness (k_{ss}) as the rate of change of shear stress (τ) with respect to shear displacement

(u) (Goodman et al., 1968). These two types of behavior (normal and shear) are treated in the following.

3.2.1 Joint normal deformation

As the normal stress on a joint increases, closure of the joint occurs. This closure depends on several factors including the relative position of both sides of the joints (mated or unmated position) and the presence of filling. Figure 3.2 shows the normal stress behavior as a function of normal displacement for a joint. This curve is mostly hyperbolic and becomes asymptotic to a vertical line when $v = -V_m$, which corresponds to the maximum joint closure (joint separation being positive). A model to describe this normal load-displacement behavior was proposed by Bandis et al. (1983):

$$\sigma_n = \frac{v\, k_{ni}\, V_m}{V_m + v} \qquad \text{or} \qquad v = \frac{\sigma_n\, V_m}{k_{ni}\, V_m - \sigma_n} \tag{3.1}$$

where joint opening and compressive stress are positive, v is the normal displacement (closure), V_m is the maximum closure (usually smaller than initial starting aperture) and k_{ni} is the initial normal stiffness of the joint. According to this model, at any normal stress level, the joint tangent normal stiffness k_{nn} is equal to:

$$k_{nn} = \frac{\partial \sigma_n}{\partial v} = k_{ni}\left(\frac{k_{ni}\, V_m - \sigma_n}{k_{ni}\, V_m}\right)^2 \tag{3.2}$$

which means that the curve starts with a slope of k_{ni} (at $\sigma_n \rightarrow 0$) and ends with an infinite slope (at $\sigma_n \rightarrow \infty$).

Empirical functions have been suggested to describe k_{ni} and V_m (Bandis et al., 1983):

$$k_{ni} = 0.02\left(\frac{JCS}{a_j}\right) + 1.75\,JRC - 7 \tag{3.3}$$

$$V_m = C\left(\frac{JCS}{a_j}\right)^D \tag{3.4}$$

where JRC is the joint roughness coefficient (which can be estimated from the joint profile), JCS is the joint wall compressive strength, a_j is the initial joint aperture, C and D are constants having suggested values of 8.57 and -0.68 respectively for rock joints.

Several experimental studies have shown that the normal load-deformation of a joint under mated and unmated conditions are different (e.g., Goodman, 1976; Bandis et al., 1983). In general, an unmated joint is more deformable than a mated one, and the maximum closure of an unmated joint is larger. Figure 3.3 shows the different normal load-axial displacement curve for a rock, a mated and an unmated joint. The measured axial displacement is dependent of the deformation properties of both the joint and the surrounding rock. The closure of the joint can then be calculated by subtracting the deformation of the rock (curve A) from the measured displacement (curve B or C).

Several authors proposed models to describe the behavior of unmated joints; Goodman (1976) proposed a hyperbolic relation, Bandis et al. (1983) proposed a semi-logarithmic function; so did Sun et al. (1985). However, these models did not correlate the normal deformability of the unmated joint to that of the mated joint. Saeb and Amadei (1989, 1990) proposed a graphical method and a mathematical model to obtain the curve of unmated joint from direct shear test under constant normal stress on a mated joint. This method relates the behavior of the unmated joint to the behavior of a mated joint after being sheared by a certain quantity. This method will be described in the next section.

During unloading, joint behavior shows an hysterisis and inelastic behavior, the unloading curve also resembling a hyperbola. Under repeated load cycling, joints display stiffening behavior, whether in interlocked or dislocated positions, and the behavior after several loading cycles remains typically non-linear (e.g., Bandis et al., 1983).

3.2.2 Joint shear behavior and strength

The shear behavior of a joint is complex and depends on several factors like the boundary conditions (e.g., initial normal stress, load path), material deformational properties, properties of filling (deformation, strength, thickness), surfaces of the joint (roughness, aperture, strength), size of the joint (area, length), and the presence of water. The shear stress versus shear displacement curve typically shows a quick rise of shear stress to a maximum value (τ_p), followed by a gradual decline to a residual value (τ_r) after a large shear displacement. Usually, joints exhibit non-linear behavior, to a greater or lesser extent (Bandis et al., 1983).

The literature on rock joint deformation is abundant (e.g., Barton and Stephansson, 1990). To assess the behavior of rock joints, a number of experimental studies have been performed on natural and artificial joints. Notable among these are the work of Patton (1966), Goodman (1970), Ladanyi and Archambault (1970), Barton and Choubey (1977), Bandis et al. (1981), Sun et al. (1985), Yoshinaka and Yamabe (1986), and Huang et al. (1993).

The shear behavior of joints can be divided in two important aspects: strength and deformation behavior. These aspects are treated separately in the followings.

A) Shear strength

To estimate the peak shear strength, several criteria have been proposed. In that matter, one should mention the early work of Newland and Allely (1957), Jaeger (1957), Krsmanovic and Langof (1964), Patton (1966), Goldstein et al. (1966) and Byerlee (1968). Following, these early studies on rock and rock joints, many authors have developed criteria to estimate the peak shear strength. Barton (1976) and Priest (1993) provide a good review of the failure criteria that have been proposed over the years. Among these, the criteria proposed by Patton (1966), Ladanyi and Archambault (1970), Jaeger (1971), and Barton (1973, 1976) are the best known.

- Barton and co-workers' model

Barton (1973) proposed an empirical relationship to estimate peak strength of rock joints:

$$\tau_p = \sigma_n \tan\left(\text{JRC} \log\left(\frac{\text{JCS}}{\sigma_n}\right) + \phi_b\right) \tag{3.5}$$

where JRC is the joint roughness coefficient (which can be estimated from the joint profile), JCS is the joint wall compressive strength, and ϕ_b is the basic friction angle (which is approximately equal to ϕ_r, the residual friction angle). For intact rock joint, JCS value is the same as C_0 (the uniaxial compressive strength) while its value can go as low as $0.25C_0$ when weathered. Barton and Choubey (1977) proposed typical profiles of joint surfaces giving JRC values ranging between 0 (for planar, smooth joints) to 20 (for rough and irregular surfaces).

To account for scale effect, Bandis et al. (1981) proposed the following relationships:

$$JRC_n \approx JRC_0 \left[\frac{L_n}{L_0} \right]^{-0.02\,JRC_0} \tag{3.6}$$

$$JCS_n \approx JCS_0 \left[\frac{L_n}{L_0} \right]^{-0.03\,JRC_0} \tag{3.7}$$

where JRC_n, JCS_n are the values for the natural block size, JRC_0, JCS_0 are the values for the nominal size sample, L_n is the natural block size and L_0 is the laboratory size joint samples (nominal 100 mm). ϕ_b (or ϕ_r) is assumed not to be scale dependent.

- Ladanyi-Archambault's model

Ladanyi and Archambault (1970) proposed a criterion, referred to as LADAR to estimate peak shear strength of joints. This curvilinear semi-empirical model for peak strength is given by:

$$\tau_p = \frac{\sigma_n \left(1 - a_s\right) \left(\dot{v} + \tan\phi_u\right) + a_s s_r}{1 - \left(1 - a_s\right) \dot{v} \tan\phi_u} \tag{3.8}$$

where a_s is the shear area ratio (ratio of the sum of areas of failed asperities to the total sample area), $\dot{v}$ is the rate of dilation at the instant of peak shear strength, ϕ_u is the angle of friction, and s_r is the shear strength of intact rock. At very low normal stress, when no asperity failure occurs ($a_s \rightarrow 0$) and $\dot{v} \rightarrow \tan i_0$, equation (3.8) reduces to the Patton (1966) model which is defined by:

$$\tau_p = \sigma_n \tan(\phi_u + i_0) \tag{3.9}$$

where i_0 is the angle of asperities (or for natural joints, the average of the first order roughness of the surface). At high normal stress, all asperities will be sheared off ($a_s \rightarrow 1$) and $\tau_p \rightarrow s_r$.

To evaluate the rock strength, the authors suggested using the equation proposed by Fairhurst (1964):

$$s_r = C_0 \frac{\sqrt{(1+N)}-1}{N}\left(1+N\frac{\sigma_n}{C_0}\right)^{1/2} \tag{3.10}$$

where C_0 is the uniaxial compressive strength of the rock and N is the ratio of compressive over tensile strength $|C_0/T_0|$.

The a_s and $\dot{v}$ values can be estimated based on empirical relationships derived from tests on surfaces with artificial roughness by:

$$\dot{v} = \left(1-\frac{\sigma_n}{\sigma_T}\right)^{k_2} \tan i_0 \tag{3.11}$$

$$a_s = 1-\left(1-\frac{\sigma_n}{\sigma_T}\right)^{k_1} \tag{3.12}$$

where σ_T is the brittle-ductile transition pressure and k_1 and k_2 are determined by testing. The authors suggested values of $k_1 = 1.5$ and $k_2 = 4$ for rough rock surfaces. Goodman (1976) recommended using C_0 for an estimate of σ_T. This model was later re-examined by Saeb (1990) and the following relation was proposed:

$$\tau_p = \sigma_n\,(1-a_s)\,\tan(i+\phi_u)+a_s\,s_r \tag{3.13}$$

where

$$i = \tan^{-1}\dot{v} = \tan^{-1}\left[\left(1-\frac{\sigma_n}{\sigma_T}\right)^{k_2}\tan i_0\right] \tag{3.14}$$

Assuming a Mohr-Coulomb criterion for the shear strength of asperities (s_r), the total shear strength can be calculated as:

$$\frac{\tau_p}{\sigma_T} = \frac{\sigma_n}{\sigma_T}(1-a_s)\tan(i+\phi_u) + a_s\left(\frac{S_0}{\sigma_T}+\frac{\sigma_n}{\sigma_T}\tan\phi_0\right) \tag{3.15}$$

where S_0 is the cohesion and ϕ_0 is the friction angle of the rock. Saeb (1990) showed that this formulation of the criterion seems to capture the two modes of failure (shearing and sliding). This formulation also plots very close to the original model of LADAR.

B) Shear deformation behavior

To describe the behavior of joints, many authors have proposed constitutive equations to model the stress-displacement relation. The models most often used in mining engineering are the Goodman model (Goodman et al., 1968; Goodman, 1976) and the Barton-Bandis model (Barton, 1973; Barton and Choubey, 1977; Bandis, 1980; Bandis et al., 1983). Nevertheless, numerous other models have been proposed for different applications, based on different mechanisms. For example, models were proposed for soil-rock interaction (e.g., Carter and Ooi, 1988; Desai et al., 1991), for block sliding (e.g., Andreaus, 1989; Li et al., 1990; Leong and Randolph, 1991), for faults (e.g., Dieterich, 1978, 1979; Ohnaka and Yamashita, 1989; Kato et al., 1993) and for earthquakes (e.g., Rice, 1983). Some of these models are based on cracks behavior (e.g., Wittke, 1990; Divakar and Fafitis, 1990), on micro-mechanics (e.g., Dong and Pan, 1996), on plasticity (e.g., Pande, 1985; Cundall and Lemus, 1990; Desai and Fishman, 1991) or on elasto-viscoplasticity (e.g., Olofson, 1985). Some of the models were proposed to take into account certain conditions like time dependency (e.g., Höwing and Kutter, 1985), progressive damage (e.g., Desai et al., 1989), temperature effects (e.g., Bilgin and Pasamehmetoglu, 1990), dynamic effects (e.g., Rice and Tse, 1986; Bro, 1992), filling properties (e.g., Pereira, 1990; Phien-wej et al., 1990; Papaliangas et al., 1993), anisotropy (e.g., Jing et al., 1992, 1994), scale effects (e.g., Pinto da Cunha, 1991; Muralha and Pinto da Cunha, 1992) and cyclic loading (e.g., Jing et al., 1993; Qiu et al., 1993; Souley et al., 1995).

3.3 BARTON-BANDIS' MODEL

In this model, the shear behavior of the joint depends on several parameters, including the peak shear angle (ϕ_p), the basic friction angle (ϕ_b), the peak dilation angle (d_n^0), the residual friction angle (ϕ_r), shear stiffness (k_s) and joint parameters (JRC and JCS). The peak shear angle is given by the relationship (Barton and Choubey, 1977):

$$\phi_p = \phi_b + d_n^0 \tag{3.16}$$

The basic friction angle can be found from tilt test. Typical values can be found in Richards (1975) and Barton and Choubey (1977). The peak dilation angle is given by (Barton and Choubey, 1977):

$$d_n^0 = \mathrm{JRC}\,\log\left(\frac{\mathrm{JCS}}{\sigma_n}\right) \tag{3.17}$$

The residual angle for joint can be estimated from the relationship (Barton and Choubey, 1977):

$$\phi_r = \left(\phi_b - 20^\circ\right) + \frac{20}{(r/R)} \tag{3.18}$$

where r is the Schmidt rebound on wet joint surfaces and R is the Schmidt rebound on dry unweathered sawn surfaces.

The shear stiffness of the joint can be considered as linear and can be estimated from (Barton and Choubey, 1977; Bandis et al., 1983):

$$k_s = \frac{\tau_p}{u_p} = \frac{\sigma_n}{u_p}\tan\left[\mathrm{JRC}\,\log\left(\frac{\mathrm{JCS}}{\sigma_n}\right) + \phi_r\right] \tag{3.19}$$

This model was later modified by Barton et al. (1985) to take into account the stress dependency of the shear strength. The stress and displacement histories of a rock discontinuity are considered by using a mobilized joint roughness coefficient (JRC_m). The failure condition for shear failure is then given by:

$$\tau_p = \sigma_n \tan\left(JRC_m \log\left(\frac{JCS}{|\sigma_n|} \right) + \phi_r \right) \tag{3.20}$$

where

$$JRC_m = \frac{\arctan(\tau_m/\sigma_n)^0 - \phi_r^0}{\log(JCS/\sigma_n)} \tag{3.21}$$

The test data can then be expressed in terms of a dimensionless ratio JRC_m/JRC_p (where JRC_p is the joint roughness coefficient at peak strength) as follows:

$$\frac{JRC_m}{JRC_p} = \frac{\arctan(\tau_m/\sigma_n)^0 - \phi_r^0}{\phi_p - \phi_r^0} \tag{3.22}$$

where $\phi_p = \arctan\left(\frac{\tau_p}{\sigma_n} \right)$ (3.23)

From these, one can use Table 3.1 that relates the shear displacement ratio (u/u_p) to the ratio of JRC.

Table 3.1 Rounded values for joints (after Barton et al., 1985)

u/u_p	JRC_m/JRC_p
0	$-(\phi_r/i)$
0.3	0
0.6	0.75
1.0	1.00
2.0	0.85
4.0	0.70
10	0.50
100	0.00

with $$i = JRC_p \log\left(\frac{JCS}{\sigma_n}\right) \tag{3.24}$$

3.4 SAEB-AMADEI'S MODEL

Saeb and Amadei (1989, 1990, 1992) developed a constitutive model for joints. This model can be seen as a generalization of the models of Goodman (1976) and Barton-Bandis. This model can be given in a graphical or a mathematical form.

As mentioned in the previous section, this model can relate the normal behavior of unmated joints to the behavior of a joint when sheared by a displacement equal to u_i. To do so, the method makes use of a series of idealized joint response curves such as those proposed by Goodman and Boyle (1985). The method is presented in Figure 3.4a to 3.4d. Figure 3.4a shows a hyperbolic joint closure versus the normal stress as defined by equation (3.1). Figure 3.4b shows a series of idealized shear stress versus shear displacement curves for a mated joint tested under constant normal stresses ranging between A and 20A, where A is an arbitrary number. Note that these curves are valid for a constant displacement model, meaning that the peak and residual shear displacement values are constants, thus independent of the applied normal stress. Figure 3.4c shows the dilatancy curves for the shear tests of Figure 3.4b. These curves show a decrease in dilatancy as the normal stresses increase from A to 20A. In these figures, the peak shear displacement is identified as u_4 and there is no change in normal displacement once u_4 has been reached (v = constant for $u > u_4$).

Figure 3.4a to 3.4c can then be used to construct the curves of normal stress versus normal displacement for unmated joint as shown in Figure 3.5. Each curve ($u=u_i$; $i = 0,4$)

corresponds to the normal displacement curve of the joint when a shear displacement of u_i has been done. The curves are constructed by using the values of σ_n and v at the points of intersection between each line $u = u_i$ and the normal displacement versus shear displacement curves in Figure 3.4c. Several aspects can be pointed out regarding Figure 3.5 (Saeb and Amadei, 1992):

- The curve $u = u_0$ which represents the joint under mated conditions is identical to the joint closure vs. normal stress curve of Figure 3.4a.
- Each curve $u = u_i$ represents the behavior of the joint under normal loading after being mismatched by a shear displacement equal to u_i.
- For the joint response shown in Figure 3.4c, for which there is no further dilatancy for values of u larger than u_4, all curves $u = u_i$ $(i > 4)$ coincide with the curve $u=u_4$, hence, the joint response is admissible if it is contained in the domain limited by the curves $u = u_0$ and $u = u_4$.
- All curves $u = u_i$ $(i = 1, 4)$ become closer to the curve $u = u_0$ as σ_n increases since joint dilatancy decreases as the joint normal stress increases.

Figures 3.5 and 3.4b can then be used to predict the behavior of the joint for any loading paths. In Figure 3.5, four different loading paths are identified. These paths originate from point A assuming that an initial normal stress $\sigma_{n0} = 4A$ was first applied without shearing. Under constant applied normal stiffness K, the joint follows the path AFGHI. Under constant normal stress (K = 0), it follows the path ABCDE. When no change in joint normal displacement is allowed (no dilatancy; $K = \infty$), it follows the path AJKLM. Path ANPQR corresponds to a joint in a rock mass with an increasing applied normal stiffness. By using the values of σ_n and u at the point of intersection of each path with the curves $u = u_i$ and using Figures 3.4b-c, the shear stress vs shear displacement curves for $\sigma_{n0} = 4A$ can be constructed for the path mentioned above. These curves are identified in

Figure 3.4a to 3.4c by dashed lines. Figure 3.4d shows the normal stress versus shear displacement curves that are constructed from the same results.

From these results, several observations can be made:

- the highest peak strength (point M on Figure 3.4b) corresponds to the constant normal displacement path due to the most increase in joint normal stress;
- the lowest peak strength (point E) corresponds to the constant normal stress path;
- the two other path leads to intermediate peak strengths (point I and R).

These observations have been partly confirmed by several experimental studies, that have shown that shear test under constant normal stiffness leads to higher peak strength than tests under constant normal stress, and that the constant normal stiffness behavior can be predicted from constant normal stress values (e.g., Leichnitz, 1985; Fortin et al., 1988; Archambault et al., 1990). This is consistent with the physical process of shearing since normal stress increases with dilatancy, and peak strength increases with normal stress.

The model can also be expressed mathematically. In the model, the dilatancy rate $\partial v/\partial u$ (which plays an important role) is described by the formulation of Goodman and St John (1977):

$$\frac{\partial v}{\partial u} = \tan i = \left(1 - \frac{\sigma_n}{\sigma_T}\right)^{k_2} \tan i_0 \quad \text{when } u \le u_r \text{ and } \sigma_n < \sigma_T \tag{3.25}$$

and

$$\frac{\partial v}{\partial u} = 0 \qquad \text{when } u > u_r \text{ or } \sigma_n \ge \sigma_T \tag{3.26}$$

When equation (3.25) is integrated, it leads to:

$$v = u\left(1-\frac{\sigma_n}{\sigma_T}\right)^{k_2} \tan i_0 \quad + \quad f(\sigma_n) \tag{3.27}$$

Since this equation must also represent the joint behavior under a mated condition (u = 0), it follows that $f(\sigma_n)$ is defined by the normal load-displacement equations (eq. 3.1) so:

$$v = u\left(1-\frac{\sigma_n}{\sigma_T}\right)^{k_2} \tan i_0 \quad + \quad \frac{\sigma_n\, V_m}{k_{ni}\, V_m - \sigma_n} \tag{3.28}$$

When $u > u_r$ (the displacement at the onset of residual strength) and $\sigma_n/\sigma_T < 1$, the joint ceases to dilate and v is equal to its value obtained by substituting $u = u_r$ in the last equation. When $\sigma_n/\sigma_T \geq 1$, the first term of the equation vanishes and no dilatation is possible during shearing. If this first term is called w, then:

$$w = u\left(1-\frac{\sigma_n}{\sigma_T}\right)^{k_2} \tan i_0 \tag{3.29}$$

$$v - w = \frac{\sigma_n\, V_m}{k_{ni}\, V_m - \sigma_n} \qquad \text{or} \qquad \sigma_n = \frac{(v-w)\, k_{ni}\, V_m}{V_m + (v-w)} \tag{3.30}$$

In this formulation, w represents the increase in joint aperture that is created due to shearing. If it is assumed that the maximum closure V_m is a reasonable estimate of the initial aperture of the joint in its mated position, then the value of w at $\sigma_n = 0$ (i.e. $w = u \tan i_0$) represents the additional initial aperture of the unmated joint created through dilatancy. The maximum additional aperture occurs when $u = u_r$ and is equal to $u_r \tan i_0$. Note that equation (3.30) represents a mathematical expression for the curves $u = u_i$ (i=1,4). If the joint is non-dilatant ($\tan i_0 = 0$), then w in equation (3.30) vanishes and the normal stress-displacement behavior is the same for all values of the shear displacement, as expected.

An incremental formulation of the model is also possible and is given by (Saeb and Amadei, 1992):

$$dv = \left(1 - \frac{\sigma_n}{\sigma_T}\right)^{k_2} \tan i_0 \, du - \frac{u\,k_2}{\sigma_T}\left(1 - \frac{\sigma_n}{\sigma_T}\right)^{k_2-1} \tan i_0 \, d\sigma_n + \frac{k_{ni}\,V_m^2}{\left(k_{ni}\,V_m - \sigma_n\right)^2} d\sigma_n \qquad (3.31)$$

or

$$d\sigma_n = \frac{dv - \left(1 - \frac{\sigma_n}{\sigma_T}\right)^{k_2} \tan i_0 \, du}{\frac{-u\,k_2}{\sigma_T}\left(1 - \frac{\sigma_n}{\sigma_T}\right)^{k_2-1} \tan i_0 + \frac{k_{ni}\,V_m^2}{\left(k_{ni}\,V_m - \sigma_n\right)^2}} \qquad (3.32)$$

Since σ_n depends on v and u, equation (3.32) can be rewritten in a more compact form as:

$$d\sigma_n = k_{nn}\,dv + k_{ns}\,du \qquad (3.33)$$

where k_{nn} and k_{ns} are two normal stiffness coefficients such that:

$$k_{nn} = \frac{\partial\sigma_n}{\partial v} = \frac{1}{\frac{-u\,k_2}{\sigma_T}\left(1 - \frac{\sigma_n}{\sigma_T}\right)^{k_2-1} \tan i_0 + \frac{k_{ni}\,V_m^2}{\left(k_{ni}\,V_m - \sigma_n\right)^2}} \qquad (3.34)$$

and

$$k_{ns} = \frac{\partial\sigma_n}{\partial u} = \frac{-\left(1 - \frac{\sigma_n}{\sigma_T}\right)^{k_2} \tan i_0}{\frac{-u k_2}{\sigma_T}\left(1 - \frac{\sigma_n}{\sigma_T}\right)^{k_2-1} \tan i_0 + \frac{k_{ni} V_m^2}{(k_{ni} V_m - \sigma_n)^2}} \qquad (3.35)$$

Note that equation (3.34) provides an analytical expression for the joint tangent normal stiffness when the joint has been sheared by an amount equal to u, and it reduces to equation (3.2) when u = 0, that is when the joint is in its mated position. Equations (3.31-3.35) are valid when $u \le u_r$ and $\sigma_n/\sigma_T < 1$. On the other hand, when $u > u_r$ and $\sigma_n/\sigma_T < 1$,

k_{ns} vanishes and k_{nn} is equal to its value at $u = u_r$. Finally, when $\sigma_n/\sigma_T \geq 1$, k_{ns} also vanishes but k_{nn} is given by equation (3.2).

An equation similar to equation (3.33) can be expressed for the shear stress τ since the latter depends in general on v and u. Then:

$$d\tau = k_{sn}\,dv + k_{ss}\,du \tag{3.36}$$

where $k_{sn} = \partial\tau/\partial v$ and $k_{ss} = \partial\tau/\partial u$ are two shear stiffness coefficients. In the literature, it has been common practice to assume that $k_{sn} = 0$ and $k_{ss} = k_s$, the unit shear stiffness of the pre-peak region of the shear stress-displacement curve. However, this assumption is not necessary and closed-form solutions can be derived. This part of the Saeb and Amadei model was proposed for the two types of assumptions made by Goodman (1976), which are the constant displacement model and the constant stiffness model.

<u>Constant displacement model</u>

This model assumes that the peak and residual displacement (u_p and u_r) are material constants and independent of normal stress. The model of Saeb and Amadei is then given by:

- for $u < u_p$:

$$k_{sn} = \frac{\partial\tau}{\partial v} = \frac{u}{u_p} k_{nn} \frac{\partial\tau_p}{\partial\sigma_n} \tag{3.37}$$

$$k_{ss} = \frac{\partial\tau}{\partial u} = \frac{u}{u_p} k_{ns} \frac{\partial\tau_p}{\partial\sigma_n} + \frac{\tau_p}{u_p} \tag{3.38}$$

- for $u_p \leq u \leq u_r$ and $\sigma_n < \sigma_T$:

$$k_{sn} = \frac{\partial\tau}{\partial v} = \frac{k_{nn}}{u_p - u_r}\left\{\frac{\partial\tau_p}{\partial\sigma_n}(u - u_r) + (u_p - u)\left[\frac{\partial\tau_p}{\partial\sigma_n}\left(B_0 + \frac{1 - B_0}{\sigma_T}\sigma_n\right) + \frac{\tau_p}{\sigma_T}(1 - B_0)\right]\right\}$$

(3.39)

$$k_{ss} = \frac{\partial\tau}{\partial u} = \frac{\tau_p - \tau_r}{u_p - u_r} + \frac{k_{ns}}{u_p - u_r}\left\{\frac{\partial\tau_p}{\partial\sigma_n}(u - u_r) + (u_p - u)\left[\frac{\partial\tau_p}{\partial\sigma_n}\left(B_0 + \frac{1 - B_0}{\sigma_T}\sigma_n\right) + \frac{\tau_p}{\sigma_T}(1 - B_0)\right]\right\}$$

(3.40)

- for $u > u_r$ and $\sigma_n < \sigma_T$:

$$k_{sn} = \frac{\partial\tau}{\partial v} = k_{nn}\left\{\frac{\partial\tau_p}{\partial\sigma_n}\left(B_0 + \frac{1 - B_0}{\sigma_T}\sigma_n\right) + \frac{\tau_p}{\sigma_T}(1 - B_0)\right\} \qquad (3.41)$$

$$k_{ss} = \frac{\partial\tau}{\partial u} = k_{ns}\left\{\frac{\partial\tau_p}{\partial\sigma_n}\left(B_0 + \frac{1 - B_0}{\sigma_T}\sigma_n\right) + \frac{\tau_p}{\sigma_T}(1 - B_0)\right\} = 0 \qquad (3.42)$$

Constant stiffness model

This model implies that the shear stiffness is a constant and independent of normal stress.

- for $u < u_p$:

$$k_{sn} = \frac{\partial\tau}{\partial v} = 0 \qquad (3.43)$$

$$k_{ss} = \frac{\partial\tau}{\partial u} = \frac{\tau_p}{u_p} \qquad (3.44)$$

- for $u_p \leq u \leq u_r$ and $\sigma_n < \sigma_T$:

$$k_{sn} = \frac{\partial\tau}{\partial v} = k_{nn}\frac{\partial\tau_p}{\partial\sigma_n}\frac{1}{\tau_p}\left(\frac{u_p\tau_r - u_r\tau_p}{u_p - u_r}\right) \tag{3.45}$$

$$k_{ss} = \frac{\partial\tau}{\partial u} = \frac{\tau_p - \tau_r}{u_p - u_r} + k_{ns}\frac{\partial\tau_p}{\partial\sigma_n}\frac{1}{\tau_p}\left(\frac{u_p\tau_r - u_r\tau_p}{u_p - u_r}\right) \tag{3.46}$$

- for $u > u_r$ and $\sigma_n < \sigma_T$:

k_{sn} and k_{ss} are similar to the constant displacement model and are given by:

$$k_{sn} = \frac{\partial\tau}{\partial v} = k_{nn}\left\{\frac{\partial\tau_p}{\partial\sigma_n}\left(B_0 + \frac{1-B_0}{\sigma_T}\sigma_n\right) + \frac{\tau_p}{\sigma_T}(1-B_0)\right\} \tag{3.41}$$

$$k_{ss} = \frac{\partial\tau}{\partial u} = k_{ns}\left\{\frac{\partial\tau_p}{\partial\sigma_n}\left(B_0 + \frac{1-B_0}{\sigma_T}\sigma_n\right) + \frac{\tau_p}{\sigma_T}(1-B_0)\right\} = 0 \tag{3.42}$$

In all these equations, τ_p is the peak shear strength, τ_r is the residual shear strength, σ_T is the transitional normal stress, and B_0 is the ratio of residual to peak strength at zero (or very low) normal stress (with $0 \leq B_0 \leq 1$).

When $\sigma_n \geq \sigma_T$, k_{ns} in equations (3.38), (3.40) and (3.46) vanishes and equations (3.39) and (3.40) or (3.45), (3.46) are replaced by equations (3.41) and (3.42) with $B_0 = 1$ and k_{nn} equals to its value at $u = 0$ for all shear displacement $u \geq u_p = u_r$.

In view of these equations, the following relations can be written between the normal and shear stiffness coefficient for both constant stiffness and displacement models:

$$k_{ss} = \frac{k_{sn} k_{ns}}{k_{nn}} + \frac{\tau_p}{u_p} \qquad \text{when } u < u_p \tag{3.47}$$

$$k_{ss} = \frac{k_{sn} k_{ns}}{k_{nn}} + \frac{\tau_p - \tau_r}{u_p - u_r} \qquad \text{when } u_p \le u \le u_r \tag{3.48}$$

$$k_{ss} = \frac{k_{sn} k_{ns}}{k_{nn}} \qquad \text{when } u > u_r \tag{3.49}$$

As we can see, τ_p, τ_r, $\partial\tau_p/\partial\sigma_n$ depend on the selected peak shear strength criterion. If the modified LADAR criterion is used with a Mohr-Coulomb criterion for the intact rock strength $s_r = s_0 + \sigma_n \tan\phi_0$, τ_p is given by equation (3.13), τ_r is obtained by substituting equation (3.13) into the model of Goodman (1976) for the variation of residual shear strength with normal stress, and given by:

$$\tau_r = \tau_p \left(B_0 + \frac{1 - B_0}{\sigma_T} \sigma_n \right) \qquad \text{when } \sigma_n < \sigma_T \tag{3.50}$$

This leads to:

$$\begin{aligned}\frac{\partial \tau_p}{\partial \sigma_n} = {} & (1 - a_s)\tan(\phi_u + i) - \frac{\sigma_n}{\sigma_T} \frac{(1 - a_s) k_2}{\cos^2(\phi_u + i)} \frac{1}{1 + \left(1 - \frac{\sigma_n}{\sigma_T}\right)^{2k_2} \tan^2 i_0} \tan i_0 \left(1 - \frac{\sigma_n}{\sigma_T}\right)^{k_2 - 1} \\ & - \frac{\sigma_n}{\sigma_T} k_1 \tan(\phi_u + i) \left(1 - \frac{\sigma_n}{\sigma_T}\right)^{k_1 - 1} + \frac{s_r}{\sigma_T} k_1 \left(1 - \frac{\sigma_n}{\sigma_T}\right)^{k_1 - 1} + a_s \tan\phi_0\end{aligned} \tag{3.51}$$

Combining equations (3.33) and (3.36), a differential formulation can be written for the rock joint deformability:

$$\begin{Bmatrix} d\sigma_n \\ d\tau \end{Bmatrix} = \begin{bmatrix} k_{nn} & k_{ns} \\ k_{sn} & k_{ss} \end{bmatrix} \begin{Bmatrix} dv \\ du \end{Bmatrix} \tag{3.52}$$

The (2 x 2) matrix is the material tangent stiffness and is, in general, non-symmetric.

Then, the shear response of a rock joint under applied constant or variable normal stiffness boundary conditions can be predicted by writing that during shearing, $d\sigma_n$ and dv must be related as follows:

$$d\sigma_n = K\,dv \tag{3.53}$$

where K is the applied stiffness which can be constant or also vary with σ_n. Substituting equation (3.53) into equation (3.33) gives two relations that change in normal stress, normal displacement and shear displacement must satisfy for the path with applied stiffness K:

$$d\sigma_n = \frac{K k_{ns}}{K - k_{nn}}\,du \tag{3.54}$$

and

$$dv = \frac{k_{ns}}{K - k_{nn}}\,du \tag{3.55}$$

Similarly, using equation (3.36), the changes in shear stress and stress displacement are related as follows:

$$d\tau = \left(\frac{k_{sn} k_{ns}}{K - k_{nn}} + k_{ss}\right) du \tag{3.56}$$

Note that if the joint is non-dilatant, i.e. tan i = 0, k_{ns} vanishes. Therefore $d\sigma_n = dv = 0$ and $d\tau = k_{ss}\,du$ with, according to equations (3.47-3.49), $k_{ss} = \tau_p/u_p$ when $u < u_p$, $k_{ss} = (\tau_p - \tau_r)/(u_p - u_r)$ when $u_p \le u \le u_r$ and $k_{ss} = 0$ when $u > u_p$. This means that a non-dilatant joint has a shear displacement response that is independent of the applied stiffness K, as expected.

Lets consider two special cases: First when the applied stiffness K vanishes (corresponding to a joint under constant normal stress boundary conditions) $d\sigma_n = 0$ and equation (3.55) reduces to $dv = -(k_{ns}/k_{nn})\, du$. Secondly, when $K = \infty$ (corresponding to constant displacement boundary conditions) $dv = 0$, it follows from equations (3.54) and (3.56) that $d\sigma_n = k_{ns}\, du$ and $d\tau = k_{ss}\, du$.

This model can be implemented in numerical code to obtain the response of discontinuities in rock masses (Saeb, 1989; Saeb and Amadei, 1990). Finally, it should be noted that this model is limited to monotonic loading. However, Souley et al. (1995) proposed a modified version of the Saeb and Amadei model that can consider cyclic loading.

3.5 FORTIN AND CO-WORKERS' MODEL

One difficulty of using graphical methods is that a limited number of points are available for the construction of the complete shear stress-shear displacement curve of the discontinuity. To help construct these curves in a more accurate manner, Fortin et al. (1988, 1990; Archambault et al., 1990) proposed an algorithm to predict the effect of a variable normal stiffness on shear strength of discontinuities. To use this algorithm, the constant normal stress direct shear test results must cover the entire field of variation of the different variables (σ, τ, u, v). This method is also only valid for progressive loading, when the shear and normal stresses are independent of the stress path. This method is described in the following.

The data required for applying the algorithm are:

- Results from direct shear tests at different constant normal stresses, including entire
  (τ, u) and (v, u) curves
- The in situ stiffness of the rock mass; This stiffness can be normal stress dependent.
- The value of the normal stress prior to any shear displacement (initial normal stress).

This algorithm makes use of the method suggested by Goodman (1980) and of a computing method developed by Gill (1971) which relies on arrays of the compiled addressed values taken at different available experimental curves and an interpolation procedure of polynomial nature. Figure 3.6 shows the interdependence of the parameters on the behavior of the joint. The method proposed by Fortin et al. (1988) is illustrated in Figure 3.7.

In the algorithm, the shear displacement is imposed step by step. For each of these steps, the corresponding normal displacement and normal stress are determined. They must satisfy both the dilatancy and rock mass stiffness requirements. If the in situ stiffness is not considered as infinite, then an iterative process allows for the adjustment of the dilatancy and of the normal stress. The variation of the shear stress is then calculated.

One important aspect of the method is that it is able to handle different rock mass stiffnesses whether they are constant, hardening or softening. A multi-linear approximation of the rock mass (v, σ) curve can be used, as shown in Figure 3.8.

Figure 3.9 shows a logical diagram of the algorithm. This algorithm was used to write a code in FORTRAN language and has been implemented on a personal computer (Fortin et al., 1988). This algorithm has been validated by making comparisons with direct shear test results under constant normal stiffness (Fortin et al., 1988; Archambault et al., 1990). The method showed good agreement with test results.

3.6 BEHAVIOR OF JOINTS AND THE PHENOMENON OF ROCKBURSTING

As it was outlined in section 2.1.4, Salamon (1974) explained the fault-slip bursts by a difference of stiffness between the loading system and the post-peak stiffness of the fault. Other evidences of the role of stiffness in the rockburst phenomenon can be found in the mechanics of stick-slip widely studied in geophysics research on earthquakes (e.g., Dieterich, 1972, 1978; Scholz et al., 1972, Rice, 1983; Li, 1987). Observations on rock friction have shown that three characteristics will affect the stick-slip behavior (Dieterich, 1978):

- Normal stress
- Stiffness of the testing system
- Surface finish effects

It was widely reported that the transition between stick-slip and stable sliding is dependent of normal stress and that a stable slip can become unstable (stick-slip) at a higher normal stress. Several studies have reported the minimum normal stress needed to obtain a stick-slip (e.g., Byerlee and Brace, 1968; Byerlee, 1970; Engelder and Scholz, 1976). However, results obtained showed a great difference depending on the authors. For Westerly granite, for example, Scholz et al. (1972) obtained a value of 1 MPa while

Byerlee and Brace (1968) reported a value of 122 MPa. This leads to the conclusion that other factors may be involved. Ohnaka (1973) reports that increased loading stiffness decreases the tendency for stick-slip as observed in metals. When Dieterich (1978) looked at the stiffness of the loading systems of the experiment of Scholz et al. (1972) and Byerlee and Brace (1968), he found values of 7,5 and 1003 GPa/m respectively. The two order of magnitude difference in stiffness may explain the two order of magnitude found in the value of the minimum normal stress needed to produce a stick-slip. In fact, when one divides the normal stress by the stiffness, results obtained are quite similar (7.5 and 8.2 m).

Several authors have also observed that surface finish and the presence of gouge have some effect on the stability of slip (Horn and Deere, 1962; Byerlee, 1967; Hoskins et al., 1968; Jaeger and Rosengren, 1969; Dieterich, 1972; Scholz et al., 1972; Ohnaka, 1973). Results from these studies suggest that the greater the surface roughness, the lesser the tendency for stick-slip (Scholz et al., 1972), and also, thicker layers of gouge have less tendency for stick-slip than thin layers (Byerlee and Summers, 1976). Figure 3.10 shows the results of Dieterich (1978) that shows the effect of the three characteristics (normal stress, stiffness and surface) on the transition between stable and stick slip for Westerly granite. From this experiment, stick-slip clearly arises from an interaction of the mechanical properties of the slip surface with the sample/machine system that exerts the stress on the surface (Dieterich, 1978).

These studies clearly show that, for a given set of conditions (normal and shear stresses, surface roughness), an unstable slip will become stable when the loading system stiffness becomes large enough.

An explanation of this phenomenon is given by Li (1987) in Figure 3.11. Figure 3.11a shows a single degree of freedom spring-block model, with loading through imposed displacement u_o, and load transmitted through a spring of stiffness k. The block is assumed to be rigid and the sliding surface of the block is govern by a slip-weakening relation shown in Figure 3.11b. The block is loaded through a spring which is pulled forward by the amount u_o. The normal stress acting on the block, as well as the temperature of the sliding surface, are assumed to remain constant during the sliding process. The force equilibrium governing the system can be written as:

$$T = \tau \tag{3.57}$$

where T is the spring force. The load and load point displacement are related by:

$$T = k(u_o - u) \tag{3.58}$$

where u_o is the displacement in front of the spring and u is the displacement of the block. Combining these two equations gives:

$$\tau = k\,u_o - k\,u \tag{3.59}$$

which expresses the equilibrium of the system on any point of the unloading line. However, for each unloading line shown, only its intercept with the τ-u curve can be the true equilibrium point since the sliding is governed by this constitutive relation. Thus a series of equilibrium points A, B, C, D may be traced as u_o is increased. The block displacement (u_A, u_B, u_C, u_D...), will accelerate faster than u_o. For the τ-u relationship and spring stiffness k shown in Figure 3.11b, equilibrium can be maintained only up to point E (when the post-peak slope of the block become larger in absolute values than k). Instability sets in at E, when equilibrium can not be maintained, followed by slip acceleration and rapid stress drop rate approaching infinity, as illustrated in Figure 3.11c. Reestablishment of equilibrium can be at any of the points F, G or H. These points are constrained by the fact that unloading of the spring must follow the unloading line EE' at instability. Furthermore, the energy loss from the spring must be converted into work of the sliding surface, which implies that:

$$\tfrac{1}{2}(\tau_E + \tau_H)(u_H - u_E) = \int_{u_E}^{u_H} \tau(u)\,du \tag{3.60}$$

which is how the point H is defined. However, if the energy is partially lost through seismic radiation (for example), then the final resting position may be at F or G. For a stiffer spring (where the stiffness of the spring is always larger than the slope of the block) and the same slip-weakening relationship (Figure 3.11d), the unloading lines are steeper and no dynamic instability occurs. The stress may drop and the slip may accelerate as in Figure 3.11e, but their time rate of change do not approach infinity and the slip is stable.

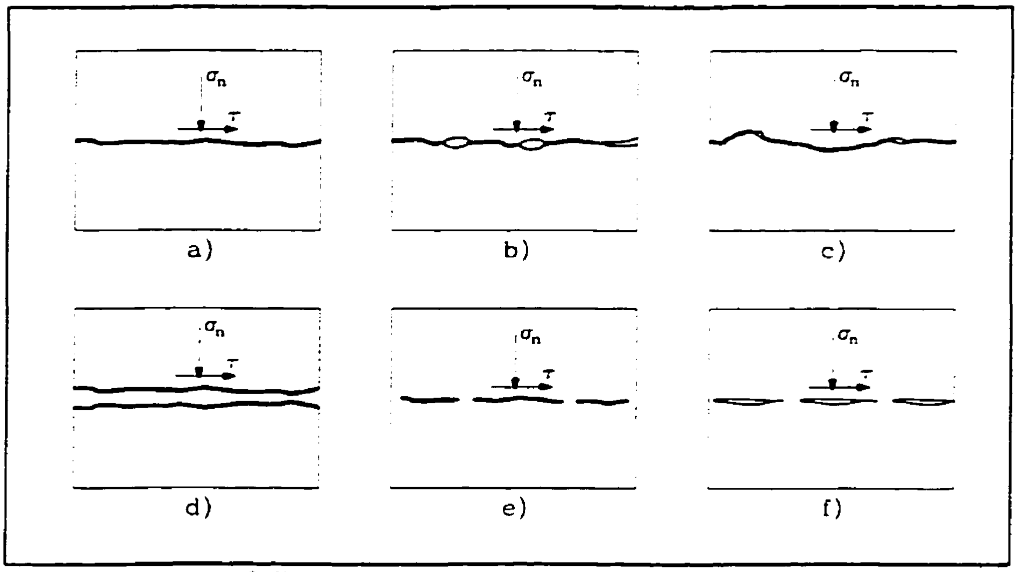

Figure 3.1: The nature of discontinuities. a) persistent discontinuity, planar, smooth or rough, closed; b) persistent discontinuity, planar, rough, not fully closed; c) persistent discontinuity, uneven, closed or not fully closed; d) persistent discontinuity, filled; e) discontinuities interrupted by rock bridging, closed; f) discontinuities interrupted by rock bridging, opened or filled (after Wittke, 1990).

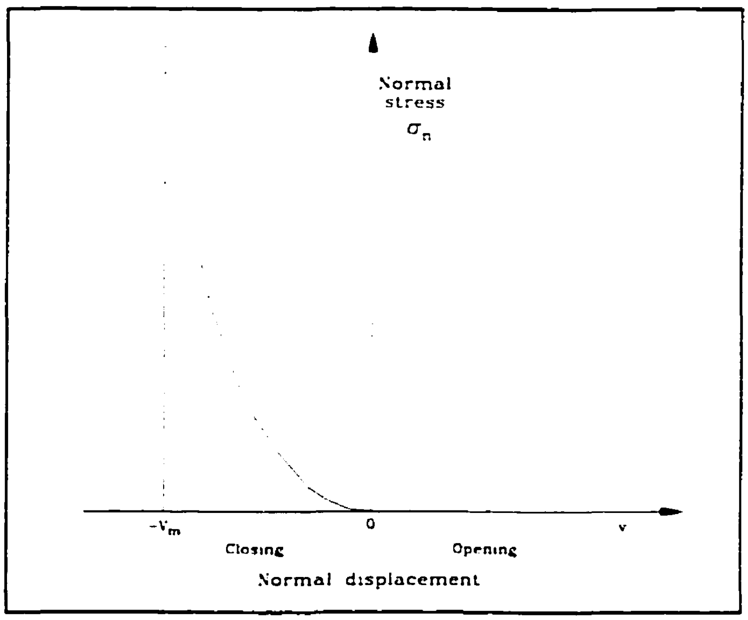

Figure 3.2: Normal stress vs normal displacement curve for a joint (after Saeb and Amadei, 1989).

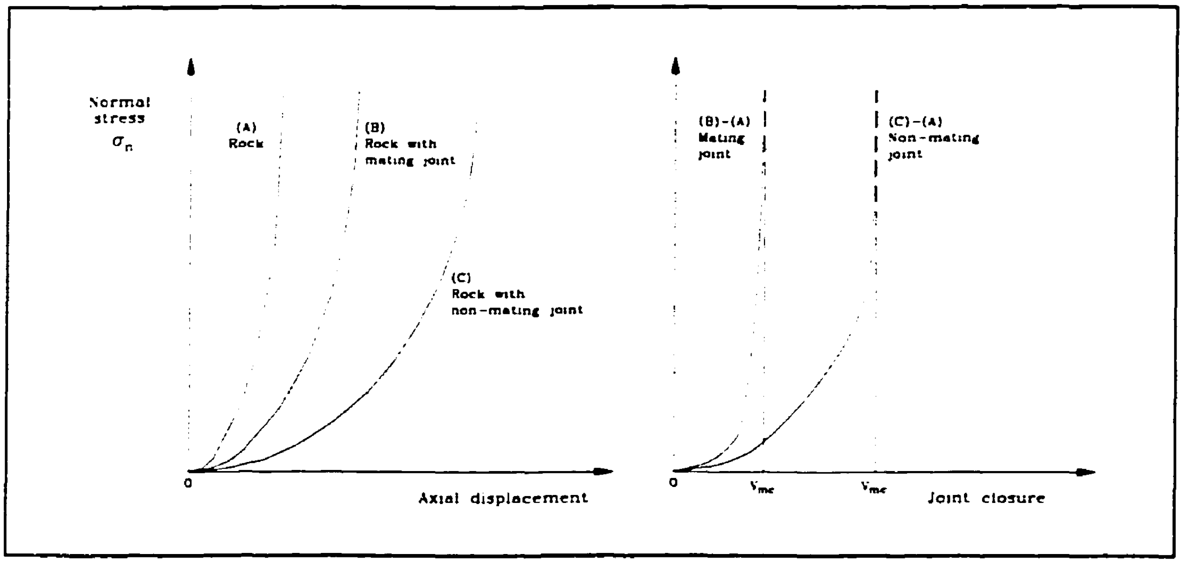

Figure 3.3: Comparison of joint normal behavior under mated and unmated conditions (after Goodman, 1976).

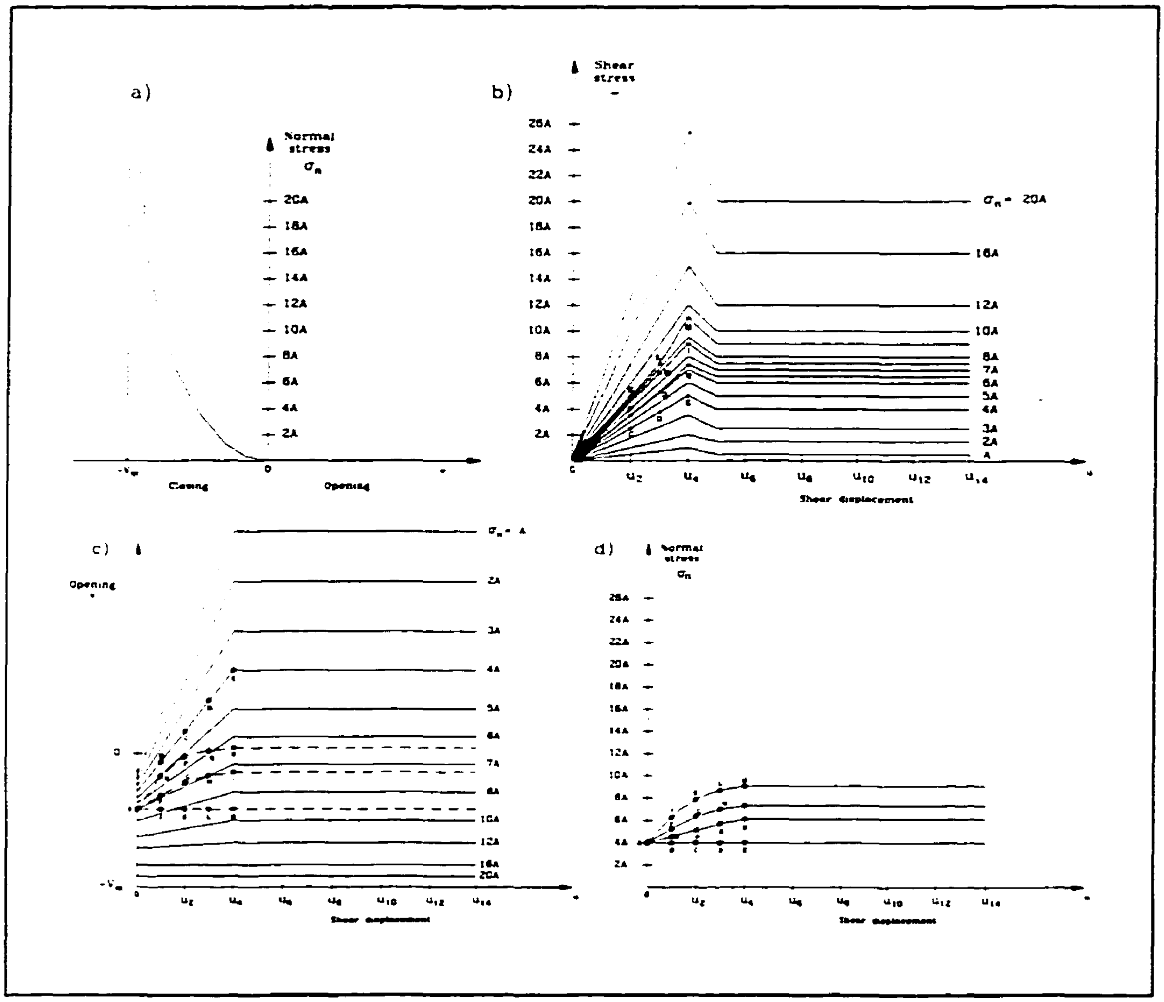

Figure 3.4: Joint response curves for normal stresses σ_n ranging between 0 and 20A (after Goodman and Boyle, 1985, and Saeb and Amadei, 1989).

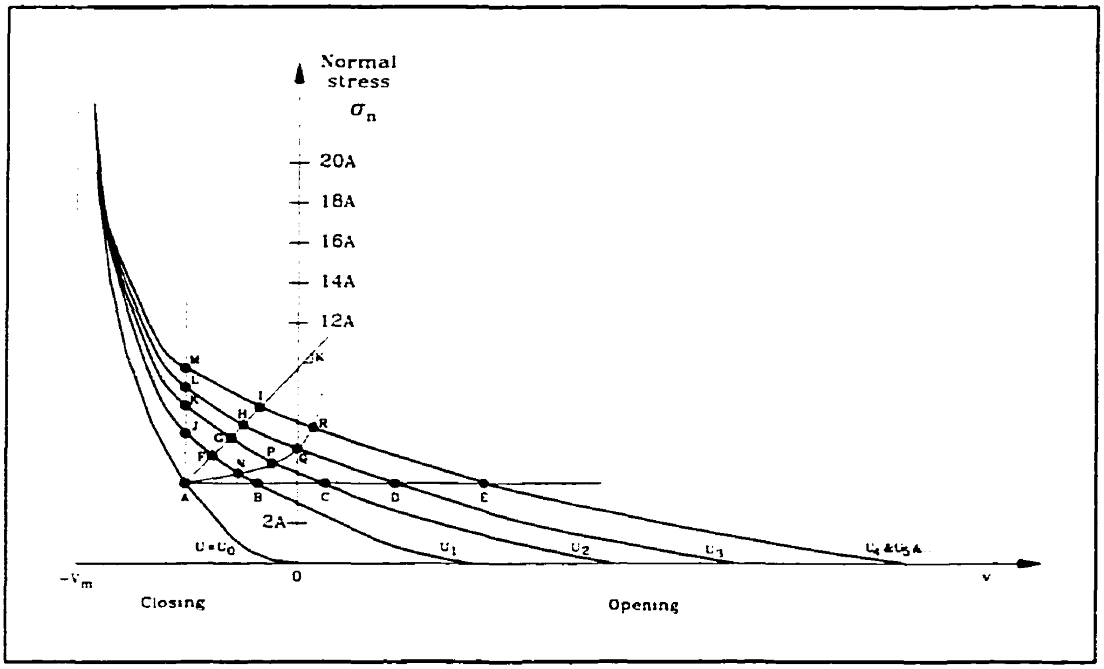

Figure 3.5: Normal stress vs. normal displacement curves at different shear displacement levels (after Saeb and Amadei, 1989).

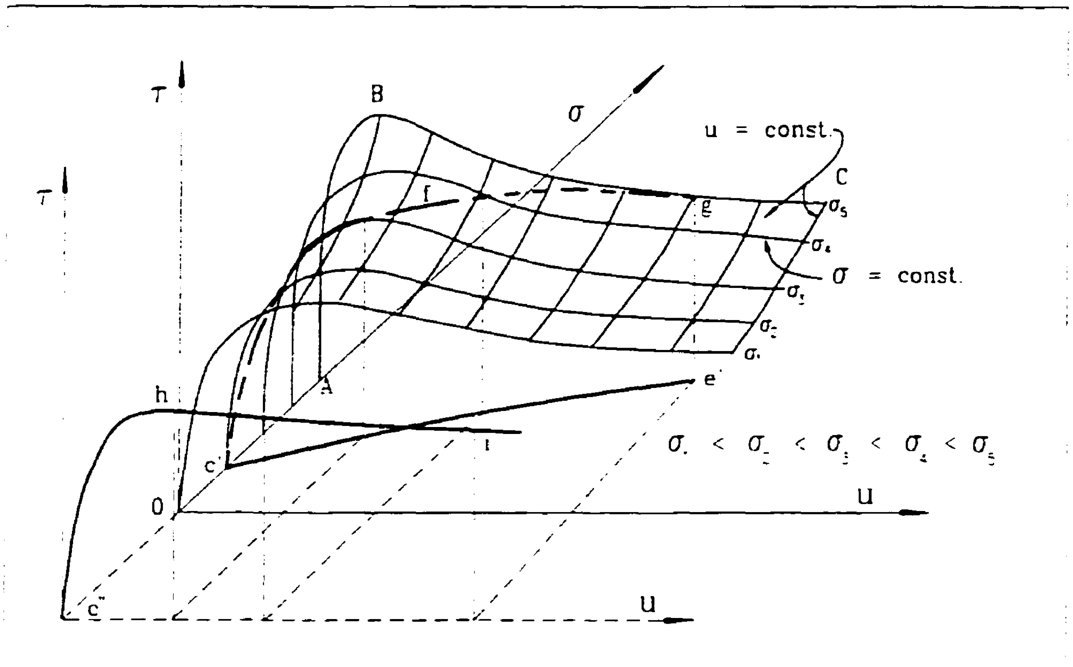

Figure 3.6a: Tridimensional surface describing the shear stress-shear displacement relationship of a dilatant discontinuity as a function of the normal stress, $f(\tau,u,\sigma) = 0$ (after Fortin et al., 1990).

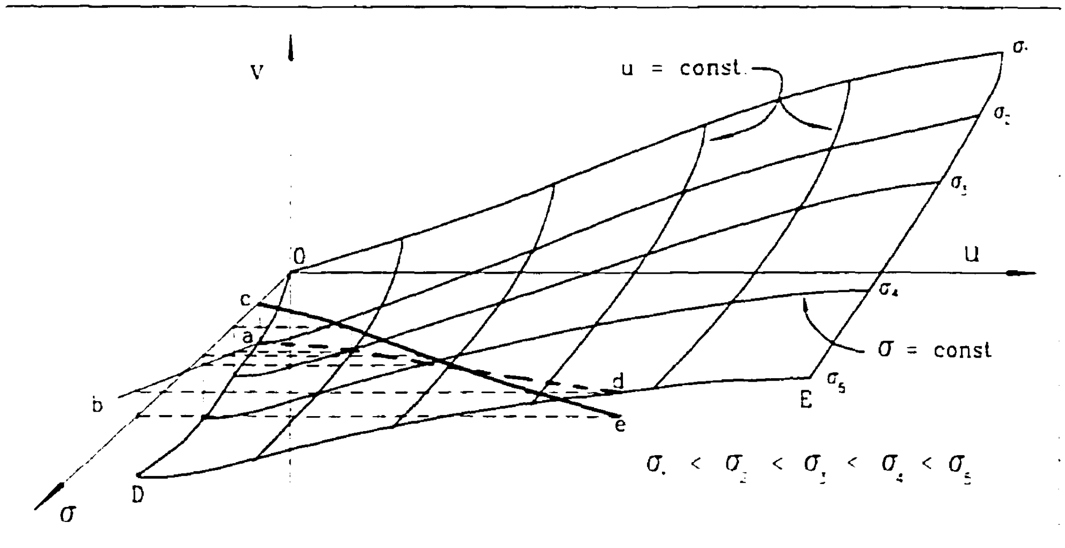

Figure 3.6b: Tridimensional surface describing the normal displacement-shear displacement relationship of a dilatant discontinuity as a function of the normal stress, $g(v,u,\sigma) = 0$ (after Fortin et al., 1990).

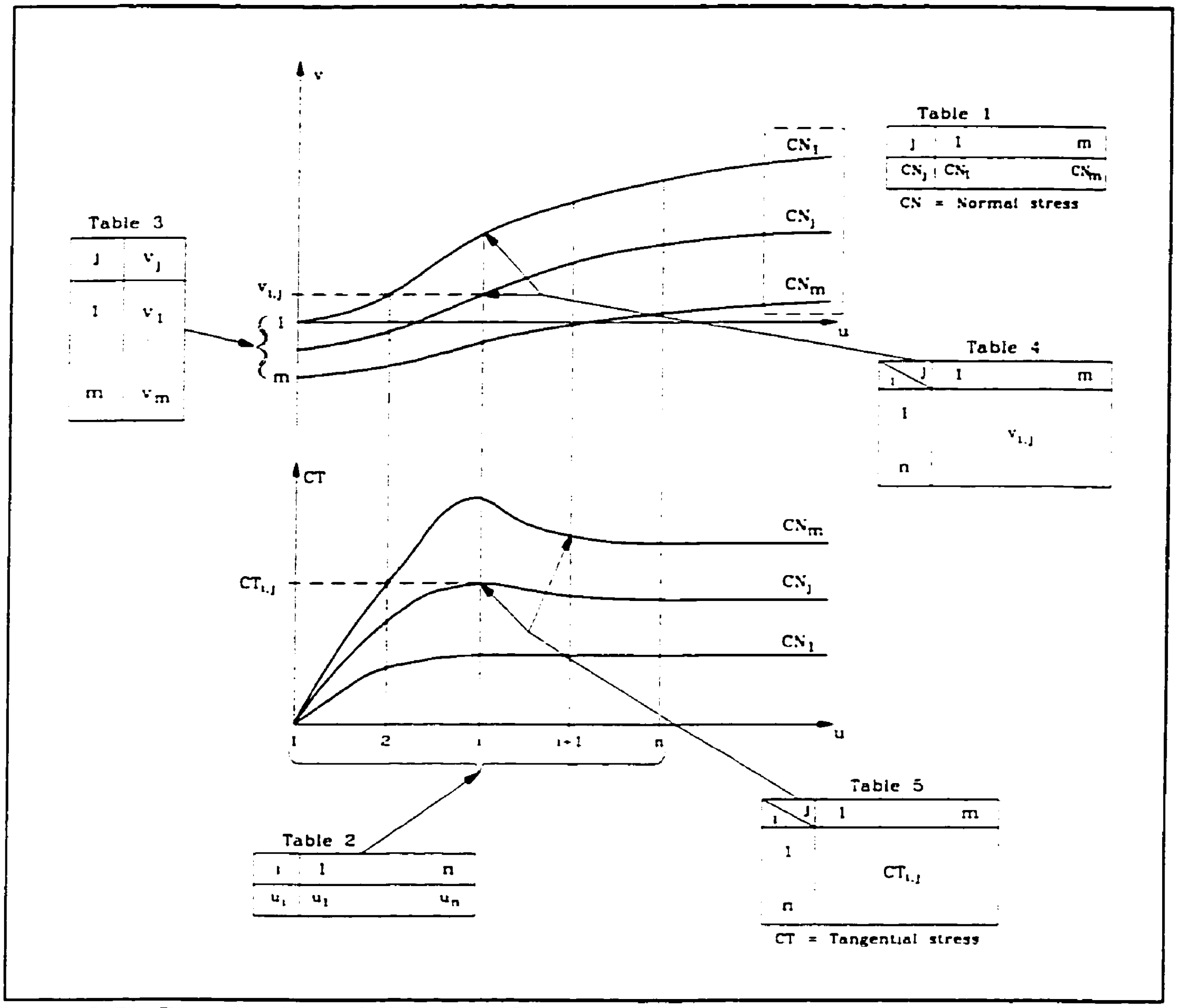

Figure 3.7: Construction of the data file from constant normal stress direct shear test results (after Fortin et al., 1988).

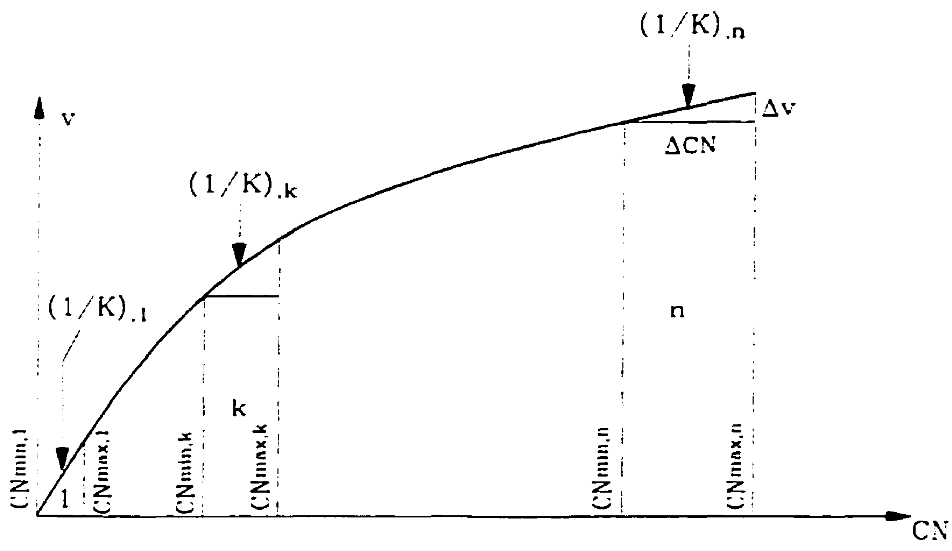

Table 6

i	1	.	k	.	n
CN_{max}	.		$CN_{max.k}$	.	
K_i	K_1	.	K_k	.	K_n

Figure 3.8: Multi-linear approximation of a non-linear rock mass stiffness and construction of the related part of the data file (after Fortin et al., 1988).

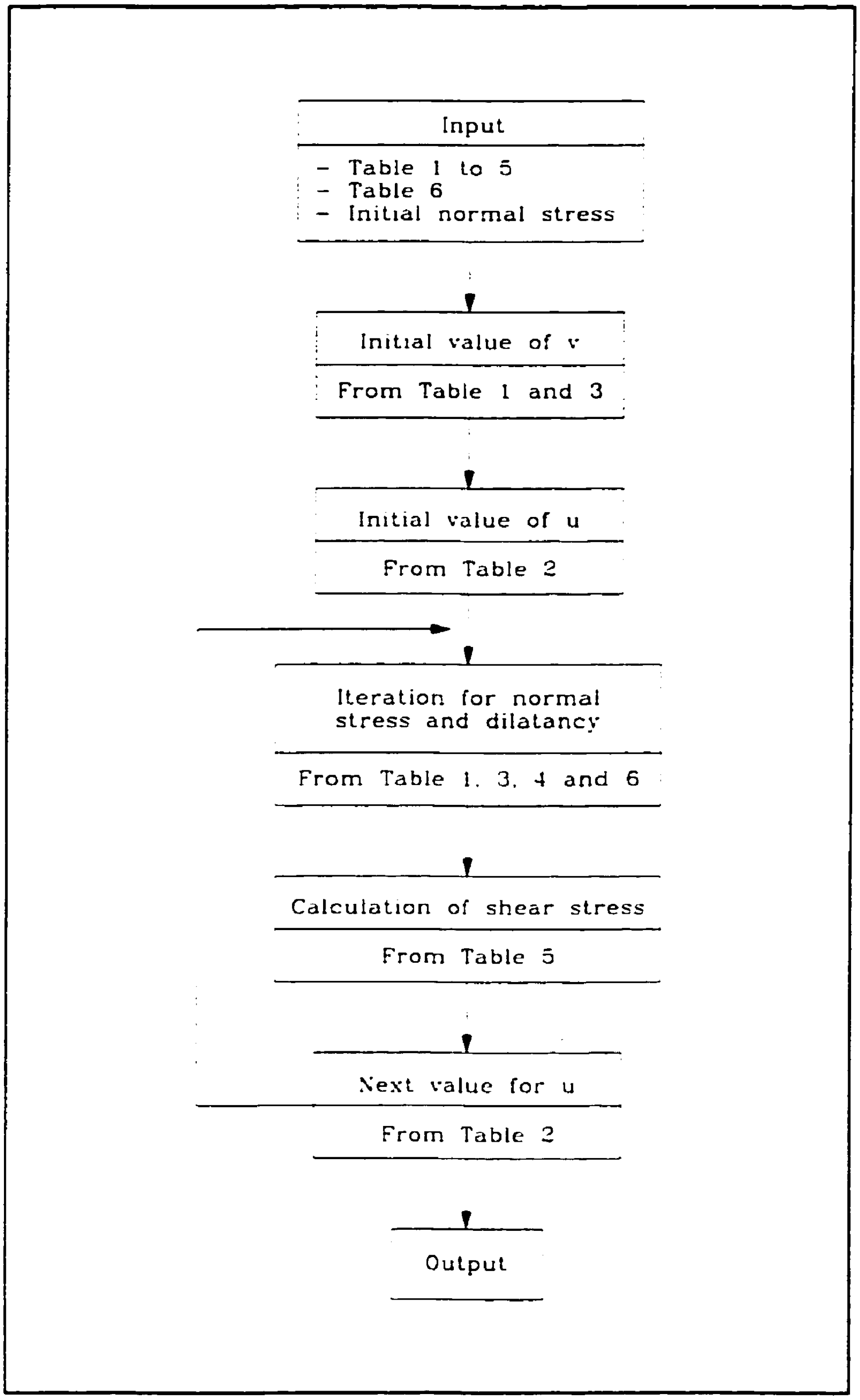

Figure 3.9: **Simplified logical diagram of the algorithm (after Fortin et al., 1988).**

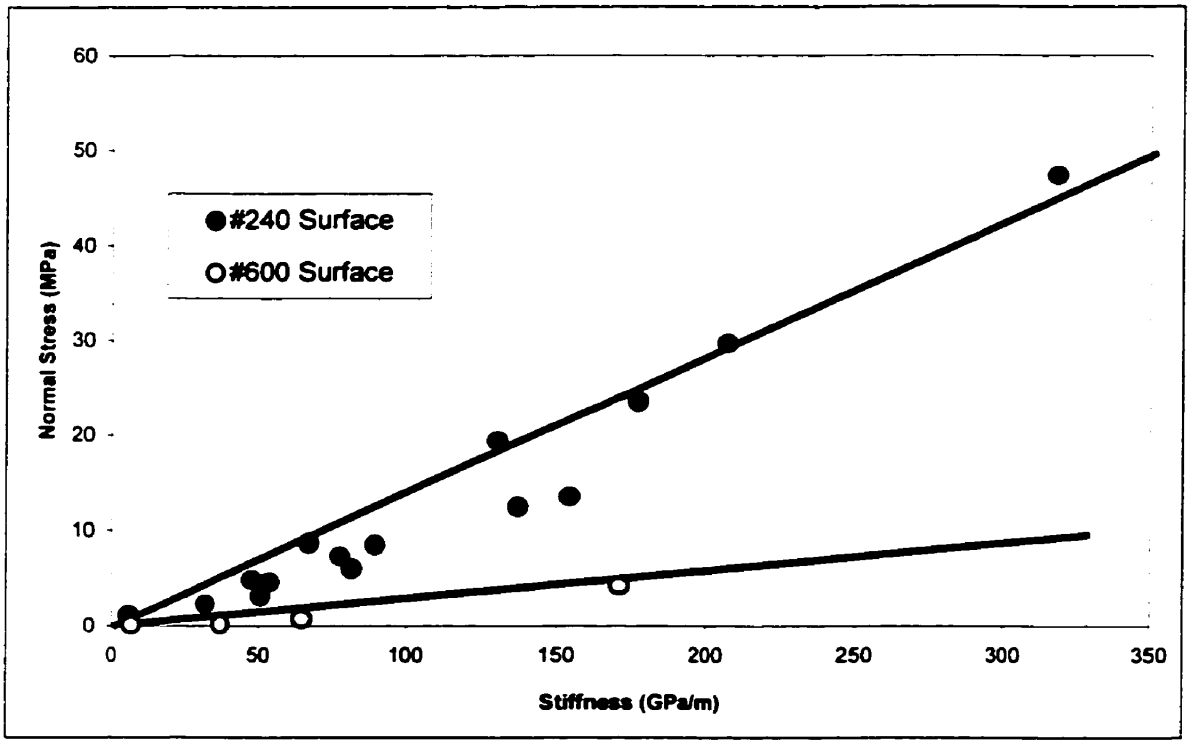

Figure 3.10: Transition from stable sliding to stick-slip as a function of normal stress, stiffness and surface finish for Westerly granite (after Dieterich, 1978).

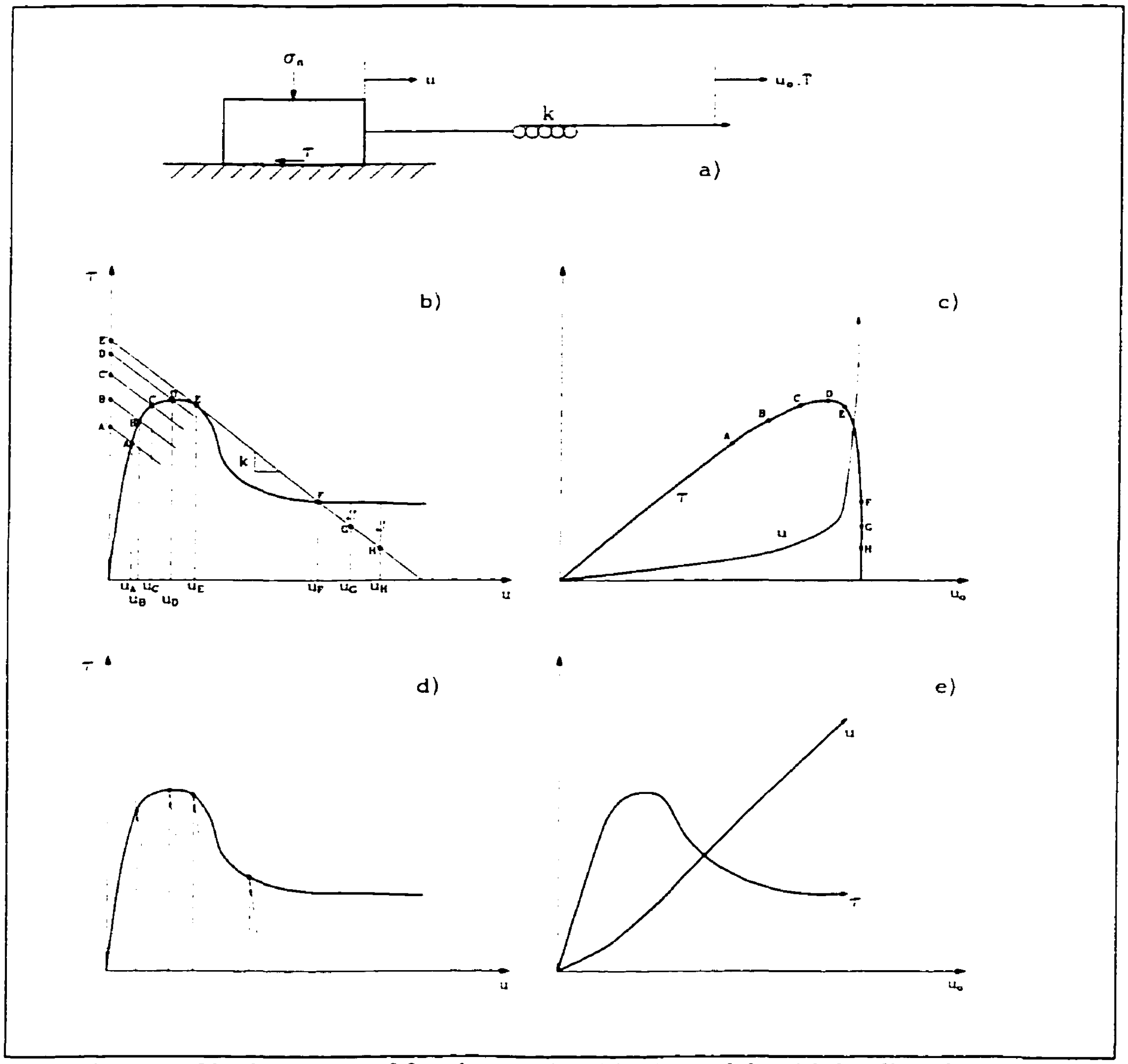

Figure 3.11: a) Single degree of freedom spring-block model, with loading through imposed displacement u_0, and load transmitted through a spring of stiffness k. b) Trace of equilibrium load and corresponding slips. c) Illustration of the stress-displacement curve as transmitted by the spring (unstable slip). d) Same situation with a stiffer spring. e) Illustration of the stress-displacement curve as transmitted by the spring (stable slip). (after Li, 1987).

CHAPTER 4
BOUNDARY ELEMENT METHODS

4.1 INTRODUCTION

In many engineering problems, it is necessary to assess some design conditions such as stresses, displacements, groundwater flow, etc. To evaluate these, one can use analytical solutions or, when the problem is more complex, numerical methods. There are three broad categories of numerical methods to evaluate the response of a continuum to loading: the finite element method (FEM), the discrete element method (DEM) and the boundary element method (BEM). In the FEM and the DEM, the domain must be defined (by a mesh or by elements) over a certain volume (or area) while with the BEM, only the domain boundaries need to be defined. Figure 4.1a shows the classification of numerical methods used to solve geomechanical problems. The relative advantages (and disadvantages) of each method are presented in Table 4.1.

Table 4.1: Relative strengths and weaknesses of numerical methods (after Hoek et al., 1991)

	Advantages	Disadvantages
Boundary element method	Far-field conditions inherently represented Only boundaries require discretization	Coefficient matrix fully populated Solution time increases exponentially with number of elements used
Finite-element and finite-difference methods	Material heterogeneity easily handled Material and geometric non-linearity handled efficiently with explicit solution techniques Matrices are banded with implicit solution techniques When explicit solution techniques are used, less skill is required from user	Entire volume must be discretized Far-field boundary conditions must be approximated For linear problems, explicit solutions techniques are relatively slow Solution time increases exponentially with number of elements used for implicit solution techniques
Discrete-element method	Data structures well suited to model systems with high degree of non-linearity from multiple intersecting joints Very general constitutive relations may be used with little penalty in terms of computational efforts Solution time increases only linearly with number of elements used	Solution time seem much slower than for linear problems Results can be sensitive to assumed values of modeling parameters

4.1.1 Finite Element and Finite Difference Methods

From a practical point of view, these two methods are similar. The difference relies in the way of solving the set of equations. Figure 4.1b shows the process that led to the present-day finite element method with interesting references. In these methods, the physical problem is modeled numerically by discretizing the problem region (i.e. dividing the domain in small elements). These methods are well suited to solve problems involving heterogeneous or non-linear materials because each element explicitly models the response of its contained material. However, since the domain must be modeled entirely, these techniques are not perfectly adapted to handle problems with *infinite* boundaries such as excavations in rock masses.

The finite element method has become very popular in many fields of engineering (the term "finite element" appears to have been first proposed by Clough, 1960). Numerous computer codes (2D and 3D) are available and have proven their reliability. The literature on the subject is extremely abundant and many books have been published. The interested reader is referred to the work of Zienkiewicz (1971, 1977; Zienkiewicz and Taylor, 1989), Bathe (1982), and Reddy (1993).

4.1.2 The discrete element methods

These methods were developed to properly model ground conditions that are often referred as "blocky" (that is where the spacing of joints is of the same order of magnitude as the dimension of the excavation). Since the joints are much more deformable than the blocks, then individual blocks may be regarded as rigid bodies. Table 4.2 presents a summary of the development of the methods.

Table 4.2: Development of discrete element methods

	References
Distinct elements	Cundall, 1971, 1974 Voegele et al., 1978 Cundall and Strack, 1979
Discontinuous deformation analysis	Shi, 1988 Shi and Goodman, 1989 Lin et al., 1994
Rigid body spring	Kawai, 1980
Modified virtual stress	Hamajima, 1993 Hamajima et al., 1994

Although discrete element methods have been used most extensively in academic environment, it is finding its way in consultant offices and mine planners and designers as well (Hoek et al., 1991). These techniques have become a useful tool for analysis in blocky ground, especially in open pits.

4.1.3 The Boundary Element Methods

The BEM have been used in mining engineering and geomechanics for the past 20 years or so. Over the years, the boundary element methods have become a useful tool for ground control, mine planning and stress analysis of underground excavations in the rock mass. This technique has been used to assist the engineer in many different applications such as: the design of underground openings (e.g., Meek, 1985); pillar size determination and pillar stability (e.g., Huang et al., 1985); evaluation of rock slope stability (e.g., Tomlin and Butterfield, 1974); evaluation of the rockburst potential of underground openings (e.g., Simon et al., 1993); and the modelling of cracks and faults (e.g., Peirce, 1991). It has also been used to resolve problems such as: the effect of mining sequences on the redistribution of stresses (e.g., Grant et al., 1993); the influence of geological discontinuities on the stress distribution around openings (e.g., Wiles and Nicholls, 1993; Fotoohi and Mitri, 1996); the behaviour of non-linear materials (e.g., Zipf, 1993); the behaviour of backfill material (e.g., Brechtel et al., 1989); the rate-dependent behaviour of a jointed rock mass (e.g., Crawford and Curran, 1983); the plasticity of rock masses (e.g., Mukherjee and Chandra, 1985); dynamic effects (e.g.. Crouch and Tian, 1988); drainage problems in geomechanics (e.g., Tomlin, 1973); and hydraulic fracturing (e.g., Vandamme and Wawrzynek, 1988).

The BEM can be divided in two categories, the direct method and the indirect method. Both methods require solving an integral equation over a boundary surface. Table 4.3 shows pertinent references of the development of the BEM.

Table 4.3: Development of boundary element methods in solid mechanics.

	References
Direct formulation	Shaw, 1966, 1969 Rizzo, 1967 Cruze, 1969, 1972, 1974 Cruze and Rizzo, 1968, 1975 Lachat, 1975 Lachat and Watson, 1975, 1976 Rizzo and Shippy, 1977, 1979 Brebbia and Dominguez, 1977 Brebbia, 1978 Brebbia and Ferrante, 1978 Brebbia and Butterfield, 1978 Telles, 1983 Henry, 1987
Indirect formulation	Chen and Schweikert, 1963 Hess and Smith, 1964, 1966 Massonet, 1965 Oliviera, 1968 Butterfield and Banerjee, 1971 Watson, 1973 Hess, 1974, 1975 Tomlin and Butterfield, 1974 Banerjee, 1971, 1976 Crouch, 1976a, 1976b, 1979 Banerjee and Butterfield, 1976 Banerjee and Driscoll, 1976 Jaswon and Symm, 1977 Crouch and Starfield, 1983

More general reviews on the BEM can be found in Banerjee and Butterfield (1981), Crouch and Starfield (1983) and Banerjee (1994).

In this report, particular emphasis is given to the indirect method for its usefulness in non-linear modeling.

4.1.4 Hybrid approaches

The main objective of a hybrid method is to combine the above methods so as to eliminate as many of the undesirable characteristics as possible while retaining as many of their advantages as possible (Hoek et al., 1991). In this way, the rock mass surrounding the openings may be modeled with finite or discrete elements while modeling the elastic far-field conditions with boundary elements. Even though the idea of coupling two numerical methods may have started with the work of Wood (1976), the hybrid approach really developed with the work of Zienkiewicz et al. (1977; Kelly et al., 1979), Brebbia and Georgiou (1979), Beer and Meek (1981), Brady and Wassyng (1981) and Lorig and Brady (1984). More examples of these coupling methods can be found in Atluri et al. (1983) and Zienkiewicz and Taylor (1989).

4.2 LINEAR ELASTICITY

It is important to state the fundamental solutions used in geomechanics. The simplest form is linear elasticity. Stresses in a rock mass in static equilibrium must satisfy these three differential equations (e.g., Timoshenko and Goodier, 1970):

$$\begin{aligned}
&\frac{\partial\sigma_{xx}}{\partial x}+\frac{\partial\sigma_{yx}}{\partial y}+\frac{\partial\sigma_{zx}}{\partial z}+\beta_x=0\\
&\frac{\partial\sigma_{xy}}{\partial x}+\frac{\partial\sigma_{yy}}{\partial y}+\frac{\partial\sigma_{zy}}{\partial z}+\beta_y=0\\
&\frac{\partial\sigma_{xz}}{\partial x}+\frac{\partial\sigma_{yz}}{\partial y}+\frac{\partial\sigma_{zz}}{\partial z}+\beta_z=0
\end{aligned}\tag{4.1}$$

where σ_{ij} are the stress components and β_i are the body forces acting in the *i* direction. Furthermore, the strain tensor can be defined as:

$$\begin{aligned}
&\varepsilon_{xx} = \frac{\partial u_x}{\partial x} \quad \varepsilon_{yy} = \frac{\partial u_y}{\partial y} \quad \varepsilon_{zz} = \frac{\partial u_z}{\partial z} \\
&\varepsilon_{xy} = \frac{1}{2}\left(\frac{\partial u_x}{\partial y} + \frac{\partial u_y}{\partial x}\right) \quad \varepsilon_{yz} = \frac{1}{2}\left(\frac{\partial u_y}{\partial z} + \frac{\partial u_z}{\partial y}\right) \quad \varepsilon_{xz} = \frac{1}{2}\left(\frac{\partial u_x}{\partial z} + \frac{\partial u_z}{\partial x}\right) \\
&\varepsilon_{yx} = \varepsilon_{xy} \quad \varepsilon_{zy} = \varepsilon_{yz} \quad \varepsilon_{zx} = \varepsilon_{xz}
\end{aligned} \tag{4.2}$$

where u_i is the displacement in the *i* direction; the normal strains ε_{ii} represent the change of length per unit length in the *i* direction; the shear strains ε_{ij} ($i \neq j$) represent half the change of right angle originally parallel to the *i* and *j* axis.

The strain and stress can be related by the generalized Hooke's law:

$$\begin{aligned}
&\varepsilon_{xx} = \frac{1}{E}\left[\sigma_{xx} - \nu\left(\sigma_{yy} + \sigma_{zz}\right)\right] \\
&\varepsilon_{yy} = \frac{1}{E}\left[\sigma_{yy} - \nu\left(\sigma_{xx} + \sigma_{zz}\right)\right] \\
&\varepsilon_{zz} = \frac{1}{E}\left[\sigma_{zz} - \nu\left(\sigma_{yy} + \sigma_{xx}\right)\right] \\
&\varepsilon_{xy} = \frac{1}{2G}\sigma_{xy} \quad \varepsilon_{yz} = \frac{1}{2G}\sigma_{yz} \quad \varepsilon_{xz} = \frac{1}{2G}\sigma_{xz}
\end{aligned} \tag{4.3}$$

with

$$G = \frac{E}{2\,(1+\nu)} \tag{4.4}$$

where G is the shear modulus, E is the Young modulus and ν is the Poisson's ratio. From Equations 4.3 and 4.4, stresses can be expressed as a function of strains:

$$\begin{aligned}
\sigma_{xx} &= \frac{2G}{1-2\nu}\left[(1-\nu)\varepsilon_{xx} + \nu\left(\varepsilon_{yy} + \varepsilon_{zz}\right)\right] \\
\sigma_{yy} &= \frac{2G}{1-2\nu}\left[(1-\nu)\varepsilon_{yy} + \nu\left(\varepsilon_{xx} + \varepsilon_{zz}\right)\right] \\
\sigma_{zz} &= \frac{2G}{1-2\nu}\left[(1-\nu)\varepsilon_{zz} + \nu\left(\varepsilon_{yy} + \varepsilon_{xx}\right)\right] \\
\sigma_{xy} &= 2G\varepsilon_{xy} \quad \sigma_{yz} = 2G\varepsilon_{yz} \quad \sigma_{xz} = 2G\varepsilon_{xz}
\end{aligned} \tag{4.5}$$

It is easier to write these equations with an index notation where the following two conventions are used: (i) a repeated literal index in any term of an expression implies summation; (ii) a comma preceding an index denotes partial differential with respect to the variable represented by that index. This example will help clarify the notation:

$$\sigma_{ij} n_j = \sum_{j=1}^{3} \sigma_{ij} n_j = \sigma_{i1} n_1 + \sigma_{i2} n_2 + \sigma_{i3} n_3$$

$$u_{i,j} = \frac{\partial u_i}{\partial x_j} \qquad u_{i,jk} = \frac{\partial^2 u_i}{\partial x_j \partial x_k}$$

$$u_{i,jj} = \frac{\partial^2 u_i}{\partial x_1^2} + \frac{\partial^2 u_i}{\partial x_2^2} + \frac{\partial^2 u_i}{\partial x_3^2}$$

Then, Equation (4.1) can be rewritten as:

$$\sigma_{ji,j} + \beta_i = 0 \tag{4.6}$$

and the strain tensor as:

$$\varepsilon_{ij} = \tfrac{1}{2}\left(u_{i,j} + u_{j,i}\right) \tag{4.7}$$

The stress-strain relations can be written as:

$$\varepsilon_{ij} = \frac{1}{2G}\left[\sigma_{ij} - \frac{\nu}{1+\nu}\sigma_{kk}\delta_{ij}\right] \tag{4.8}$$

$$\sigma_{ij} = 2G\left[\varepsilon_{ij} + \frac{\nu}{1-2\nu}\varepsilon_{kk}\delta_{ij}\right] \tag{4.9}$$

where δ_{ij} is the Kronecker delta, which is defined by:

$$\delta_{ij} = \begin{cases} 1 & \text{if } i = j \\ 0 & \text{if } i \neq j \end{cases} \tag{4.10}$$

4.3 THE FICTITIOUS STRESS METHOD (FSM)

The fictitious stress method is considered as an indirect method of boundary elements. This method uses the solution of Kelvin's problem for plane strain. Sections 4.3 to 4.5 are largely taken from Crouch and Starfield (1983).

4.3.1 Kelvin's problem for plane strain

Figure 4.2 illustrates the problem that was solved by the Scottish physicist William Thompson (who later became Lord Kelvin) in 1848 (Davis and Selvadurai, 1993). A force $F_i = (F_x, F_y)$ is applied along the *z* axis in an infinite elastic solid. The components $F_x > 0$ and $F_y > 0$ have dimensions of force/length (e.g., N/m). The solution to this problem can be expressed in terms of a function g(x,y), defined by:

$$g(x,y) = \frac{-1}{4\pi(1-\nu)} \ln\left(\sqrt{x^2 + y^2}\right) \tag{4.11}$$

and the displacements can be written as:

$$\begin{aligned} u_x &= \frac{F_x}{2G}\left[(3-4\nu)g - xg_{,x}\right] + \frac{F_y}{2G}\left[-yg_{,x}\right] \\ u_y &= \frac{F_x}{2G}\left[-xg_{,y}\right] + \frac{F_y}{2G}\left[(3-4\nu)g - yg_{,y}\right] \end{aligned} \tag{4.12}$$

In the same manner, stresses are given by:

$$\begin{aligned}
\sigma_{xx} &= F_x\left[2(1-\nu)g_{,x} - xg_{,xx}\right] + F_y\left[2\nu g_{,y} - yg_{,xx}\right] \\
\sigma_{yy} &= F_x\left[2\nu g_{,x} - xg_{,yy}\right] + F_y\left[2(1-\nu)g_{,y} - yg_{,yy}\right] \\
\sigma_{xy} &= F_x\left[(1-2\nu)g_{,y} - xg_{,xy}\right] + F_y\left[(1-2\nu)g_{,x} - yg_{,xy}\right]
\end{aligned} \tag{4.13}$$

The derivatives of g(x,y) are found from (4.11) and are given by:

$$\begin{aligned}
g_{,x} &= \frac{-1}{4\pi(1-\nu)}\frac{x}{x^2+y^2} \\
g_{,y} &= \frac{-1}{4\pi(1-\nu)}\frac{y}{x^2+y^2} \\
g_{,xy} &= \frac{1}{4\pi(1-\nu)}\frac{2xy}{\left(x^2+y^2\right)^2} \\
g_{,xx} &= -g_{,yy} = \frac{1}{4\pi(1-\nu)}\frac{x^2-y^2}{\left(x^2+y^2\right)^2}
\end{aligned} \tag{4.14}$$

Note however that the displacements in this solution are unbounded at large distances from the origin due to the logarithmic function in g(x,y).

4.3.2 Constant tractions over a line segment

By integration of Kelvin's problem, one can solve the problem of constant traction $t_x = P_x$ and $t_y = P_y$ applied to the line segment $|x| \le a,\ \ y = 0$ in an infinite elastic solid. If the line segment is divided into elements of length $d\xi$ (as shown in Figure 4.3), the resultant force (per unit length perpendicular to the *x*, *y* plane) on the element centered at point $x = \xi,\ \ y = 0$ is then:

$$F_i(\xi) = P_i\, d\xi \tag{4.15}$$

where *i* represents either *x* or *y*. The solution can be found by substituting forces $F_x(\xi)$ and $F_y(\xi)$ into Equation (4.12) and (4.13), replacing *x* by *x-ξ* and integrating the resulting expressions with respect to ξ between *-a* and *+a*. If a function *f*(x,y) is defined as:

$$f(x,y) = \int_{-a}^{a} g(x-\xi, y)d\xi \tag{4.16}$$

then:

$$\begin{aligned} u_x &= \frac{P_x}{2G}\left[(3-4\nu)f + yf_{,y}\right] + \frac{P_y}{2G}\left[-yf_{,x}\right] \\ u_y &= \frac{P_x}{2G}\left[-yf_{,x}\right] + \frac{P_y}{2G}\left[(3-4\nu)f - yf_{,y}\right] \end{aligned} \tag{4.17}$$

and

$$\begin{aligned} \sigma_{xx} &= P_x\left[(3-2\nu)f_{,x} + yf_{,xy}\right] + P_y\left[2\nu f_{,y} + yf_{,yy}\right] \\ \sigma_{yy} &= P_x\left[-(1-2\nu)f_{,x} - yf_{,xy}\right] + P_y\left[2(1-\nu)f_{,y} - yf_{,yy}\right] \\ \sigma_{xy} &= P_x\left[2(1-\nu)f_{,y} + yf_{,yy}\right] + P_y\left[(1-2\nu)f_{,x} - yf_{,xy}\right] \end{aligned} \tag{4.18}$$

The integral in Equation (4.16) can then be evaluated by:

$$f(x,y) = \frac{-1}{4\pi(1-\nu)}\left[\begin{array}{l} y\left(\arctan\left(\frac{y}{x-a}\right) - \arctan\left(\frac{y}{x+a}\right)\right) - (x-a)\ln\sqrt{\left[(x-a)^2 + y^2\right]} \\ + (x+a)\ln\sqrt{\left[(x+a)^2 + y^2\right]} \end{array}\right] \tag{4.19}$$

The derivatives of f(x,y) are then given by:

$$
\begin{aligned}
f_{,x} &= \frac{1}{4\pi(1-\nu)}\left[\ln\sqrt{\left[(x-a)^2+y^2\right]} - \ln\sqrt{\left[(x-a)^2+y^2\right]}\right] \\
f_{,y} &= \frac{-1}{4\pi(1-\nu)}\left[\arctan\frac{y}{x-a} - \arctan\frac{y}{x+a}\right] \\
f_{,xy} &= \frac{1}{4\pi(1-\nu)}\left[\frac{y}{(x-a)^2+y^2} - \frac{y}{(x+a)^2+y^2}\right] \\
f_{,xx} &= -f_{,yy} = \frac{1}{4\pi(1-\nu)}\left[\frac{x-a}{(x-a)^2+y^2} - \frac{x+a}{(x+a)^2+y^2}\right]
\end{aligned}
\qquad (4.20)
$$

Here again, the displacements are unbounded at large distances from the origin, because of the logarithmic terms in f(x,y). Hence, the displacements are specified only in a relative sense, meaning that in any particular problem, a reference point will be selected and the displacement will be measured with respect to this point.

4.3.3 Numerical procedure for the FSM in geomechanics

The solutions presented in section 4.3.1 and 4.3.2 can be used to solve numerically general mixed boundary value problems in elasticity. A stress boundary value problem is shown in Figure 4.4a. The cavity is assumed to be long so the analysis can be considered as plane strain. The local coordinates *n* and *s* are respectively perpendicular and tangent to the boundary C: therefore, they vary from one point to the other. Suppose that the wall of the cavity is subjected to a uniform normal stress σ_n = -p (negative = compression) with no shear stress (σ_s = 0). What needs to be determined is the displacements and stresses in the body due to that loading.

To solve this problem, we can proceed as follows. The boundary C is approximated by N straight line segments, joined end to end as shown in Figure 4.4. The length of a typical boundary element i is denoted as $2\overset{i}{a}$. When the elements are small enough, the approximation of C will be close. It then may be considered that each element is subjected to a normal stress σ_n = -p along its entire length and that σ_s = 0. The boundary conditions become:

$$\overset{i}{\sigma_n} = -p, \quad \overset{i}{\sigma_s} = 0 \qquad \text{for} \quad i = 1 \text{ to } N \tag{4.21}$$

The problem can then be solved numerically using the model shown in Figure 4.4b. The dashed curve C' has the same shape as C used to define the boundary. However, C' does not represent a boundary but marks the locations of line segments that are coincident with the boundary elements of Figure 4.4a. Then the constant resultant normal and shear stresses are applied to each element along C'. For element j, the shear stress and normal stress applied to this segment are denoted as $\overset{j}{P_s}$ and $\overset{j}{P_n}$.

The notation P is used instead of σ to point out that the stresses applied are not the actual stresses along C'.

Using the solution found in section 4.3.2, and accounting for the orientations of the line segments, the actual stresses $\overset{i}{\sigma_s}$ and $\overset{i}{\sigma_n}$ at the midpoint of each element of curve C' can be computed, for i = 1 to N. The results can be written as:

$$\left.\begin{aligned} \overset{i}{\sigma_s} &= \sum_{j=1}^{N} \overset{ij}{A_{ss}} \overset{j}{P_s} + \sum_{j=1}^{N} \overset{ij}{A_{sn}} \overset{j}{P_n} \\ \overset{i}{\sigma_n} &= \sum_{j=1}^{N} \overset{ij}{A_{ns}} \overset{j}{P_s} + \sum_{j=1}^{N} \overset{ij}{A_{nn}} \overset{j}{P_n} \end{aligned}\right\} \quad i = 1 \text{ to } N \tag{4.22}$$

where $\overset{ij}{A_{ss}}$ etc., are the boundary stress influence coefficients for the problem. The coefficient $\overset{ij}{A_{sn}}$, for example, gives the actual shear stress at the midpoint of the i^{th} segment ($\overset{i}{\sigma_s}$) due to a constant unit normal stress applied to the j^{th} segment ($\overset{j}{P_n} = 1$).

If one can find the applied stresses $\overset{j}{P}_s$ and $\overset{j}{P}_n$ for $j = 1$ to N such that the actual stresses $\overset{i}{\sigma}_s$ and $\overset{i}{\sigma}_n$ in Equation (4.22) have the values specified in (4.21), then the physical problem is solved in an approximate manner. Combining the last two equations, then:

$$\left.\begin{aligned} 0 &= \sum_{j=1}^{N} \overset{ij}{A}_{ss} \overset{j}{P}_s + \sum_{j=1}^{N} \overset{ij}{A}_{sn} \overset{j}{P}_n \\ -p &= \sum_{j=1}^{N} \overset{ij}{A}_{ns} \overset{j}{P}_s + \sum_{j=1}^{N} \overset{ij}{A}_{nn} \overset{j}{P}_n \end{aligned}\right\} \quad i = 1 \text{ to } N \tag{4.23}$$

which is a system of 2N simultaneous linear equations with as many unknowns. $\overset{j}{P}_s$ and $\overset{j}{P}_n$ are fictitious quantities introduced to find the numerical solution of the problem and have no physical meaning. Once (4.23) has been solved, the displacements and stresses at any point in the body can be found.

The method to solve the problem consists of five separate steps, namely:

(1) Define the locations of all boundary elements and specify displacement or stress boundary conditions for each one.

(2) Compute the boundary influence coefficients, and set up the appropriate system of simultaneous linear equations by considering the boundary conditions at each element.

(3) Solve the system of equations from step 2.

(4) Compute the displacements and stresses at each boundary element.

(5) Compute the influence coefficients for specified points within the region of interest, and hence compute the displacements and stresses at these points.

4.4 THE DISPLACEMENT DISCONTINUITY METHOD (DDM)

In many rock mechanics problems, thin, slit-like openings or cracks are involved. Because of the effects of elements placed along one crack surface are indistinguishable from the effect of elements placed along the other side, the fictitious stress method can not be used to solve this kind of problem. Another method, the displacement discontinuity method (DDM), was developed to solve this type of problem. This method is based on the analytical solution to the problem of a constant discontinuity displacement over a finite segment in the *x, y* plane of an infinite elastic solid.

4.4.1 Displacement discontinuity in an infinite solid

The problem of a constant displacement discontinuity over a finite line segment in the *x, y* plane of an infinite elastic solid is specified by the condition that the displacements must be continuous everywhere except over the line segment in question. The line segment may be chosen to occupy a certain portion of the *x* axis, such as $|x| \leq a, \quad y = 0$. If this segment is considered as a crack, the two surfaces can be distinguished as one being on the positive side of $y = 0$ ($y = 0_+$), and the other on the negative side ($y = 0_-$). From one side to the other, the displacements undergo a constant specified change in value $D_i = \left(D_x, D_y\right)$. The displacement discontinuity D_i can be defined as the difference in displacement between the two sides of the segment such as:

$$D_i = u_i\left(x_1, 0_-\right) - u_i\left(x_1, 0_+\right) \tag{4.24}$$

or

$$\begin{aligned} D_x &= u_x(x, 0_-) - u_x(x, 0_+) \\ D_y &= u_y(x, 0_-) - u_y(x, 0_+) \end{aligned} \tag{4.25}$$

Since u_x and u_y are positive in the positive *x* and *y* coordinate directions, D_x and D_y are positive as shown in Figure 4.5. It should be noted that with this formulation, there can be an overlap of surface ($D_y > 0$) which is physically impossible.

The solution to the problem was given by Crouch (1976a, b). The displacements and stresses can be written as:

$$\begin{aligned} u_x &= D_x\left[2(1-\nu)f_{,y} - yf_{,xx}\right] + D_y\left[-(1-2\nu)f_{,x} - yf_{,xy}\right] \\ u_y &= D_x\left[(1-2\nu)f_{,x} - yf_{,xy}\right] + D_y\left[2(1-\nu)f_{,y} - yf_{,yy}\right] \end{aligned} \tag{4.26}$$

and

$$\begin{aligned} \sigma_{xx} &= 2G\left(D_x\left[2f_{,xy} + yf_{,xyy}\right] + D_y\left[f_{,yy} + yf_{,yyy}\right]\right) \\ \sigma_{yy} &= 2G\left(D_x\left[-yf_{,xyy}\right] + D_y\left[f_{,yy} - yf_{,yyy}\right]\right) \\ \sigma_{xy} &= 2G\left(D_x\left[f_{,yy} + yf_{,yyy}\right] + D_y\left[-yf_{,xyy}\right]\right) \end{aligned} \tag{4.27}$$

where f(x, y) is the same as in Equation (4.19):

$$f(x,y) = \frac{-1}{4\pi(1-\nu)}\left[\begin{aligned} & y\left(\arctan\left(\frac{y}{x-a}\right) - \arctan\left(\frac{y}{x+a}\right)\right) - (x-a)\ln\sqrt{\left[(x-a)^2 + y^2\right]} \\ & + (x+a)\ln\sqrt{\left[(x+a)^2 + y^2\right]} \end{aligned}\right]$$

The derivatives of the function are given by Equation (4.20). The third-order derivatives are:

$$
\begin{aligned}
f_{,xyy} &= -f_{,xxx} = \frac{1}{4\pi(1-\nu)}\left[\frac{(x-a)^2 - y^2}{\{(x-a)^2 + y^2\}^2} - \frac{(x+a)^2 - y^2}{\{(x+a)^2 + y^2\}^2}\right] \\
f_{,yyy} &= -f_{,xxy} = \frac{2y}{4\pi(1-\nu)}\left[\frac{x-a}{\{(x-a)^2 + y^2\}^2} - \frac{x+a}{\{(x+a)^2 + y^2\}^2}\right]
\end{aligned} \tag{4.28}
$$

4.4.2 Numerical procedure for the DDM

The numerical procedure for the DDM is illustrated in Figure 4.6. The crack presented here is curved, but it is assumed that it can be represented with sufficient accuracy by N straight line segments, joined end to end. If the crack surfaces are subjected to stress, there will be a relative displacement from one face to the other. The DDM is a way of finding a discrete approximation to the smooth distribution of the real relative displacement. Each subdivision in Figure 4.6a is a boundary element and represents an elemental displacement discontinuity. Each element is defined with respect to local coordinates *s* and *n*. Figure 4.6b shows a single elemental displacement discontinuity at the j^{th} segment of the crack. The discontinuity components are denoted $\overset{j}{D}_s$ and $\overset{j}{D}_n$ and are defined by:

$$
\begin{aligned}
\overset{j}{D}_s &= \overset{j}{u}_s^- - \overset{j}{u}_s^+ \\
\overset{j}{D}_n &= \overset{j}{u}_n^- - \overset{j}{u}_n^+
\end{aligned} \tag{4.29}
$$

where $\overset{j}{u}_s$ and $\overset{j}{u}_n$ are the shear and normal displacement of the j^{th} segment of the crack, with reference to the positive and negative crack surfaces. These local displacements are the two components of a vector, and they are positive in the positive direction of *s* and *n*. Then, $\overset{j}{D}_n$ is positive if the crack surfaces displace toward one another (closure). $\overset{j}{D}_s$ is positive if the positive surface moves to the left (or *s* negative) with respect to the negative surface. These are best illustrated on Figure 4.6b, where the displacements are positive.

The shear and normal stresses at midpoint of the i^{th} element in Figure 4.6b can be expressed in terms of displacement discontinuity components at the j^{th} element as follows:

$$\left.\begin{aligned} \overset{i}{\sigma}_s &= \sum_{j=1}^{N} \overset{ij}{A}_{ss} \overset{j}{D}_s + \sum_{j=1}^{N} \overset{ij}{A}_{sn} \overset{j}{D}_n \\ \overset{i}{\sigma}_n &= \sum_{j=1}^{N} \overset{ij}{A}_{ns} \overset{j}{D}_s + \sum_{j=1}^{N} \overset{ij}{A}_{nn} \overset{j}{D}_n \end{aligned}\right\} \quad i = 1 \text{ to } N \qquad (4.30)$$

where $\overset{ij}{A}_{ss}$ etc., are the boundary stress influence coefficients for the problem. The coefficient $\overset{ij}{A}_{ns}$, for example, gives the normal stress at the midpoint of the i^{th} segment ($\overset{i}{\sigma}_n$) due to a constant unit shear displacement discontinuity over the j^{th} segment ($\overset{j}{D}_s = 1$).

When the stress values are specified for each element of the cracks, then Equations (4.30) are a system of 2N simultaneous linear equations with 2N unknowns, namely the elemental displacement discontinuity components $\overset{i}{D}_s$ and $\overset{i}{D}_n$ for i = 1 to N. When the equations above have been solved, the displacements and stresses at designated points in the body can be found by using the principle of superposition. The displacements along the cracks in Figure 4.6a are given by:

$$\left.\begin{aligned} \overset{i}{u}_s &= \sum_{j=1}^{N} \overset{ij}{B}_{ss} \overset{j}{D}_s + \sum_{j=1}^{N} \overset{ij}{B}_{sn} \overset{j}{D}_n \\ \overset{i}{u}_n &= \sum_{j=1}^{N} \overset{ij}{B}_{ns} \overset{j}{D}_s + \sum_{j=1}^{N} \overset{ij}{B}_{nn} \overset{j}{D}_n \end{aligned}\right\} \quad i = 1 \text{ to } N \qquad (4.31)$$

where $\overset{ij}{B}_{ss}$ etc., are the boundary displacement influence coefficients for the problem.

4.5 APPLICATION OF THE BEM TO ROCK MECHANICS

Problems in rock mechanics usually imply bodies that are subjected to an initial state of stress, contrary to most problems in applied mechanics. Before an excavation is created, the rock mass is subjected to initial stress due to the gravity, the Poisson effect, and tectonics. When an opening is created, the initial stress state is disturbed. The total stresses σ_{ij} at any point in the rock mass can then be represented as the sum of the initial stresses $(\sigma_{ij})_0$ and the induced stresses σ'_{ij} due to the opening:

$$\sigma_{ij} = \left(\sigma_{ij}\right)_0 + \sigma'_{ij} \tag{4.32}$$

The displacements can also be represented in the same manner:

$$u_i = \left(u_i\right)_0 + u'_i \tag{4.33}$$

Usually the initial displacements $(u_i)_0$ are considered nil, so the total and induced displacements are the same.

This kind of problems involving underground excavations in rock masses can be solved in three steps:

(1) Postulate the initial state of stress;

(2) Define and solve the induced stress boundary value problem;

(3) Add the induced stresses to the initial stresses to find the total stresses in the rock.

This method of superposition is valid when the material is linear elastic. The definition of the induced stress boundary value problem is eased by the introduction of the concepts of initial tractions $(t_i)_0$, induced tractions t'_i and total tractions t_i. For a plane with outward normal n_j, the relationships between tractions and stresses are:

$$t_i = \sigma_{ji} n_j$$
$$\left(t_i\right)_0 = \left(\sigma_{ji}\right)_0 n_j \qquad (4.34)$$
$$t'_i = \sigma'_{ji} n_j$$

then:

$$t_i = \left(t_i\right)_0 + t'_i \qquad (4.35)$$

and

$$t'_i = t_i - \left(t_i\right)_0 \qquad (4.36)$$

Equation (4.36) is used to specify traction boundary conditions for the induced stress problem. Once the boundary conditions have been defined, the induced stress problem can be solved.

4.5.1 Elastic joint elements

For modeling purposes, a joint can be considered as a long, thin crack with a compressible filling. A segment of the joint can then be modeled as an elemental displacement discontinuity whose opposite surfaces are connected by a spring, with the normal and shear stiffnesses of the spring chosen to be representative of the properties of the joint-filling material. The values of the displacement discontinuity components at a joint element will then be related to the normal and shear stresses acting on the element.

This method assumes that the element obeys simple one-dimensional stress-strain relations for compression and shear. These relations are illustrated on Figure 4.7. A single joint element is represented with two degrees of freedom, and its thickness *h* is considered small compared to its length. Stresses shown here are total stresses, and hence, the deformations of the joint must be considered in two parts, initial and induced. If it is assumed that the initial deformations are zero and that the joint element deforms only in response to the induced stresses σ'_{yy} and σ'_{xy}, then the induced normal and shear strain are given from Equation (4.2):

$$\varepsilon'_{yy} = \frac{\partial u'_y}{\partial y}$$
$$\varepsilon'_{xy} = \frac{1}{2}\left(\frac{\partial u'_x}{\partial y} + \frac{\partial u'_y}{\partial x}\right)$$

If it is assumed that the element is compressed by a constant amount along the *x* direction, then $\partial u'_y / \partial x = 0$ and the equation can be rewritten:

$$\begin{aligned} \varepsilon'_{yy} &= \frac{u'_y(x, h/2) - u'_y(x, -h/2)}{h} \\ \varepsilon'_{xy} &= \frac{u'_x(x, h/2) - u'_x(x, -h/2)}{2h} \end{aligned} \tag{4.37}$$

When h is small, the numerators of (4.37) are equivalent to displacement discontinuity components $-D'_y$ and $-D'_x$ so that the displacements are given by:

$$\begin{aligned} \varepsilon'_{yy} &= -\frac{D'_y}{h} \\ \varepsilon'_{xy} &= -\frac{D'_x}{2h} \end{aligned} \tag{4.38}$$

If the joint filling behaves in a linear elastic fashion with Young's modulus E_0 and shear modulus G_0, then the induced normal and shear stresses and strain are related as follows:

$$\begin{aligned} \sigma'_{yy} &= E_0 \varepsilon'_{yy} = -E_0 \frac{D'_y}{h} \\ \sigma'_{xy} &= 2G_0 \varepsilon'_{xy} = -G_0 \frac{D'_x}{h} \end{aligned} \tag{4.39}$$

which can be written in function of the *n* and *s* coordinate system:

$$\sigma'_n = -E_0 \frac{D'_n}{h}$$
$$\sigma'_s = -G_0 \frac{D'_s}{h} \tag{4.40}$$

or

$$\sigma'_n = -k_n D'_n$$
$$\sigma'_s = -k_s D'_s \tag{4.41}$$

where k_n and k_s are the normal and shear stiffnesses of the spring of Figure 4.7.

4.5.2 Numerical procedure for rock mechanics problems

The previous results can be used to model problems in rock mechanics. For example, consider the problem of an underground excavation intersected by a joint. The excavation boundary can be modeled by fictitious stress elements and the joint by the special compressible displacement discontinuity elements. If there are *N* elements altogether, with *M* fictitious stress elements and *N-M* displacement discontinuity elements, then the induced stresses at any element are given by:

$$\overset{i}{\sigma'}_s = \sum_{j=1}^{M} (\overset{ij}{A}_{ss} \overset{j}{P}_s + \overset{ij}{A}_{sn} \overset{j}{P}_n) + \sum_{j=M+1}^{N} (\overset{ij}{A}_{ss} \overset{j}{D'}_s + \overset{ij}{A}_{sn} \overset{j}{D'}_n)$$
$$\overset{i}{\sigma'}_n = \sum_{j=1}^{M} (\overset{ij}{A}_{ns} \overset{j}{P}_s + \overset{ij}{A}_{nn} \overset{j}{P}_n) + \sum_{j=M+1}^{N} (\overset{ij}{A}_{ns} \overset{j}{D'}_s + \overset{ij}{A}_{nn} \overset{j}{D'}_n) \tag{4.42}$$

where $\overset{ij}{A}_{ss}$, etc., are the boundary influence coefficients. The total stresses at element *i* are obtained by adding the initial stresses and the induced stresses. The first 2M equations in the system are then given by:

$$\left.\begin{aligned} -(\overset{i}{\sigma}_s)_0 &= \sum_{j=1}^{N}(\overset{ij}{A}_{ss}\overset{j}{X}_s + \overset{ij}{A}_{sn}\overset{j}{X}_n) \\ -(\overset{i}{\sigma}_n)_0 &= \sum_{j=1}^{N}(\overset{ij}{A}_{ns}\overset{j}{X}_s + \overset{ij}{A}_{nn}\overset{j}{X}_n) \end{aligned}\right\} 1 \le i \le M \tag{4.43}$$

and the remaining 2(N-M) equations are given by combining (4.41) and (4.42):

$$\left.\begin{aligned} 0 &= \overset{i}{k}_s \overset{i}{X}_s + \sum_{j=1}^{N}(\overset{ij}{A}_{ss}\overset{j}{X}_s + \overset{ij}{A}_{sn}\overset{j}{X}_n) \\ 0 &= \overset{i}{k}_n \overset{i}{X}_n + \sum_{j=1}^{N}(\overset{ij}{A}_{ns}\overset{j}{X}_s + \overset{ij}{A}_{nn}\overset{j}{X}_n) \end{aligned}\right\} M+1 \le i \le N \tag{4.44}$$

where
$$\begin{aligned} &\overset{j}{X}_n = \overset{j}{P}_n \quad \text{and} \quad \overset{j}{X}_s = \overset{j}{P}_s \quad \text{for} \quad 1 \le j \le M \\ &\overset{j}{X}_n = \overset{j}{D}'_n \quad \text{and} \quad \overset{j}{X}_s = \overset{j}{D}'_s \quad \text{for} \quad M+1 \le j \le N \end{aligned} \tag{4.45}$$

These equations can be solved by standard numerical methods.

In the precedent equations, it was assumed that no deformations occurred on the joint before the creation of the excavation. However, the initial stress field may have been distorted before the creation of the opening, due to deformation of the joint (or fault) in geological time under the action of the far-field stresses. Assuming that this possibility exists, then the initial stress would include induced components due to initial fault deformations. Then:

$$(\sigma_{ij})_0 = (\sigma_{ij})_0^\infty + (\sigma'_{ij})_0 \tag{4.46}$$

where $(\sigma_{ij})_0^\infty$ are the far-field stresses and $(\sigma'_{ij})_0$ are the initial induced stresses. Similarly, the initial displacements are given by:

$$(u_i)_0 = (u_i)_0^\infty + (u'_i)_0 \tag{4.47}$$

where $(u'_i)_0$ are the initial induced displacements due to initial fault or joint deformations, and $(u_i)_0^\infty$ are assumed to be zero.

The total initial stresses at element *i* are then given by:

$$\begin{aligned} \overset{i}{(\sigma_s)_0} &= -\overset{i}{k_s}\overset{i}{(D_s)_0} \\ \overset{i}{(\sigma_n)_0} &= -\overset{i}{k_n}\overset{i}{(D_n)_0} \end{aligned} \qquad (4.48)$$

and the initial induced stresses at element *i* are given by:

$$\begin{aligned} \overset{i}{(\sigma'_s)_0} &= \sum_{j=1}^{N}[\overset{ij}{A_{ss}}\overset{i}{(D_s)_0} + \overset{ij}{A_{sn}}\overset{i}{(D_n)_0}] \\ \overset{i}{(\sigma'_n)_0} &= \sum_{j=1}^{N}[\overset{ij}{A_{ns}}\overset{i}{(D_s)_0} + \overset{ij}{A_{nn}}\overset{i}{(D_n)_0}] \end{aligned} \qquad (4.49)$$

Combining these last equations leads to:

$$\left.\begin{aligned} -\overset{i}{(\sigma_s)_0^\infty} &= \overset{i}{k_s}\overset{i}{(D_s)_0} + \sum_{j=1}^{N}[\overset{ij}{A_{ss}}\overset{i}{(D_s)_0} + \overset{ij}{A_{sn}}\overset{i}{(D_n)_0}] \\ -\overset{i}{(\sigma_n)_0^\infty} &= \overset{i}{k_n}\overset{i}{(D_s)_0} + = \sum_{j=1}^{N}[\overset{ij}{A_{ns}}\overset{i}{(D_s)_0} + \overset{ij}{A_{nn}}\overset{i}{(D_n)_0}] \end{aligned}\right\} \quad \text{for } i = 1 \text{ to } N \quad (4.50)$$

The stresses $\overset{i}{(\sigma_s)_0^\infty}$ and $\overset{i}{(\sigma_n)_0^\infty}$ are known, or postulated so this brings a system of 2N equations to find the joint deformations. The initial induced stresses and displacements at any point in the rock mass can be computed in the usual way, and Equations (4.46) and (4.47) are used to specify the values of $(\sigma_{ij})_0$ and $(u_i)_0$ at these points.

4.5.3 Mohr-Coulomb elements

It was assumed in the previous section that the filling is behaving as linear elastic. In reality, joints often behave inelastically. To include inelastic deformations, one can impose a constraint such as:

$$|\overset{i}{\sigma_s}| \leq \overset{i}{c} + (-\overset{i}{\sigma_n})\tan\overset{i}{\phi} \tag{4.51}$$

where $\overset{i}{c}$ and $\overset{i}{\phi}$ are the cohesion and angle of friction of the fill material. A joint element subjected to such a constraint is called a Mohr-Coulomb element. This type of element will behave like a joint element but the total shear stress can not exceed the value specified by Equation (4.51). This means that elements are allowed to undergo a certain amount of inelastic deformations or permanent slip.

As it was shown in Chapter 3, slip along a joint is a non-linear, path-dependent phenomenon. Thus, it must be modeled by an incremental process. One problem arises however, because, in rock mechanics, the load does not start from zero toward the final load value, but rather starts from a certain value and then reaches its final value. One way to take this into account, is to model the creation of the excavation by incrementally relaxing the boundary tractions from their initial value to zero.

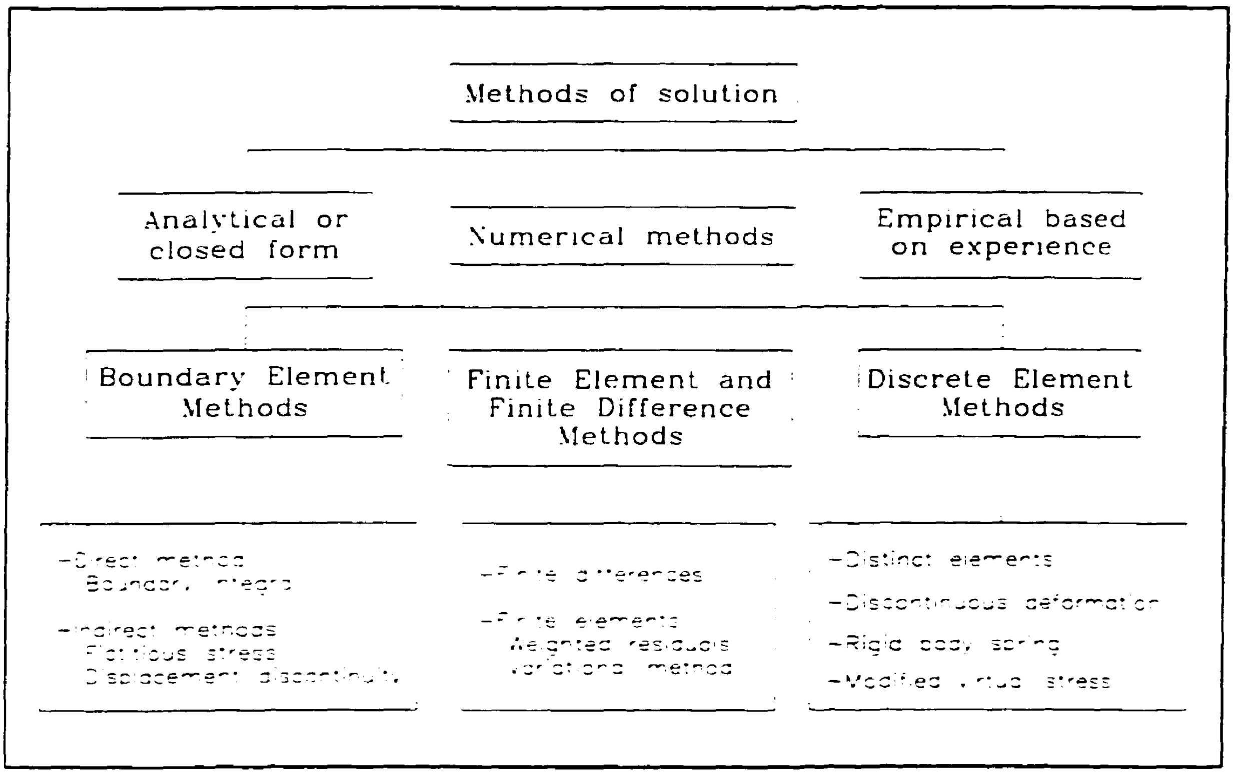

Figure 4.1a: **Solution of geotechnical problem by numerical methods (adapted from Desai and Christian, 1977)**

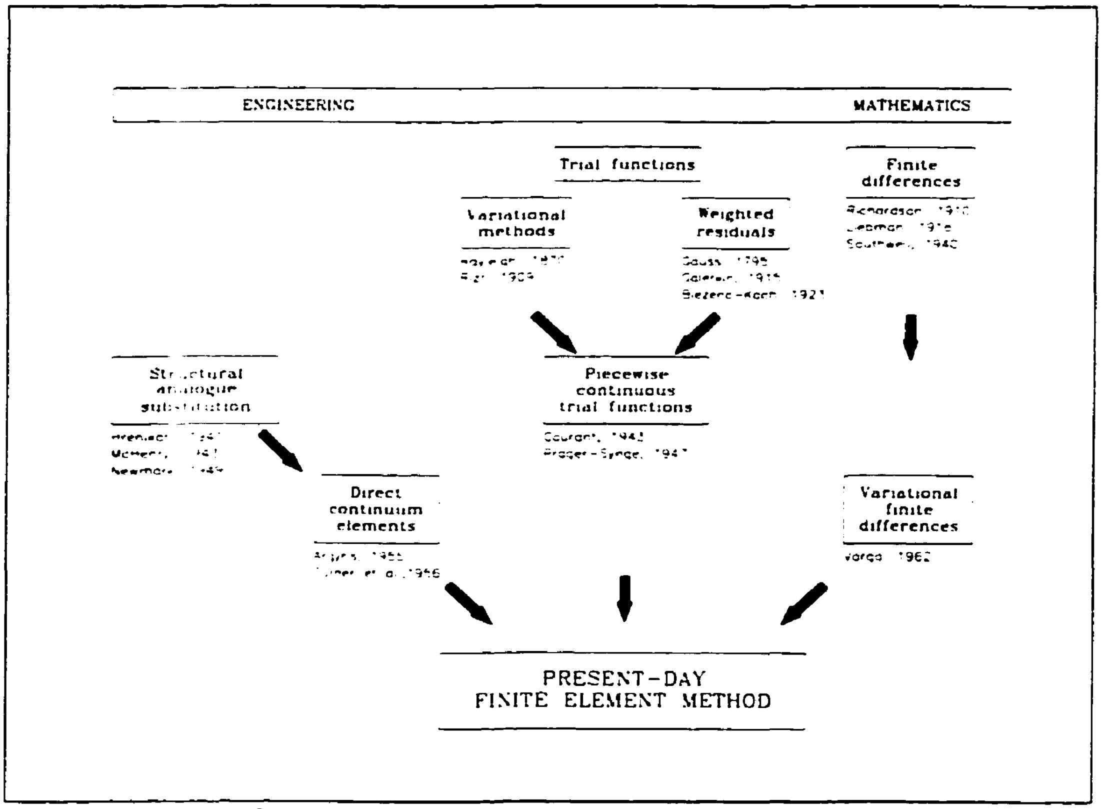

Figure 4.1b: Process of evolution which led to the present-day concepts of finite element analysis (after Zienkiewicz and Taylor, 1989).

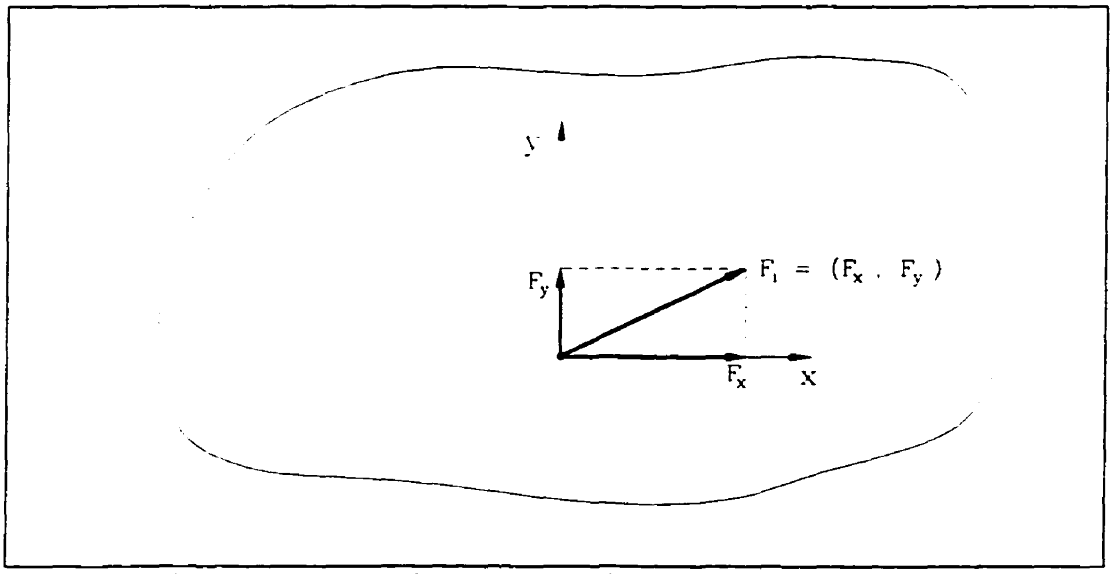

Figure 4.2: Kelvin's problem of a force F_i applied in an infinite elastic solid in plane strain (after Crouch and Starfield, 1983).

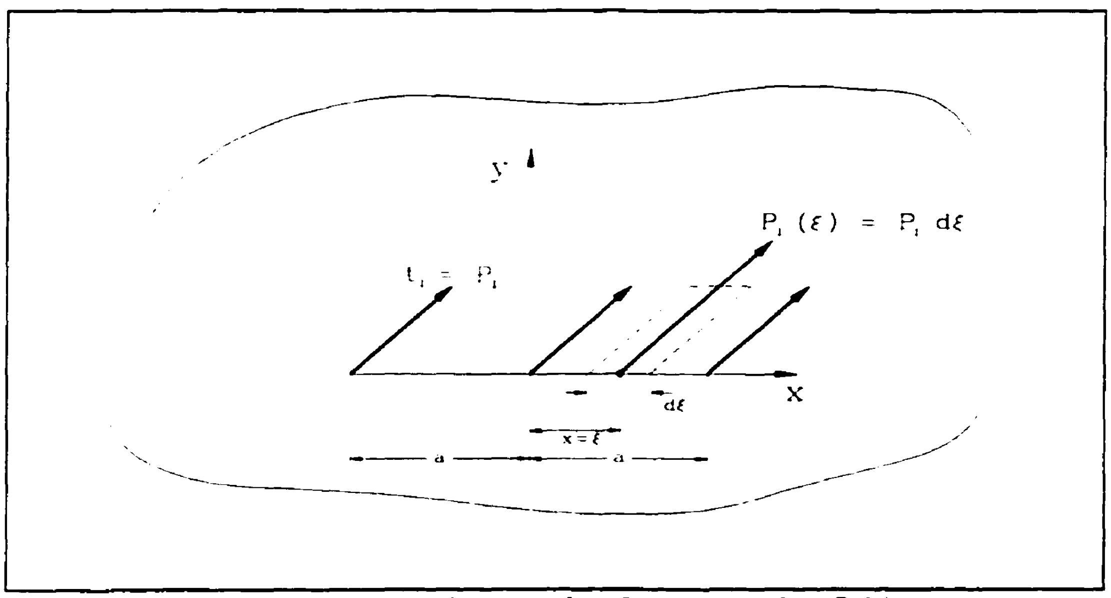

Figure 4.3: Integration of Kelvin's solution (after Crouch and Starfield, 1983).

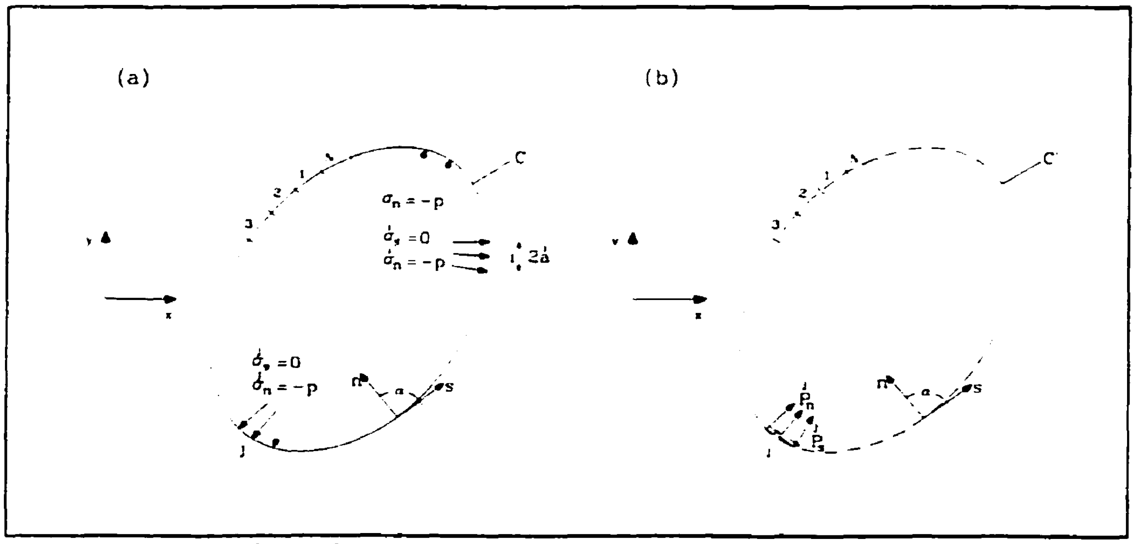

Figure 4.4: The boundary element method for a cavity problem. (a) Physical problem; (b) Numerical model (after Crouch and Starfield, 1983).

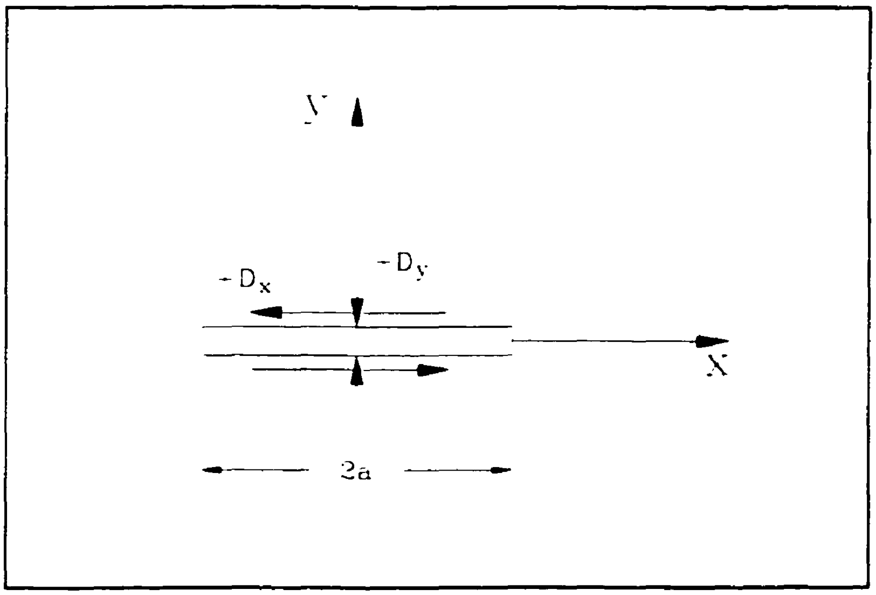

Figure 4.5: The constant displacement discontinuity components D_x and D_y (after Crouch and Starfield, 1983).

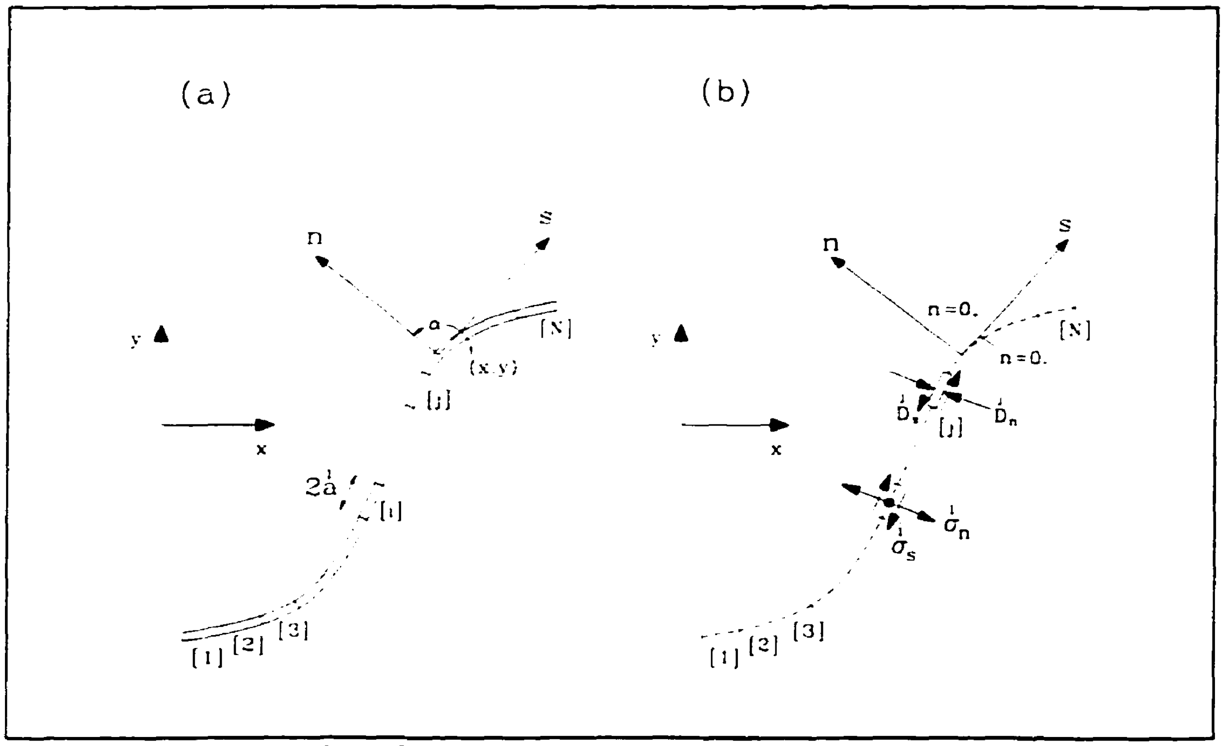

Figure 4.6: Representation of a crack by N elemental displacement discontinuities (after Crouch and Starfield, 1983).

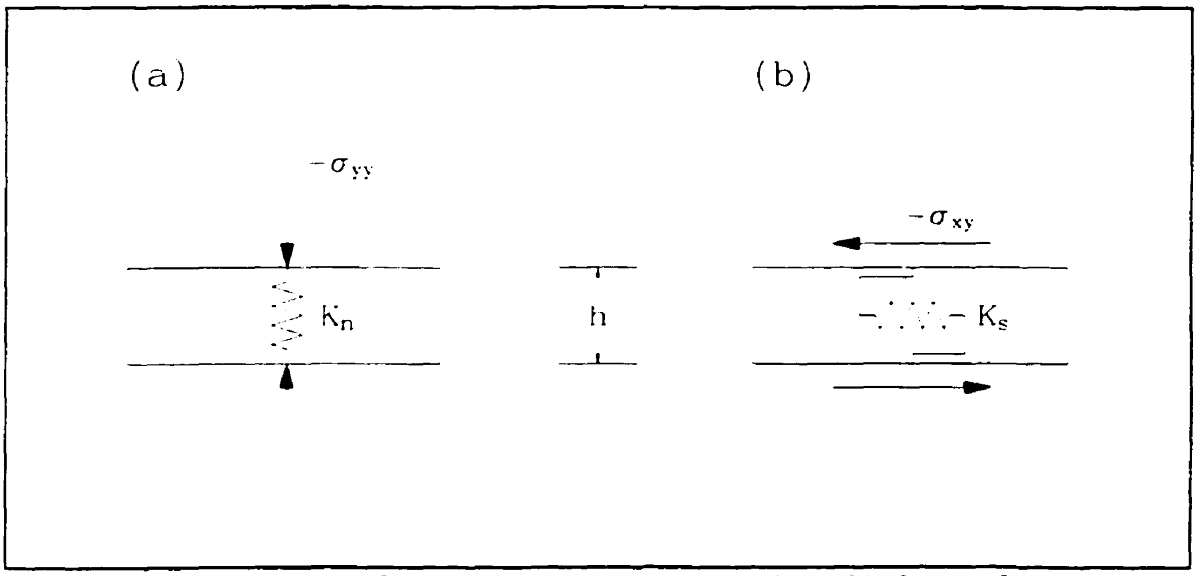

Figure 4.7: Representation of a joint element (a) compression; (b) shear (after Crouch and Starfield, 1983).

CHAPTER 5

DEVELOPMENT OF A NON-LINEAR CONSTITUTIVE MODEL FOR ROCK JOINTS AND FAULTS

5.1 INTRODUCTION

As it was shown in section 3.6, the fault-slip phenomenon can be explained by comparing the post-peak behavior of the joint and the stiffness of the loading system. Thus, it is essential for the constitutive model used to follow as closely as possible the post-peak behavior of the joint. A good progress in that domain was given with the model of Saeb-Amadei presented in Chapter 3. However, in cases of strain softening, this model cannot always follow the non-linear behavior of the joint, especially when the normal stress is constant. Figure 5.1 illustrates the limitations of the Saeb-Amadei model in situations of strain softening.

From Figure 5.1a, one can see that the Saeb-Amadei becomes a linear model when the normal stress stays constant. Since it is the strain softening behavior that may cause unstable slip along a discontinuity, there was a need to develop a model that could follow the non-linear behavior of the joint.

5.2 DEVELOPMENT OF A NEW NON-LINEAR CONSTITUTIVE MODEL

5.2.1 Shear stress-shear displacement relationship

To obtain a non-linear relation, several formulations could be used. The formulation chosen here has the general form of:

$$F(u) = \tau = a + b\exp(-c\,u) - d\exp(-e\,u) \tag{5.1}$$

where τ is the shear stress in MPa, u is the shear displacement in mm and a to e are the model parameter with the condition of $c < e$ (a, b, c, d, e >0). A mathematically similar stress formulation was proposed by Chapuis (1990) for granular materials. This formulation is based on a statistical approach to relate deformation to the transformation of the internal structure (Chapuis, 1990). Figure 5.2 shows the type of curve that can be obtained from Equation 5.1.

From Equation 5.1, some conclusions can be drawn. At u=0, the shear stress must be nil, so one can write:

$$F(0) = a + b\exp(-c \bullet 0) - d\exp(-e \bullet 0) = 0 \tag{5.2}$$

or $$a + b = d \tag{5.3}$$

At large displacement $u \gg 0$, the residual strength (τ_r) must be attained and Equation 5.1 leads to:

$$F(u \gg 0) = \tau_r \cong a \tag{5.4}$$

thus $$a = \tau_r \tag{5.5}$$

Moreover, since $a = \tau_r$, we must have at u_r:

$$F(u_r) = a + b\exp(-c \bullet u_r) - d\exp(-e \bullet u_r) = \tau_r \tag{5.6}$$

then $$b\exp(-cu_r) - d\exp(-eu_r) = \tau_r - a = 0 \tag{5.7}$$

To properly capture the τ-u curve, one must impose that c<e, so the exponential of (-e u_r) will tend toward zero much faster than the exponential of (-c u_r). From several curves shown in Appendix, it appears that 0.07 can be considered a small enough value of the exponential (in a first approximation) to be considered negligible, then we obtain:

$$\exp(-cu_r) \cong 0.07 \tag{5.8}$$

and $$c \approx 5/u_r \tag{5.9}$$

The general equation can then be rewritten by:

$$\begin{aligned}\tau &= a + b\exp(-cu) - d\exp(-eu)\\ &= \tau_r + [d - \tau_r]\exp\left(-\frac{5u}{u_r}\right) - d\exp(-eu)\\ &= \tau_r\left[1 - \exp\left(-\frac{5u}{u_r}\right)\right] + d\left[\exp\left(-\frac{5u}{u_r}\right) - \exp(-e\,u)\right]\end{aligned} \tag{5.10}$$

At the peak displacement u_p, we have a maximum of the function (peak strength). The derivative of F(u) is given by:

$$\frac{\partial F(u)}{\partial u} = -\frac{5}{u_r}(d - \tau_r)\exp\left(-\frac{5u}{u_r}\right) + de\exp(-e\,u) \tag{5.11}$$

If we have a maximum of the function at u_p, then the derivative must equal zero and:

$$\left.\frac{\partial F(u)}{\partial u}\right|_{u=u_p} = -\frac{5}{u_r}(d - \tau_r)\exp\left(-\frac{5u_p}{u_r}\right) + de\exp(-e\,u_p) = 0 \tag{5.12}$$

$$\frac{5}{u_r}(d - \tau_r)\exp\left(-\frac{5u_p}{u_r}\right) = de\exp(-e\,u_p) \tag{5.13}$$

$$\frac{d\,e\,u_r}{5\,(d-\tau_r)} = \frac{\exp\left(-\dfrac{5u_p}{u_r}\right)}{\exp(-eu_p)} = \exp\left[u_p\left(e-\frac{5}{u_r}\right)\right] \tag{5.14}$$

$$\frac{d\,e\,u_r}{5\,(d-\tau_r)} - \exp\left[u_p\left(e-\frac{5}{u_r}\right)\right] = 0 \tag{5.15}$$

At peak displacement, $F(u_p)$ must be equal to the peak strength τ_p:

$$F(u_p) = a + b\exp(-c \bullet u_p) - d\exp(-e \bullet u_p) = \tau_p \tag{5.16}$$

$$\tau_p = \tau_r\left[1-\exp\left(-\frac{5u_p}{u_r}\right)\right] + d\left[\exp\left(-\frac{5u_p}{u_r}\right) - \exp(-eu_p)\right] \tag{5.17}$$

thus $$\tau_p - \tau_r\left[1-\exp\left(-\frac{5u_p}{u_r}\right)\right] - d\left[\exp\left(-\frac{5u_p}{u_r}\right) - \exp(-eu_p)\right] = 0 \tag{5.18}$$

or $$d = \frac{\tau_p - \tau_r\left[1-\exp\left(-\dfrac{5u_p}{u_r}\right)\right]}{\exp\left(-\dfrac{5u_p}{u_r}\right) - \exp(-eu_p)} \tag{5.19}$$

We then have two non-linear equations (5.15 and 5.18) to solve to find the unknown parameters d and e. This set of non-linear equations can be solved by standard iterative methods (e.g., Gerald and Wheatley, 1989). However, proper care must be taken when solving Equation 5.15 because it has two roots of e, one being lower than c. Then one root violates the initial condition ($c < e$). Figure 5.3 shows Equation 5.15 given as a function F(e).

To solve Equations 5.15 and 5.18, the Newton method can be used (e.g., Gerald and Wheatley, 1989). First, an initial value of d (d_{init}) is obtained by the following procedure. If e >> c, then Equation 5.17 can be reduced to:

$$\tau_p - a[1-\exp(-cu_p)] - d[\exp(-cu_p)] \approx 0 \qquad (5.20)$$

then $$d_{init} = \frac{\tau_p - a[1-\exp(-cu_p)]}{\exp(-cu_p)} = \frac{\tau_p - \tau_r\left[1-\exp\left(-\frac{5u_p}{u_r}\right)\right]}{\exp\left(-\frac{5u_p}{u_r}\right)} \qquad (5.21)$$

which leads to a first approximation of d. This approximation is then used to solve Equation 5.15. The Newton's method to solve non-linear equations is given by (Gerald and Wheatley, 1989):

$$x_{i+1} = x_i - \frac{f(x_i)}{f'(x_i)} \qquad (5.22)$$

where x_{i+1} is the value of the next step and x_i is the value obtained for the previous step. This method is known to converge rapidly, once an initial value is given to start the process. It could be shown that the root to which the method will converge depends of the initial value of x. As we can see on Figure 5.3, F(e) passes through a maximum before getting to the wanted root (the larger one). Then, if the initial value used for e is larger than the value of e at the maximum, the method will always converge towards the larger root. Hence, the initial value of e (let it be e_{init}) must be larger than e_p, the value at the maximum of F(e). We know that the derivative of F(e) at e_p will equal zero, then from Equation 5.14 we get:

$$\frac{\partial F(e)}{\partial e} = \frac{d}{bc} - u_p \exp[u_p(e-c)] = 0 \qquad (5.23)$$

The solution leads to e_p:

$$e_p = \frac{\ln\left(\dfrac{d}{bcu_p}\right)}{u_p} + c \tag{5.24}$$

Since e_{init} must be larger than e_p, if we add one unit to e_p, we get an initial value that will always converge towards the wanted root:

$$e_{init} = \frac{\ln\left(\dfrac{d}{bcu_p}\right)}{u_p} + c + 1 \tag{5.25}$$

Then, using Equation 5.22, we get:

$$e_{i+1} = e_i - \frac{de_i / bc - \exp[u_p(e_i - c)]}{d / bc - u_p \exp[u_p(e_i - c)]} \tag{5.26}$$

The model can also be expressed in an incremental formulation with

$$k_{ss} = \frac{\partial \tau}{\partial u} = de\exp(-e\,u) - bc\exp(-c\,u) \tag{5.27}$$

$$k_{sn} = \frac{\partial \tau}{\partial v} = 0 \tag{5.28}$$

Then $\quad d\tau = k_{sn}dv + k_{ss}du = k_{ss}du \qquad (5.29)$

The different terms of the model are summarized in Table 5.1.

Table 5.1: Parameters terms of the new model

Parameter	Value	Condition
a	τ_r	
b	d-a	
c	$5/u_r$	$c < e$
Non-linear equations to be solved		
$$d = \frac{\tau_p - a[1-\exp(-cu_p)]}{\exp(-cu_p)-\exp(-eu_p)} = \frac{\tau_p - \tau_r\left[1-\exp\left(-\frac{5u_p}{u_r}\right)\right]}{\exp\left(-\frac{5u_p}{u_r}\right)-\exp(-eu_p)}$$ with $d_{init} = \frac{\tau_p - a[1-\exp(-cu_p)]}{\exp(-cu_p)} = \frac{\tau_p - \tau_r\left[1-\exp\left(-\frac{5u_p}{u_r}\right)\right]}{\exp\left(-\frac{5u_p}{u_r}\right)}$		
$$\frac{de}{bc} - \exp[u_p(e-c)] = 0$$ with $e_{init} = \frac{\ln\left(\frac{d}{bcu_p}\right)}{u_p} + c + 1$		

As it can be seen in Table 5.1, all the model parameters can be determined from four joint parameters easily determined in laboratory, which are the peak and residual strength (τ_p, τ_r) and the peak and residual displacement (u_p, u_r). The peak strength can be determined from any peak strength criterion such as the Ladanyi-Archambault model as modified by Saeb (1990) and given by Equation 3.15. The residual strength is then given by Equation 3.50. Both peak and residual displacements are considered to be constants for a given joint. The residual displacement is considered to be the displacement at which the dilatancy level remains constant. If Equations 3.15 and 3.50 are used to define the strengths, then the model parameters are defined from these joint physical parameters:

B_0: ratio of the residual to peak strength at very low normal stress ($0 \leq B_0 \leq 1$)

i_o: average angle of the asperities

S_0: cohesion of the rock walls (using a Mohr-Coulomb criterion)

u_p: displacement at peak strength

u_r: displacement at residual strength (displacement at which dilatancy stops)

ϕ_0: friction angle of the rock walls (using a Mohr-Coulomb criterion)

ϕ_u: friction angle of the joint

σ_n: applied normal stress

σ_T: brittle-ductile transition stress for the asperities (usually taken as the uniaxial compressive strength)

Finally, the model can be expressed by:

$$\tau = \tau_r + [d - \tau_r]\exp\left(-\frac{5u}{u_r}\right) - d\exp(-eu) \tag{5.30}$$

Figure 5.4 shows the comparison between the model and a few laboratory test results under constant normal stress. As it can be seen on Figure 5.4, the model shows a good correlation with the data. In all, 27 curves were plotted to evaluate the correlation with data taken from literature (other curves are given in the appendix). These comparisons showed a correlation factor (R^2) of 0.900 (a factor of 1.0 gives an exact correlation). Moreover, the Saeb-Amadei model gave a correlation factor of 0.739, which demonstrates clearly that the new model can follow more closely the behavior of the joint under constant normal stress, especially in the post-peak region.

5.2.2 Normal displacement - shear displacement relationship

An exponential formulation can also be used to describe the normal displacement (v) - shear displacement (u) relationship. This relationship can be given in the form:

$$v = \beta_1 + \beta_2 \exp(-\beta_3 u) - \beta_4 \exp(-\beta_5 u) \tag{5.31}$$

where v is the normal displacement, u is the shear displacement and β_1 to β_5 are model parameters. Figure 5.5 shows the type of curve that can be obtained with such a formulation as well as the curve obtained from the Saeb-Amadei model (Equation 3.28). However, it is sometimes difficult to relate all the parameters of Equation (5.31) to physical parameters that can be easily obtained through standard laboratory tests. For such reason, a simpler form of the relation is adopted (neglecting initial closure of joints):

$$v = \beta_1 - \beta_2 \exp(-\beta_3 u) \tag{5.32}$$

The parameters β_1 to β_3 can be determined from the following. From this formulation, we get at u = 0 (no shear displacement):

$$\begin{aligned} v &= \beta_1 - \beta_2 \exp(-\beta_3 * 0) \\ &= \beta_1 - \beta_2 \end{aligned} \tag{5.33}$$

The normal displacement at u = 0 must then be a function of the normal stress to reflect the normal behavior of the joint. If the model proposed by Bandis et al. (1983) is used (Equation 3.1), then at u = 0, we also have:

$$v = \frac{\sigma_n V_m}{k_{ni} V_m - \sigma_n}$$

where σ_n is the normal stress, V_m is the maximum closure of the joint and k_{ni} is the initial normal stiffness of the joint. Combining the last equations leads to:

$$\beta_1 - \beta_2 = \frac{\sigma_n V_m}{k_{ni} V_m - \sigma_n} \tag{5.34}$$

and $$\beta_2 = \beta_1 - \frac{\sigma_n V_m}{k_{ni} V_m - \sigma_n} \tag{5.35}$$

From Equation 5.32, it can be seen that at large displacement (u >> 0), the normal displacement will be equal to β_1 (which will represent the maximum normal displacement V_m). If we consider that the Saeb-Amadei model gives a good approximation of this maximum normal displacement, then we can use the Saeb-Amadei formulation to evaluate β_1. The maximum normal displacement with the Saeb-Amadei formulation is given by using Equation 3.28 at $u = u_r$ (where the dilatancy level remains constant). Then we get:

$$\beta_1 = u_r \left(1 - \frac{\sigma_n}{\sigma_T}\right)^{k_2} \tan i_0 + \frac{\sigma_n V_m}{k_{ni} V_m - \sigma_n} \tag{5.36}$$

where i_0 is the angle of asperities of the joint and k_2 is the constant of the Ladanyi-Archambault peak strength model (and considered to be equal to 4).

The last parameter (β_3) can be related to the residual displacement (u_r). Based on several test results obtained from literature, it was found that β_3 can be given by:

$$\beta_3 \cong \frac{1.5}{u_r} \tag{5.37}$$

Figure 5.6 shows the comparison of Equation 5.37 with the value obtained by curve fitting on 15 tests found in literature (these curves are given in appendix).

Combining Equations 5.35 to 5.37 into Equation 5.32, we get:

$$v = \left[u_r\left(1-\frac{\sigma_n}{\sigma_T}\right)^{k_2}\tan i_0 + \frac{\sigma_n V_m}{k_{ni}V_m - \sigma_n}\right]\left[1-\exp\left(-\frac{1.5u}{u_r}\right)\right] + \left(\frac{\sigma_n V_m}{k_{ni}V_m - \sigma_n}\right)\exp\left(-\frac{1.5u}{u_r}\right)$$

$$= \left[u_r\left(1-\frac{\sigma_n}{\sigma_T}\right)^{k_2}\tan i_0\right]\left[1-\exp\left(-\frac{1.5u}{u_r}\right)\right] + \frac{\sigma_n V_m}{k_{ni}V_m - \sigma_n} \quad (5.38)$$

An incremental formulation can also be given by:

$$d\sigma_n = k_{nn}dv + k_{sn}du \quad (5.39)$$

with

$$k_{nn} = \frac{\partial\sigma_n}{\partial v} = \frac{1}{\dfrac{k_2 u_r}{\sigma_T}\left(1-\dfrac{\sigma_n}{\sigma_T}\right)^{k_2-1}\tan i_0 + \dfrac{k_{ni}V_m^2}{(k_{ni}V_m - \sigma_n)^2}} \quad (5.40)$$

and

$$k_{ns} = \frac{\partial\sigma_n}{\partial u}$$

$$= \frac{1.5(k_{ni}V_m - \sigma_n)\left(1-\dfrac{\sigma_n}{\sigma_T}\right)\left[(k_{ni}V_m - \sigma_n)\left[u_r\left(1-\dfrac{\sigma_n}{\sigma_T}\right)^{k_2}\tan i_0 - v\right] + \sigma_n V_m\right]}{u_r\left[k_2[V_m\sigma_n - v(k_{ni}V_m - \sigma_n)] - (V_m + v)(k_{ni}V_m - \sigma_n)\left(1-\dfrac{\sigma_n}{\sigma_T}\right)\right]} \quad (5.41)$$

5.3 Evaluation of fault-slip rockbursts potential

As it was mentioned in the presentation of the relative stiffness approach (section 2.3), to establish if failure will be violent or gradual, one needs to compare the post-peak stiffness of the failed element with the stiffness of the material surrounding this failed element. Thus, in cases where a slip along a discontinuity is anticipated, the stiffnesses that need to be determined are the shear post-peak stiffness of the discontinuity and the shear stiffness of the surrounding rock mass. A proposed method to obtain these stiffnesses is detailed in this section.

5.3.1 Shear post-peak stiffness of a discontinuity k'_p

Lets consider a direct shear test on a rock discontinuity as illustrated in Figure 5.7a. As it was shown in the previous section, the model developed can reproduce fairly well the behavior of the discontinuity for this situation (Figure 5.7b). Thus, the model can be used to evaluate the post peak stiffness of the discontinuity. The value that needs to be used for the comparison will of course be the largest value possible (in absolute value) of the slope in its post-peak phase, or the smallest value since the slope is negative in the post-peak phase. In the case where the normal stress stays constant, the value of the slope is given by Equation 5.27:

$$k_{ss} = d e \exp(-e\ u) - b c \exp(-c\ u)$$

The smallest value can then be determined by the derivative of the slope and given by:

$$\frac{\partial k_{ss}}{\partial u} = bc^2 \exp(-c\ u) - de^2 \exp(-e\ u) = 0 \qquad (5.42)$$

Solving this equation will lead to the critical displacement u_{crit} where the slope will be the smallest:

$$u_{crit} = \frac{\ln\left(de^2 / bc^2\right)}{(e-c)} \qquad (5.43)$$

It could be shown that since the maximum slope given by the formulation of the model is at the origin (u = 0), that the critical displacement obtained by Equation 5.43 is always a minimum. Then, computing the value of the slope at u_{crit} will lead to the smallest value of the slope given by:

$$(k_{ss})_{min} = k_p^{'} = de\exp(-e\ u_{cnt}) - bc\exp(-c\ u_{cnt}) \quad (5.44)$$

Special attention must be given to the units used. The value obtained with Equation 5.44 is in MPa/mm or GPa/m. It should be noted that stiffness coefficients should be expressed in pounds per inch or meganewtons per metre as it is in most publications. Then, the value obtained with Equation 5.44 should be multiplied by the area of the sample perpendicular to the normal load.

In the case where the normal load is not constant, then the parameters a,b,d and e will vary and Equations 5.43 and 5.44 cannot be used. In this case, the stiffness can be calculated by plotting the slope (using a spreadsheet) and finding the smallest value.

To extend this concept at the rock mass level, numerical modeling is mandatory. The use of a non-linear approach is needed to be able to model the behavior of the joint near openings where normal and shear stresses are not constant throughout the rock mass. Thus, the model developed in section 5.2 was introduced in a boundary element code named SATURN that was originally developed at McGill University by Fotoohi (1993). A description of SATURN and of the implementation of the new model is given in the following sections.

The stiffness of the fault can then be computed using the results provided by the SATURN output. Each segment of the fault that has failed can then be analyzed to obtain its post-peak behavior. The value of the post-peak shear stiffness k'_p will be given by the largest value of the slope (in absolute values). Examples of application are given in chapter 6.

5.3.2 Shear stiffness of the surrounding rock mass k_e

The shear stiffness of the surrounding rock mass can be estimated through a process similar as the one proposed for fracturing of the rock mass (section 2.3.4). It consists of replacing the fault elements that failed with fictitious shear stresses. Then, the shear displacements along these elements are computed. A graph of σ_s*L vs u (where σ_s is the resultant shear stress, L is the length of the fault that failed and u is the shear displacement) is plotted. The slope of this graph represents the shear stiffness k_e of the surrounding rock mass. Examples of application are given in Chapter 6.

5.3.3 Burst-potential ratio for joints (BPR_j)

To evaluate if there is a fault-slip rockburst potential, one must compare the post-peak shear stiffness of the failed fault elements with that of the surrounding rock mass. If the post-peak stiffness of the failed element is larger (in absolute values) than that of the surrounding rock mass, there is a fault-slip rockburst potential. Otherwise, the failure will be gradual.

For comparison purpose, it might be easier to compare the stiffness in a relative manner. Then a Bursting Potential Ratio for joints, or BPR_j, can be used (similar to the one defined for rock mass failure in section 2.3.4). This index is then given by:

$$BPR_j = \left| \frac{k_p^{'}}{k_e} \right| \tag{5.45}$$

A BPR_j value well above unity would indicate a clear potential of rockbursting while a value near unity might require further investigation (like more laboratory testing to get more accurate values for the fault model).

5.4 THE PROGRAM SATURN

The SATURN software system was developed by Fotoohi (1993) in a Ph.D. thesis. SATURN (for Stress Analysis of Tunnels and Underground Rock excavation with Non-linear discontinuities) consists in three modules, the pre-processor (DRAW), the main program (SATURN) and the post-processor (SHOW).

Program SATURN uses a combination of fictitious stress and displacement discontinuity methods (BEM) that are used for stress analysis of rock masses containing major faults. The program employs the indirect boundary element method with a technique of incremental relaxation of the boundary tractions representing the mining induced stress relief at the boundary of mine openings. The equilibrium of the system for each increment step is achieved by iterations. SATURN can also take advantage of symmetry to reduce the computing effort. Two models of joint behavior were available: the Mohr-Coulomb model and the Barton-Bandis model.

5.4.1 Non-linear analysis

The non-linear analysis performed by SATURN uses an incremental iteration technique. The creation of the excavation is modeled by incremental relaxation of the fictitious boundary tractions for the fictitious stress elements. The size of the load step increment is determined by dividing the initial boundary stresses into L equal segments. The displacement discontinuity elements can follow either the Mohr-Coulomb or the Barton-Bandis models to calculate the shear stress-displacement relation along a fault. The Mohr-Coulomb model assumes that both the shear and normal stiffness are constant during the incremental loading analysis, whereas the Barton-Bandis model uses non-linear relationships for both normal and shear stresses so their corresponding stiffness is not constant.

A system of 2N algebraic equations based on Equations (4.43) and (4.44) is obtained. The system of algebraic equation of iteration j from load increment k for i = 1, N can be written as follows:

$$\left[\mathbf{A}_k^j\right]\left\{\mathbf{X}_k^j\right\} = \left\{\mathbf{B}_k\right\} \tag{5.46}$$

where the matrix [**A**] is a full asymmetric known matrix that represents parameters $\overset{ij}{A}_{ss}$, etc. from Equation (4.43) and (4.44), the vector {**X**} is unknown and represents the parameters $\overset{j}{P}_s$ and $\overset{j}{D}_s$, etc. from these equations, and vector {**B**} represents the left end side of these equations. Each of vector {**X**} and {**B**} has 2N entries.

5.4.2 SATURN algorithm

The structure of SATURN can be resumed in 5 steps as shown in Figure 5.8. First, the geometry of boundary and physical property of the domain are generated. Then, the traction vectors on boundary are constructed. The third step is the calculation of influence coefficients of traction vectors over all elements and the set up of the system of equations. Then, the system of equations to determine the unknown fictitious stresses or displacement discontinuities is solved. Finally, the stresses and displacements at any point inside the domain (using superposition of fictitious stresses or displacement discontinuities) are calculated.

Particular interest is given to step 2 to 4 in Figure 5.8. The generation of traction vectors (step 2) consists in constructing $\{\mathbf{B}\}$. The traction vector for all fictitious stress elements is calculated from in situ (or pre-mining) stresses. The traction vector for all displacement discontinuity elements (DDE) is set equal to zero. However, the real traction vector for DDE are equal to $k_i * D_i$ ($i = n$ or s) which are moved into matrix $[\mathbf{A}]$ in step 3. In step 3, the influence coefficients of every element are calculated and the matrix $[\mathbf{A}]$ is assembled. In step 4, the system of algebraic equation $[\mathbf{A}]\{\mathbf{X}\} = \{\mathbf{B}\}$ is solved and the unknown vector of fictitious stresses or displacement discontinuities is determined. The solution procedure uses the Gauss elimination method. Finally, the stresses and displacement at any point around the openings are calculated (step 5) by superposition of fictitious stresses or displacement discontinuity parameters. The number of calculation of influence coefficients for each point is equal to 2*N where N is the total number of elements.

5.4.3 Implementation of the new model into SATURN

For the non-linear analysis, the numerical algorithm used in SATURN is based on incremental relaxation of the boundary tractions. The initial tractions are divided into L equal increments and are applied step by step. After each step, the characteristics of the fault are updated using either Barton-Bandis' or the proposed model. Figure 5.9 shows the flowchart for the incremental procedure. The computation steps are repeated L times from step 2 to step 4 (of Figure 5.8). For each iteration, the traction vector $\{\mathbf{B}\}$ is calculated before step 2, which is based on k/L of total tractions. The parameter k_i*D_i are included in the matrix [A] after step 3 for displacement discontinuity elements. After step 4, the normal and shear displacements and stresses are calculated for all elements along opening boundaries and faults. Then, the calculation of the limiting stress using a failure criterion for each displacement discontinuity element is performed and compared with the shear stress of that element. Finally, the element stiffness k_{nn} and k_{ss} are modified appropriately. If the convergence criterion is satisfied, then the next load step is considered. Otherwise, the iteration restarts from step 2.

Figure 5.10 and 5.11 show the flowcharts for the set up of matrix [A] and vector {B}. For the proposed model, the procedure is identical as that of the Barton-Bandis model. Figure 5.12 shows the flowchart for the failure criteria of each joint model available in SATURN. First, the maximum shear stress τ_m is calculated for the model used. Figure 5.13 shows how the maximum shear stress is calculated for the proposed model. As it was mentioned in section 5.2, an iterative procedure is used to determine parameters d and e of Equation (5.1). First, the peak and residual stress are evaluated with the modified Ladanyi-Archambault model (Equations 3.15 and 3.50 respectively). Then, Newton's method is used to solve d and e. Finally, the maximum shear stress is calculated using Equation (5.30). Figure 5.14 shows how the shear stiffness is modified for the proposed model. If the resultant shear displacement Vx(I) is smaller than the peak displacement u_p, then K_{ss} is given by:

$$K_{ss} = \frac{\tau_p}{u_p} \tag{5.47}$$

A linear relation is used before the peak because the proposed model was developed for monotonous loading. This implies that the shear stress allowed by the model at u=0 is nil. However, in the rock mass, in situ normal and shear stresses usually exist even if the displacement is nil. Since the allowed shear stress for the model is nil at u=0, then no stress could be transferred to the joint because SATURN uses a secant stiffness approach.

If the resultant displacement is larger than the peak displacement, then the resultant shear stress σ_s is compared with the calculated maximum shear stress τ_m. If σ_s exceeds τ_m, then a Kodfal value of 3 is attributed, meaning that the program must proceed to another iteration. The shear stiffness is then given by:

$$K_{ss} = \frac{\tau_m}{Vx(I)} \tag{5.48}$$

This procedure is repeated until the resultant shear stress does not exceed τ_m. Figure 5.15 shows schematically how the program will converge towards the joint behavior by "relaxing" the shear stiffness.

For the normal stiffness, the Saeb-Amadei model is used for its simplicity. For that model, the normal-shear displacement relationship is given by Equation (3.28):

$$v = u\left(1-\frac{\sigma_n}{\sigma_T}\right)^{k_2} \tan i_0 \quad + \quad \frac{\sigma_n V_m}{k_{ni} V_m - \sigma_n}$$

Then, the secant normal stiffness is given by:

$$K_{nn} = \frac{\sigma_n}{v} = \frac{\sigma_n}{u\left(1-\frac{\sigma_n}{\sigma_T}\right)^{k_2} \tan i_0 + \frac{\sigma_n V_m}{k_{ni} V_m - \sigma_n}} \tag{5.49}$$

5.5 OUT-OF-BALANCE INDEX OBI

The stiffness comparison is a method that can be used to evaluate the fault-slip rockburst potential but it is not the only avenue that can be explored. A second approach is illustrated on Figure 5.16. Figure 5.16a shows an excavation near a geological discontinuity. As the mining progress towards the discontinuity, the stress state along the discontinuity will be modified. In the situation shown here, one can expect, at point A, an increase in shear stress and a decrease in normal stress. Figure 5.16b shows the evolution of shear strength and applied shear stress at point A at each mining step. The shear strength gets lower at each mining step because of the decrease in normal stress. As the mining steps are achieved, the shear stress applied along the discontinuity increases. If the applied stress becomes larger than the strength, the equilibrium becomes out of balance. One can then define an "Out-of-Balance Index" (OBI) given by:

$$\mathrm{OBI} = \frac{F_{ob}}{F_{res}} \tag{5.50}$$

where F_{ob} is the applied shear stress minus the shear strength and F_{res} is the shear strength. The larger this OBI value will be, the larger the rockburst potential should be. This is based on the hypothesis that if at one moment in time, the OBI value is large enough (and positive), then there will be enough energy to produce a seismic event. The program SATURN was modified to make this calculation. However, to allow for the stress to be larger than the strength, the shear stiffness K_{ss} stays constant and is at every step given by Equation 5.47.

5.6 Verification of the implementation

To insure that the program SATURN works efficiently and that the implementation was done correctly, some verifications are mandatory. The best way to verify that the implementation was done correctly is to reproduce direct shear tests. SATURN can model either external (e.g. openings) or internal (e.g. direct shear tests) problems. Fotoohi (1993) made some verifications for external problems for simple openings such as circular, elliptical and square (with rounded corners) openings. SATURN showed good agreement for such shapes of openings. However, no verifications were made for internal problems or for external problems involving faults. Thus, four kind of verifications are made here: First, a thick-wall cylinder in compression is analyzed (to verify the validity of internal problems); Secondly, cases of a circular opening near a fault in an elastic field are analyzed (to verify the accuracy of DD elements); Then, direct shear tests are reproduced under either constant normal stress or constant normal stiffness (to verify the implementation of the proposed model).

5.6.1 Thick-wall cylinder

Lamé (1852) developed an analytical solution for a thick wall cylinder submitted to uniform internal (p_i) and external (p_e) pressures, as illustrated on Figure 5.17. The analytical solution of Lamé is given by:

$$\begin{aligned} \sigma_r &= \frac{b^2 p_e - a^2 p_i}{b^2 - a^2} - \frac{(p_e - p_i)a^2 b^2}{r^2(b^2 - a^2)} \\ \sigma_t &= \frac{b^2 p_e - a^2 p_i}{b^2 - a^2} + \frac{(p_e - p_i)a^2 b^2}{r^2(b^2 - a^2)} \end{aligned} \tag{5.51}$$

where σ_r is the radial stress, σ_t is the tangential stress, a and b are the internal and external radius, r is the radius at the point of interest, and p_i and p_e are the internal and external pressures (compression is positive). The parameters for the case analyzed are:

$b = 5$; $a = 1$, $p_e = 10$; $p_i = 0$.

Figure 5.18 shows the comparison between the analytical solution and the results from SATURN. As it can be seen, SATURN compares well with the analytical solution. It can then be concluded that SATURN can model correctly such internal problems.

5.6.2 Circular opening near a fault (elastic analysis)

To evaluate if SATURN can accurately calculate stresses on DD elements, two cases of a circular opening near a fault are analyzed. The first case analyzed is a circular opening intersected by a plane of weakness at an angle of 45° as shown on Figure 5.19 (details of the analytical solution of this situation can be found in Brady and Brown, 1993, p. 202). Components p and 0.5p define the far field stresses. The normal (σ_n) and shear (τ) stress components along the plane, based on Kirsch (1898) solution, are given by (Brady and Brown, 1993):

$$\begin{aligned} \sigma_n &= \frac{p}{2} * 1.5\left(1 + \frac{a^2}{r^2}\right) \\ \tau &= \frac{p}{2} * 0.5\left(1 + \frac{2a^2}{r^2} - \frac{3a^4}{r^4}\right) \end{aligned} \qquad (5.52)$$

where a is the radius of the opening and r is the radius along the plane of weakness. The variation of the ratio τ/σ_n is plotted on Figure 5.20. As it can be seen, SATURN's results compare well with the analytical solution. However, there is some discrepancy of the results near the opening. This could be explained by the fact that the opening is modeled in SATURN by straight segments and not by a real circle. This affects the accuracy of the results near the opening.

The second case analyzed is a circular opening close but not intersecting the plane of weakness, as shown on Figure 5.21 (details of the analytical solution of this situation can be found in Brady and Brown, 1993, p. 203). The far-field stress is taken as hydrostatic. The normal and shear stresses, also based on Kirsch (1898) solution, are given by (Brady and Brown, 1993):

$$\sigma_n = p\left(1 - \frac{a^2}{r^2}\cos 2\alpha\right)$$
$$\tau = p\frac{a^2}{r^2}\sin 2\alpha \tag{5.53}$$

The variation of the ratio τ/σ_n is plotted on Figure 5.22. Here again, SATURN results show good agreements with the analytical solution.

5.6.3 Direct shear tests under constant normal stress

To evaluate if the implementation of the proposed model has been done correctly, reproduction of direct shear tests were performed. Figure 5.23a to 5.23d show the results obtained from SATURN, along with the proposed model and the test data taken from literature (more details on the test data can be found in appendix). As it can be seen from these figures, the implementation is adequate since the results obtained by SATURN follow closely the behavior of the proposed model obtained from the mathematical formulation. However, some differences can be observed at certain points on several curves. This can be explained by the fact that a difference of 10% between the resultant shear stress (σ_s) and the maximum allowed shear stress (τ_m) is allowed to ease the convergence process.

5.6.4 Direct shear tests under constant normal stiffness

The results of section 5.6.3 have shown that SATURN can efficiently reproduce the shear behavior of joints as given by the proposed model. To verify that the normal joint behavior is also modeled correctly, direct shear tests under constant normal stiffness were modeled. However, it is not possible to impose two normal boundary conditions in

SATURN (to impose the stiffness and the initial normal stress). So SATURN was modified to make possible the modeling of such a situation. After each iteration, the applied normal stress was given by:

$$(\sigma_n)_i = (\sigma_n)_{ini} + K * (v_{i-1} - v_0) \qquad (5.54)$$

where $(\sigma_n)_i$ is the applied normal stress at the iteration i, $(\sigma_n)_{ini}$ is the initial normal stress, K is the applied normal stiffness, v_{i-1} is the normal displacement at iteration $i-1$ and v_0 is the initial normal displacement (at u = 0). Figure 5.24 shows the result obtained for tests under different constant normal stiffnesses. Figure 5.25 shows the results for several tests taken from literature. Here again, results from SATURN compare well with the mathematical formulation of the proposed model.

Thus, based on all the verifications performed, it can be considered that the implementation of the proposed model was done adequately and that SATURN can be used in order to model openings near faults. In the next chapter, it will be shown how SATURN can be used to evaluate the fault-slip rockburst potential.

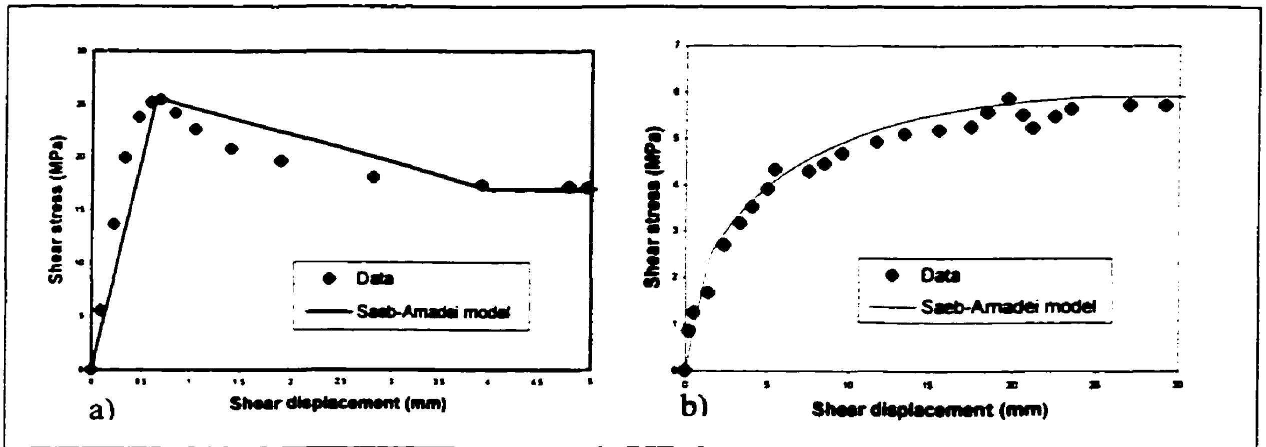

Figure 5.1 Comparison of the Saeb-Amadei model with typical joint behavior. a) Shear test under constant normal load (data from Flamand et al., 1994). b) Shear test under constant normal stiffness (data from Skinas et al., 1990).

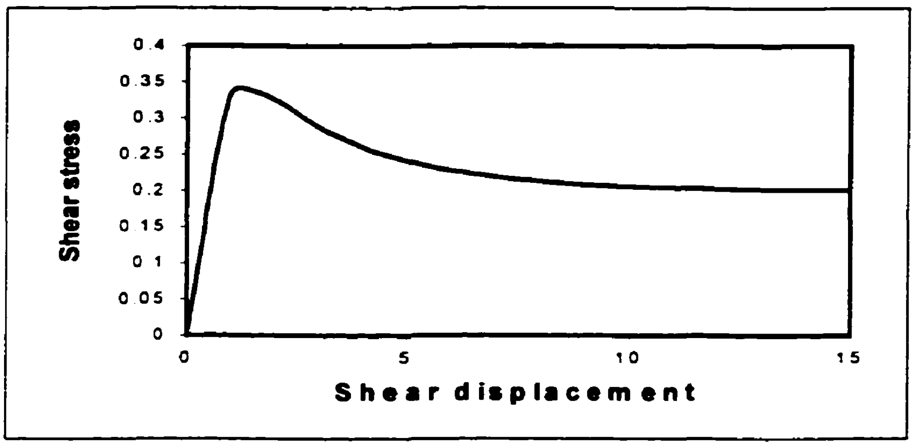

Figure 5.2 Typical shear stress-shear displacement curve obtained from Equation 5.1

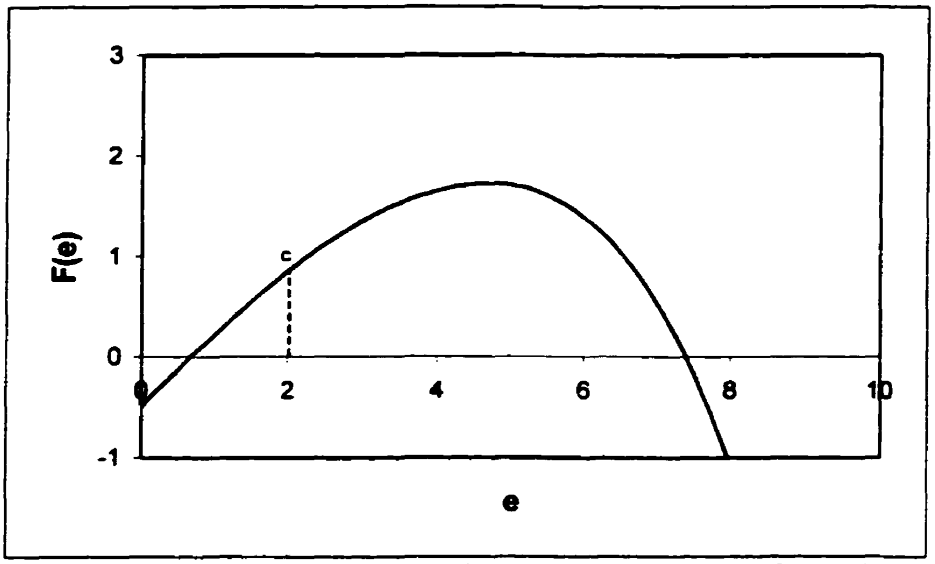

Figure 5.3: Graph of the function F(e) given by Equation 5.15 for typical values.

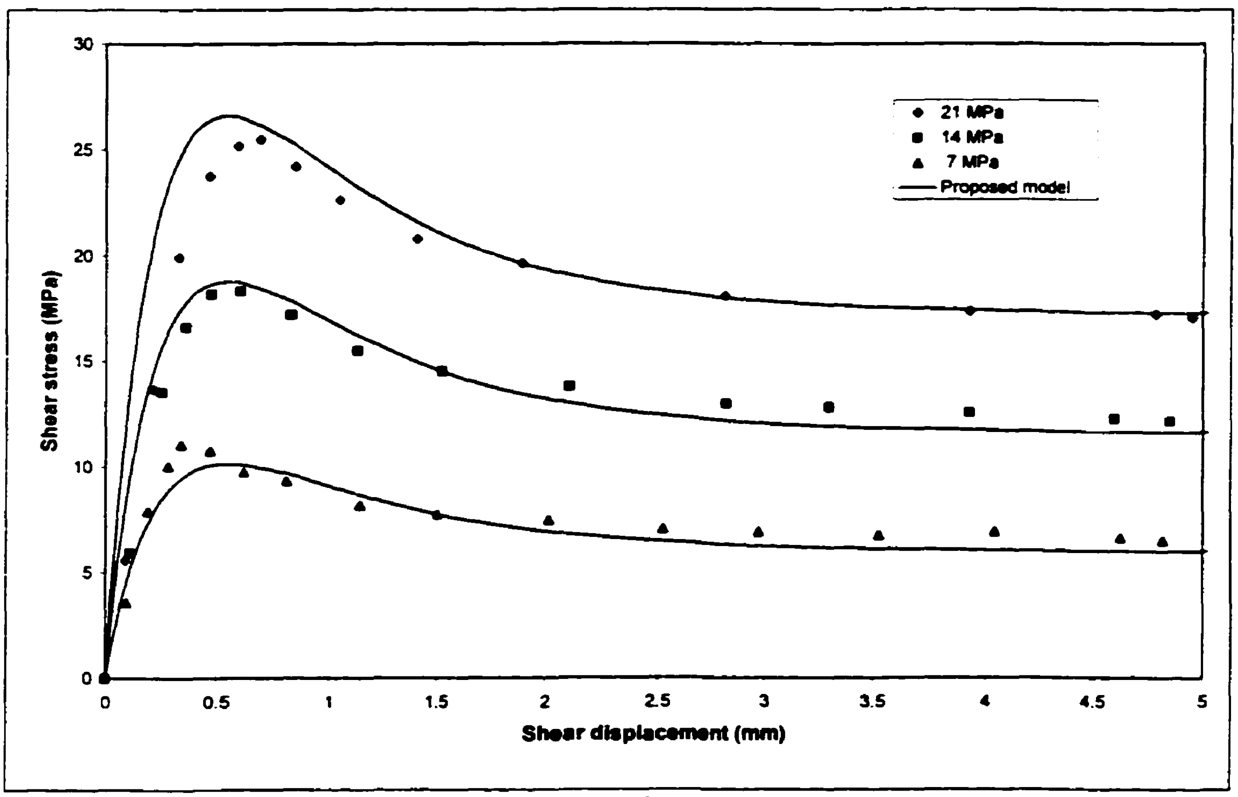

Figure 5.4a: Comparison between the proposed model and actual shear test result for rock joint replica made of cement mortar under different constant normal stresses (data taken from Flamand et al., 1994).

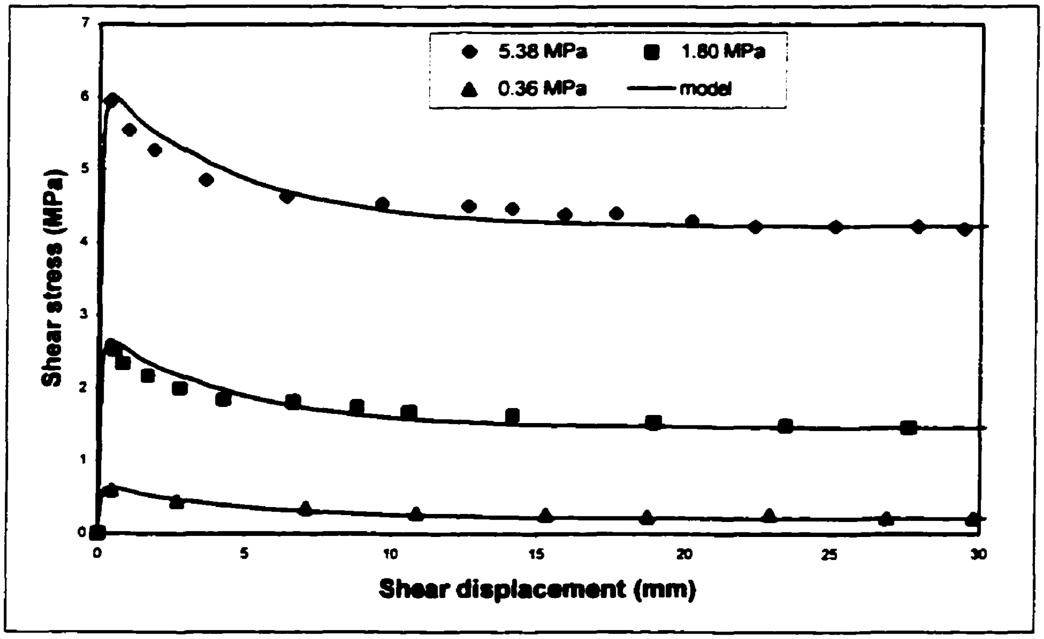

Figure 5.4b: Comparison between the proposed model and actual shear test result for an artificial fracture on a sandstone rock under different constant normal stresses (data taken from Leichnitz, 1985).

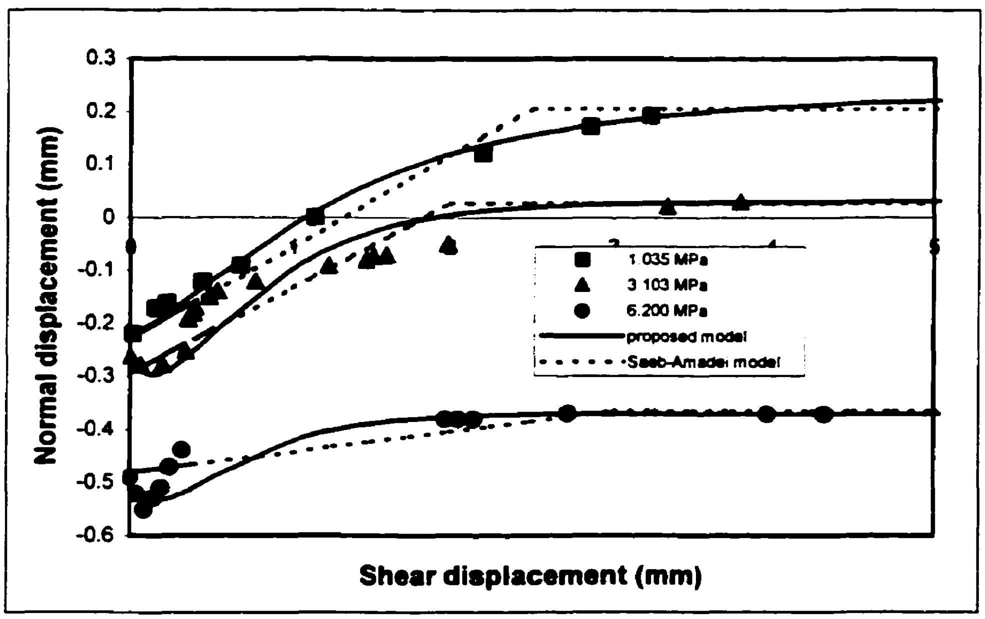

Figure 5.5: Typical normal displacement - shear displacement curve of a direct shear test on a rock joint under constant normal stress showing the Saeb-Amadei model and the proposed model (data from Bertrand, 1989).

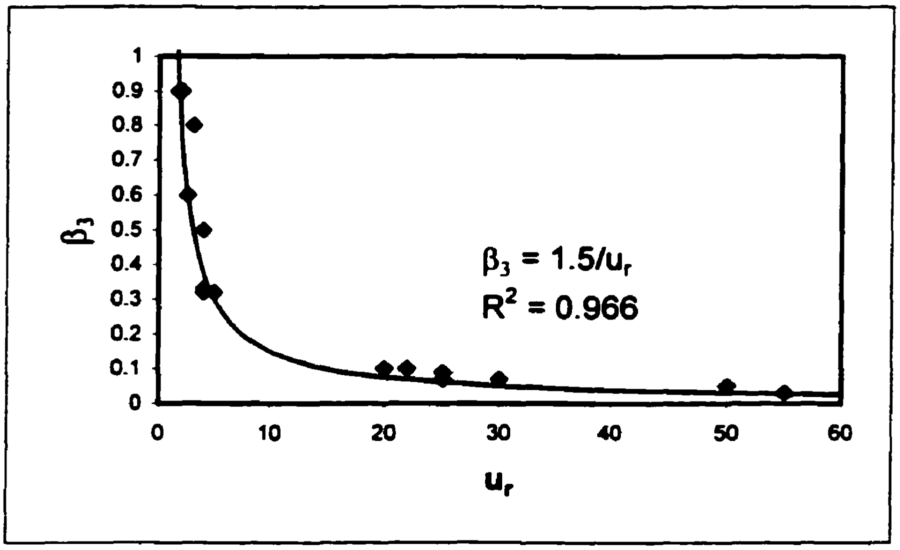

Figure 5.6: Correlation of parameter β_3 with Equation 5.37 (data from curves given in Appendix A).

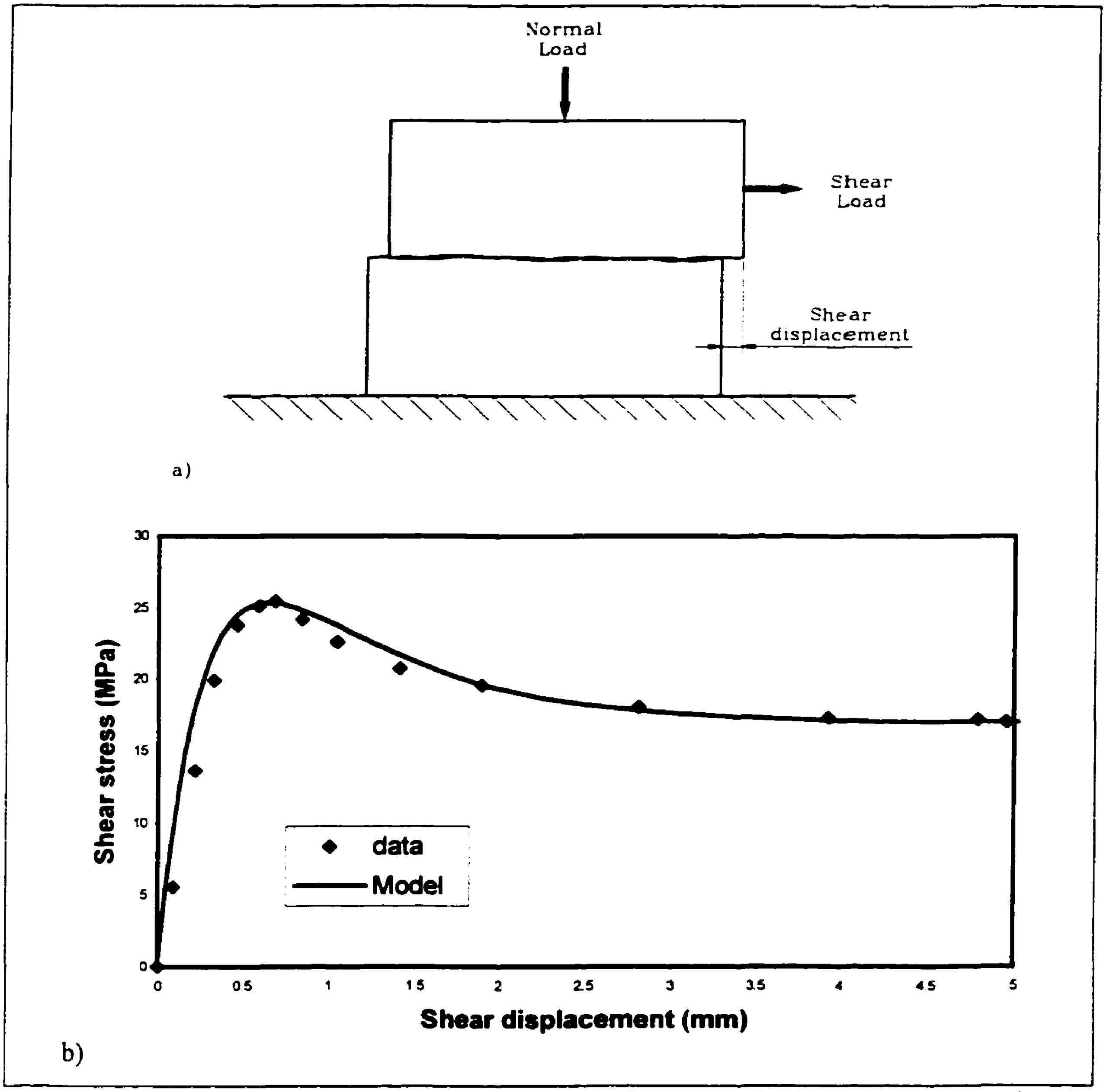

Figure 5.7 a) Direct shear test under constant normal load. b) Typical shear stress - shear displacement curve obtained with the proposed model (data from Flamand et al., 1994).

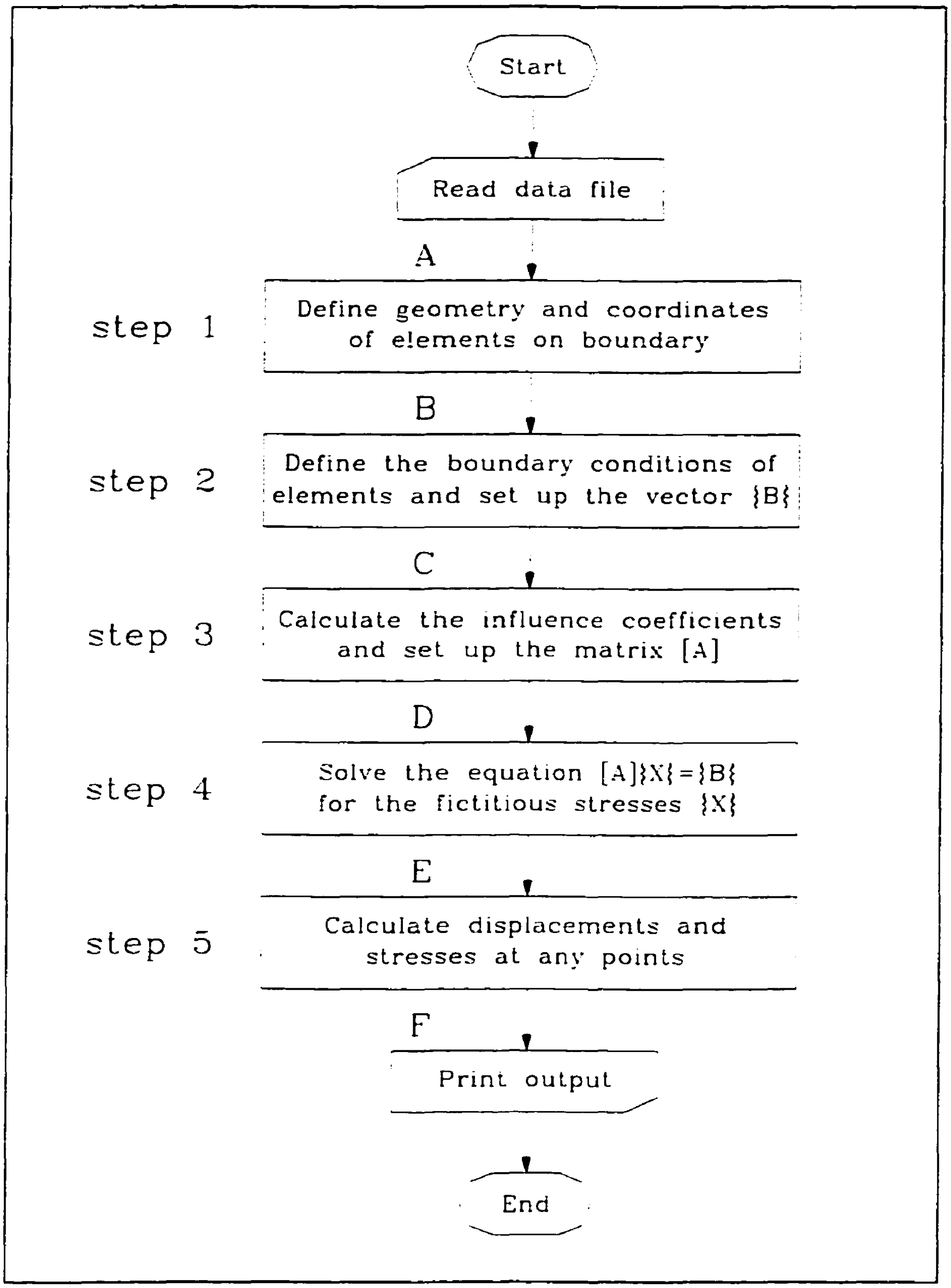

Figure 5.8: General flowchart of SATURN (after Fotoohi, 1993).

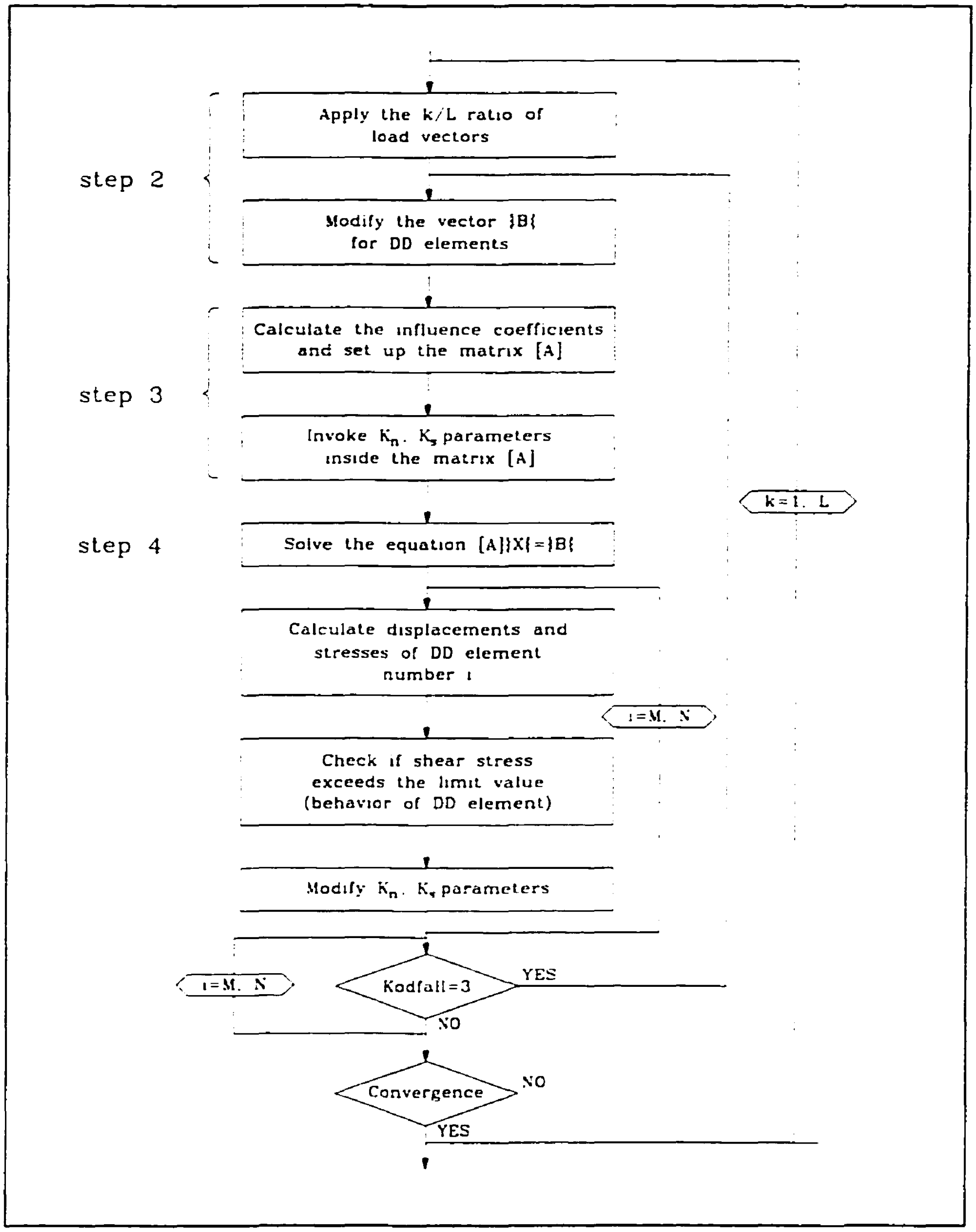

Figure 5.9: General flowchart of the incremental technique (after Fotoohi, 1993).

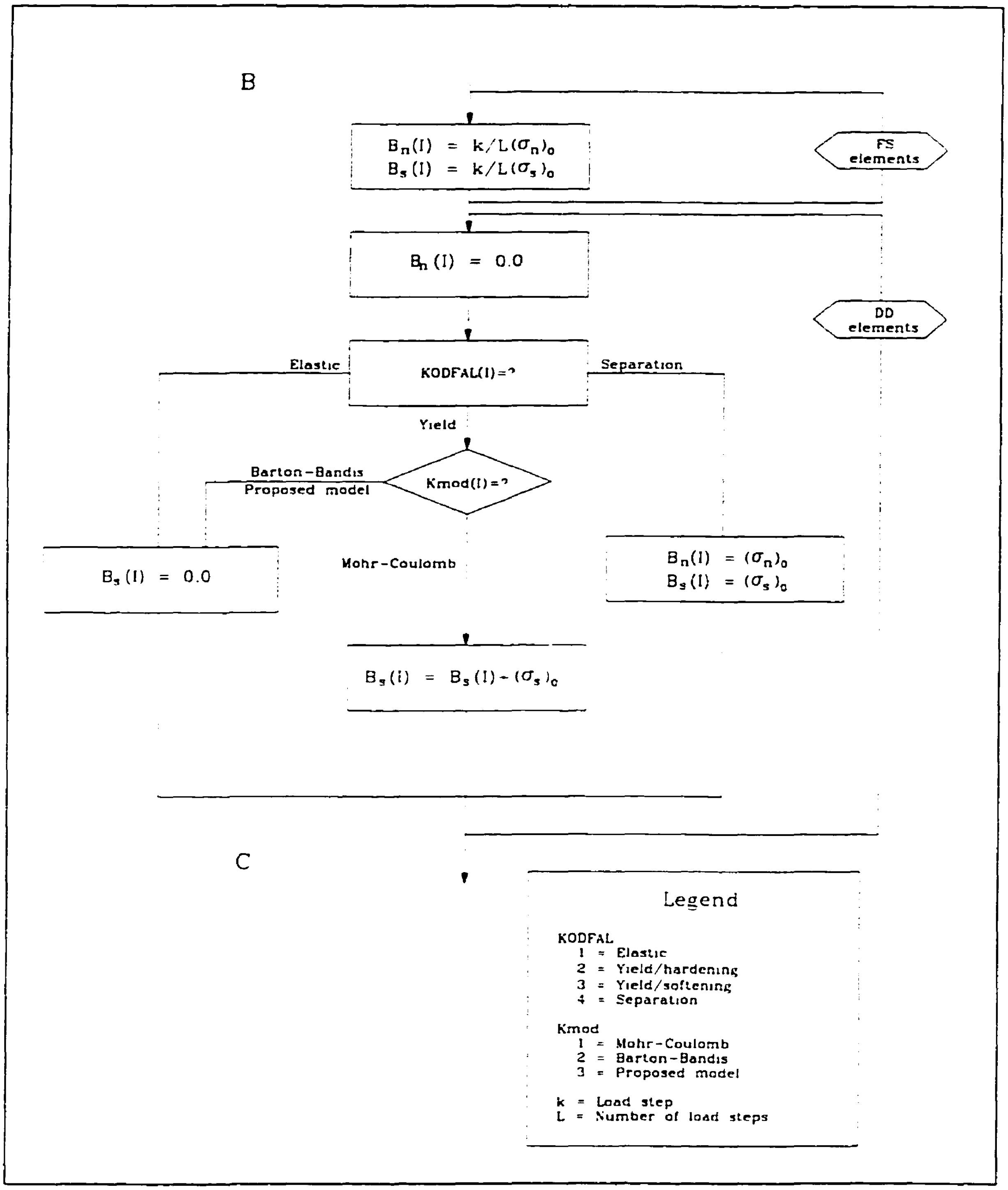

Figure 5.10: The flowchart of modification of vector **{B}** (adapted from Fotoohi, 1993).

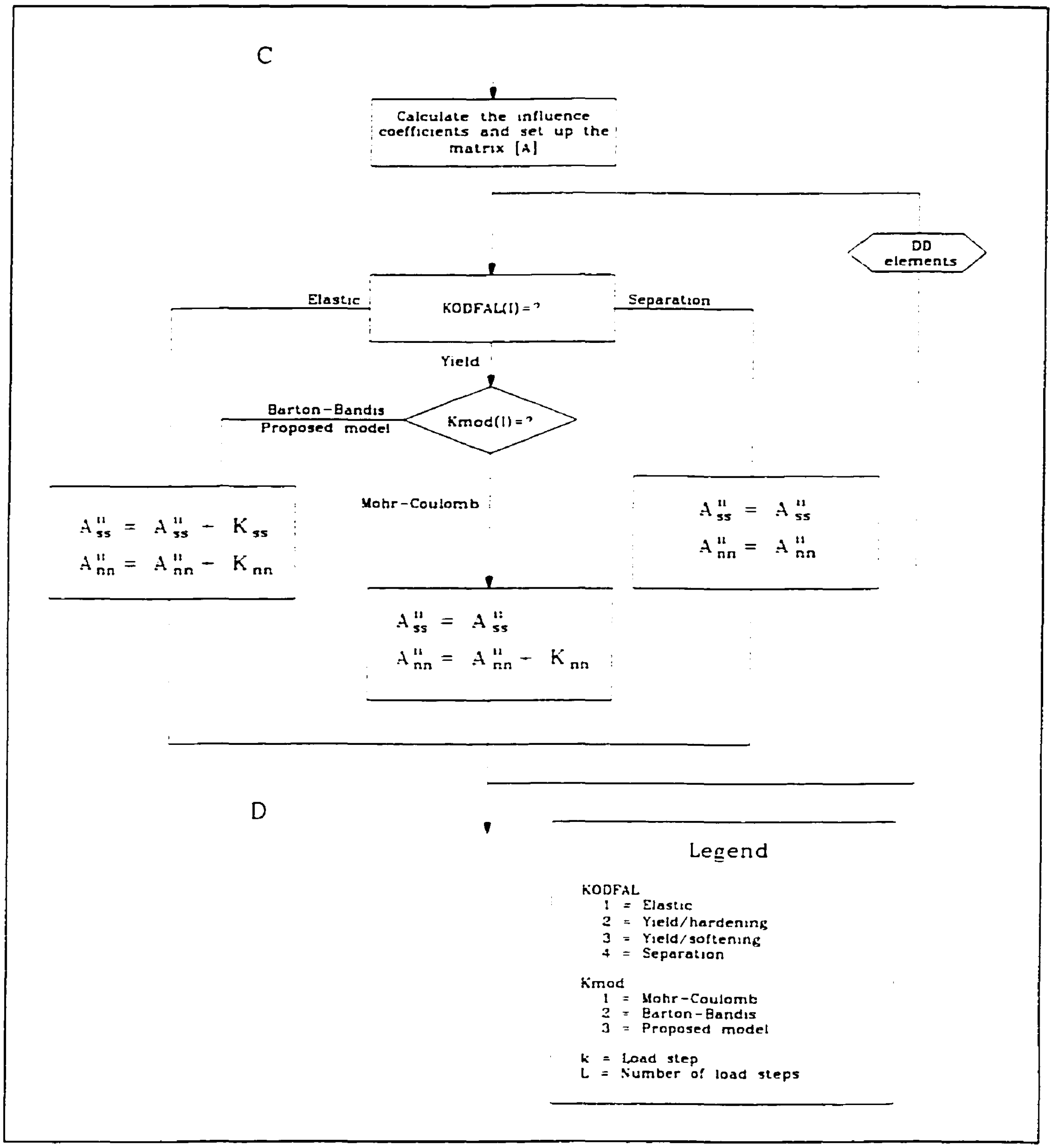

Figure 5.11: The flowchart of set up of matrix [A] (adapted from Fotoohi, 1993).

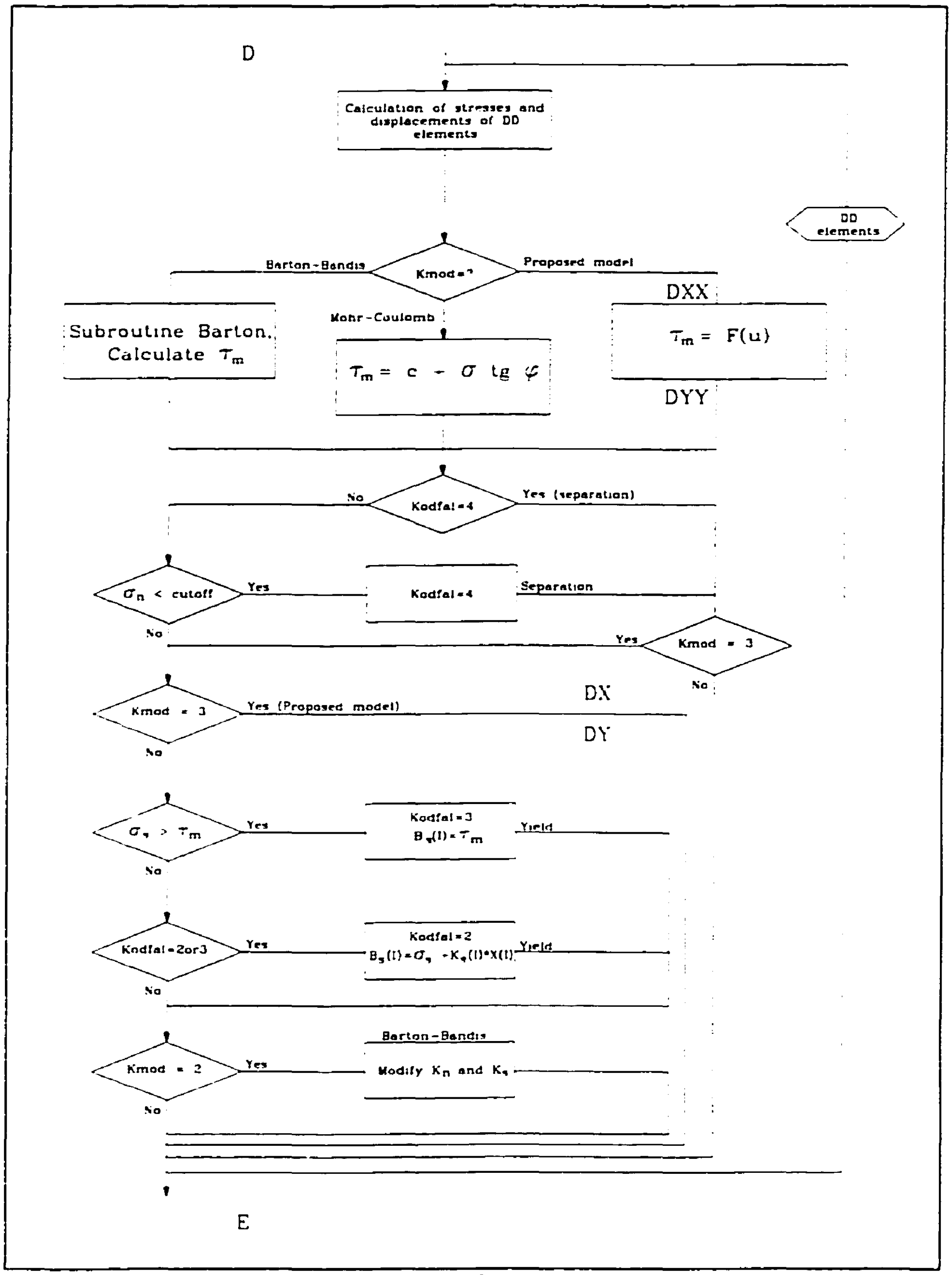

Figure 5.12: The flowchart of failure criteria for DD elements (adapted from Fotoohi, 1993).

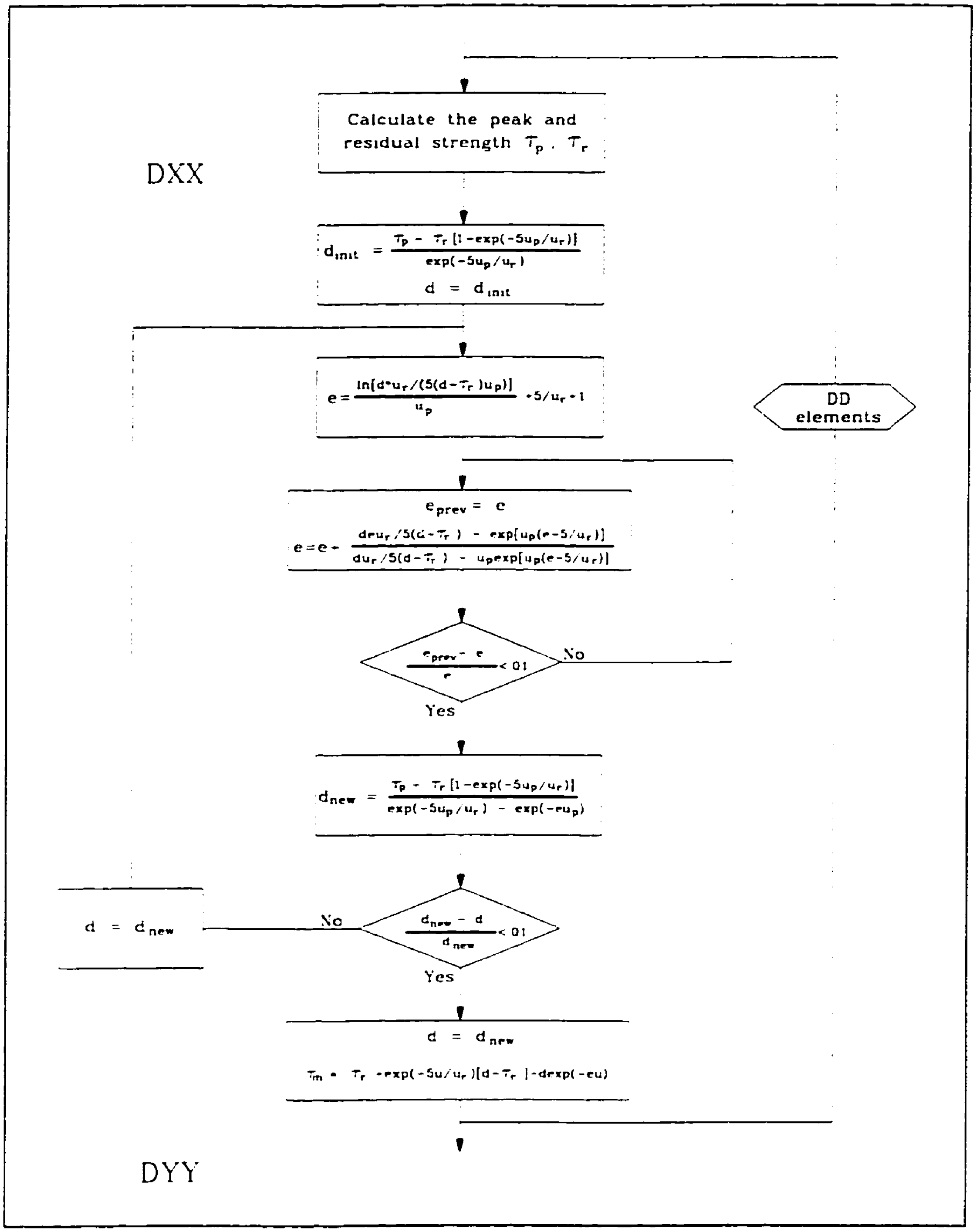

Figure 5.13: **The flowchart of calculating parameters *d* and *e* and the determination of τ_m for the proposed model.**

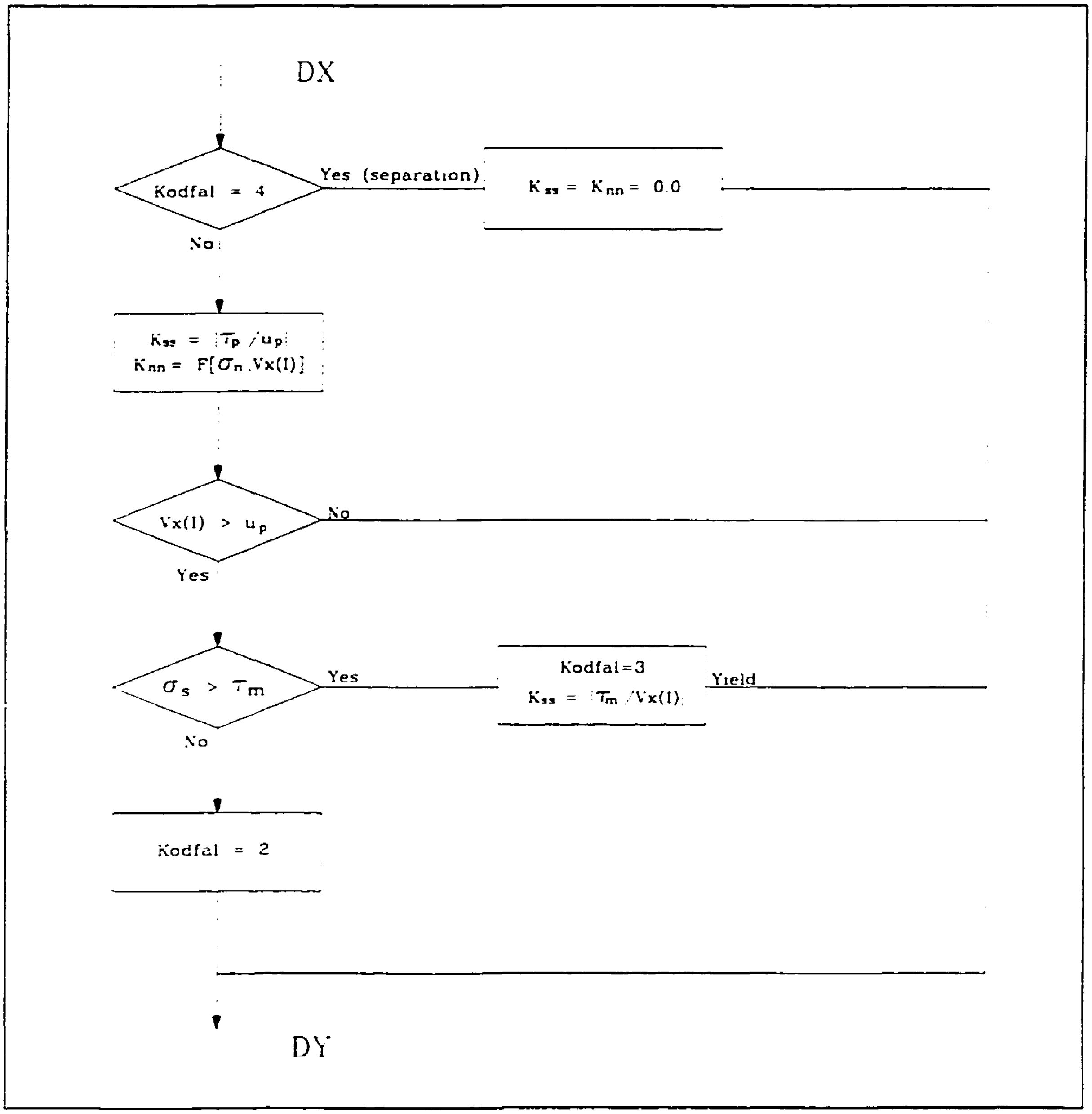

Figure 5.14: **The flowchart of modification of stiffness parameters for the proposed model.**

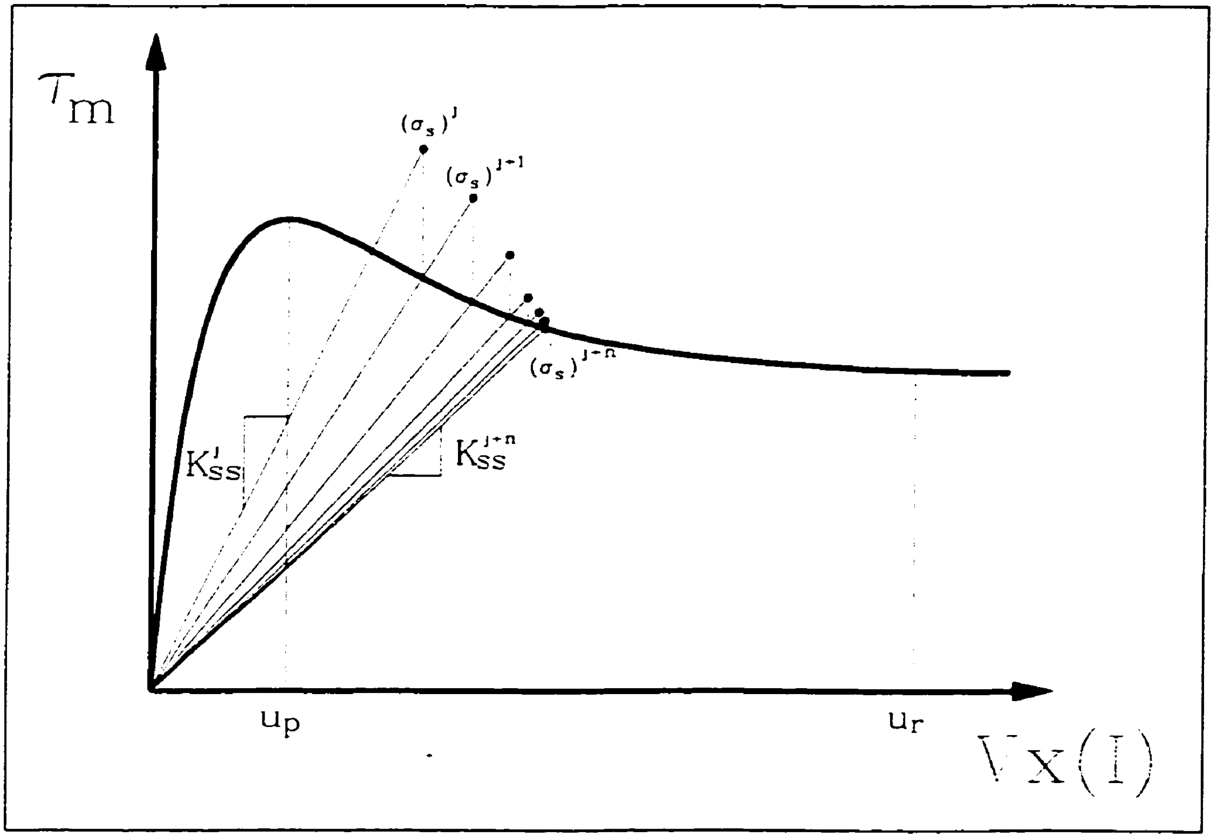

Figure 5.15: Schematic representation of the iterative process of modifying K_{ss} for the proposed model starting from iteration j and converging at iteration $j+n$.

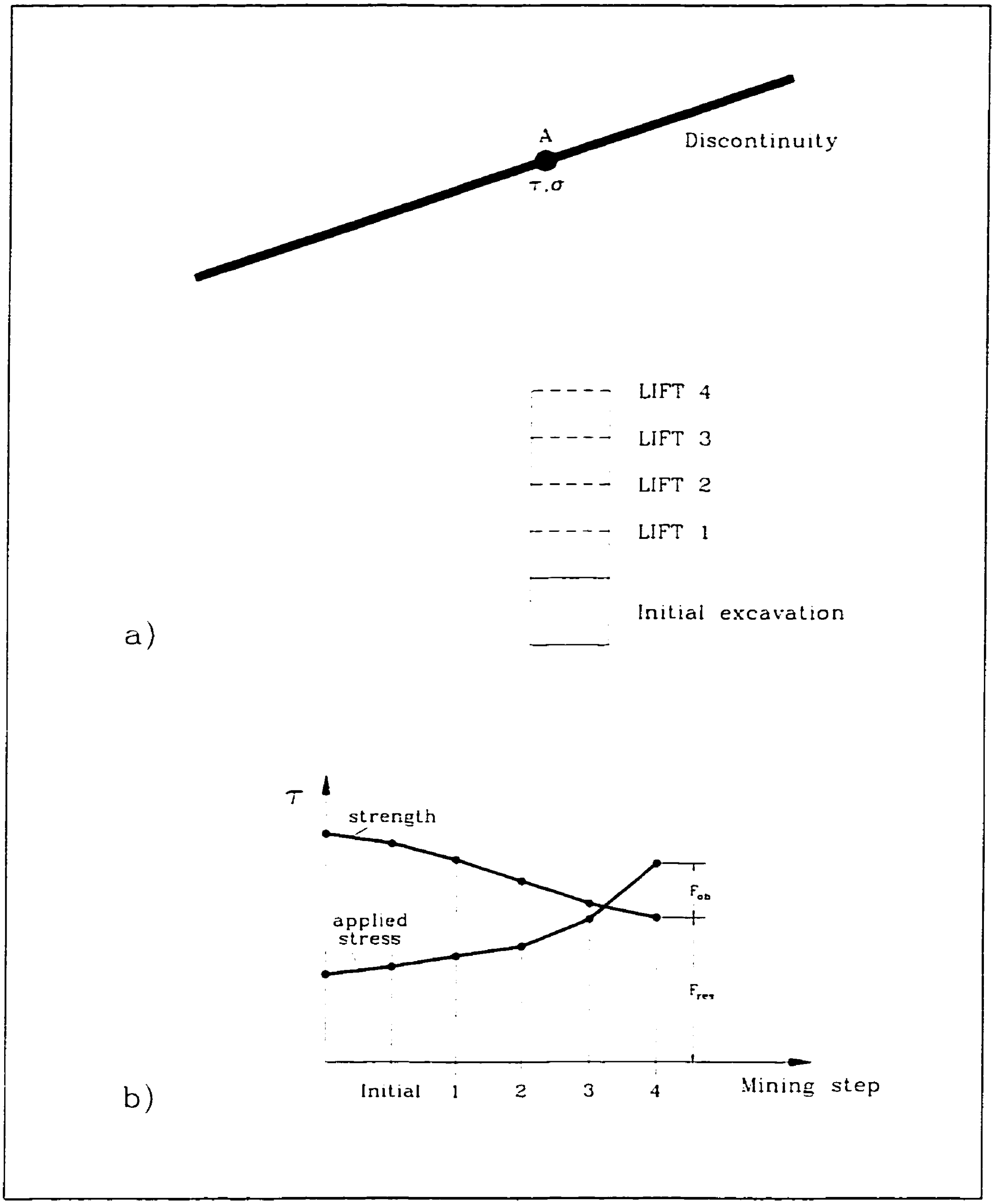

Figure 5.16: a) **Mining of a stope near a geological discontinuity. b) Shear strength and applied shear stress at point A at each mining step.**

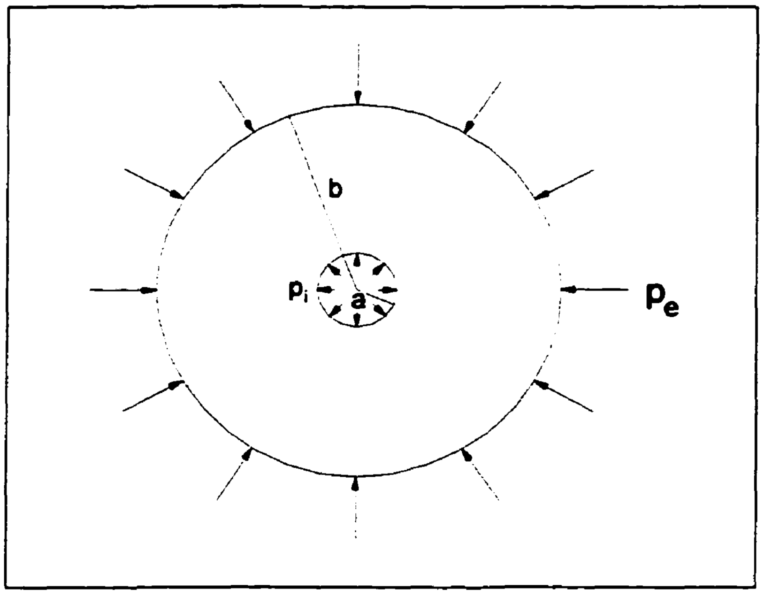

Figure 5.17: Hollow cylinder of internal radius *a* and external radius *b* under internal (p_i) and external (p_e) pressures.

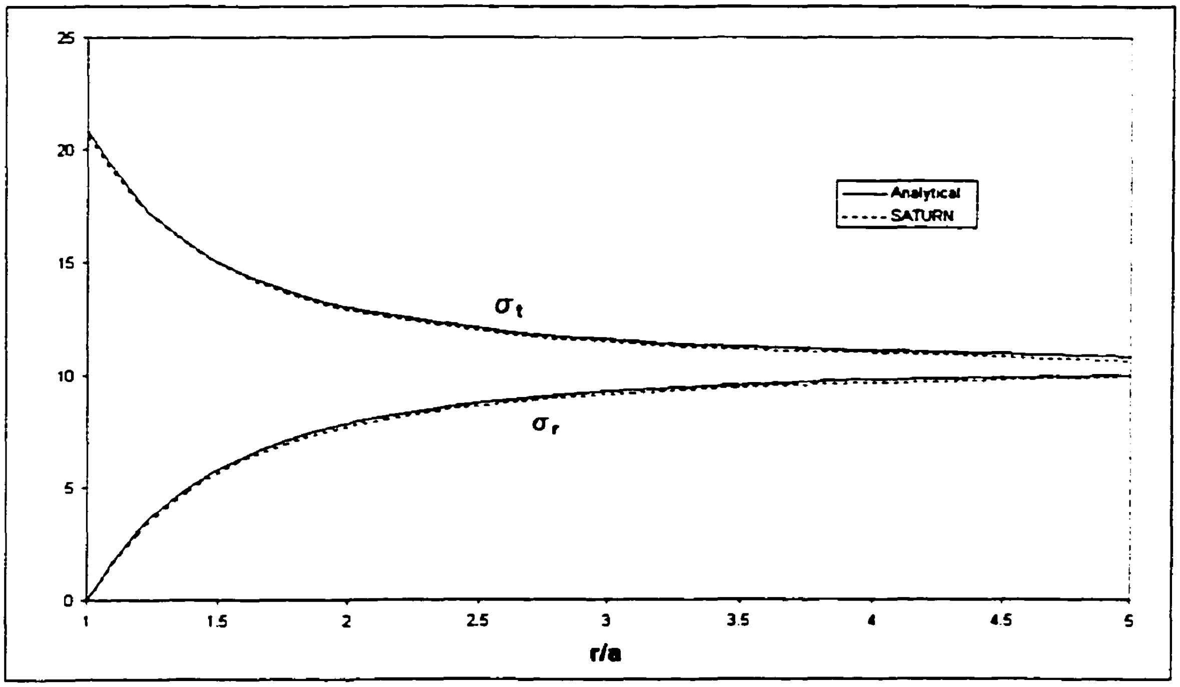

Figure 5.18: Comparison of tangential (σ_t) and radial (σ_r) stress results between an analytical solution and SATURN for a hollow cylinder under internal and external pressures.

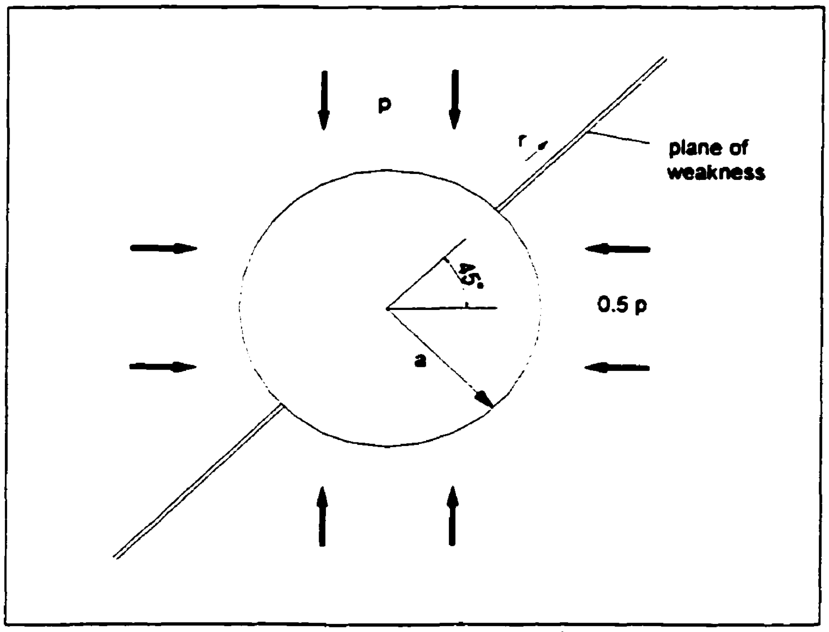

Figure 5.19: An inclined, radially oriented plane of weakness intersecting a circular excavation (after Brady and Brown, 1993).

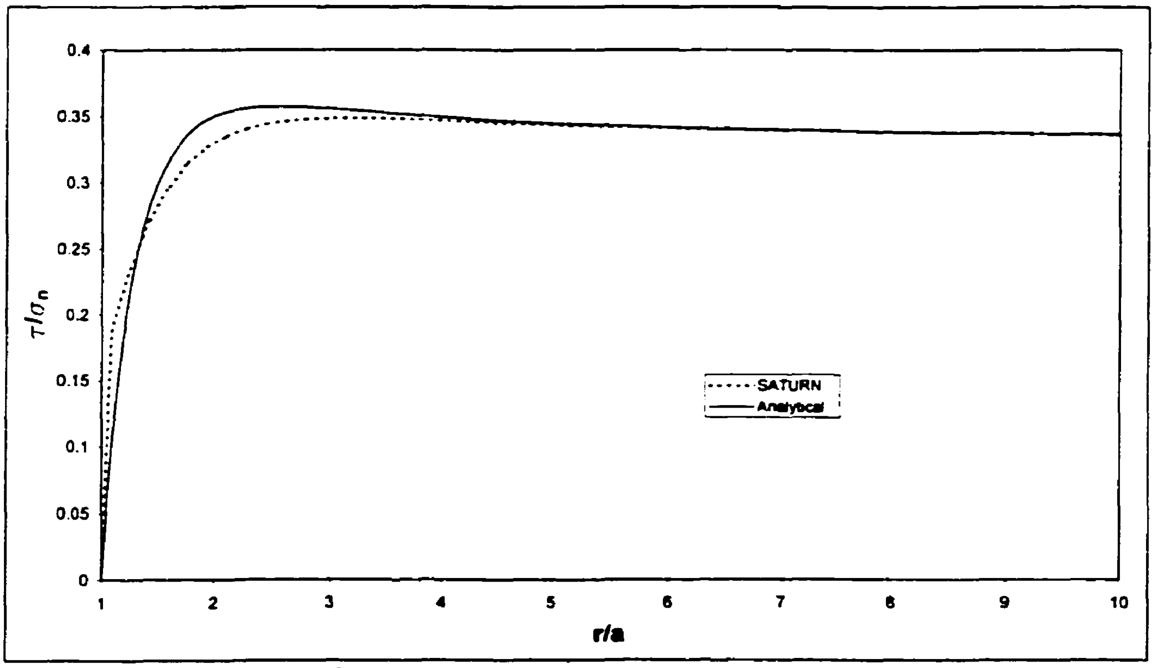

Figure 5.20: Comparison of the ratio of shear stress over normal stress between SATURN and an analytical solution.

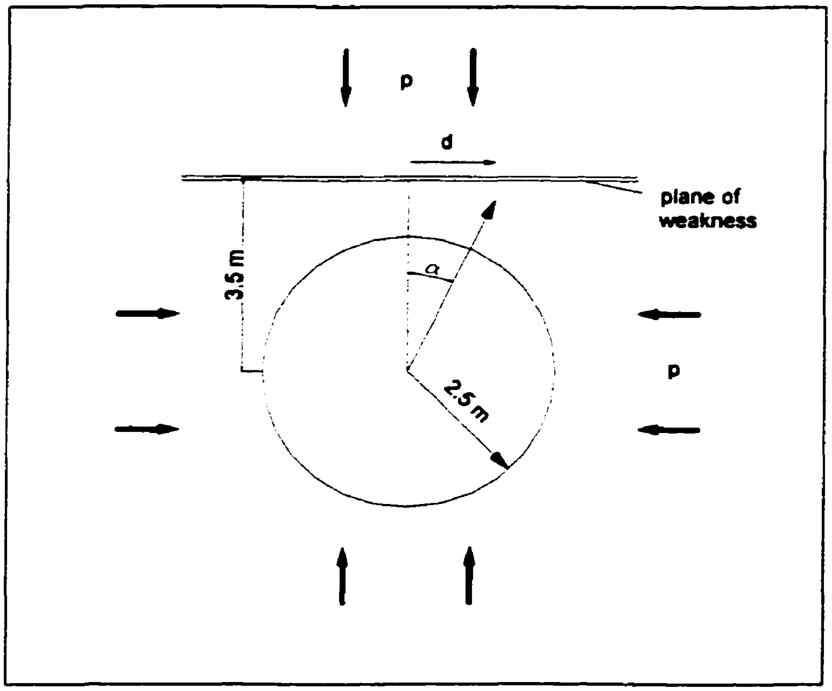

Figure 5.21: Plane of weakness close to, but not intersecting, a circular excavation (after Brady and Brown, 1993).

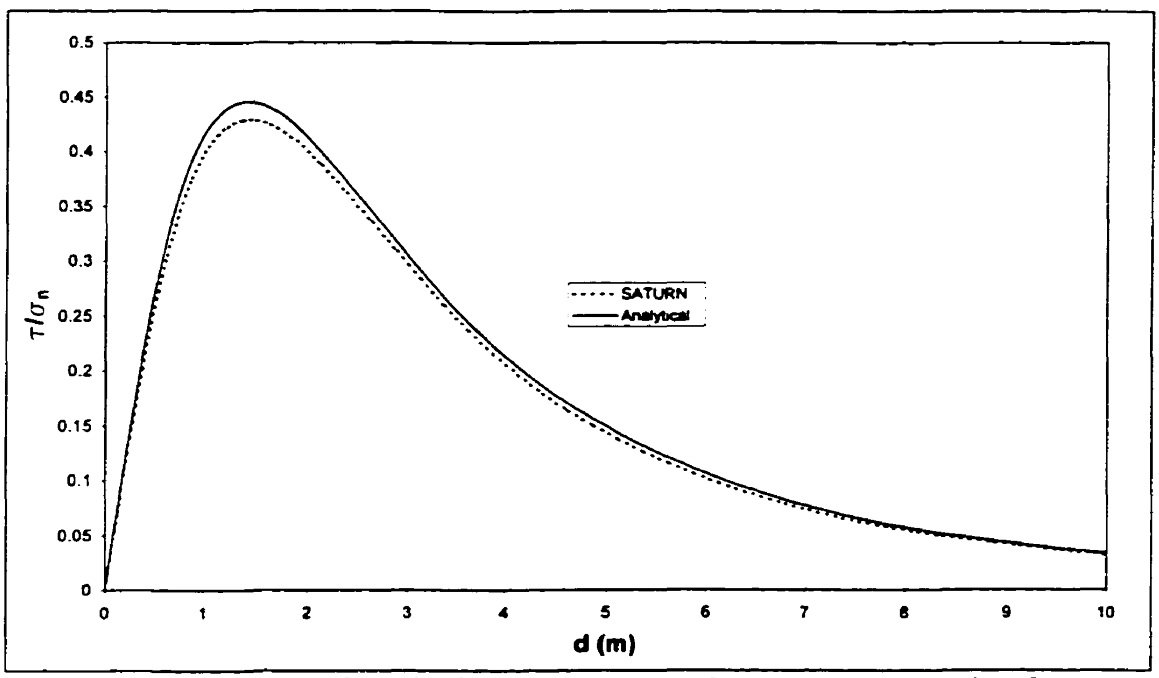

Figure 5.22: Comparison of results from SATURN and an analytical solution for a circular opening close to a plane of weakness.

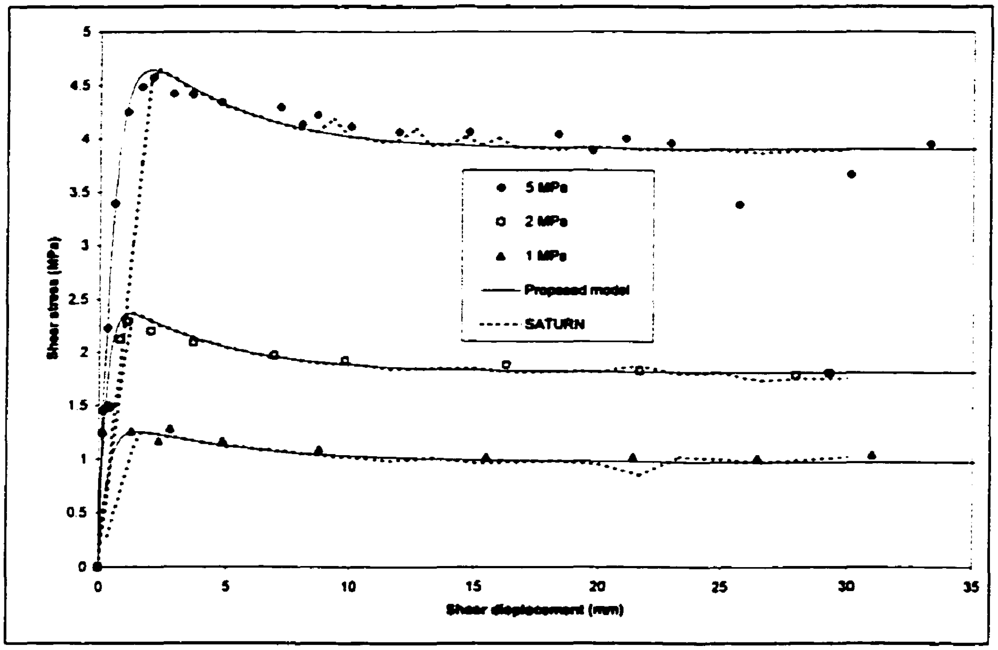

Figure 5.23a: Comparison of results obtained from SATURN and the proposed model for direct shear tests under different constant normal stresses (data taken from Skinas et al., 1990).

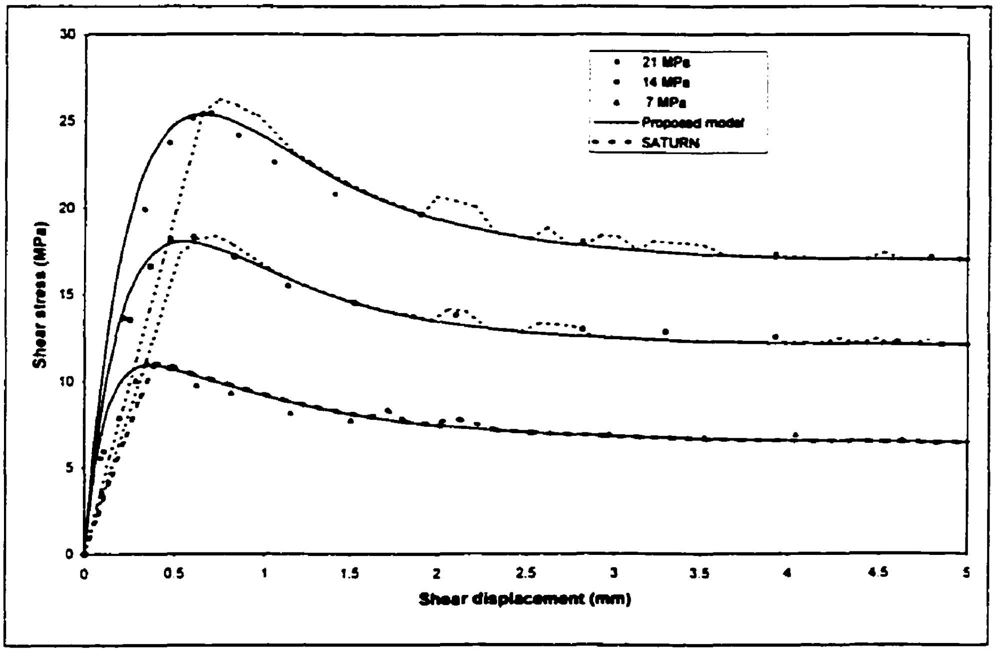

Figure 5.23b: Comparison of results obtained from SATURN and the proposed model for direct shear tests under different constant normal stresses (data taken from Flamand et al., 1994).

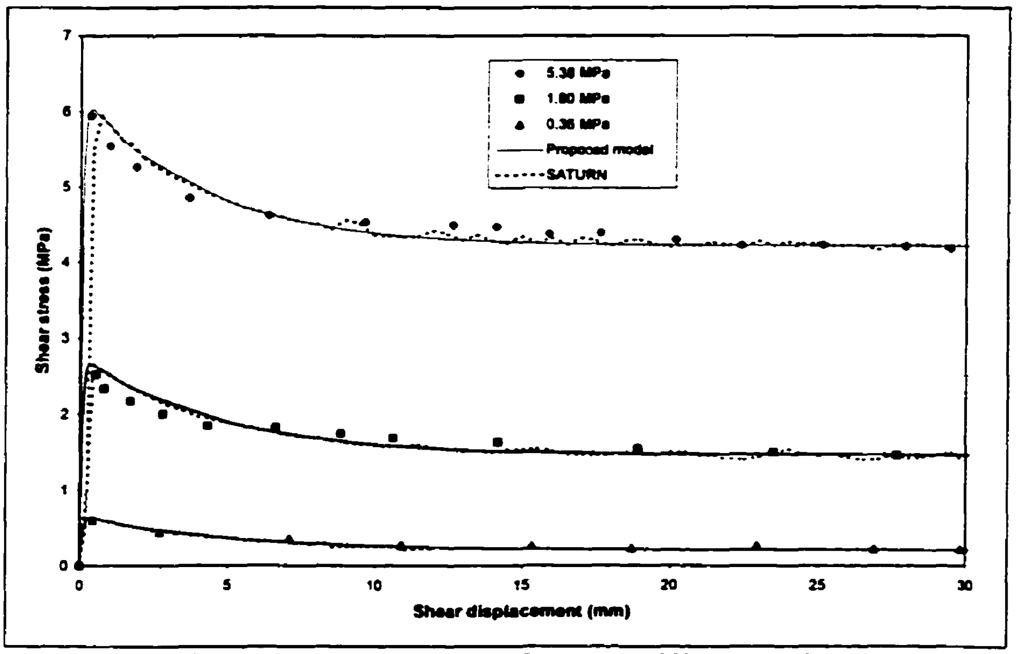

Figure 5.23c: Comparison of results obtained from SATURN and the proposed model for direct shear tests under different constant normal stresses (data taken from Leichnitz, 1985).

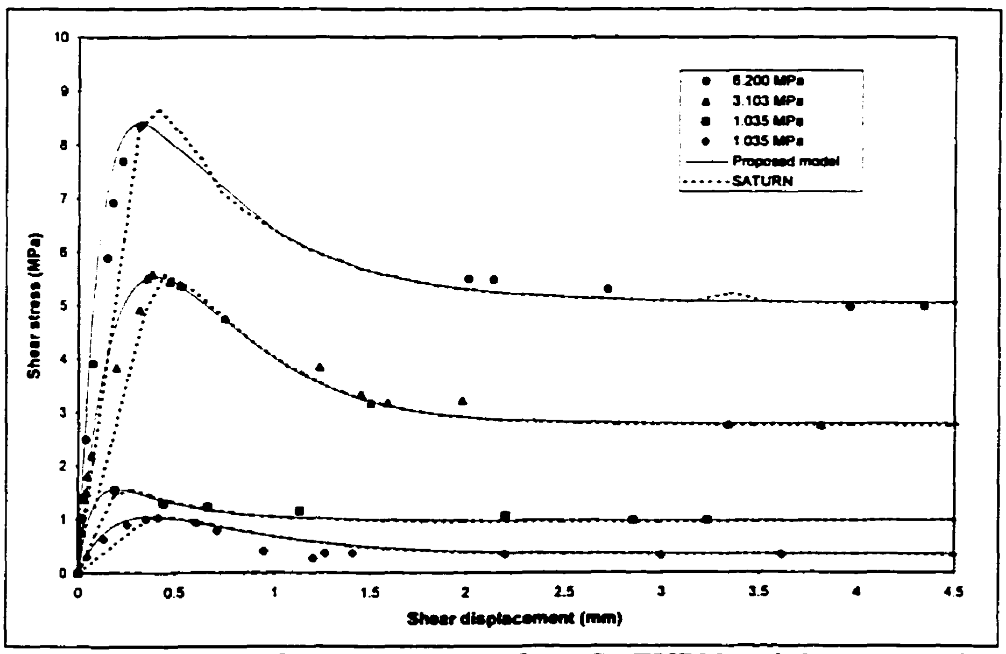

Figure 5.23d: Comparison of results obtained from SATURN and the proposed model for direct shear tests under different constant normal stresses (data taken from Bertrand, 1989).

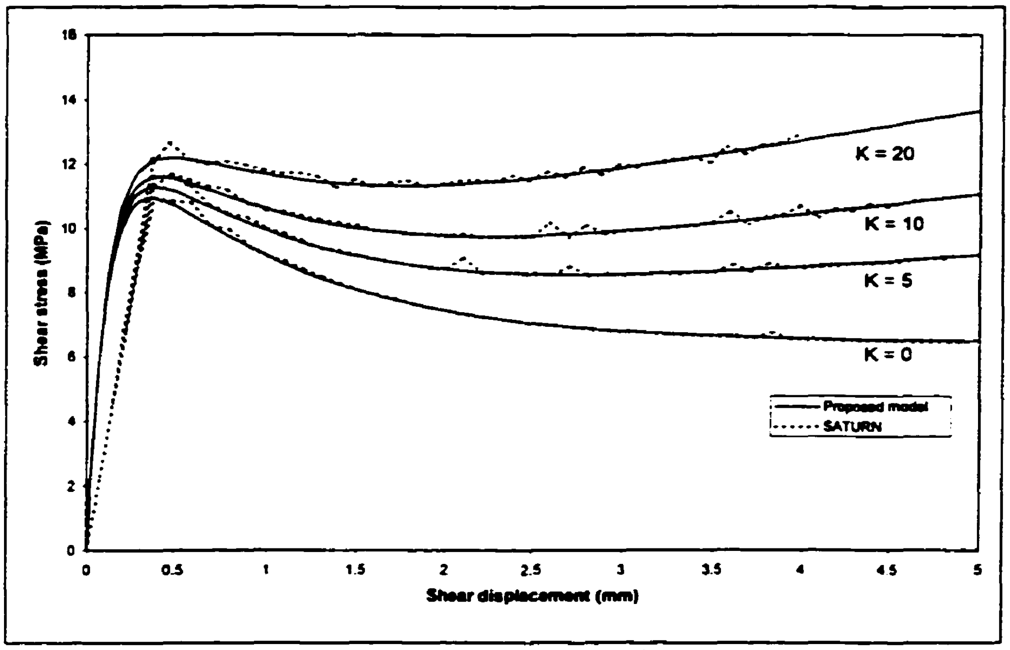

Figure 5.24a: Shear stress - shear displacement curves for direct shear test under different constant normal stiffness K.

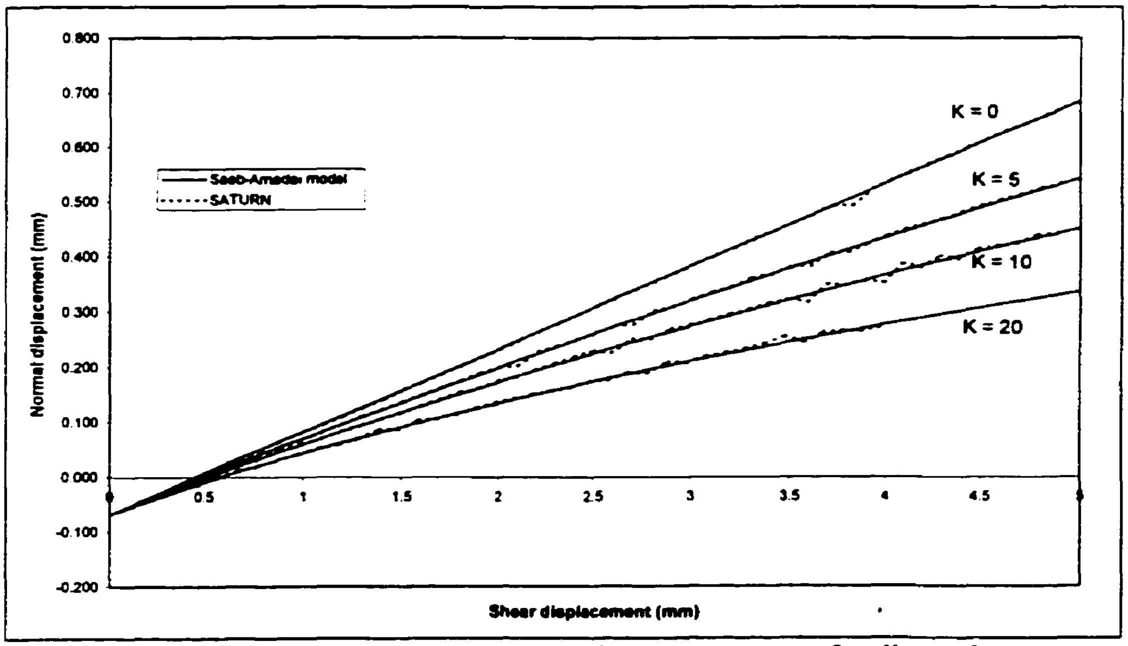

Figure 5.24b: Normal displacement - shear displacement curves for direct shear test under different constant normal stiffness K.

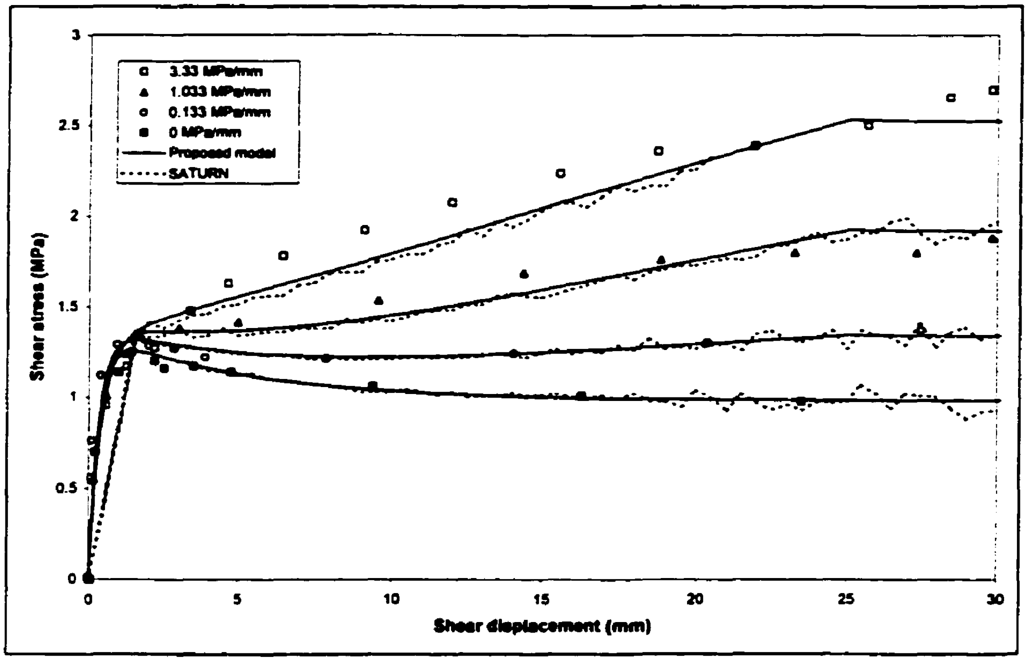

Figure 5.25: Comparison of results obtained from SATURN and the proposed model with direct shear tests under different constant normal stiffness with an initial normal stress of 1 MPa (data taken from Skinas et al., 1990).

CHAPTER 6

PARAMETRIC ANALYSES AND SIMPLE CASE STUDIES

To demonstrate how the tools developed in Chapter 5 can be used to evaluate the fault-slip rockburst potential of underground openings, several cases are presented in the second section of this chapter. In the first section, a sensitivity analysis of the proposed model is performed to evaluate which parameters of the model have more influence on the joint behavior.

6.1 SENSITIVITY ANALYSIS OF THE PROPOSED MODEL

As it was shown in Chapter 5, the proposed constitutive model for rock joints can be studied from two separate relationships: the shear stress-shear displacement relationship and the normal to shear displacement relationships. Hence, these topics are treated separately in the following.

6.1.1 Shear stress - shear displacement relationship

For all the cases that are studied, the model parameters value are given in Table 6.1 (except for the studied parameter).

Table 6.1: Parameters value used in the sensitivity analysis

σ_n (MPa)	u_p (mm)	u_r (mm)	B_0	σ_T (MPa)	i_o (°)	ϕ_u (°)	ϕ_0 (°)	S_0 (MPa)
10	1	5	0.5	100	10	40	40	5

Figure 6.1 shows the influence of the normal stress on the shear stress curve. As the normal stress increases, the strength of the joint increases also, leading to a higher peak strength. The stress drop from the peak strength to the residual strength also increases as the normal stress increases. This leads to a larger post-peak stiffness at higher normal stress.

Figure 6.2 and 6.3 show the influence of the peak and residual displacement. As could be expected, the closer these displacements are to each other, the larger the post-peak stiffness is (the region where the stress drop must take place being reduced). These graphs reveal that these parameters are very important values to be determined in the assessment of the fault-slip rockburst potential. Another important parameter is the peak to residual strength ratio (B_0), as shown in Figure 6.4. This parameter controls (in part) the stress drop that is occurring after the peak, hence having a direct impact on the post-peak shear stiffness of the joint.

Figure 6.5 presents the control of the stress ratio (σ_n/σ_T) on the shear stress-displacement curve. As it can be seen in that figure, a stress ratio increase leads to a larger peak strength but does not increase the post-peak stiffness. In fact, the post-peak stiffness is smaller as the residual strength is increasing in a larger fashion than the peak strength.

Finally, Figure 6.6 to 6.9 shows the influence of the initial angle of asperities, friction angle of the joint and the failure parameters of the rock walls (cohesion and angle of friction). These parameters all have an effect on the peak strength of the joint, the most influent being the angle of asperities and the friction angle of the joint.

6.1.2 Normal displacement - shear displacement relationship

For all the cases that are studied, the model parameters value are the same as in Table 6.1 plus the values in Table 6.2. From Equation (5.38), which formulate the relation between the normal and shear displacements, the parameters that affect the dilatancy curve are the normal stress, the residual displacement, the stress ratio, the initial angle of asperities, the initial normal stiffness and the maximum closure. All the other parameters used in the model (u_p, B_0, S_0, ϕ_u, ϕ_0) have no effect on the dilatancy curve.

Table 6.2 Other parameters value used in the sensitivity analysis

k_{ni} (MPa/mm)	V_m (mm)
1000	10

Figure 6.10 presents the influence of the normal stress on the dilatancy curve. As it can be seen (and as one would expect), any increase of normal stress limits the dilatancy of the joint. Thus, in situations of constant normal stiffness, this leads to a maximum rate of increase of normal stress in the beginning of the shearing process that diminishes as the dilatancy rate is lowered by the increase of normal stress.

Figure 6.11 shows the influence of the residual displacement on the dilatancy curve. At small displacement, this parameter has minimal effect on the curve. Moreover, if the residual displacement is large compared to the peak displacement (as it is often the case; see Appendix A), u_r will have no effect on the curve before the peak displacement.

Figure 6.12 presents the influence of the stress ratio (σ_n/σ_T). As can be seen, this ratio has a great effect on the dilatancy of the joint. As the ratio increases, the dilatancy rate decreases considerably. This could be explained by the fact that as the normal stress approaches the strength of the rock asperities, a larger portion of these asperities are sheared, hence limiting the dilatancy. Another parameter that has the same kind of effect is the initial angle of asperities, as shown in Figure 6.13. Evidently, if this angle is nil, there is no dilatancy at all. Then, when this angle increases, not only the peak strength increases but also does the dilatancy, even for small differences in the angle value.

Figure 6.14 shows the effect of the initial normal stiffness on the curve. What can be observed by varying this parameter is that the shape of the curve is not affected by this parameter. Only the initial value of normal displacement is affected by this parameter. Hence, this does not affect the rate of dilatancy or the increase in normal stress due to dilatancy.

Finally, the last parameter that influence dilatancy is the maximum closure. In the same fashion as the initial normal stiffness, this parameter has no effect on the rate of dilatancy as shown in Figures 6.15a and 6.15b for different values of k_{ni}. Moreover, as the initial normal stiffness increases (Figure 6.15b), the effect of the maximum closure becomes negligible.

In conclusion of all these sensitivity analyses, it appears that some parameters have more influence on the model and should be determined more carefully. These parameters are the peak and residual displacements (u_p, u_r), the residual to peak strength ratio (B_0), the initial angle of asperities (i_o), the friction angle of the joint (ϕ_u) and the transitional stress (σ_T) that determines the stress ratio.

6.2 EXAMPLES OF APPLICATION

To illustrate how one can use the tools that were developed to evaluate the possibility of a violent slip along a fault near a mine opening, a few fictitious cases are presented here.

6.2.1 Mine stope approaching a fault

Figure 6.16 shows a typical cut-and-fill stope mined in several steps that comes in the vicinity of a major geological discontinuity. For this hypothetical case, the far field or in situ stresses are:

Horizontal stress: $\sigma_h = 60$ MPa

Vertical stress: $\sigma_v = 25$ MPa

These bring a ratio of horizontal over vertical stress of 2.4, a situation that can be encountered in a few Canadian underground mines. The elastic properties of the rock mass are:

Elastic modulus: $E_m = 50$ GPa

Poisson's ratio: $\nu = 0.30$

The characteristics of the fault used in this analysis are given in Table 6.3.

Table 6.3: Characteristics of the fault used in the analysis

u_p (mm)	u_r (mm)	B_0	σ_T (MPa)	i_o (°)	ϕ_u (°)	ϕ_0 (°)	S_0 (MPa)	k_{ni} (MPa/mm)	V_m (mm)
1	20	0.75	50	4	30	50	9.1	1000	10

The analyses performed at each step shows that at step 5, failure occurs on the fault on the right side of the stope (Figure 6.17). Figure 6.18 shows the major and minor principal stress induced by the stope. As we can see on Figure 6.17, failure occurs on the length of 5 meters (element 47-48).

To evaluate if the failure will be stable or violent, a stiffness comparison must be made. Figure 6.19 shows the shear behavior of element 47 and 48 at each load step of the final stage of mining. We can then calculate the maximum slope (in absolute values) of each element after the peak displacement is reached. Multiplying the slope by the element length brings the post-peak shear stiffness of the failed element. These values are compiled in Table 6.4.

Table 6.4: Post-peak shear stiffness k'_p of the failed elements (in MPa)

47	48
-9034	-14512

To obtain the shear stiffness of the surrounding rock mass k_e, the method is to replace the failed elements by fictitious shear stresses (σ_s) and to compute the displacement along these elements. The slope of the graph of σ_s*L (shear stress times the length of failed elements) versus the shear displacement (at mid-distance of the failed zone) is plotted. Figure 6.20 shows the results of this process. The value of the slope obtained is -15243 MPa.

To evaluate if there is a risk of violent failure, we can then calculate the Bursting Potential Ratio for joints (BPR_j) given by:

$$BPR_j = \left| \frac{k_p^{'}}{k_e} \right| = \frac{14512}{15243} = 0.95$$

This indicates that the failure would be gradual in this case since the value of BPR_j is lower than unity. However, since the value obtained is very close to 1.0, it might be judicious (in a real situation) to perform more parametric analyses to evaluate if variability in the fault parameter's values would induce a violent failure.

As it was described in Chapter 5, another method that was investigated to evaluate the fault-slip rockburst potential was through the Out-of-Balance Index (OBI). The same case was analyzed to evaluate this OBI. Figure 6.21 shows the values obtained at the last mining stage. As we can see, there are two elements on the right side that have a positive value of OBI (meaning that the peak strength was exceeded). Figure 6.22 shows the progression of the OBI value for elements 47 and 48 after each mining stage. The largest value obtained is 0.31 for element 47. However, at this point, it is impossible to give values of OBI that would indicate a fault-slip rockburst potential.

6.2.2 Mine opening intersecting a fault

Figure 6.23 shows a mine opening intersected by a major geological discontinuity. For this hypothetical case, the far field or in situ stresses are:

Horizontal stress: $\sigma_h = 60$ MPa

Vertical stress: $\sigma_v = 25$ MPa

The elastic properties of the rock mass are:

Elastic modulus: $E_m = 50$ GPa

Poisson's ratio: $\nu = 0.30$

The characteristics of the fault used in this analysis are given in Table 6.5.

Table 6.5: Characteristics of the fault used in the analysis

u_p (mm)	u_r (mm)	B_0	σ_T (MPa)	i_o (°)	ϕ_u (°)	ϕ_0 (°)	S_0 (MPa)	k_{ni} (MPa/mm)	V_m (mm)
0.5	20	0.75	60	4	30	50	9.1	1000	10

This case is analyzed in only one mining step since the opening is perpendicular to the discontinuity. Figure 6.24 shows the results of the analysis. There is failure on the right side fault on a length of 1.8 m. Figure 6.25 shows the behavior of the failed fault element at each loading step. As we can see on this figure, this situation is not of an increasing shear stress that leads to failure but rather a relaxing process. When the opening is created, the stresses on the fault start from the in situ stress field to a situation where the shear stress is less than before. The fact is that the normal stress is reduced considerably when the opening is created, which in turns leads to a failure (as the peak strength is lowered). From this graph, we can also evaluate the post-peak shear stiffness of the failed portion. Multiplying the slope by length of the failed element, we get:

$$k'_p = -1671 \text{ MPa}$$

The shear stiffness of the surrounding rock mass is given by replacing the failed portion by fictitious shear stresses and by plotting the graph of σ_s*L (shear stress times the length of failed elements) versus the shear displacement. Figure 6.26 shows the graph obtained. The value of k_e is then -9190 MPa

Then, the Bursting Potential Ratio for joint is given by:

$$BPR_j = \left| \frac{k'_p}{k_e} \right| = \frac{1671}{9190} = 0.18$$

This value indicates that the failure would be gradual.

The OBI was also evaluated for this case. Figure 6.27 shows the OBI values obtained along the fault. The OBI value obtained for the portion that failed is 0.22. Here again, it is impossible to give values of OBI that would indicate a fault-slip rockburst potential.

6.3 CASE STUDY

To illustrate furthermore how the developed tools can be used in actual mine situation, a case study that was performed by Fotoohi (1993) is re-analyzed here with the proposed model. Figure 6.28 shows the situation of mining stopes approaching 2 faults (plan view). First, stope A is mined, then B and so on. The stopes are relatively high compared with their plan dimensions so the case was analyzed in plan view. To analyzed this case, Fotoohi (1993) has used these parameters:

North-South horizontal stress:	39 MPa
East-West horizontal stress:	52 MPa
Rock mass elastic modulus:	67 GPa
Poisson's ratio:	0.28

For the faults, these parameters were used:

k_{ni}:	13000 MPa/m
V_m	9 mm
u_p	9 mm
ϕ_u	33°
$\sigma_T = \sigma_c$:	160 MPa

The other parameters were not determined since they are not used with the Barton-Bandis model. Hence, they are estimated here:

$B_0 = 0.75$

$S_0 = 9$ MPa

$\phi_0 = 60^{\circ}$

$u_r = 90$ mm

$i_o = 5^{\circ}$

Figure 6.29 shows the major and minor principal stress after the last stage. These stresses compare fairly well with the results obtained by Fotoohi (1993). However, there are major differences in the displacement results. Fotoohi (1993) recalls obtaining shear displacement of more than 108 mm on the fault nearest to the stopes. In this analysis, results show a maximum of 4.5 mm on the same fault. This analysis also shows no signs of failure since the displacements obtained are below the peak displacement of 9 mm. To insure that no mistake was done in the analysis, another analysis was performed using Barton-Bandis model and using the data reported by Fotoohi (1993). The results of this analysis showed no failure and a maximum shear displacement on the fault of 2.6 mm. In addition, when analyzing the results reported by Fotoohi (1993), these results showed on an element a shear stress of 16 MPa for a normal stress of 47 MPa, leading to a friction angle of 20^{0} while the residual friction angle was 33°. It is then in the author's opinion that some mistake may have occurred while preparing the data file that may have led to these results.

Since no failure occurs for the data used, there are evidently no fault-slip rockburst potential in this case (for the data used). The OBI values were also calculated and the results for the most critical element are presented in Figure 6.30. Figure 6.31 shows the

OBI values along the faults for the last mining stage. These results show that there is no fault-slip rockburst potential since the OBI values are negative.

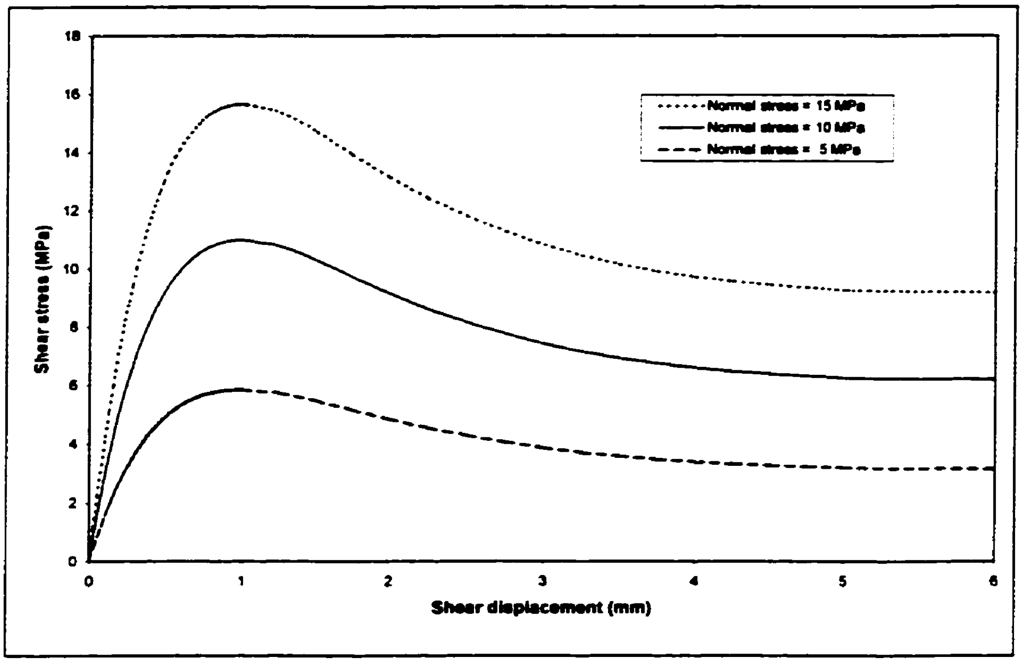

Figure 6.1: Influence of normal stress (σ_n) on the shear stress - shear displacement curve of the proposed model.

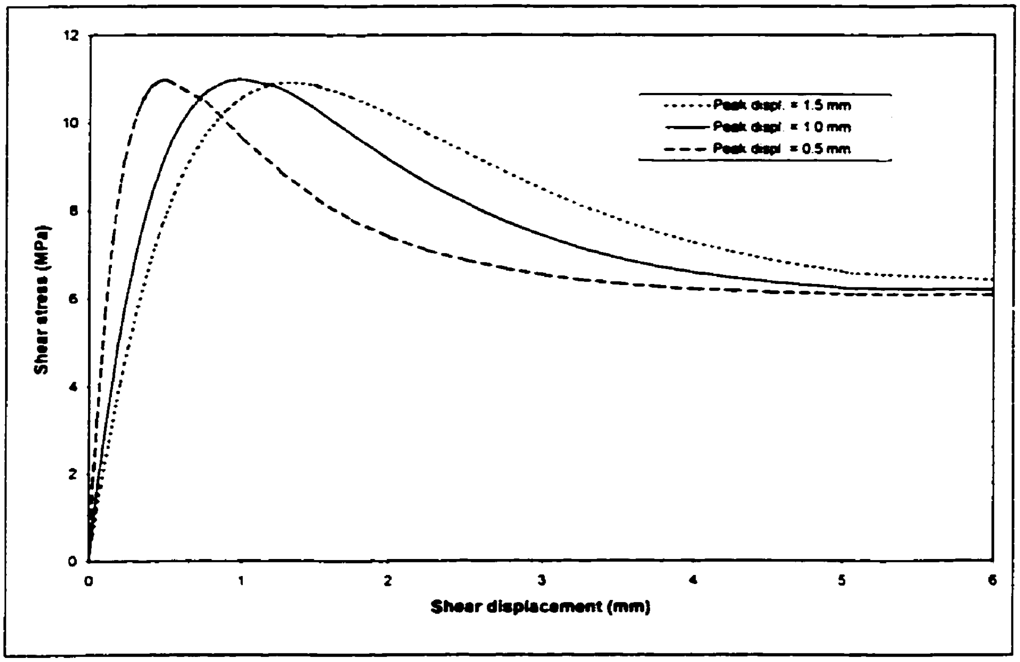

Figure 6.2: Influence of peak displacement (u_p) on the shear stress - shear displacement curve of the proposed model.

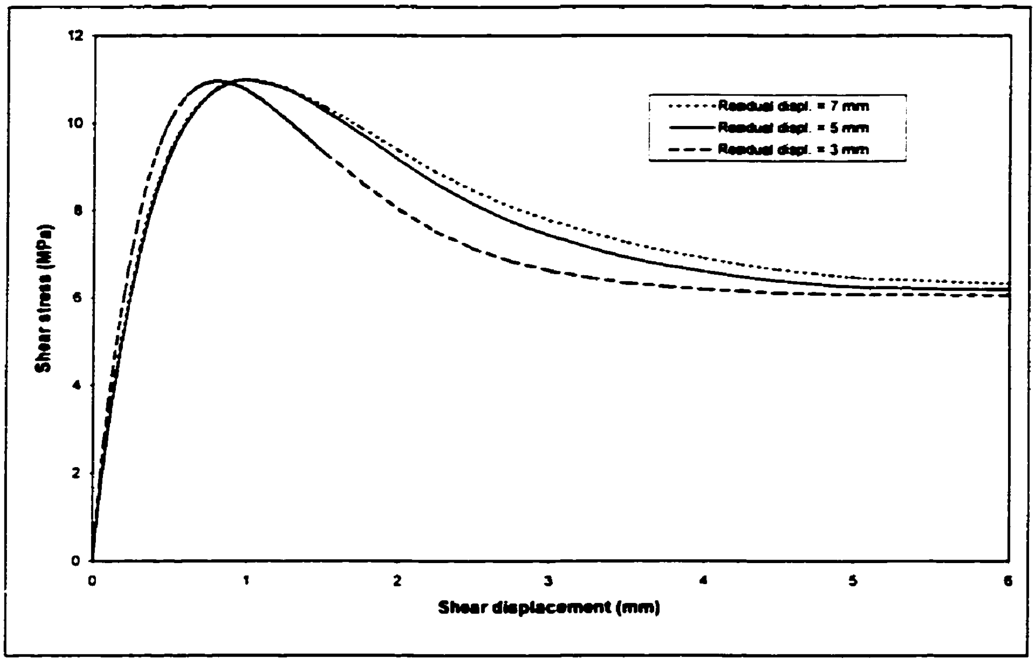

Figure 6.3: Influence of residual displacement (u_r) on the shear stress - shear displacement curve of the proposed model.

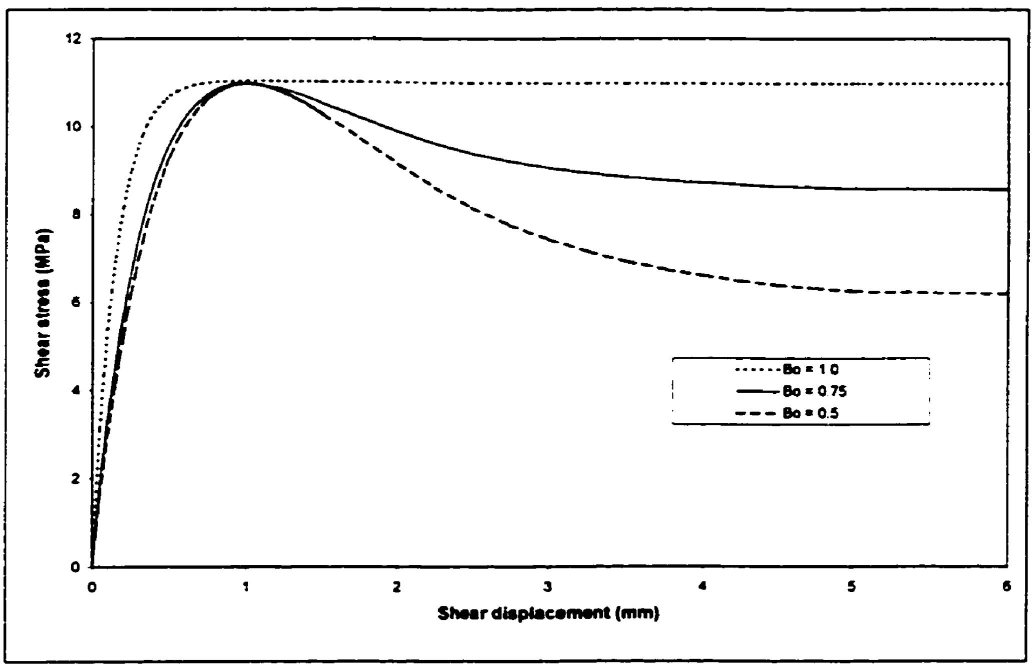

Figure 6.4: Influence of residual to peak strength ratio (B_0) on the shear stress - shear displacement curve of the proposed model.

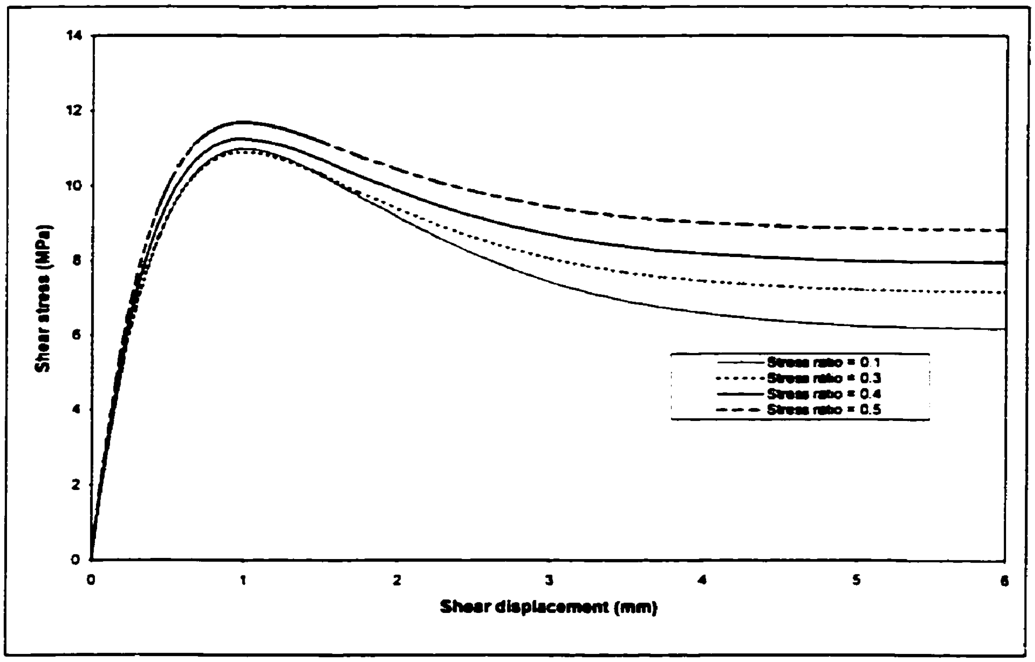

Figure 6.5: Influence of stress ratio (σ_n/σ_T) on the shear stress - shear displacement curve of the proposed model.

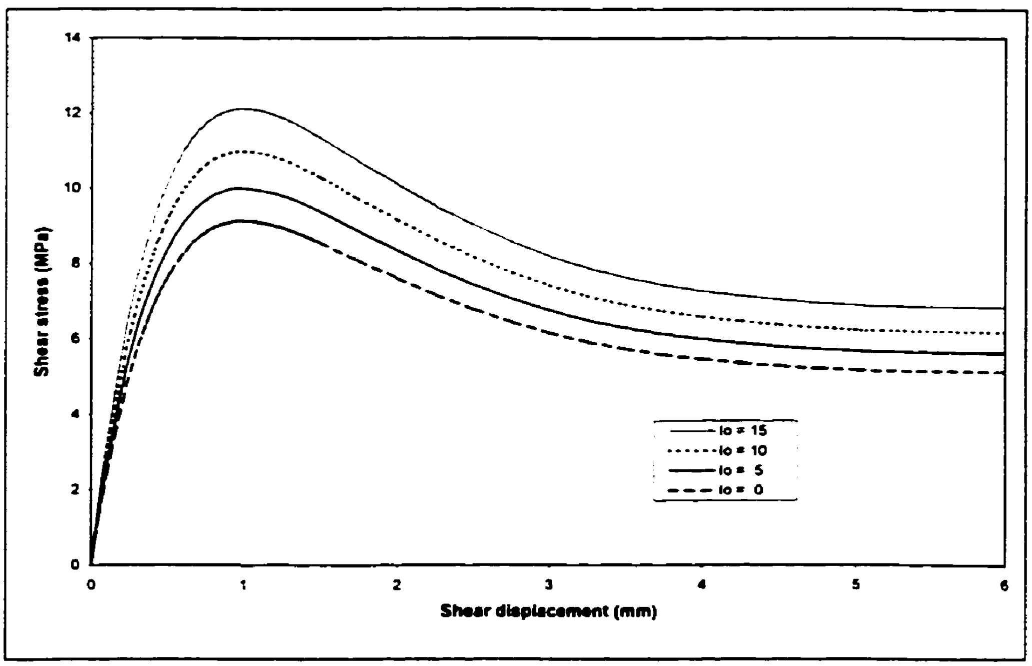

Figure 6.6: Influence of initial angle of asperities (i_o) on the shear stress - shear displacement curve of the proposed model.

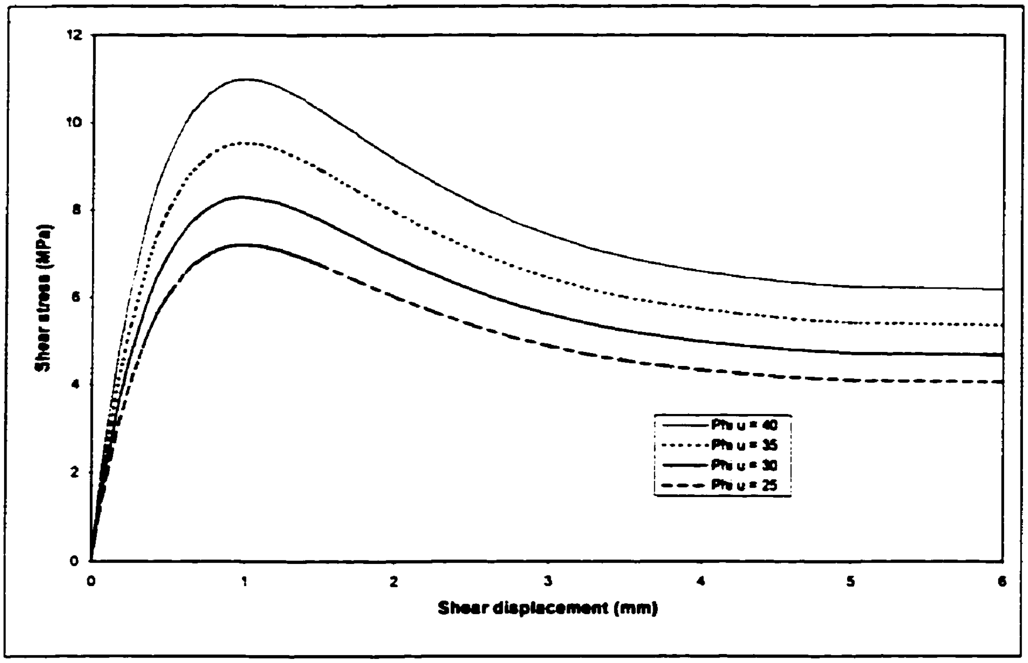

Figure 6.7: Influence of the friction angle of the joint (ϕ_u) on the shear stress - shear displacement curve of the proposed model.

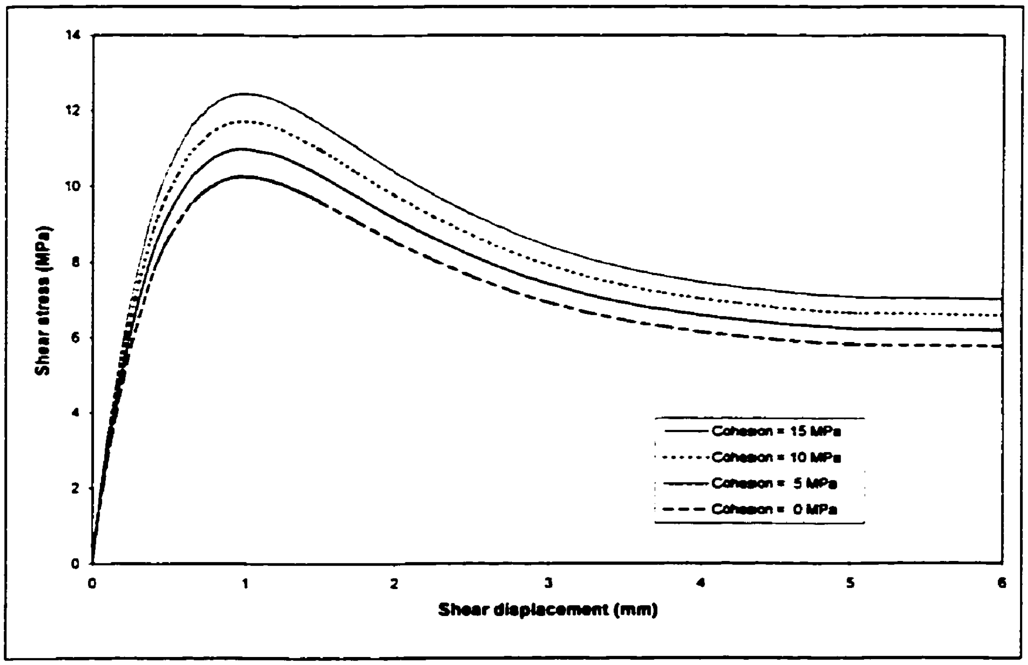

Figure 6.8: Influence of the rock walls cohesion (S_0; using a Mohr-Coulomb criterion) on the shear stress - shear displacement curve of the proposed model.

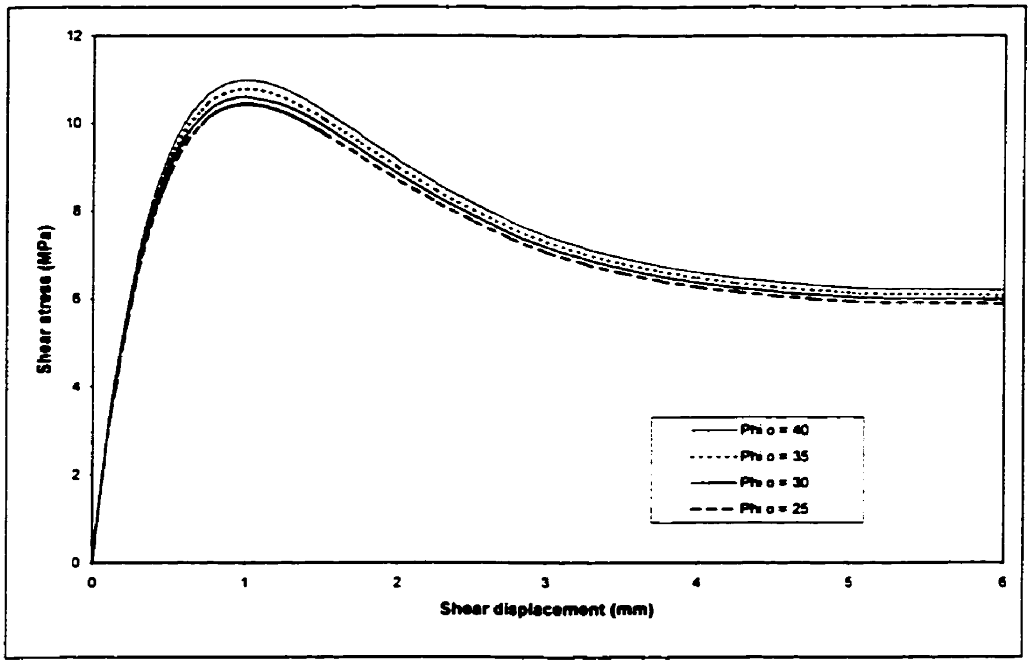

Figure 6.9: Influence of rock walls friction angle (ϕ_0; using a Mohr-Coulomb criterion) on the shear stress - shear displacement curve of the proposed model.

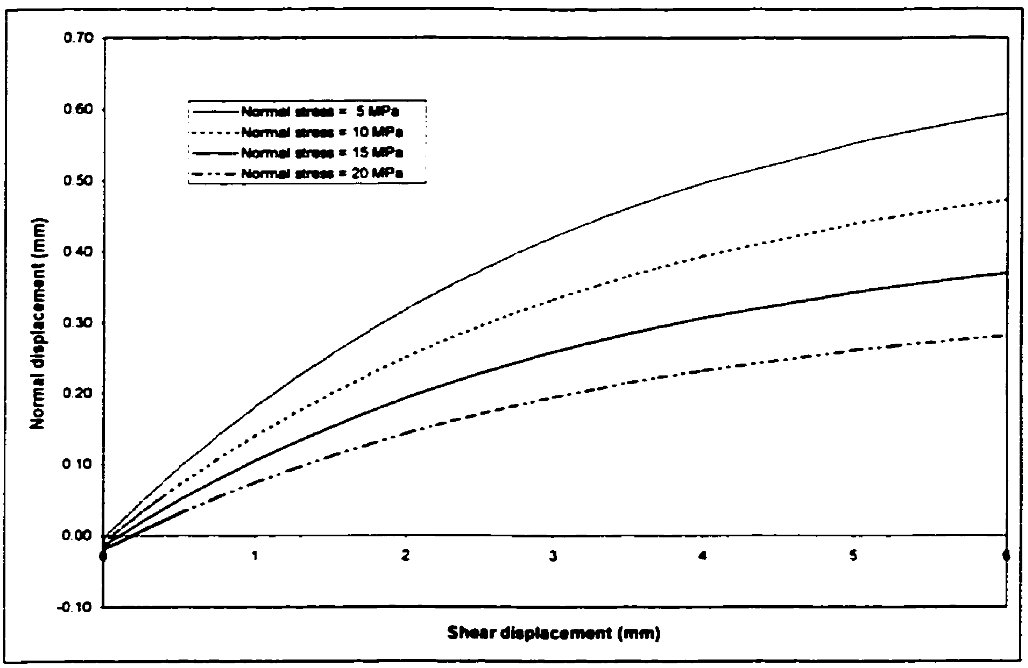

Figure 6.10: Influence of normal stress (σ_n) on the normal displacement - shear displacement curve of the proposed model.

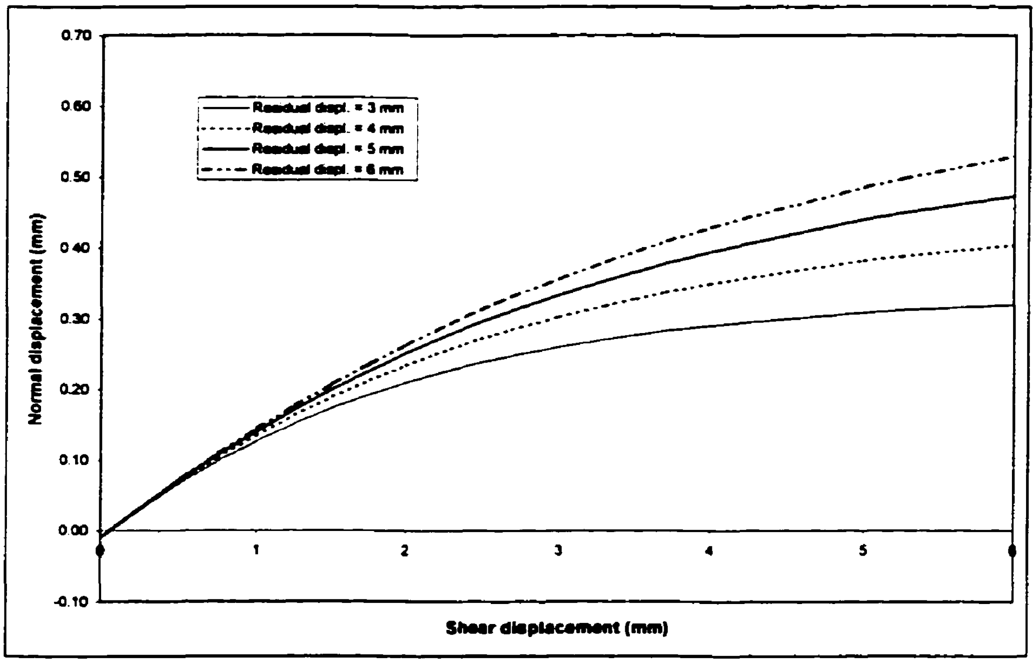

Figure 6.11: Influence of residual displacement (u_r) on the normal displacement - shear displacement curve of the proposed model.

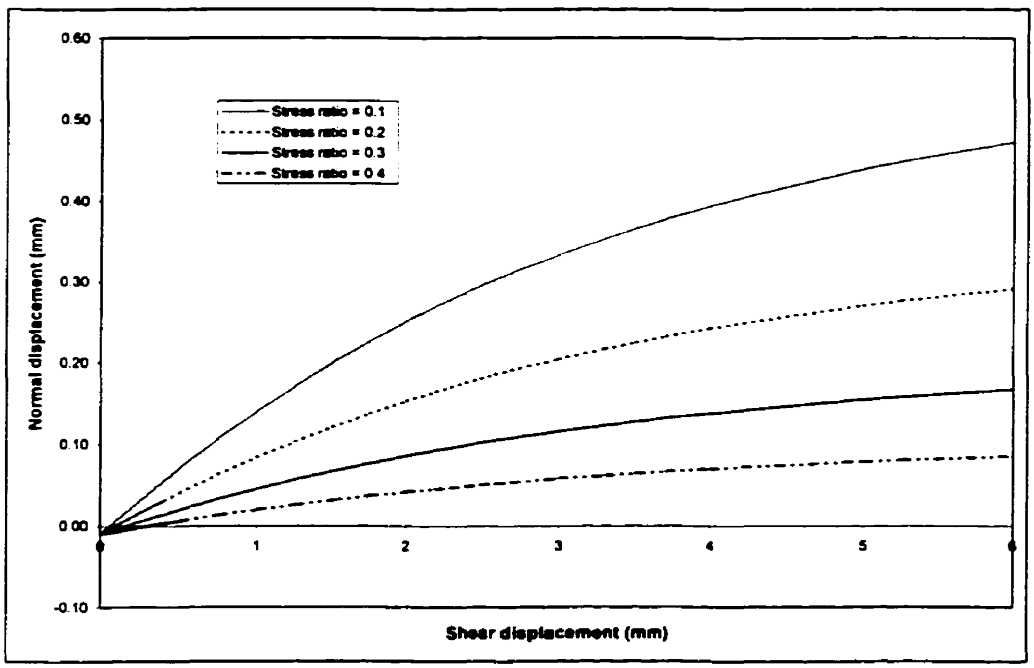

Figure 6.12: Influence of the stress ratio (σ_n/σ_T) on the normal displacement - shear displacement curve of the proposed model.

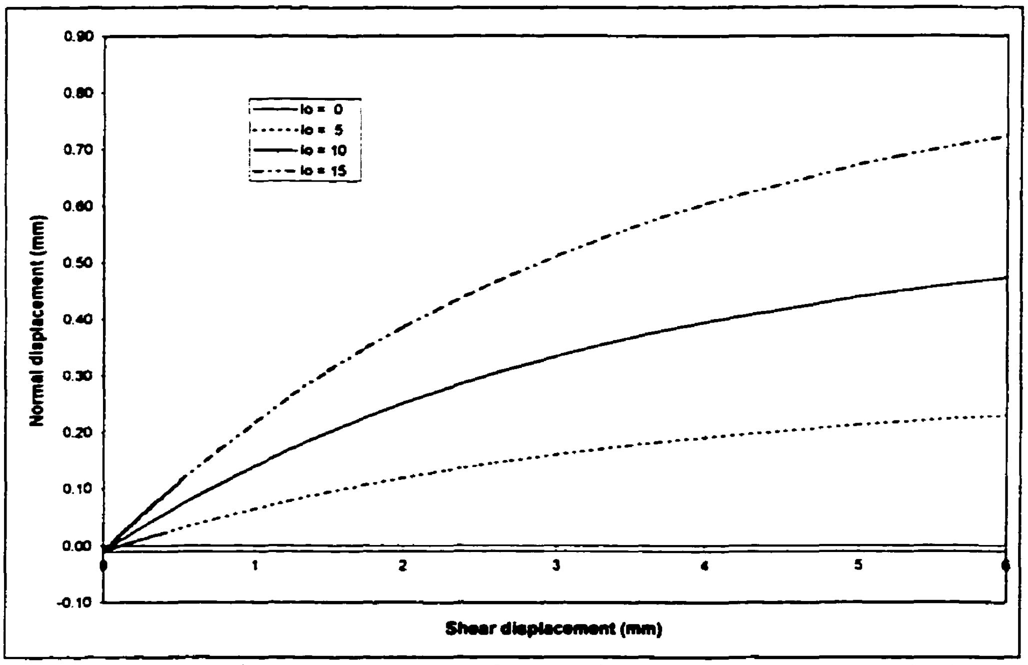

Figure 6.13: Influence of the initial angle of asperities (i_o) on the normal displacement - shear displacement curve of the proposed model.

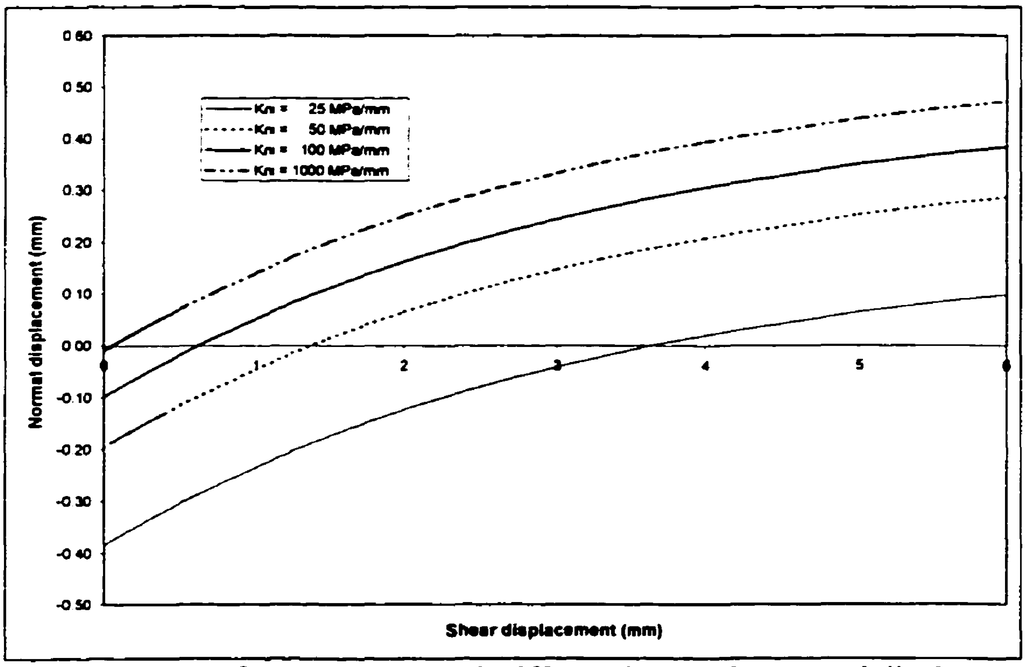

Figure 6.14: Influence of the initial normal stiffness (k_{ni}) on the normal displacement - shear displacement curve of the proposed model.

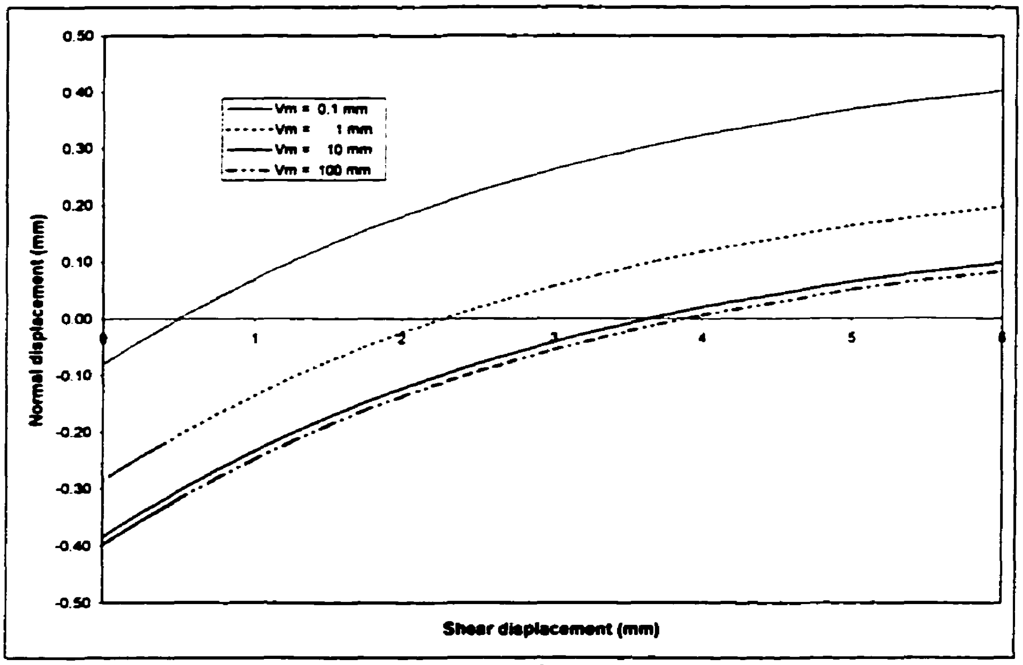

Figure 6.15a: Influence of maximum closure of the joint (V_m) on the normal displacement - shear displacement curve of the proposed model (k_{ni} = 25 MPa/mm).

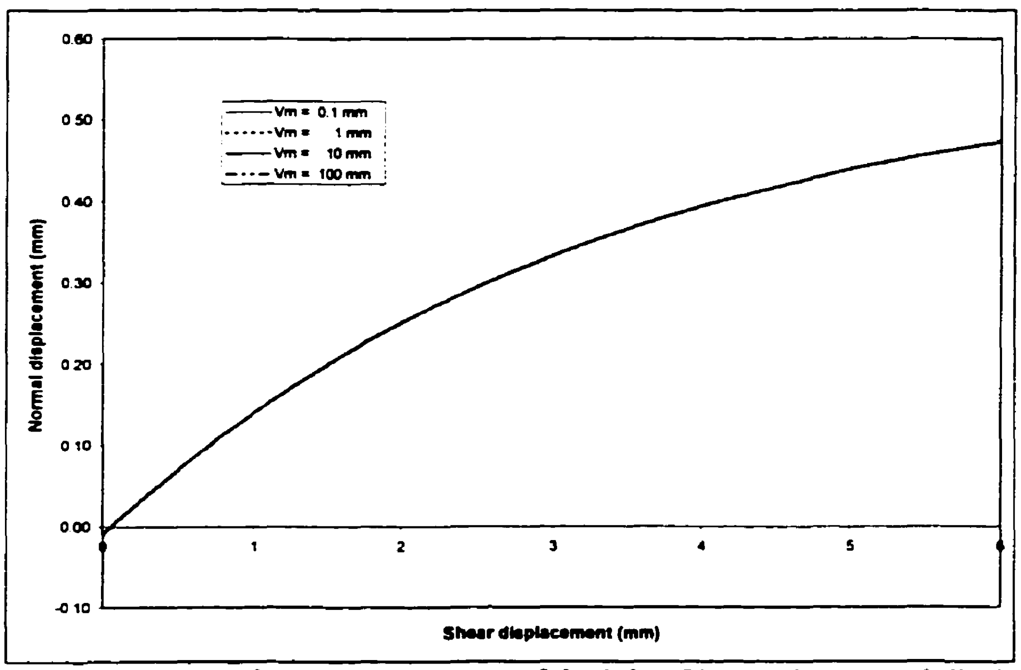

Figure 6.15b: Influence of maximum closure of the joint (V_m) on the normal displacement - shear displacement curve of the proposed model (k_{ni} = 1000 MPa/mm).

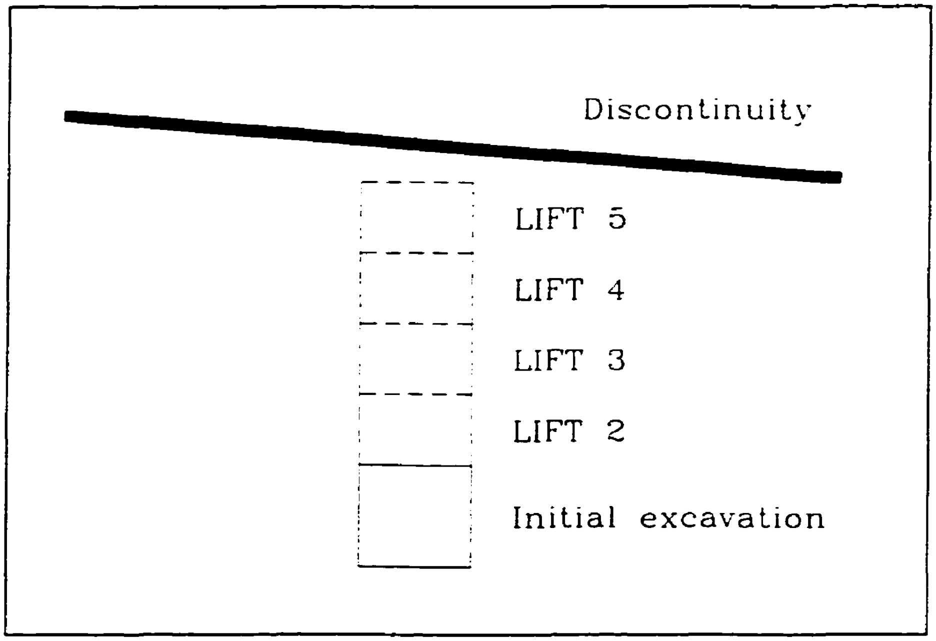

Figure 6.16: Cut-and-fill stope approaching a major geological discontinuity.

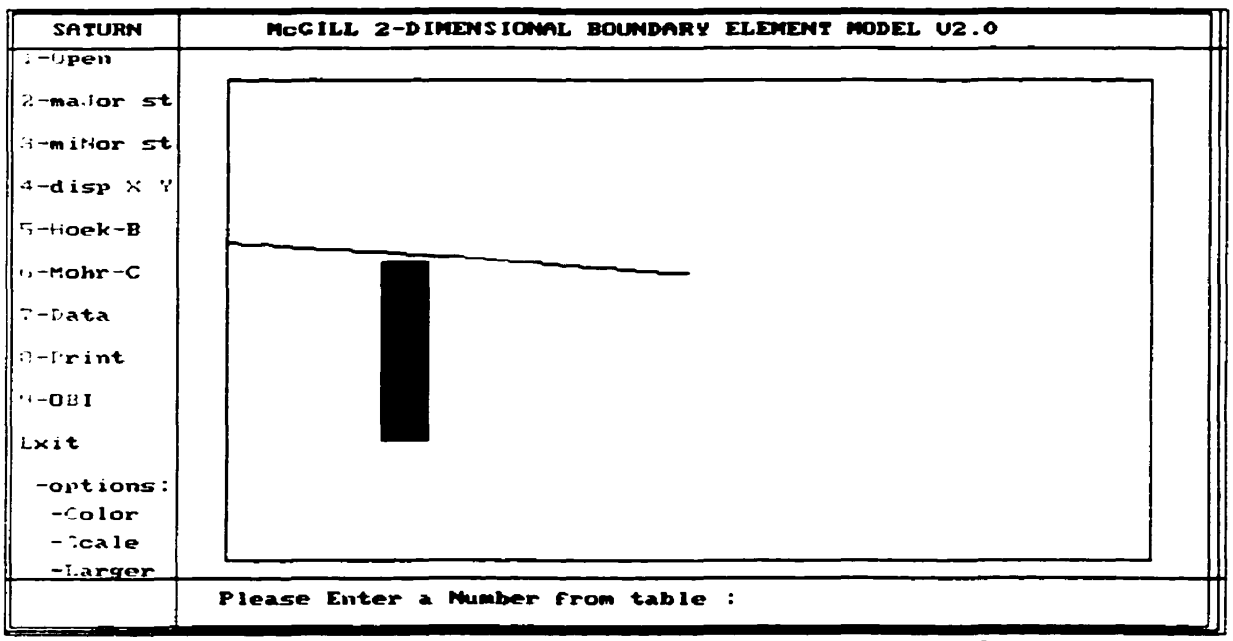

Figure 6.17: Results from the analysis for Case 6.2.1. Grey area on the fault indicate failure.

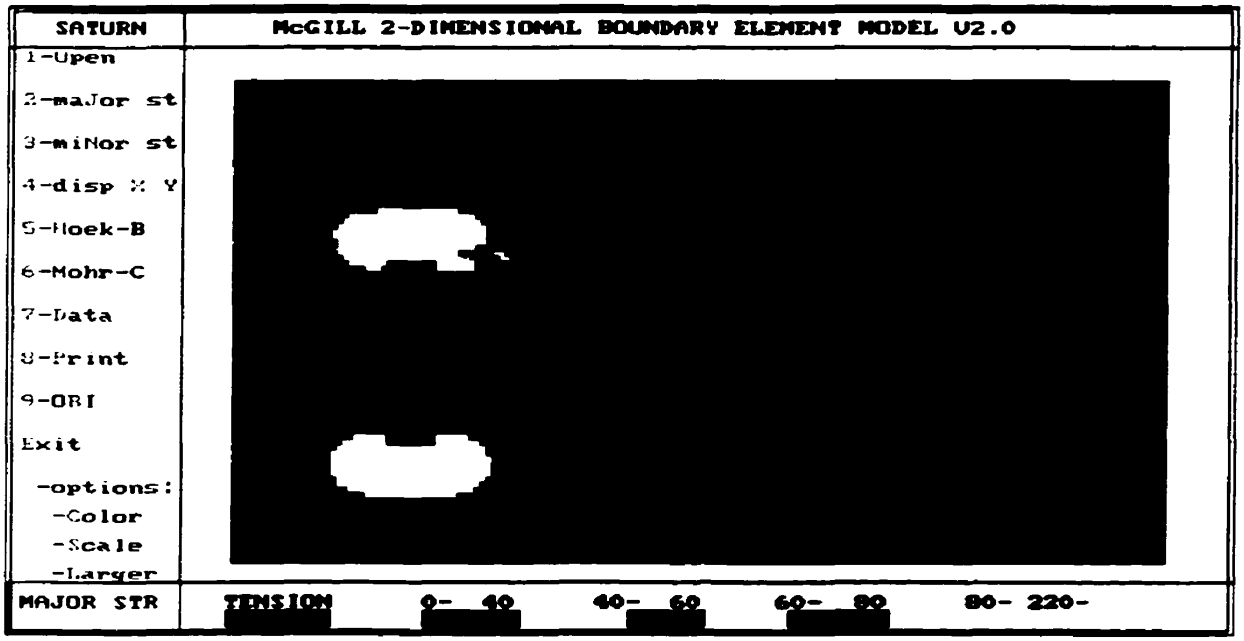

Figure 6.18a: Major principal stress (σ_1) obtained with SATURN.

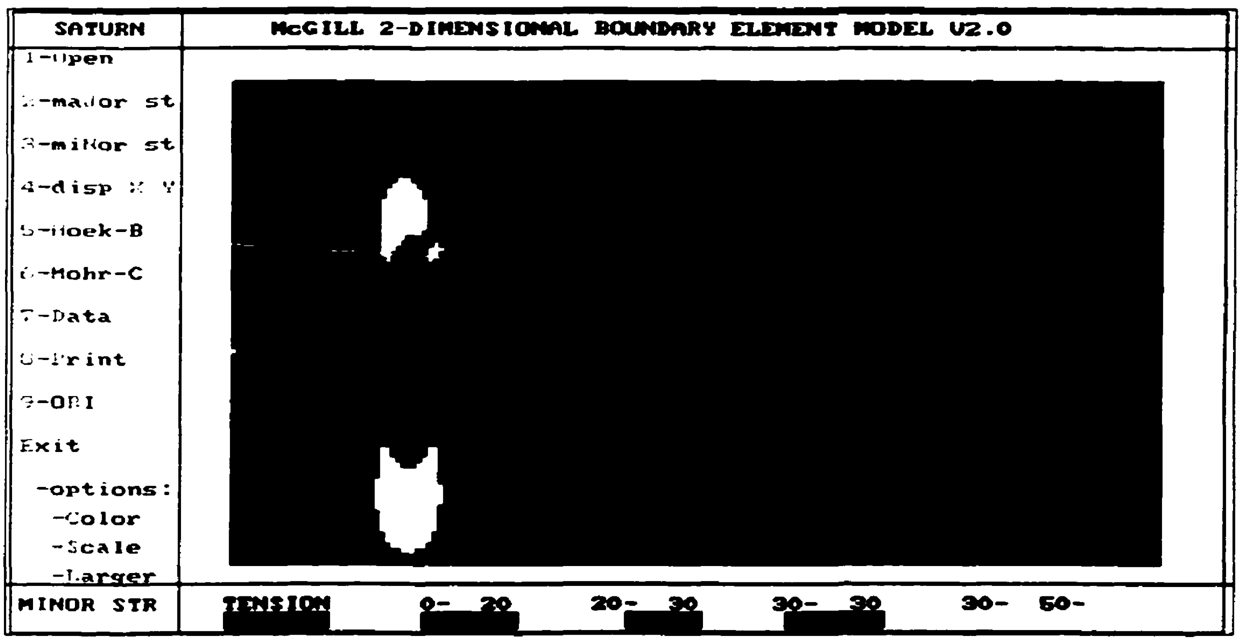

Figure 6.18b: Minor principal stress (σ_3) obtained with SATURN.

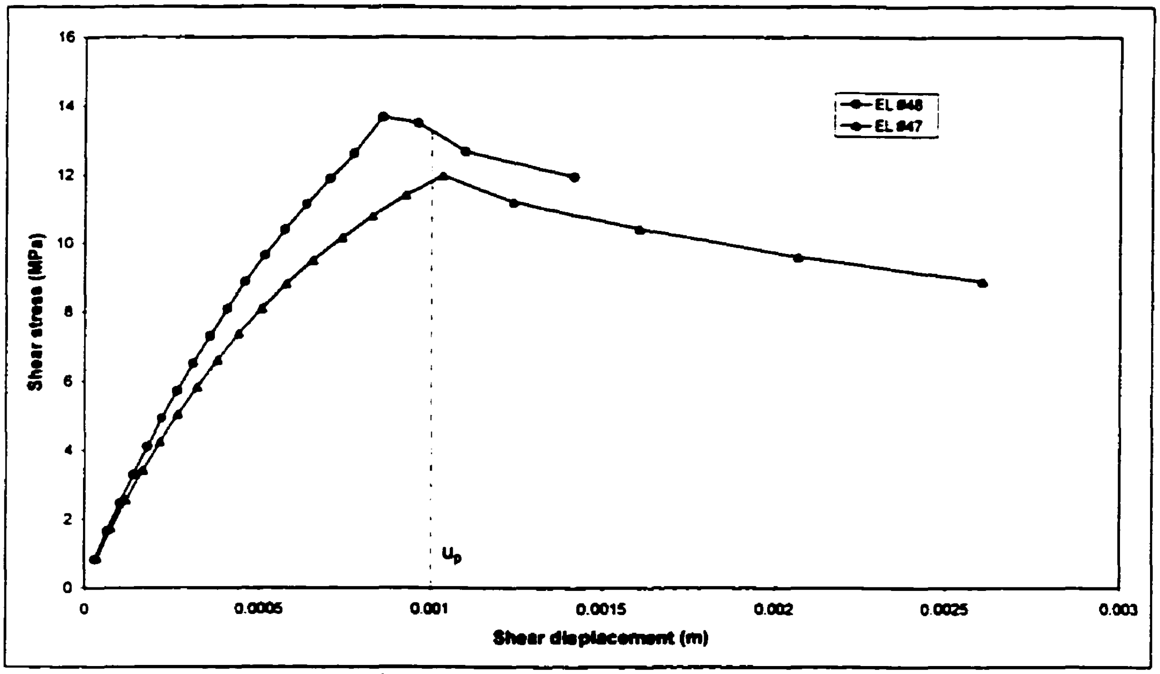

Figure 6.19: Shear behavior of failed elements after each load step of mining stage 5.

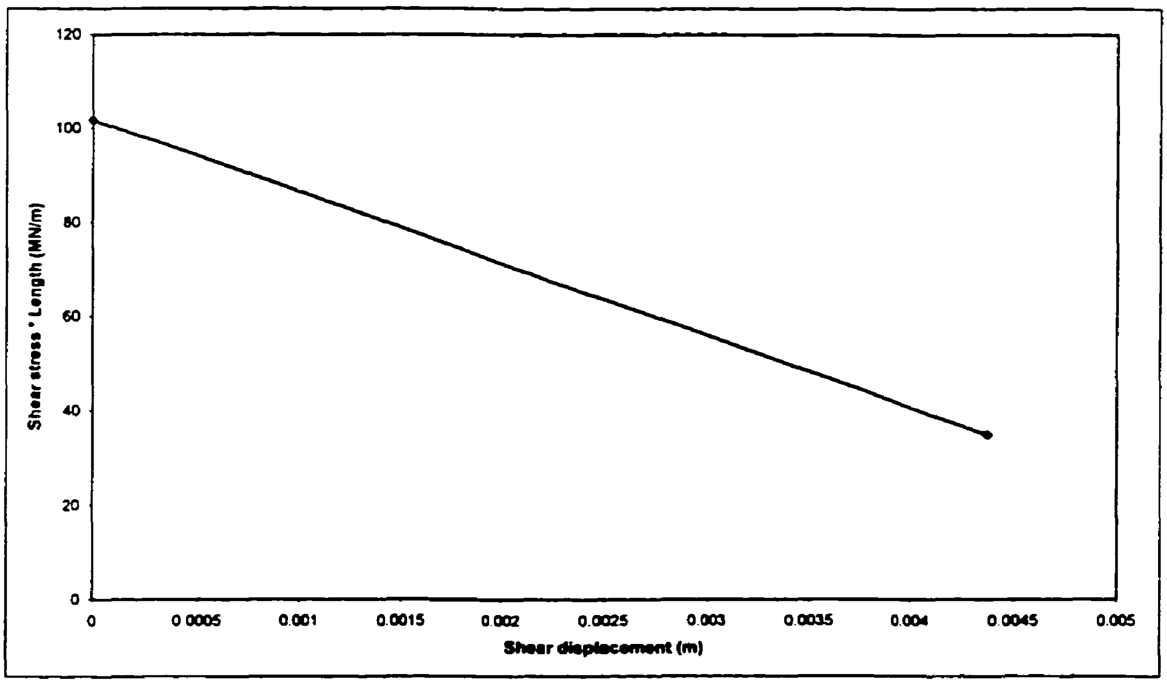

Figure 6.20: Graph of σ_s*L versus the displacement. The slope gives the surrounding rock mass stiffness k_e.

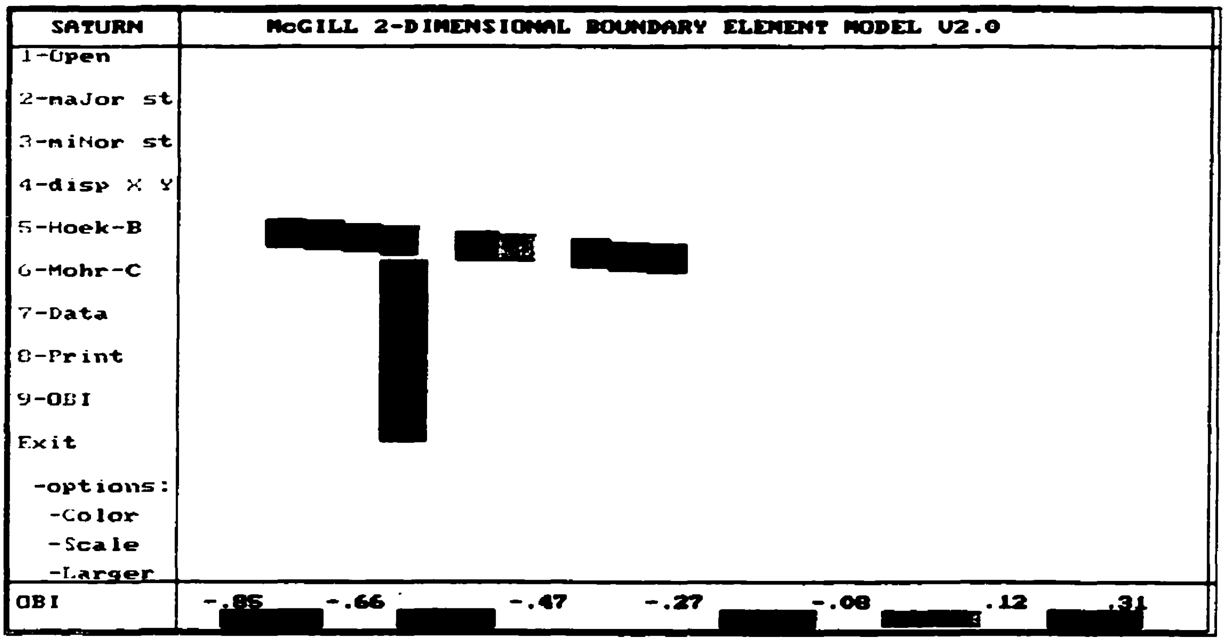

Figure 6.21: OBI values along the fault for mining stage 5.

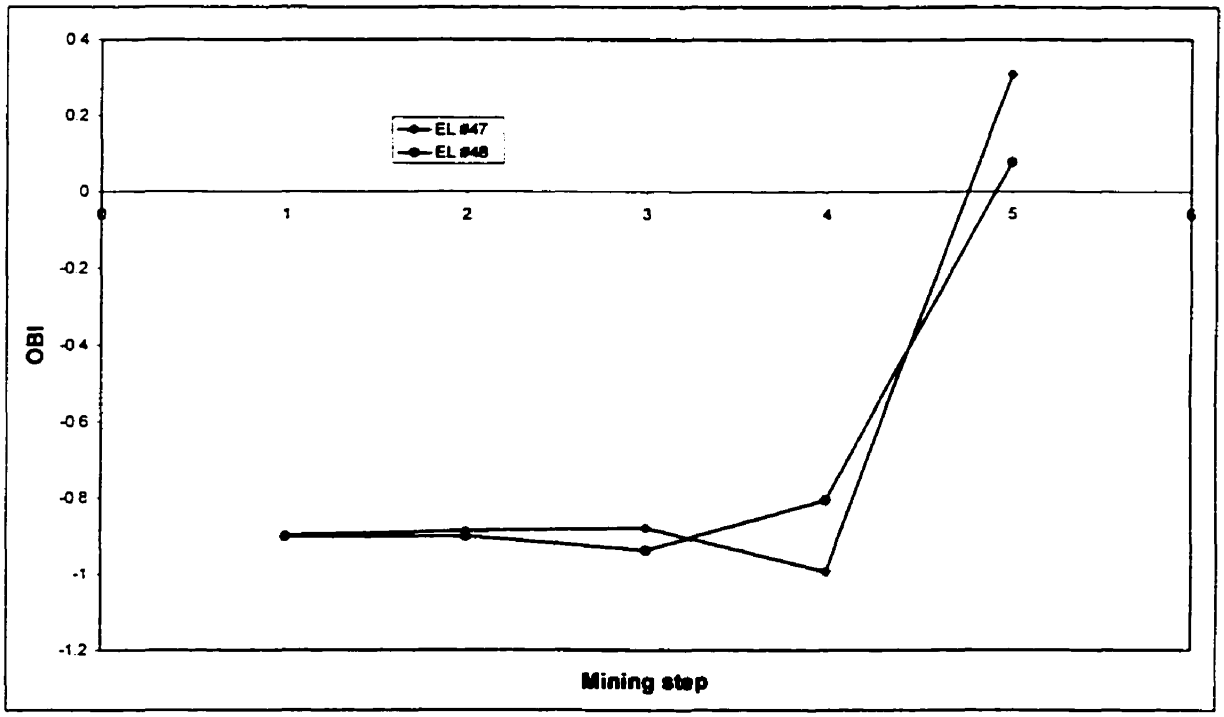

Figure 6.22: OBI values for two elements after each mining stage.

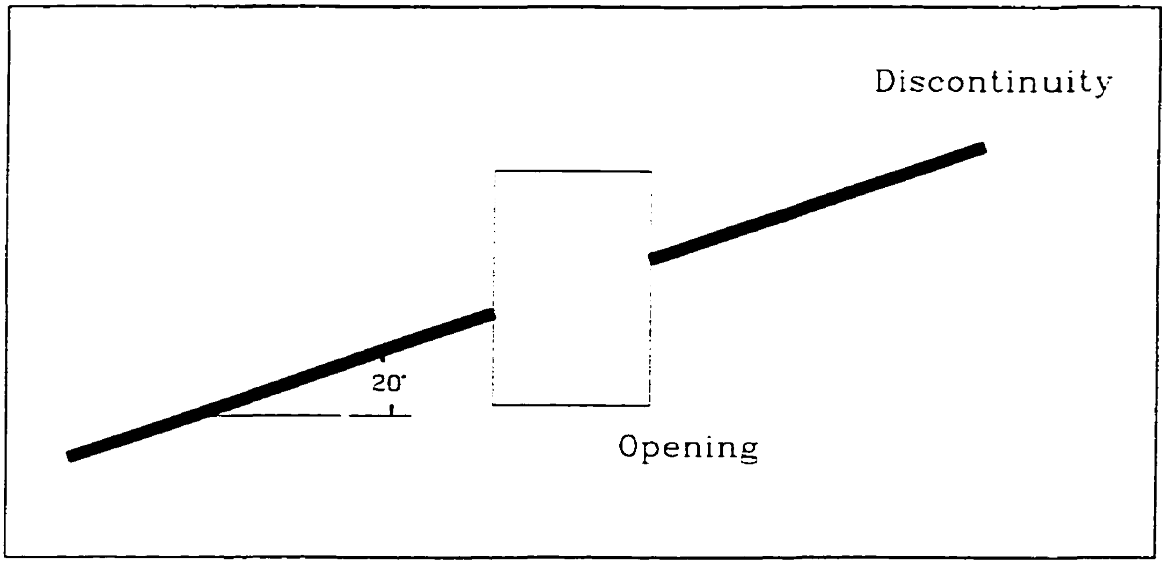

Figure 6.23: Opening intersecting a major geological discontinuity.

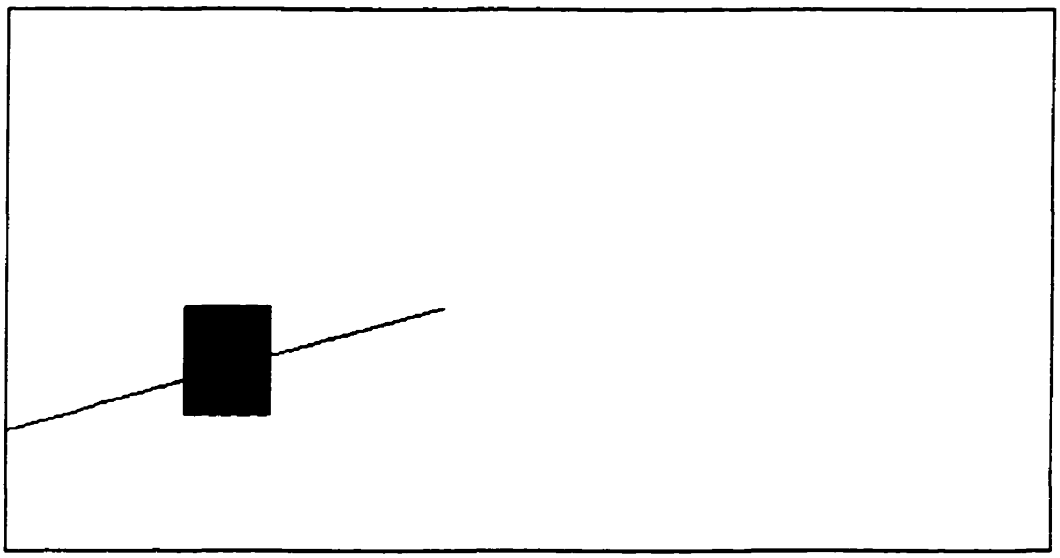

Figure 6.24: Results from the analysis for Case 6.2.2. Grey area on the fault indicate failure.

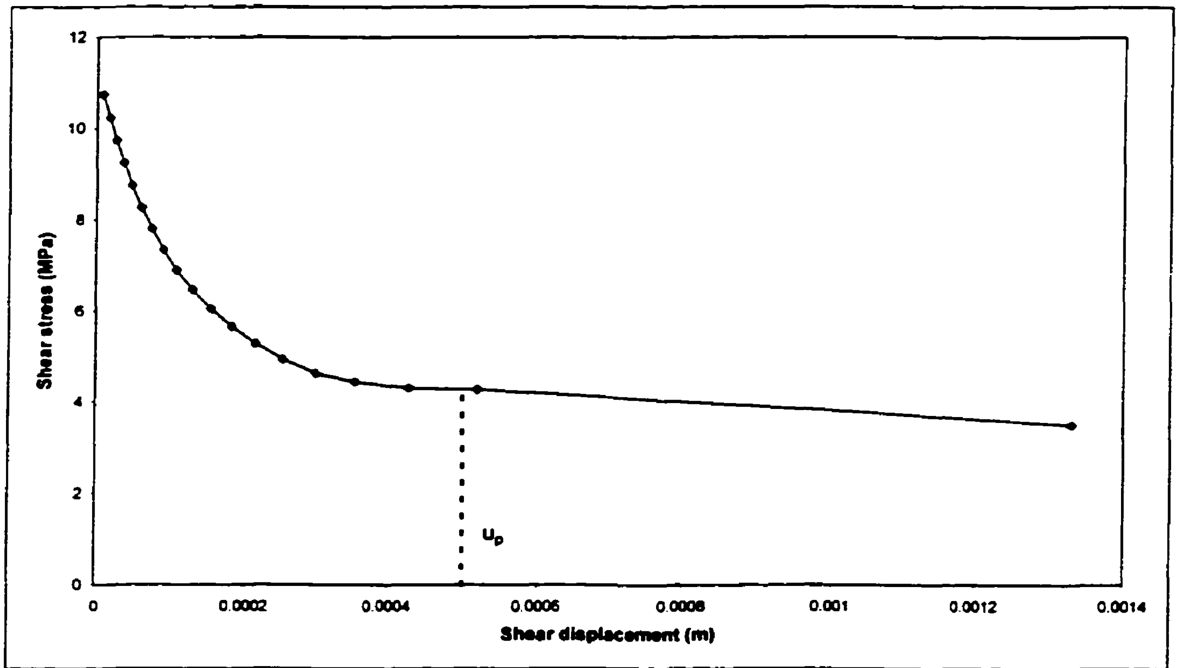

Figure 6.25: Shear behavior of the failed element after each load step.

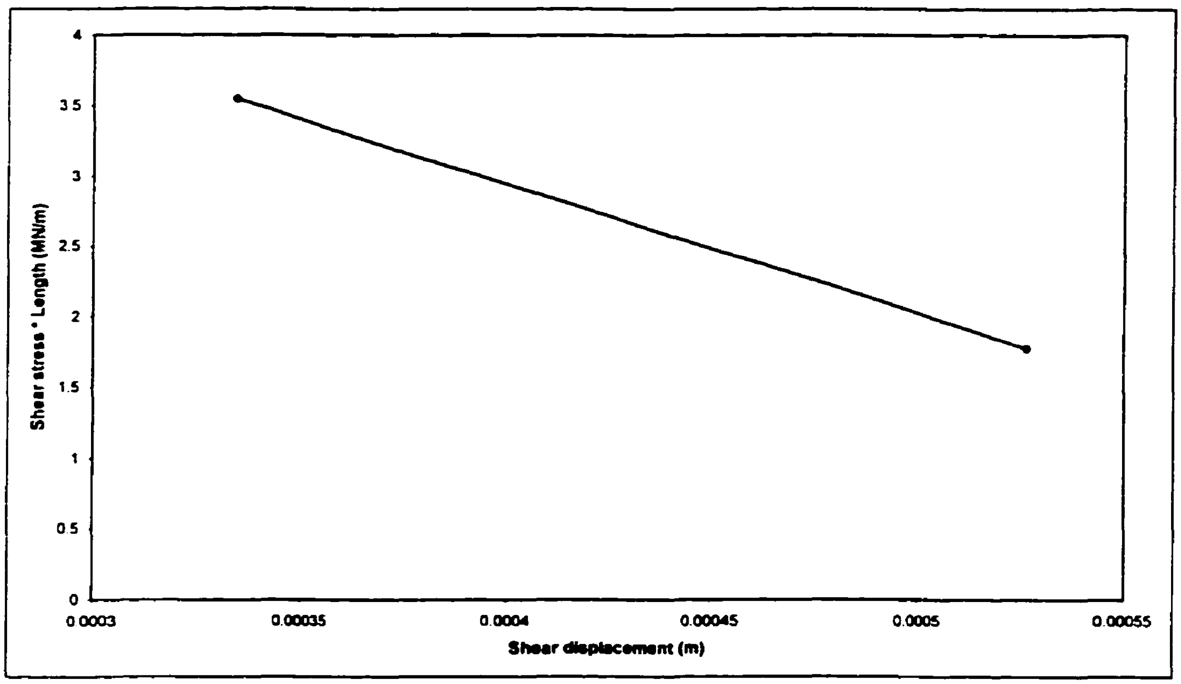

Figure 6.26: Graph of σ_s*L versus the displacement. The slope gives the surrounding rock mass stiffness k_c.

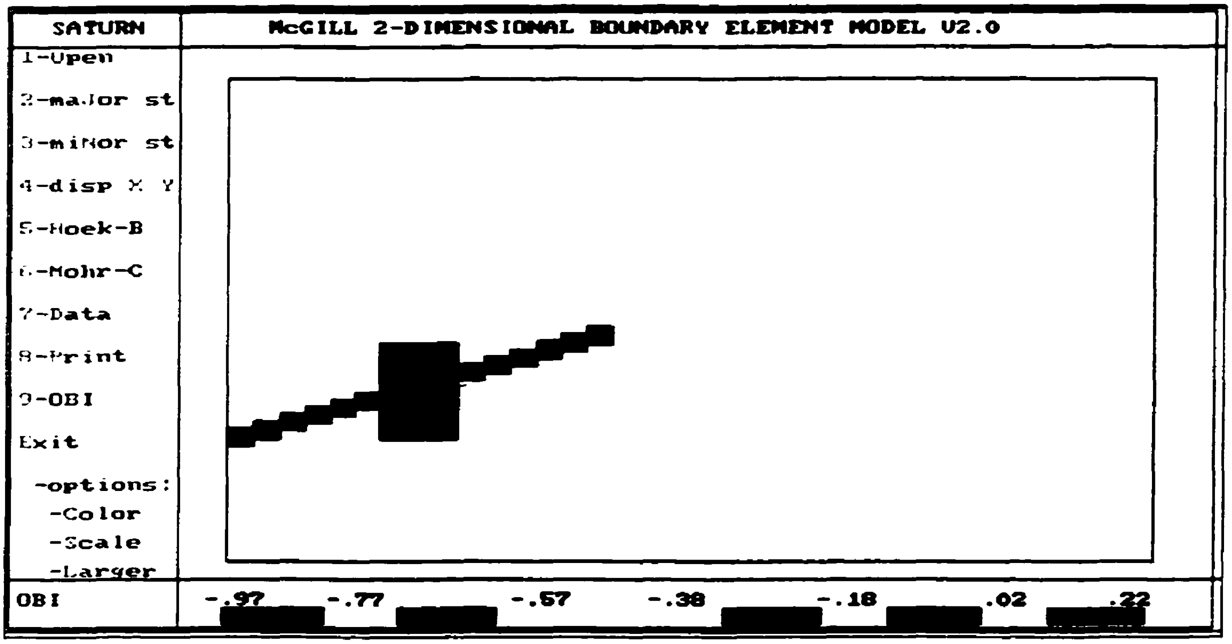

Figure 6.27: OBI values along the fault.

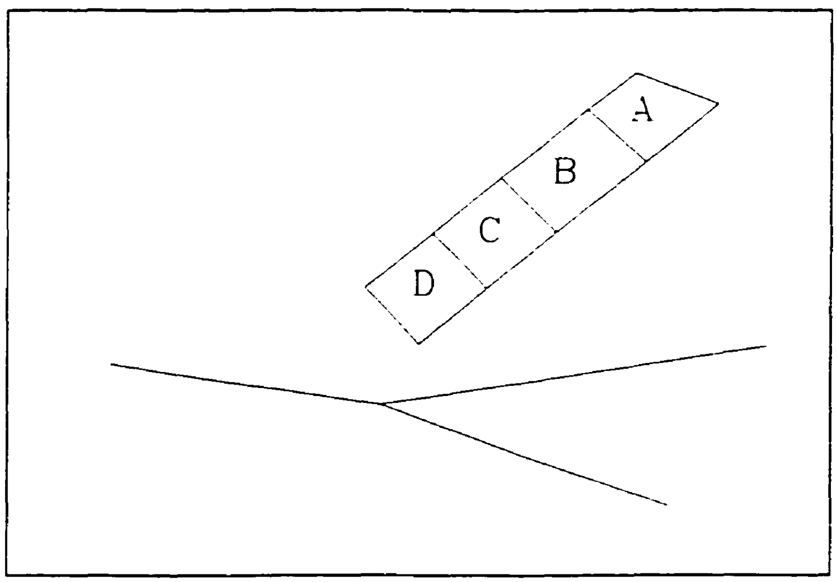

Figure 6.28: Stopes mined in sequence near faults in plan view (after Fotoohi, 1993).

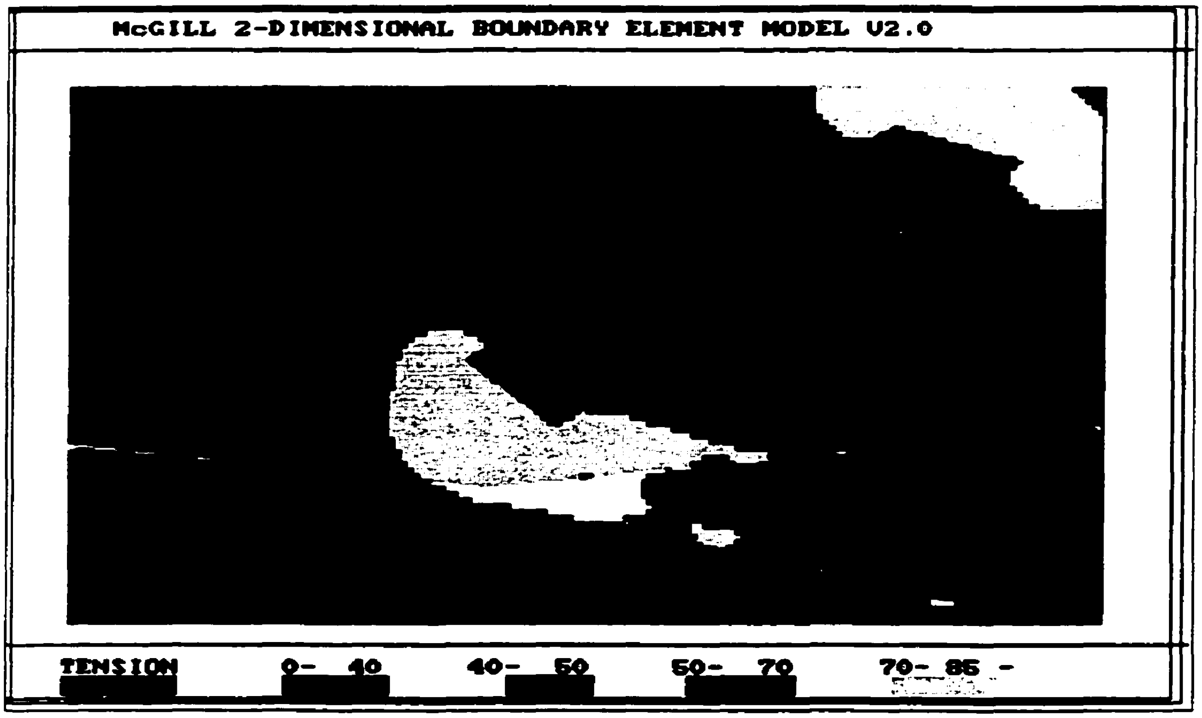

Figure 6.29a: Major principal stress (σ_1) after stope D has been mined.

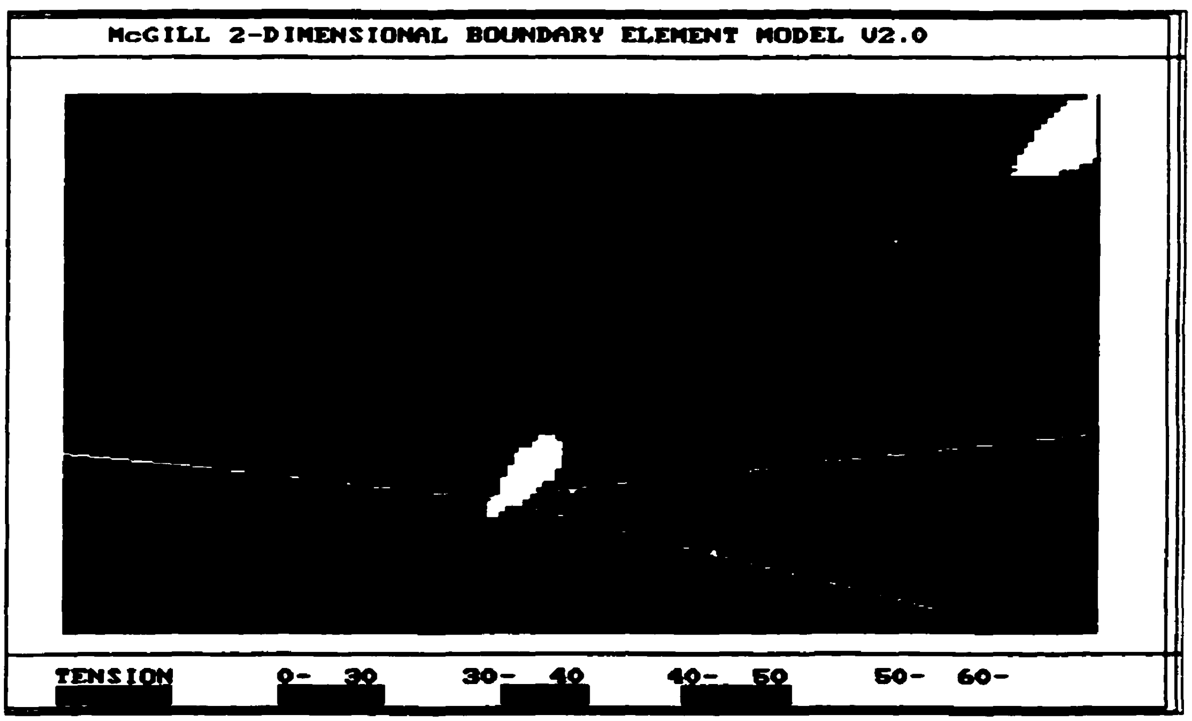

Figure 6.29b: Minor principal stress (σ_3) after stope D has been mined.

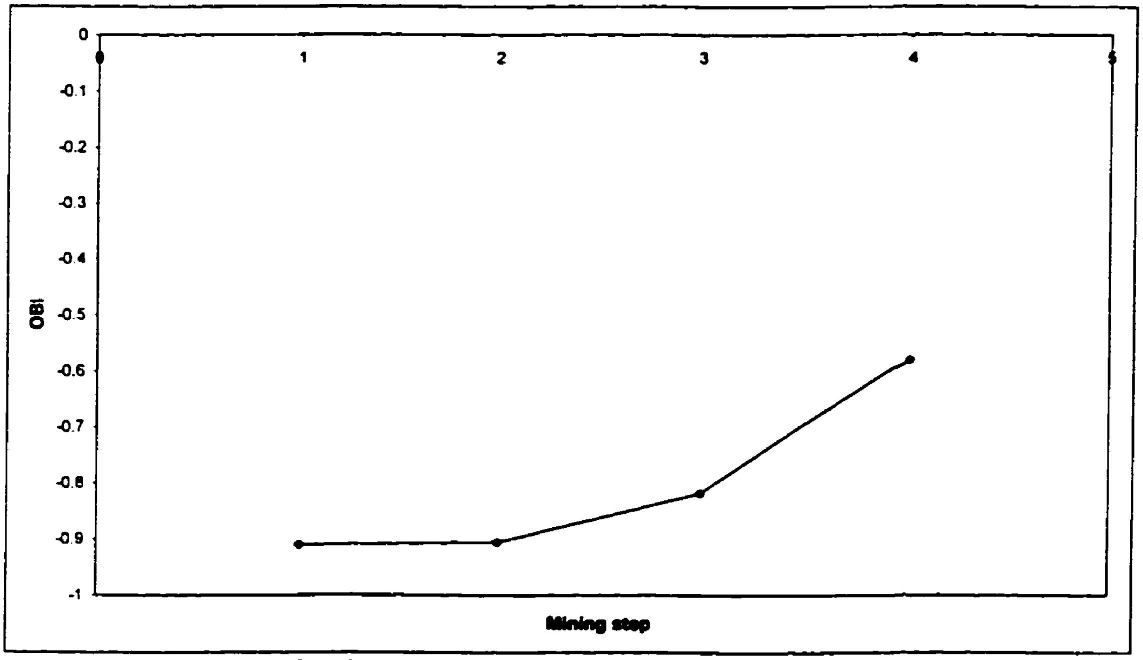

Figure 6.30: OBI values for the most critical element.

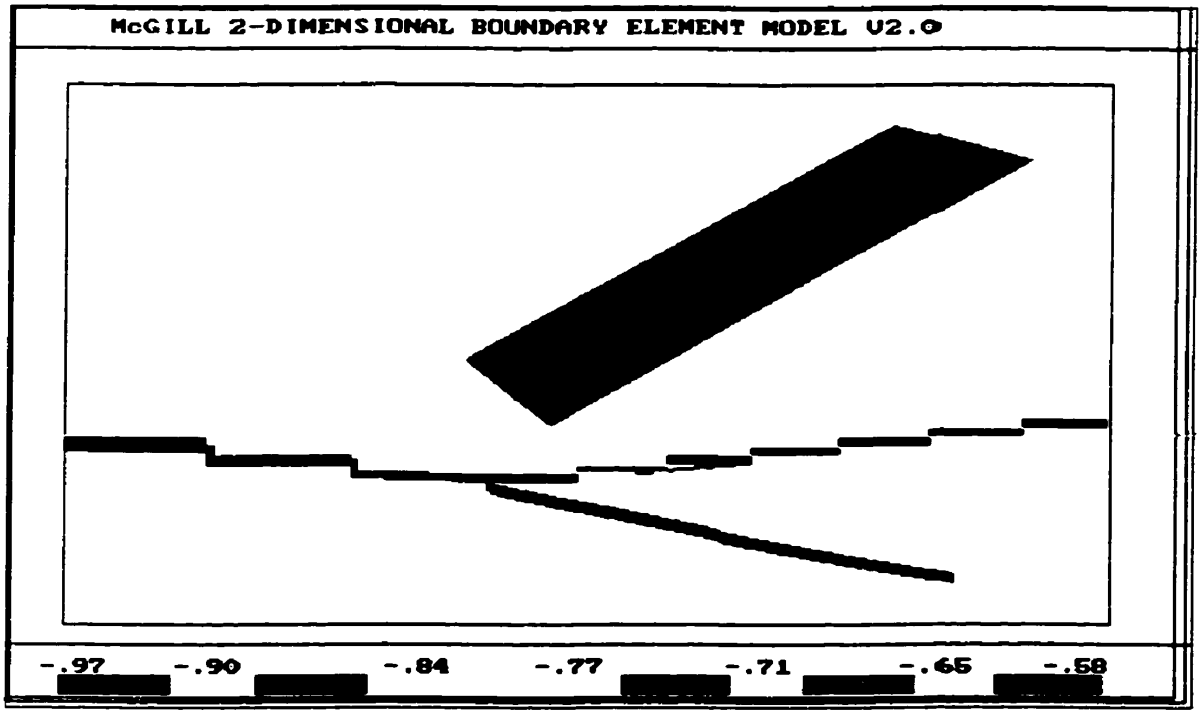

Figure 6.31: OBI values along the fault after the last stope is mined.

CHAPTER 7
DISCUSSION

In the preceding chapters of this thesis, it was shown how certain tools could be used to evaluate the rockburst potential when geological discontinuities are involved. In this chapter, some aspects of the proposed methodology and of the tools developed are further discussed.

7.1 CONSTITUTIVE MODEL FOR ROCK JOINTS

As it was mentioned before, existing constitutive model for rock joints are not always adequate in the modeling of the post-peak behavior of rock joints. Even models like the one proposed by Saeb and Amadei (1989, 1990, 1992), although very representative in constant normal stiffness (CNS) tests, does not follow closely the real behavior of the joint in constant normal stress (CNL) tests where a stress drop can be observed. CNL situations are of particular interest when investigating rockburst situation since this may lead to a violent failure along a discontinuity generated by the energy liberated by the stress drop. The proposed constitutive model, as it was shown, can follow, in a very close way, the stress drop behavior of tests under CNL conditions. The correlation factor obtained for several curves (R^2 = 0.90) proves that this new model can be very representative of the shear stress-shear displacement behavior of rock joints. This model relies on four parameters: the peak and residual strength (τ_p, τ_r) and the peak and residual displacement (u_p, u_r). This model can be related to two different phenomena occurring in a shear test: shearing of asperities and friction. If we start from Equation (5.30):

$$\tau = \tau_r + [d - \tau_r]\exp\left(-\frac{5u}{u_r}\right) - d\exp(-eu)$$

Rearranging this equation leads to:

$$\tau = \tau_r \left[1 - \exp\left(-\frac{5u}{u_r}\right)\right] + d\left[\exp\left(-\frac{5u}{u_r}\right) - \exp(-eu)\right] \tag{7.1}$$

or

$$\tau = F_1 + F_2 \tag{7.2}$$

with

$$\begin{aligned} F_1 &= \tau_r \left[1 - \exp\left(-\frac{5u}{u_r}\right)\right] \\ F_2 &= d\left[\exp\left(-\frac{5u}{u_r}\right) - \exp(-eu)\right] \end{aligned} \tag{7.3}$$

Figure 7.1 shows how these functions vary with shear displacement. Function F_1 can be seen as the friction component while F_2 represents the shearing of asperities. At small shear displacement, the deformation of asperities plays a major role in the mobilization of shear resistance while sliding along surfaces (i.e. friction) is minimal. As some asperities are being sheared off, the friction along surfaces increases (replacing in part the deformation of asperities). When most asperities have been sheared off (which seems to occur just before peak displacement), the shearing component decreases rapidly and the friction component represents the larger part of shear resistance. Finally, when all asperities have been sheared off (when residual displacement is attained), only friction is accountable for the shear resistance. Then, F_1 and F_2 can be regarded as being statistical functions describing the transformation of shear resistance of asperities into friction along sheared surfaces.

A constitutive model was also proposed for the dilatant behavior of joint (v-u). This model was mostly inspired by the equations proposed in the Saeb-Amadei model. Both models have two points in common, the beginning of the curve (u=0) and the residual value ($u=u_r$). In the Saeb-Amadei model, the behavior between these two points is linear while the proposed model follows an exponential shape. Here again, the proposed model relies on physical basis to explain the dilatancy curve. At the start of the shearing process, all asperities are intact. Thus, this should lead to a maximum dilatancy rate (dv/du) in the beginning of the process (Figure 7.2). Then, as some asperities are being sheared, the dilatancy rate slows down and becomes zero when all asperities have been sheared (at $u=u_r$). The proposed model reflects this phenomenon.

Although very promising, the proposed constitutive model has also some flaws and limitations. The first problem with the proposed model is that at least a few direct shear tests must be performed to obtain all the parameters. It is no secret that very few mines (if none) investigate the mechanical behavior of their discontinuity in laboratory. The biggest advantage of the Barton-Bandis model is that the fault characteristics can be approximated through very simple tests and observations that can be performed on site at very low costs.

Since the proposed model (at least for the shear stress - shear displacement behavior) can be determined strictly from four parameters (τ_p, τ_r, u_p, u_r), any strength criterion could be used. The reason behind the choice of the Ladanyi-Archambault strength criterion is that it relies on parameters that are also used in the dilatancy formulation.

Also, as can be seen on Figure 6.3, when the peak and residual displacements values (u_p, u_r) are close to one another ($u_r \leq 3\ u_p$), the model no longer goes through the peak strength (τ_p) at u_p when the stress drop is large. However, from the test results compiled in this thesis, it appears that u_r is usually larger than 8 times u_p.

The proposed model has proven its efficiency in describing tests under constant normal load. However, in situation of tests under constant normal stiffness (see Figure 5.25 for instance), the model presents sometimes a stress drop after the peak displacement that is not always corroborated by the data.

The principal limitations of the proposed model are:

- it is a 2D model; rock joints and faults are planes of weakness which means that they are 3D structures. Several studies (e.g. Huang and Doong, 1990; Jing et al., 1992, 1994) have shown that rock joints usually present some degree of anisotropy;
- it has been develop for monotonous loading; rock joints and faults in a rock mass are already loaded before nearby openings will be created. It is not clear if the model can accurately reflect the behavior of joints under these conditions;
- the model does not account for directional shearing; experimentation (e.g., Jing et al., 1994) have shown that rock joints do not always show the same behavior when tested back and forth along the same axis. This phenomenon is caused by the fact that asperities are usually not symmetric and thus, the average initial angle of asperities might not be the same in the X^+ than in the X^- direction;
- peak and residual displacement (u_p, u_r) are considered as material constant. As it can be observed in several direct shear test series (see Figure A2a and A5a for example), these parameters are not always constant for a given joint. However, like with any other rocklike material, one will often find some variability in mechanical parameters. This is the reason why good engineering practice will always recommend to perform some parametric analyses. The same reasoning applies here;
- the model is only valid for $\sigma_n \leq \sigma_T$; when the normal stress becomes larger than the rock strength, rock failure will occur and the model is no longer valid as another type of behavior will occur;

- scale effects; another aspect that was not addressed in this research is the scale effect on discontinuity behavior and how the proposed model could be adapted to take into account such situations. For the moment, it is presumed that the parameters entered in the model reflect the behavior of the discontinuity at the scale of the problem.

The parametric analyses showed that some parameters of the model have more impact on the behavior of the joint. In regards of the rockburst potential, the most important parameters are of course the peak and residual displacements (u_p, u_r) and the residual to peak strength ratio (B_0). The displacements parameters affect the length (of displacement) along which the stress drop will occur while the strength ratio affects the value of the stress drop. Hence, a smaller value of B_0 and/or of the displacement ratio (defined here as the residual over the peak displacement u_r/u_p) increases the value of the post-peak shear stiffness of the joint. This in turn increases the fault-slip rockburst potential.

7.2 THE SATURN PROGRAM

The proposed constitutive model has been implemented successfully into SATURN a boundary element code that uses both the fictitious stress method and the displacement discontinuity method. Several reproductions of direct shear tests under either constant normal load or constant normal stiffness have shown that the implementation is adequate. However, SATURN has at the moment several limitations. First of all, it is a 2D program and 2D analyses are not always appropriate to evaluate actual complex mine situations. Moreover, although SATURN can model different rock mass materials, it would be extremely difficult to a non-familiar user to model more than one material. To do so, the user must adapt the data file "manually" as no options allows this in the DRAW module.

Also, in SATURN, the rock mass is considered to present a linear elastic behavior. Although this assumption is usually considered as adequate for hard rock mining, it is not always appropriate for certain categories of rock masses.

But the most important limitation of SATURN at the moment is that it runs only in DOS mode. With the implementation of the new model, the program size has increased dramatically. This poses a problem because the live memory in DOS mode is very limited. In fact, at the moment, only 15 fault elements can be modeled when using the new fault model. This limits the complexity of problems that can be analyzed and the accuracy of the results.

If the goal of any research on the rockburst problem is to provide mine engineers with useful tools and techniques in the alleviation of rockburst hazards, then these aspects should be addressed in the near future.

7.3 Evaluation of rockburst potential

Gill and Aubertin (1988) developed a methodology to evaluate the rockburst potential of existing and future underground excavations. Until now, this methodology was of limited interest for rockburst involving a slip along a geological discontinuity because it was impossible to evaluate if the slip would be violent or gradual. The constitutive model and the tools associated allow to complete this methodology, as shown in Figure 7.3.

The process to obtain the different stiffness was described in Chapter 5 and examples of applications were presented in Chapter 6. It should be noted however, that the cases presented are hypothetical. While performing these analyses, no parametric studies where performed. Nonetheless, in real analyses of rockburst, these parametric studies should be performed to evaluate the influence of the fault characteristics on the rockburst potential. These analyses were not performed here since the cases were presented only to illustrate the methodology.

Furthermore, before one can consider the methodology validated, back-analyses of actual rockbursts situations involving fault-slip must be performed. However, these back-analyses could be difficult to achieve because of extremely limited data of fault characteristics in actual mines or to the complexity of the geology at hand.

Nevertheless, a methodology to evaluate *a priori* if there is a risk of fault-slip rockbursting is now available to mine engineers. Still, as it was mentioned in the preceding section, the tools necessary to evaluate this type of rockburst potential is not at the moment really accessible to mine engineers as SATURN is not a software often used in Canadian underground mines. Nonetheless, the work performed in this research could lead to a more user-friendly version of SATURN or to the implementation of the proposed model into existing commercial codes.

The Out-of Balance Index (OBI) is another tool that was also developed for the evaluation of rockburst potential involving discontinuities. The OBI is a very simple tool that can be easily implemented in any type of numerical modeling code with a minimum effort. It was shown that the OBI values show a great increase when failure is near. At this moment, it is not possible to give boundary values to state what is a critical value for this index. To get these values, case studies should be performed. However, although it is a simple tool, the OBI index could in the future prove to be very useful in the evaluation of rockburst potential.

Finally, it should be noted that a violent failure on a fault will produce a seismic event but not necessarily a rockburst. A rockburst was defined in Chapter 2 as being a seismic event that produce damages in mine openings. It is nonetheless conservative to conclude on a rockburst potential if it is evaluated that there is a possibility of violent failure. Damages in opening will depend on several factors like the energy generated by the failure, the distance from the opening, the stress state around the opening and the strength of the rock mass.

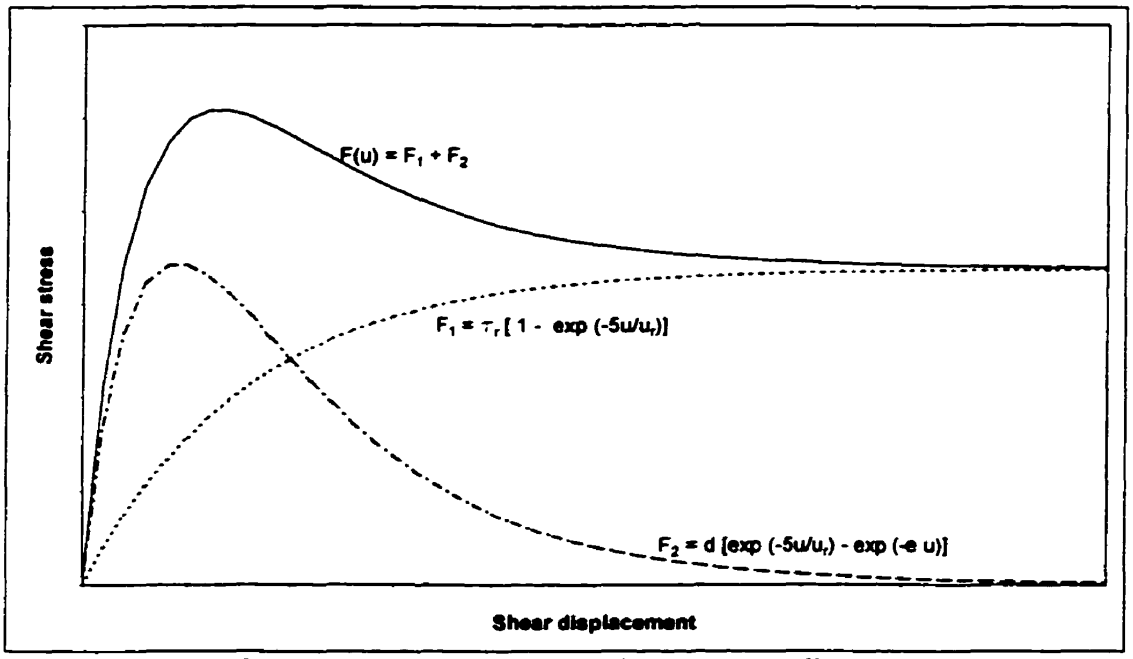

Figure 7.1: Graph showing the two different functions leading to the resultant shear stress.

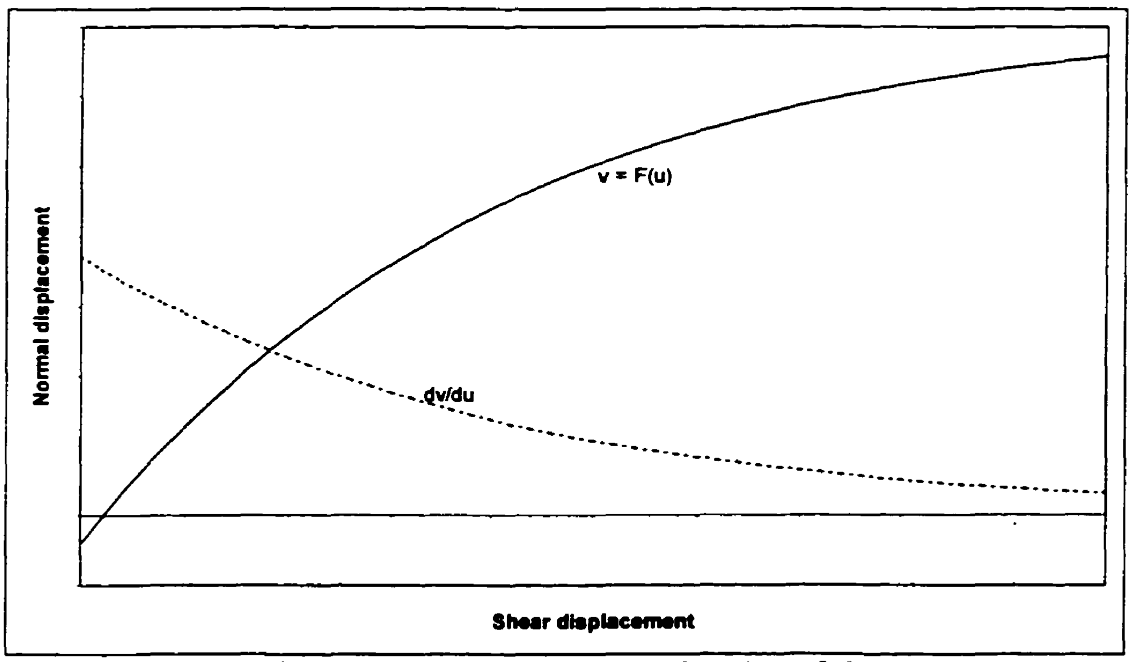

Figure 7.2: Evolution of the dilatancy rate (dv/du) in function of shear displacement.

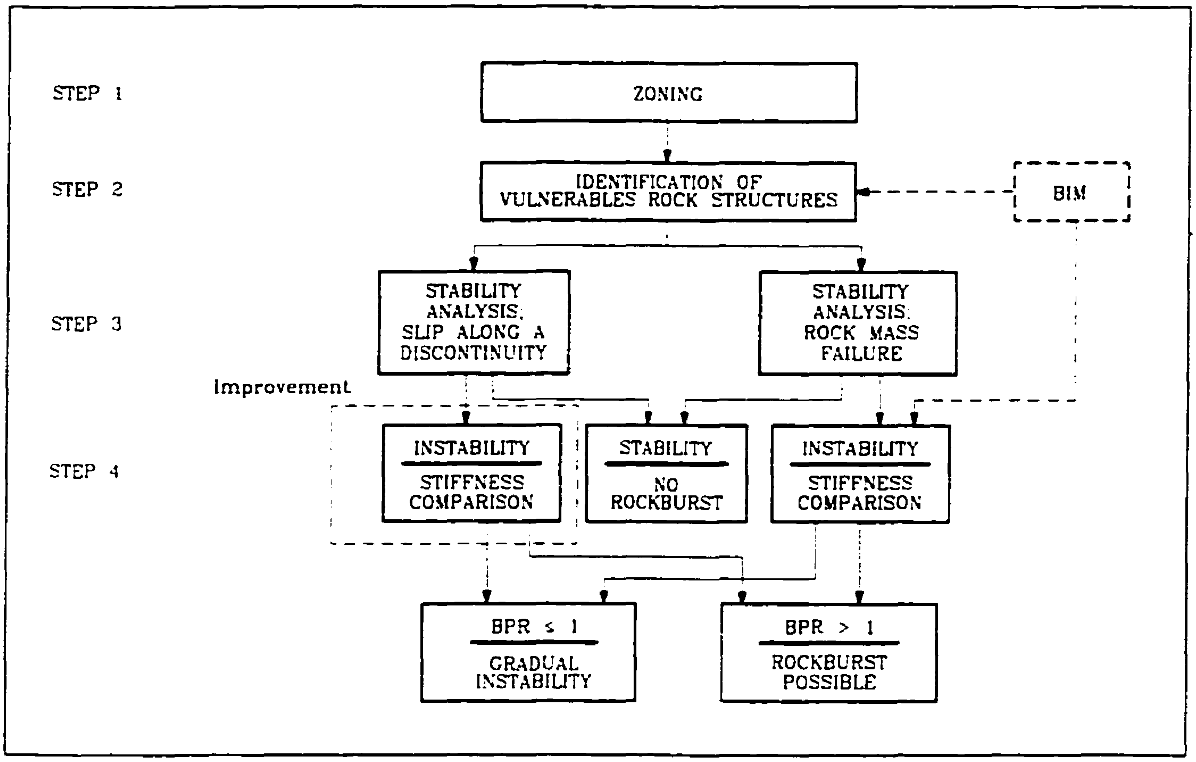

Figure 7.3: **Logical diagram showing the methodology proposed for the evaluation of rockburst potential (adapted from Gill and Aubertin, 1988 and Simon et al., 1998).**

CHAPTER 8
CONCLUSIONS

8.1 SUMMARY AND CONCLUSIONS

For more than a century, rockbursts have been a problem for many underground mines. As deeper orebodies are mined with higher extraction ratio, mining engineers will most probably have to deal with this problem more often. Moreover, mines in Canada are most likely to operate at greater depth in the near future. Due to the "unpredictability" and the recurrence nature of the phenomenon, rockbursts might just be the biggest challenge facing rock mechanics engineers in hard rock mines.

Although rockbursts do not occur in the majority of Québec underground mines, it is a problem that presents a high risk of fatalities in mines where the problem exists. In that regard, some efforts have been initiated over the last decade to provide tools to help rock mechanics engineers to assess the rockburst potential of their openings. On that matter, Gill and Aubertin (1988; see also Aubertin et al., 1992; Gill et al., 1993; Simon et al., 1998) proposed a methodology that makes use of standard rock mechanics tools, which attempts to evaluate rockburst potential of rock structures. This methodology, called the ERP method, is based on the stiffness comparison between the failed rock and the surrounding rock mass, as was proposed initially by Cook (1965b). However, this comparison could only be established for instabilities involving the fracturing of the rock mass. To make this comparison possible for instabilities involving slip on pre-existing discontinuities (the second type of rockbursts) several tools were developed and a methodology was proposed.

First, a new constitutive model for rock joints was developed. This new model allows to follow the post-peak shear behavior of rock joint in a relatively close manner. This model relies on four basic parameters such as the peak and residual strength, and the peak and residual displacement. To evaluate the peak strength, it was proposed to use the well-known Ladanyi-Archambault criterion as modified by Saeb (1990). Compared with test results from literature, the model showed a correlation factor R^2 of 0.90. A new formulation for the dilatancy behavior of joint was also proposed based on the formulation that was developed by Saeb and Amadei (1992). Parametric analyses were performed on the model which showed that the most influential parameters (in relation with the post-peak shear stiffness) were the peak and residual displacement and the residual to peak strength ratio.

The new model was implemented into a boundary element code called SATURN, which was originally developed by Fotoohi (1993). Verifications were made and showed that SATURN could reproduce direct shear tests and follow adequately the behavior of the proposed model.

A methodology was then elaborated to evaluate the post-peak shear stiffness of failed segment on a fault and the shear stiffness of the surrounding rock mass. Similarly to strainbursts pillar bursts, an index was proposed, called the Bursting Potential Ratio for joints BPR_j, to compare these stiffnesses. The BPR_j index was defined as the post-peak shear stiffness of the failed segment over the shear stiffness of the surrounding rock mass. If the BPR_j index is larger than unity, this indicates a potential of fault-slip.

Examples of application of the methodology and of the developed tools were given to better illustrate how to use them. Detailed fictitious and real cases were presented.

Concurrently, another approach on the evaluation of rockburst led to the development of another index called the Out-of-Balance Index. This index represents the ratio of the exceeding stress over the strength. It is postulated that the larger this value is, the larger the rockburst potential. This index was also implemented into SATURN. The same cases were analyzed and showed some correlation with the stiffness comparison approach.

8.2 RECOMMENDATIONS FOR FURTHER RESEARCH

The research work presented in this thesis can be further extended in the following directions:

1- Transformation of SATURN into a WINDOWS based software. This would allow to make use of the full computer memory available and the analyses of cases requiring a larger number of elements. The proposed model could also be implemented in more popular numerical modeling codes like MAP3D or PHASE^2. These commercial softwares are used more frequently in the mining industry than SATURN.

2- Development of a non-linear approach for the rock mass in SATURN to take into account rock masses that present this type of behavior.

3- Investigation on the scale effects on the proposed model. This would allow a better representation of the parameters used in analyses of actual mine openings.

4- Development of formulation of the model for other peak strength criteria such as the well-known Barton-Bandis model.

5- Development of a 3D formulation for the model.

6- Validation of the approach developed through back-analyses of actual rockburst cases involving fault-slip.

7- Uses of the new model to predict the post-peak behavior of intact rock in uniaxial compression tests. The failure plane of the sample could then be modeled as a rock joint and its post-peak behavior analyzed consequently. This would allow an estimation of the post-peak modulus when its determination in laboratory is impossible.

STATEMENT OF CONTRIBUTION

A method to evaluate the rockburst potential of situations involving a possible slip along major geological discontinuities was developed. This method is based on the comparison of the post-peak shear stiffness of the fault with the shear stiffness of the surrounding rock mass. To evaluate the post-peak shear stiffness of a discontinuity, a new non-linear constitutive model for rock joint was developed. This model is based on two exponential formulations expressing the two phenomena taking part in the shearing process: friction resistance along surfaces and shearing of asperities. The model was then implemented in an existing boundary element code to evaluate the interaction between underground openings and nearby geological discontinuities. Verification of the implementation was done by reproducing direct shear tests on a discontinuity. Methods to obtain the different stiffnesses involved in the violent slip process were developed. Examples of applications were given to illustrate the proposed methodology. In addition, an alternative method to evaluate the fault-slip rockburst potential was developed. This new method relies on a linear analysis and the calculation of a new index called the Out-of-Balance Index or OBI. These methods will allow mine engineers to perform an evaluation of the risk of having a fault-slip rockburst near existing underground excavations and for future ones.

REFERENCES

AMMQ, Éditeur (1988): Compte Rendu du 4e Colloque sur le Contrôle du Terrain. Val d'Or.

Andreaus, U. (1989): A frictional model for sliding of jointed blocks. Advances in Constitutive Laws for Engineering Materials, Jinghong and Murakami (eds), Pergamon Press, 249-254.

Archambault, G., Fortin, M., Gill, D.E., Aubertin, M., Ladanyi, B. (1990): Experimental investigation for an algorithm simulating the effect of variable normal stiffness on discontinuities shear strength. Proc. Int. Conf. on Rock Joints, Loen, Norway, 141-148.

Argyris, J.H. (1960): Energy Theorems and Structural Analysis. Butterworth, (reprinted from Aircraft Eng., 1954-5).

Arjang, B. (1996): In situ ground stresses in the Abitibi Mining District. CIM Bulletin, 89, 65-71.

Arjang, B., Herget, G. (1997): In situ ground stresses in the Canadian hard rock mines: An update. Proc. 36th U.S. Rock Mech. Symp., In Int. J. Rock Mech. & Mining Sci., 34, paper 15.

Atluri, S.N., Gallagher, R.H., Zienkiewicz, O.C. (eds) (1983): Hybrid and Mixed Finite Element Methods. Wiley.

Aubertin, M., Gill, D.E. (1988): Une méthodologie d'évaluation du potentiel de coups de terrain dans les mines d'Abitibi. Colloque sur le Contrôle de Terrain (AMMQ), Val d'Or.

Aubertin, M., Gill, D.E., Simon, R. (1992): Évaluation du potentiel de coups de terrain dans les mines; Phase II - Validation de la méthodologie proposée. Final Report presented to the Institut de Recherche en Santé et Sécurité au Travail (IRSST), September 1992.

Aubertin, M., Gill, D.E., Simon, R. (1994a): On the use of the brittleness index modified (BIM) to estimate the post-peak behavior or rocks. Proc. First North American Rock Mech. Symposium, Balkema, 945-952.

Aubertin, M., Gill, D.E., Simon, R. (1994b): Une étude sur l'utilisation de l'indice de fragilité modifié (BIM). Rapport EPM/RT-94/13, École Polytechnique.

Aubertin, M., Simon, R., Auer, L. Gill, D.E. (1997): Une étude sur le potentiel de coups de terrain à la mine Sigma en relation avec les effets du dynamitage de préfracturation -Rapport Final. Rapport de projet réalisé dans le cadre de l'entente Canada/Québec sur le développement minéral.

Bandis, S.C. (1980): Experimental Studies of Scale Effects on Shear Strength and Deformation of Rock Joints, Ph.D. thesis, University of Leeds.

Bandis, S.C., Lumsden, A.C., Barton, N.R. (1981): Experimental studies of scale effects on the shear behaviour of rock joints. Int. J. Rock Mech. Min. Sci., 18, 1-21.

Bandis, S.C., Lumsden, A.C., Barton, N.R. (1983): Fundamentals of rock joint deformation. Int. J. Rock Mech. Min. Sci., 20, 249-268.

Banerjee, P.K. (1971): Foundations within a finite elastic layer - application of the integral equation method. Civ. Engng, 1197-1202.

Banerjee, P.K. (1976): Integral equation methods for analysis of piece-wise non-homogeneous three-dimensional elastic solids of arbitrary shape. Int. J. Mech. Sci., 18, 293-303.

Banerjee, P.K. (1994): Boundary Element Methods in Engineering. McGraw-Hill.

Banerjee, P.K., Butterfield, R. (1976): Boundary element methods in geomechanics. Finite Elements in Geomechanics, Gudehus (ed.), Wiley, chapter 16.

Banerjee, P.K., Butterfield, R. (eds.) (1979): Developments in Boundary Element Method - 1. Applied Science Pub. Ltd.

Banerjee, P.K., Butterfield, R. (1981): Boundary Element Methods in Engineering Science. McGraw-Hill.

Banerjee, P.K., Driscoll, R.M.C. (1976): Three-dimensional analysis of raked pile groups. Proc. Inst. Civ. Eng. Res. and Theory, 91, 653-671.

Barron, K., Yang, T. (1992): Influence of specimen size and shape on strength of coal. Proc. Workshop on Coal Pillar Mechanics and Design, Santa Fe, USBM IC 9315, 5-24.

Barton, N.R. (1973): Review of a new shear strength criterion for rock joints. Engng. Geology, 7, 287-332.

Barton, N. (1976): Rock mechanics review - The shear strength of rock and rock joints. Int. J. Rock Mech. Min. Sci. & Geomech. Abstr., 13, 255-279.

Barton, N., Choubey, V. (1977): The shear strength of rock joints in theory and practice. Rock Mech., 10, 1, 1-54.

Barton, N., Stephansson, O. (eds.) (1990): Rock Joints. Proc. Int. Symp. on Rock Joints, Balkema.

Barton, N., Lien, R., Lunde, J. (1974): Engineering classification of rock masses for the design of tunnel support. Rock Mech., 6, 189-239.

Barton, N., Bandis, S., Bakhtar, K. (1985): Strength, deformation and conductivity coupling of rock joints. Int. J. Rock Mech. Min. Sci. & Geomech. Abstr., 22, 121-140.

Bathe, K.J. (1982): Finite Element Procedures in Engineering Analysis. Prentice-Hall.

Beghoul, M.N., Lauriault, R.A., Plouffe, M. (1996): Relation spatio-temporelle du taux d'extraction et la réponse séismique minière induite. C.R. du 11^e Colloque en Contrôle de Terrain, AMQ (ed.), Val d'Or.

Beer, G., Meek, J.L. (1981): The coupling of boundary and finite element methods for infinite domain problems in elasto-plasticity. Boundary Element Methods, Brebbia (ed.), 575-591.

Bertrand, L. (1989): Étude expérimentale des relations contrainte-déplacement sur des discontinuités structurales. Projet de fin d'étude (unpublished), Université du Québec à Chicoutimi.

Bieniawski, Z.T. (1967): Mechanism of brittle fracture of rock. Part I Theory of the fracture process; Part II Experimental studies; Part III Fracture in tension and under long-term loading. Int. J. Rock Mech. and Min. Sci., 4, 395-430.

Bieniawski, Z.T. (1973): Engineering classification of jointed rock masses. The Civil Engineer in S. Afr., 15, 335-344.

Bieniawski, Z.T. (1975): The significance of in situ test on large rock specimens. Int. J. Rock Mech. Min. Sci., 12, 101-113.

Bieniawski, Z.T. (1984): Rock Mechanics Design in Mining and Tunnelling. A.A. Balkema.

Biezeno, C.B., Koch, J.J. (1923): Over een nieuwe methode ter berekening van vlokke platen. Ing. Grav., 38, 25-36.

Bilgin, H.A., Pasamehmettoglu, A.G. (1990): Shear behaviour of shale joints under heat in direct shear. Rock Joints, Barton & Stephansson (eds), Balkema, 179-184.

Blaha, F. (1990): Some principles of rock mass failure in the case of rock bursts. Mechanics of Jointed and Faulted Rock. Rossmanith (ed.), 757-762.

Blake, W. (1972): Rockburst mechanics. Quarterly of the Colorado School of Mines, 67, 1-64

Blake, W. (1982): Microseismic Applications for Mining - A Practical Guide. U.S. Dept. of the Interior, Bureau of Mines, Contract J0215002.

Blake, W. (1984): Rock preconditioning as a seismic control measure in mines. Proc. of Symp. on Rockbursts and Seismicity in Mines, S. Afr. Inst. Min. Metall., 225-230.

Bolstad, D.D. (1990): Keynote Lecture: Rockburst control research by the US Bureau of Mines. Rockbursts and Seismicity in Mines, Fairhurst (ed.), Balkema, 371-375.

Brady, B.H.G., Brown, E.T. (1981): Energy changes and stability in underground mining: design application of boundary elements methods. Trans. Int. Min. Metall., 90, A61-A68.

Brady, B.H.G., Brown, E.T. (1985): Rock Mechanics for Underground Mining. George Allen & Unwin.

Brady, B.H.G., Brown, E.T. (1993): Rock Mechanics for Underground Mining. 2nd Ed., Chapman & Hall.

Brady, B.H.G., Wassyng, A. (1981): A coupled finite element-boundary element method of stress analysis. Int. J. Rock Mech. Min. Sci. & Geom. Abstr., 18, 475-485.

Brebbia, C.A. (1978): The Boundary Element Method for Engineers. Wiley & Sons

Brebbia, C.A., Dominguez, J. (1977): The boundary element method for potential problems. Appl. Math. Modelling, Vol. 1, No. 7.

Brebbia, C.A., Butterfield, R. (1978): The formal equivalence of the direct and inderect boundary element method. Appl. Math. Model., vol. 2, no 2.

Brebbia, C.A., Ferrante, A. (1978): Computational Methods for the Solution of Engineering Problems. Pentech Press.

Brebbia, C.A., Georgiou, P. (1979): Combination of boundary and finite elements in elastostatics. Appl. Math. Modell., 3, 212-220.

Brechtel, C.E., Hardy, M.P., Baz-Dresch, J., Knowlson, J.S. (1989): Application of high-strength backfill at the Cannon Mine. Proc. 4th Int. Symp. on Mining with Backfill., 105-117.

Bro, A. (1992): Stick-slip behaviour of smooth joints. Int. J. Rock Mech. Min. Sci. & Geomech. Abstr., 29, 171-177.

Brown, E.T. (ed.) (1981): Rock Characterization, Testing and Monitoring: ISRM Suggested Methods. Pergamon Press.

Brown, E.T. (1984): Rockbursts: Prediction and control. Tunnels and Tunnelling, April, 17-19.

Brown, E.T. (1993): The nature and fundamentals of rock engineering. In Comprehensive Rock Engineering - Principles, Practice & Projects, Hudson (ed.), Vol. 1, 1-23.

Brummer, R.K. (1990): Case studies on large rockbursts in South African gold mines. Rockbursts and Seismicity in Mines, Fairhurst (ed.), Balkema, 323-329.

Budavari, S. (1983): Response of the rock mass to excavations underground. Rock Mech. in Mining Practice, S. Afr. Inst. Min. Metall., Monograph Series, 5, 55-76.

Butterfield R., Banerjee, P.K. (1971): The problem of pile-cap pile-group interaction. Géotechnique, 21, 135-142.

Byerlee, J.D. (1967): Theory of friction based on brittle fracture. J. Appl. Phys., 38, 2928-2934.

Byerlee, J.D. (1968): Frictional characteristics of granite under high confining pressure. J. Geophys. Res., 72, 3639-3648.

Byerlee, J.D. (1970): The mechanics of stick-slip. Tectonophys., 9, 475-486.

Byerlee, J.D., Brace, W.F. (1968): Stick-slip, stable sliding, and earthquakes-effect of rock type, pressure, strain rate, and stiffness. J. Geoph. Res., 73, 6031-6037.

Byerlee, J., Summers, R. (1976): A note on the effect of fault gouge thickness on fault stability. Int. J. Rock Mech. Min. Sci. & Geomech. Abstr., 13, 35-36.

Calder, P.N., Archibald, J.F., Moroz, B., Semadeni, T., Korenberg, M., Mcilroy, P. (1986): Rockburst prediction studies at Queen's University. Can. Min. J., 107, 33-39.

Carter, J.P., Ooi, L.H. (1988): Application of a joint model to concrete-sandstone interfaces. Numerical Methods in Geomechnics, Swoboda (ed.), Balkema, 880-893.

Chapuis, R.P. (1990): A constitutive equation for granular materials from consideration of their internal structure. Yielding, Damage, and Failure of Anisotropic Solids, EGF5, Boehler (ed.), Mechanical Engineering Publications, 277-287.

Chen, X., Barron, K., Chan, D. (1995): Finite element model for the outbursts in underground mines. Proc. 3rd Can. Conf. on Computer Applications in the Mineral Industry, CAMI'95, McGill University, 256-267.

Chen, L.H., Schweikert, J. (1963): Sound radiation from an arbitrary body. J. Acoust. Soc. Am., 35, 1626-1632.

Clough, R.W. (1960): The finite element in plane stress analysis. Proc. 2nd A.S.C.E. Conf. on Electronic Computation, Pittsburg.

Coates, D.F. (1965): Pillar loading Part I: Literature survey and new hypothesis. R168, Mines Branch (CANMET) Research Report, Queen's Printer, Canada

Coates, D.F., Dickhout, M. (1970): Elements of planning in deep mines. Can. Min. J., 91, 74-78.

Cook, N.G.W. (1965a): The failure of rock. Int. J. Rock Mech. Min. Sci., 2, 389-403.

Cook, N.G.W. (1965b): A note on rockbursts considered as a problem of stability. J. S. Afr. Inst. Min. Metall., March, 515-523.

Cook, N.G.W. (1978): An Industry Guide to the Amelioration of Hazards of Rockbursts and Rockfalls. Chamber of Mines of South Africa.

Cook, N.G.W. (1983): Origin of rockburst. Proc. Rockburst Prediction and Control, IMM, London, 1-9.

Cook, N.G.W., Hoek, E., Pretorius, J.P.G., Ortlepp, W.D., Salamon, M.D.G. (1966): Rock mechanics applied to the study of rockbursts. J. S. Afr. Inst. of Min. and Metall., 66, 435-528.

Corthésy, R., Leite, M.H., Gill, D.E. (1997): Élaboration d'un modèle de prédiction des contraintes in situ dans le Nord-Ouest québécois. Rapport présenté à l'Institut de Recherche en Santé et en Sécurité du Travail du Québec (IRSST), Rapport R-173.

Courant, R. (1943): Variational methods for the solution problems of equilibrium and vibration. Bull. Am. Math. Soc., 49, 1-23.

Cox, S.J.D., Meredith, P.G. (1993): Microcrack formation and material softening in rock measured by monitoring acoustic emissions. Int. J. Rock Mech. Min. Sci. and Geomech. Abstr., 30, 11-24.

Crawford, A.M., Curran, J.H. (1983): A discontinuity displacement approach to modelling the creep behaviour of rock and its discontinuities. Int. J. for Num. and Analytical Methods in Geomech., 7, 245-268.

Crouch, S.L. (1976a): Solution of plane elasticity problems by the displacement discontinuity method. Int. J. Num. Methods Engng, 10, 301-343.

Crouch, S.L. (1976b): Analysis of stresses and displacements around underground excavations: an application of the displacement discontinuity method. Geomech. report to the National Science Foundation, Minneapolis, University of Minnesota.

Crouch, S.L. (1979): Computer simulation of mining in faulted ground. J. S. Afr. Inst. Min. Metall., 79, 159-173.

Crouch, S.L., Starfield, A.M. (1983): Boundary Element Method in Solid Mechanics. George Allen & Unwin.

Crouch, S.L., Tian, Y. (1988): A two-dimensional direct boundary integral method for elastodynamics. Int. J. Rock Mech. Min. Sci. & Geomech. Abstr., 25, 149-158.

Cruse, T.A. (1969): Numerical solutions in three-dimensional elastostatics. Int. J. Solids and Struct., 5, 1259-1274.

Cruse, T.A. (1972): Application of the boundary integral equation method in solid mechanics. Proc. Int. Conf. Southampton Univ., Tottenham & Brebbia (eds), vol. 2.

Cruse, T.A. (1974): An improved boundary integral equation method for three-dimensional stress analysis. Computers and Struct., 4, 741-757.

Cruse, T.A., Rizzo, F.J. (1968): A direct formulation and numerical solution of the general transient elasto-dynamic problem. J. Math. Anal. Appl., 22, 244-259.

Cruse, T.A., Rizzo, F.J. (eds) (1975): Boundary integral equation methods - computational applications in applied mechanics. Proc. ASME Conf. on Boundary Integral Methods.

Cundall, P.A. (1971): A computer model for simulating progressive large-scale movement in blocky rock system. Rock Fracture: proc. of the Int. Symposium on Rock Mech., Nancy, Paper 2-8.

Cundall, P.A. (1974): A computer model for rock-mass behavior using interactive graphics for the input and output of geometric data. Report AD/A-001 602, U.S. National Technical Information Service.

Cundall, P.A., Lemos, J.V. (1990): Numerical simulation of fault instabilities with a continuously-yielding joint model. Rockbursts and Seismicity in Mines, Fairhurst (ed.), Balkema, 147-152.

Cundal, P.A., Strack, O.D.L. (1979): A discrete numerical model for granular assemblies. Geotechnique, 29, 47-65.

Daihua, Z., Miller, H.D.S. (1987): A proposed mechanism of rock failure and rockbursting. Proc. 6th Int. Cong. on Rock Mech., Montréal, 1357-1362.

Davis R.O., Selvadurai, A.P.S. (1993): Elasticity and Geomechanics. Dept. Civil Engng, McGill University.

Denkhaus, H.G., Roux, A.J.A., Grobbelaar, C. (1958): A study into the mechanical properties of rocks with special reference to their bearing on the occurrence of rockburst. S. Afr. Mech. Eng., 8, 67-85.

Dennison, P.J.G., van Aswegen, G. (1993): Stress modelling and seismicity on the Tanton fault: A case study in a South African gold mine. Rockbursts and Seismicity in Mines, Young (ed.), Balkema, 327-335.

Desai, C.S., Christian, J.T. (eds) (1977): Numerical Methods in Geotechnical Engineering. McGraw-Hill.

Desai, C.S., Fishman, K.L. (1991): Plasticity-based constitutive model with associated testing for joints. Int. J. Rock. Mech. Min. Sci. & Geomech. Abstr., 28, 15-26.

Desai, C.S., Armaleh, S., Katti, D., Ma, Y. (1991): Disturbed state concept for modelling soils and joints. Computer Methods and Advances in Geomechanics, Beer, Booker & Carter (eds), Balkema, 321-327.

Desai, C.S., Wathugala, G.W., Navayogarajah, N. (1989): Developments in hierarchical modelling for solids and discontinuities and applications. Advances in Constitutive Laws for Engineering Materials, Jinghong and Murakami (eds), Pergamon Press, 43-53.

Diest, F.H. (1965): A non-linear continuum approach to the problem of fracture zones and rockbursts. J. S. Afr. Inst. Min. Metall., 65, 502-522.

Dieterich, J.H. (1972): Time-dependent friction in rocks. J. Geophys. Res., 77, 3690-3697.

Dieterich, J.H. (1978): Time-dependent friction and the mechanics of stick-slip. Pure Appl. Geophys., 116, 790-806.

Dieterich, J.H. (1979): Modelling rock friction 1. Experimental results and constitutive equations. J. Geophys. Res., 84, 2161-2175.

Divakar, M.P., Fafitis, A. (1990): A micromechanics based rough crack model. Micromechanics of Failure of Quasi-Brittle Materials, Shah, Swartz & Wang (eds), 482-493.

Dong, J.-J., Pan, Y.-W. (1996): A hierchical model of rough rock joints based on micromechanics. Int. J. Rock. Mech. Min. Sci. & Geomech. Abstr., 33, 111-123.

Engelder, J.T., Scholz, C.H. (1976): The role of asperity indentation and ploughing in rock friction: II. Influence of relative hardness and normal load. Int. J. Rock Mech. Min. Sci. & Geomech. Abstr., 13, 155-163.

Fairhurst, C. (1964): On the validity of the Brazilian test for brittle materials. Int. J. Rock Mech. Min. Sci., 1, 535-546.

Falmagne, V. (1991): Rock mechanics and microseismic monitoring at Ansil. CIM Bulletin, 84, 955, 46-51.

Farmer, I. (1983): Engineering Behavior of Rocks. Chapman & Hall.

Filcek, H. (1980): Geomechanical criteria of rockburst hazard. Zeszyty Naukowe AGH, Górnictwo no. 4, Kraków, (in polish).

Flamand, R., Archambault, G., Gentier, S., Riss, J., Rouleau, A. (1994): An experimental study of the shear behavior of irregular joints based on angularities and progressive degradation of the surfaces. Proc. Can. Geotech. Conf., 253-262.

Fortin, M., Archambault, G., Aubertin, M., Gill, D.E. (1988): An algorithm for predicting the effect of a variable normal stiffness on shear strength of discontinuities. Proc. 15th Can. Rock Mech. Symp., 109-117.

Fortin, M., Gill, D.E., Ladanyi, B., Aubertin, M., Archambault, G (1990): Simulating the effect of a variable normal stiffness on shear behavior of discontinuities. Mechanics of Jointed and Faulted Rock, Rossmanith (ed.), Balkema, 381-388.

Fotoohi, K. (1993): Nonlinear Boundary Element Analysis of Rock Mass With Discontinuities. Ph.D. Thesis, McGill University.

Fotoohi, K., Mitri, H.S. (1996): Nonlinear fault behaviour near underground excavations - a boundary element approach. Int. J. Num. & Anal. Methods in Geomech., 20, 173-190.

Galerkin, B.G. (1915): Series solution of some problems of elastic equilibrium of rods and plates. (In Russian), Vestn. Inzh. Tech., 19, 897-908.

Gauss, C.F. (1795) see *Carl Friedrich Gauss Werk*, Vol. VII, Göttingen, 1871.

Gay, N.G., Spencer, D., Van Wyk, J.J., Van Der Heever, P.K. (1982): The control of geological and mining parameters on seismicity in the Klerksdorp Gold Mine District. Proc. of Symp. on Seismicity in Mines, S. Afr. Nat. Group on Rock Mech., paper 3.

Gerald, C.F., Wheatley, P.O. (1989): Applied Numerical Analysis, Fourth Ed., Addison-Wesley Publishing Co.

Gibowicz, S.J. (1990): Keynote Lecture: The mechanism of seismic events induced by mining - A review. Rockbursts and Seismicity in Mines, Fairhurst (ed.), Balkema, 3-27.

Gill, D.E. (1971): Note du cours 6.541 (unpublished). Département de génie minier, École Polytechnique de Montréal.

Gill, D.E. (1982): Mécanique des roches (6.502). Notes de cours (unpublished) Département de génie minéral, École Polytechnique de Montréal.

Gill, D.E., Aubertin, M. (1988): Évaluation du potentiel de coups de terrain dans les mines d'Abitibi. Rapport de recherche de l'URSTM présenté à l'Institut de Recherche en Santé et Sécurité du Travail (IRSST).

Gill, D.E., Aubertin, M., Simon, R. (1993): A practical engineering approach to the evaluation of rockburst potential. Rockbursts and Seismicity in Mines, Young (ed.), Balkema, 63-68.

Glazer, S.N. (1997): Applied mine seismology: A Vaal Reefs perspective. Rockbursts and Seismicity in Mines, Gibowick and Lasocki (eds), Balkema, 227-231.

Glowacka, E. (1993): Excavated volume and long-term seismic hazard evaluation in mines. Rockburst and Seismicity in Mines, Young (ed.), Balkema, 69-73.

Goldstein, M., Goosev, B., Pyrogovsky, N., Tulinov, R., Turovskaya, A. (1966): Investigation of mechanical properties of cracked rock. Proc. 1st Cong. ISRM, Vol. 1, 521-524.

Goodman, R.E. (1970): The deformability of joints. ASTM Spec. Tech. Publ. 477.

Goodman, R.E. (1976): Methods of Geological Engineering in Discontinuous Rocks. West, St-Paul, MN.

Goodman, R.E. (1980): Introduction to Rock Mechanics. John Wiley and Sons.

Goodman, R.E., Boyle, W. (1985): Non-linear analysis for calculating the support of a rock block with dilatant joint faces. Presented at the 34th Geomechanics Colloquy, Salzburg, Austria.

Goodman, R.E., St John, C. (1977): Finite element analysis for discontinuous rocks. In Numerical Methods in Geotechnical Engineering, 148-175.

Goodman, R.E., Taylor, R.L., Brekke, T.A. (1968): A model for the mechanics of jointed rock. J. Soil Mech. Fdns Div., Proc. Am. Soc. civ. Engrs, 94 (SM3), 637-659.

Grant, D.R., Potvin, Y., Rocque, P. (1993): Three dimensional stress analysis techniques applied to mine design at Golden Giant Mine. Proc. First Can. Symp. on Num. Modell. Applications in Min. and Geomech., 5-15.

Hakami, H. (1988): Post-failure Behaviour of Brittle Rock. Doctoral Thesis, Luleå University of Technology, Sweden.

Hamajima, R. (1993): Discontinuous analysis considering the deformation of elements by modified virtual stress method and modified virtual displacement method. NACTAM, Japan, 263-264.

Hamajima, R., Suzuki, T., Nakai, Y., Han, S. (1993): Analysis for discontinuous medium considering elemental deformation. Computer Methods and Advances in Geomechanics, Siriwardane & Zaman (eds), vol. 1, 821-826.

Harvey, A., Major, C., Plouffe, M., Labrie, D. (1996). Essai de dynamitage de préfracturation à la mine Sigma: Contexte de l'expérimentation et premiers résultats. Compte-rendus du 11e Colloque en contrôle de terrain, Val d'Or.

Hasegawa, H.S., Wetmiller, R.J., Gendzwill, D.J. (1989): Induced seismicity in mines in Canada - An overview. Pure and Appl. Geophysics, 129, 423-453.

Hasegawa, H.S., Wetmiller, R.J., Plouffe, M., Cajka, M.G. (1990): Investigation of natural and mining-related seismic activity in northern Ontario. Rockbursts and Seismicity in Mines, Fairhurst (ed.), Balkema, 249-254.

Hedley, D.G.F. (1991): A five-year review of the Canada-Ontario industry rockburst project. CANMET Special Report SP90-4E.

Hedley, D.G.F. (1992): Rockburst Handbook for Ontario Hardrock Mines. CANMET Special Report SP92-1E.

Hedley, D.G.F., Udd, J.E. (1987): The Canada-Ontario-industry rockburst project. Fred Leighton Memorial Workshop on Mining Induced Seismicity, ISRM-CIM, Montréal, 115-127.

Hedley, D.G.F., Ronburgh, J.W., Muppaleneni, S.W. (1984): A case history of rockbursts at Elliot Lake. Stability in Underground Mining II, Szwilski and Brawner (eds.), AIME, 210-234.

Hedley, D.G.F., Bharti, S., West, D., Blake, W. (1985): Fault-slip rockbursts at the Falconbridge Mine. CANMET Division Report MRP/MRL 85-114.

Henry, D.P. (1987): Advanced Development of the Boundary Element Method for Elastic and Inelastic thermal stress analysis. Ph.D. Thesis, State University of New York at Buffalo.

Herget, G. (1987): Stress assumptions for underground excavations in the Canadian Shield. Int. J. Rock Mech. Min. Sci., 24, 95-97.

Hess, J.L., Smith, A.M.O. (1964): Calculations of nonlifting potential flow about an arbitrary three-dimensional bodies. J. Ship Res., 8, 22-44.

Hess, J.L., Smith, A.M.O. (1966): Calculations of potential flow about arbitrary bodies. Progress in Aeronautical Sciences, Pergamon Press, 8, 1-138.

Hodgson, K., Joughin, N.C. (1967): The relationship between energy release rate, damage, and seismicity in deep mines. Proc. 8th Symp. Rock Mech., 194-203.

Hoek, E., Brown, E.T. (1980): Underground Excavations in Rock. Inst. Min and Metall, London.

Hoek, E., Brown, E.T. (1988). The Hoek-Brown failure criterion - a 1988 update. Proc. 15th Can. Rock Mech. Symp., 31-38.

Hoek, E., Grabinsky, M.W., Fiederichs, M.S. (1991): Numerical modelling for underground excavation design. Trans. Instn Min. Metall., 100, A22-A30.

Holmes, R.D., Reeson, J.A. (1990): Excess shear stress (ESS) - A case study. Rockbursts and Seismicity in Mines, Fairhurst (ed.), Balkema, 331-336.

Homand, F., Piguet, J.P., Revalor, R. (1990): Dynamic phenomena in mines and characteristics of rocks. Rockbursts and Seismicity in Mines, Fairhurst (ed.), Balkema, 139-142.

Horn, H., Deere, D.N. (1962): Frictional characteristics of minerals. Geotechnique, 12, 319-335.

Hoskins, E.R., Jaeger, J.C., Rosengren, K.J. (1968): A medium-scale direct shear experiment. Int. J. Rock Mech. Min. Sci., 4, 143-154.

Hou F., Jia Y. (1988): The relation between rockburst and surrounding rock stress in underground chambers -with a tentative gradation of rockburst intensity. Proc. Intl. Symp. on Engng. in Complex Rock Foundations, Beijing, 497-505.

Höwing, K.-D., Kutter, H.K. (1985): Time-dependant shear deformation of filled rock joints - A keynote lecture. Proc. Int. Symp. on Fundamentals of Rock Joints, Stephansson (ed.), 113- 122.

Hrenikoff, A. (1941): Solution of problems in elasticity by the framework method. J. Appl. Mech., A8, 169-175.

Huang, T.H., Doong, Y.S. (1990): Anisotropic shear strength of rock joints. Rock Joints, Barton & Stephansson (eds), Balkema, 211-218.

Huang, J., Ma, G., Yang, Z. (1985): The application of the boundary element method (BEM) to mining engineering of Golden River Underground Phosphorus Mine. Fifth Int. Conf. on Num. Meth. in Geomech., 1557-1563.

Huang, X., Haimson, B.C., Plesha, M.E., Qiu, X. (1993): An investigation of the mechanics of rock joints - Part I. Laboratory investigation. Int. J. Rock. Mech. Min. Sci. & Geomech. Abstr., 30, 257-269.

Hucka, V., Das, B. (1974): Brittleness determination of rocks by different methods. Int. J. Rock. Mech. Min. Sci., 11, 389-392.

Hueckel, T. (1987): Hysteresis evolution and failure in cyclic loading of dilatant rocks. Constitutive Laws for Engng. Materials: Theory and Applications, Desai C.S. et al. (ed.), Elsevier Science Pub., 565-572.

Jaeger, J.C. (1959): The frictional properties of joints in rock. Geofis. Pura Appl., Milano, 43, 148-158.

Jaeger, J.C. (1971): Friction of rock and the stability of rock slopes. Géotechnique, 21, 97-134.

Jaeger, J.C., Cook, N.G.W. (1979): Fundamentals of Rock Mechanics. Chapman and Hall, 3nd ed.

Jaeger, J.C., Rosengren, K.J. (1969): Friction and sliding joints. Austral. Inst. Min. Metall. Proc., 229, 93-104.

Jaswon, M.A., Symm, G.T. (1977): Integral Equation Methods in Potential Theory and Elasto-statics. Academic Press.

Jing, L., Nordlund, E., Stephansson, O. (1992): An experimental study on the anisotropy and stress-dependency of the strength and deformability of rock joints. Int. J. Rock Mech. Min. Sci. & Geomech. Abstr., 29, 535-542.

Jing, L., Stephansson, O., Nordlund, E. (1993): Study of rock joints under cyclic loading conditions. Rock Mech. and Rock Engng, 26, 215-232.

Jing, L., Nordlund, E., Stephansson, O. (1994) A 3-D constitutive model for rock joints with anisotropic friction and stress dependency in shear stiffness. Int. J. Rock Mech. Min. Sci. & Geomech. Abstr., 31, 173-178.

Jumikis, A.R. (1979): Rock Mechanics. Trans Tech Publications.

Kaiser, P.K. (1993): Keynote address: Support of tunnels in burst-prone ground - Toward a rational design methodology.

Kaiser, P.K., McCreath, D.R., Tannant, D.D. (1996): Rockburst Support Handbook. Geomechanics Research Center Draft, (to be published).

Kato, N., Yamamoto, K., Yamamoto, H., Hirisawa, T. (1993): A stress-corrosion model for strain-rate dependence of the frictional strength of rocks. Int. J. Rock Mech. Min. Sci. & Geomech. Abstr., 30, 551-554.

Kawai, T. (1980): Some considerations on the finite element method. Int. J. for Numerical Methods in Engineering, 16, 81-119.

Kelly, D., Mustoe, W., Zienkiewicz, G.G.W. (1979): Coupling boundary element methods with other numerical methods. Developments in Boundary Element Method - 1, Banerjee & Butterfield (eds.), Applied Science Pub. Ltd, 251-285.

Kidybinski, A. (1981): Bursting liability indices in coal. Int. J. Rock Mech. Min. Sci., 18, 295-304.

Kirsch, G. (1898): Die theorie der elastizitat und die bedürfnisse der festigkeitslehre. Veit. Ver. Deut. Ing., 42, 797-807.

Kleczek, Z., Zorychta, A. (1993): Coal bumps induced by mining tremors. Rockburst and Seismicity in Mines, Young (ed.), Balkema, 87-89.

Kleczek, Z., Zorychta, A. (1991): Geomechanical conditions defining the mining tremors occurrence. Applications of the Geophysical Methods in Mining, Krakow.

Krawiec, A., Stanislaw, T. (1977): Rock bursting in Polish deep coal mines in the light of research and practical observation. Trans. Soc. Min. Eng., Am. Inst. Mech. Eng., 262, 30-36.

Krsmanovic, D., Langof, Z. (1964): Large scale laboratory tests of the shear strength of rocky material. Rock Mech Eng. Geol., Suppl. 1, 20-30.

Lachat, J.C. (1975): Further developments of the boundary integral techniques for elasto-statics. Ph.D. Thesis, Southampton University.

Lachat, J.C., Watson, J.O. (1975): A second generation boundary integral equation program for three-dimensional elastic analysis. Proc. ASME Conf. on Boundary Integral Methods, Cruse & Rizzo (eds).

Lachat, J.C., Watson, J.O. (1976): Effective numerical treatment of boundary integral method equations: a formulation for three-dimensional elasto-statics. Int. J. Num. Meth. in Engng, 10, 991-1005.

Ladanyi, B. (1960): Étude des relations entre les contraintes et les déformations lors du cisaillement des sols pulvérulents. Annales des Travaux Publics de Belgique, 3, 1-30.

Ladanyi, B., Archambault, G. (1970): Simulation of the shear behaviour of a jointed rock mass. Proc. 11th Symp. Rock Mech. (AIME), 105-125.

Lamé, G. (1852): Leçons sur la Théorie Mathématique de l'Élasticité des Corps Solides. Gauthier-Villars, Paris.

Leichnitz, W. (1985): Mechanical properties of rock joints. Int. J. Rock Mech. Min. Sci. & Geomech. Abstr., 22, 313-321.

Leong, E.C., Randolph, M.F. (1991): Modelling of sliding behaviour at rock interfaces. Computer Methods and Advances in Geomechanics, Beer, Booker & Carter (eds), Balkema, 365-369.

Li, V.C. (1987): Mechanics of shear rupture. In Fracture Mechanics of Rock, Atkinson (ed.), Academic Press, chapter 9, 351-428.

Li, V.C., Rice, J.R. (1983a): Preseismic rupture progression and great earthquake instabilities at plate boundaries. J. Geophys. Res., 88, 4231-4246.

Li, V.C., Rice, J.R. (1983b): Precursory surface deformation in great plate boundary earthquake sequences. Bull. Seism. Soc. Am., 73, 1415-1434.

Li, C., Stephansson, O., Savilahti, T. (1990): Behaviour of rock joints and rock bridges in shear testing. Rock Joints, Barton & Stephansson (eds), Balkema, 259-266.

Liebman, H. (1918): Die angenäherte ermittlung: harmonischen, functionen und konformer abbildung. Sitzber. Math. Physik Kl. Bayer Akad. Wiss. München, 3, 65-75.

Lin, C.T., Amadei, B., Sture, S. (1994): Using an Augmented Lagrangian method and block fracturing in the DDA method. Computer Methods and Advances in Geomechanics, Siriwardane & Zaman (eds), vol. 1, 837-842.

Lorig, L.J., Brady, B.H.G. (1984): A hybrid computational scheme for excavation and support design in jointed rock media. Design and Performance of Underground Excavations: ISRM Symp., Brown & Hudson (eds), 105-112.

Massonet, C.E. (1965): Numerical use of integral procedures. Stress Analysis, Zienkiewicz & Holister (eds), Wiley, chapter 10.

McCreary, R.G., Grant, D., Falmagne, V. (1993): Source mechanisms, three-dimensional boundary-element modelling, and underground observations at Ansil Mine. Rockbursts and Seismicity in Mines, Young (ed.), Balkema, 227-232.

McHenry, D. (1943): A lattice analogy for the solution of plane stress problems. J. Inst. Civ. Eng., 21, 59-82.

McMahon, T. (1988): Rock burst research and the Coeur d'Alene District. U.S.B.M., IC 9186.

Meek, J.L. (1985): Recent experience with numerical analysis of mining engineering related problems. Fifth Int. Conf. on Num. Meth. in Geomech., 93-103.

Mei, J., Lu, J. (1987a): The phenomena, prediction and control of rockburst in some Chinese underground engineering. Preprints 2nd Int. Symp. on Field Measurements in Geomechanics, 1065-1079.

Mei, J., Lu, J. (1987b): The phenomena, prediction and control of rockburst in China. Proc. 6th Int. Cong. Rock Mech., ISRM, Vol. 2, 1135- 1140.

Mitri, H.S. (1996a): Study of rockburst potential at Sigma mine, Val d'Or, Quebec using numerical modelling - Final report. Report submitted to le Centre de Développement Technologique (CDT), École Polytechnique de Montréal, In Aubertin et al., 1997.

Mitri, H.S. (1996b): Numerical modelling of mining-induced energy in rockburst problems. In Workshop Notes: Numerical Modelling of Ground Burst Problems, NARMS'96, June 22 1996, 1-20.

Mitri, H.S., Rizkalla, M. (1995): Study of rockburst potential in hard rock mining using numerical modelling. Rapport d'étape No 2, in Aubertin et al., 1997.

Mitri, H.S., Suriyachat, P. (1990): Energy based postprocessor for 2-D F.E.A. of mine openings. Proc. Int. Conf. on Struc. Engng and Computation, 917-925.

Mitri, H.S., Scoble, M.J., McNamara, K. (1988): Numerical studies of destressing mine pillars in highly-stressed rock. 41st Canadian Geotechnical Conf., Univ. of Waterloo, 50-56.

Mitri, H.S., Hassani, F.P., Kebbe, R. (1993): A strain energy approach for the prediction of rockburst potential in underground hard rock mines. Proc. First Can. Symp. on Numerical Modelling Applications in Mining and Geomech., Montréal, McGill University, 228-239.

Momoh, O.A., Mitri, H.S., Rizkalla, M. (1996): Numerical modelling of destress blasting. Proc. 2nd North Amer. Rock Mech. Symp., NARMS'96, Aubertin, Hassani and Mitri (eds), 1911-1918.

Morrison, R.G.K. (1942): Report on the rockburst situation in Ontario mines. Trans. Can. Inst. Min. and Met., 45, 225-272.

Morrison, R.G.K. (1976): A philosophy of ground control - A bridge between theory and practice. Dept. of Mining and Metallurgical Engineering, McGill University.

Morrison, R.G.K., Coates, D.F. (1957): Rockbursts and ground control mining in Canada. Proc. 6th Commonwealth Min. and Metall. Cong., 365-375.

Mottahed, P. (1992): Atelier sur les coups de toit. Organisé par CANMET et l'AMQ, Val-d'Or.

Mukherjee, S., Chandra, A. (1985): Boundary element formulations for large strain - Large deformation problems of plasticity and viscoplasticity. Dev. in Boundary Element Methods-3, Elsevier Applied, Science, 27-57.

Muralha, J., Pinto da Cunha, A. (1992): Mathematical modelling of scale effects in rock joints. Proc. ISRM Symp. Eurock'92, 287-292.

Musial, J. (1987): Predicting rockbursts. The Northern Miner Mag., November 1987, 51-55.

Newland, P.L., Allely, B.H. (1957): Volume changes in drained triaxial tests on granular materials. Géotechnique, 7, 17-34.

Neyman, B., Szecowka, Z., Zuberek, W. (1972): Effective methods for fighting rock burst in Polish collieries. Proc. 5th Int. Strata Control Conf., 23.1-23.9.

Newmark, N.M. (1949): Numerical methods of analysis in bars, plates and elastic bodies. In Numerical Methods in Analysis Engineering, Grinter (ed.), Macmillan.

Obert, L., Duvall, W.I. (1967): Rock Mechanics and the Design of Structures in Rock. John Wiley.

Ohnaka, M. (1973): Experimental studies of stick-slip and their application to the earthquake source mechanism. J. Phys. Earth, 21, 285-303.

Ohnaka, M., Yamashita, T. (1989): A cohesive zone model for dynamic faulting based on experimentally inferred constitutive relation and strong motion source parameters. J. Geophys. Res., 94, 4089-4104.

Oliviera, E.R.A. (1968): Plane stress analysis by a general integral method. J. ASCE, Engng Mech. Div., 79-85.

Olofsson, T. (1985): A non-linear model for the mechanical behaviour of continuous rock joints. Proc. Int. Symp. on Fundamentals of Rock Joints, Stephansson (ed.), 395-404..

Ortlepp, W.D. (1983): The mechanics and control of rockbursts. Rock Mechanics in Mining Practice, Budavari (ed.), SAIMM, Johannesburg, 257-282.

Ortlepp, W.D. (1984): Rockbursts in South African gold mines: A phenomenological view. Proc. 1st Int. Cong. Rockbursts and seismicity in Mines, SAIMM, Johannesburg 1982, 164-178.

Pande, G.N. (1985): A constitutive model of rock joints. Proc. Int. Symp. on Fundamentals of Rock Joints, Stephansson (ed.), 429-440.

Papaliangas, T., Hencher, S.R., Lumsden, A.C., Manolopoulous, S. (1993): The effect of frictional fill thickness on the shear strength of rock discontinuities. Int. J. Rock Mech. Min. Sci. & Geomech. Abstr., 30, 81-91.

Paterson, M.S. (1978): Experimental Rock Deformation - The Brittle Field. Spinger-Verlag.

Patton, F.D. (1966): Multiple modes of shear failure in rock. Proc. 1st Cong. ISRM, Vol. 1, 509-513.

Peirce, A.P. (1991): Efficient multigrid solution of boundary element models of cracks and faults. Int. J. for Num. and Analytical Methods in Geomech., 15, 549-572.

Pereira, J.P. (1990): Shear strength of filled discontinuities. Rock Joints, Barton & Stephansson (eds), Balkema, 283-287.

Petukhov, I.M. (1957): Rockbursts in Kizel Coalfield Mines (in Russian). Perm. Publ., Perm.

Petukhov, I.M. (1987): Forecasting and combating rockbursts: recent developments. Proc. 6th Cong. IRSM, Vol. 2, 1207-1210.

Petukhov, I.M. (1990): Theory of rockbursts and their classification. Rockbursts-global experience, Paper presented at Fifth Plenary Scientific Session of Working Group on Rockbursts of International Bureau of Strata Mechanics, 1-10.

Phien-wej, N., Shrestha, U.B., Rantucci, G. (1990): Effect of infill thickness on shear behavior of rock joints. Rock Joints, Barton & Stephansson (eds), Balkema, 289-294.

Pininska, J., Lukaszewski, P. (1991): The relationships between post-failure state and compressive strength of sudetic fractured rocks. Bul. Intl. Ass. Engng. Geol., 43, 81-86.

Pinto da Cunha, A. (1991): Scale effects in the determination of mechanical properties of joints and rock masses. Proc. 7th ISRM Congress, Aachen, Vol. 1, 311-318.

Plouffe, M., Asudeh, I., Lachance, D.V., Aguila, R., Turgeon, L. (1993a): The Agnico-Eagle Mine seismic survey. Rockbursts and Seismicity in Mines, Young (ed.), Balkema, 393-397.

Plouffe, M., Mottahed, P., Lebel, D., Côté, M. (1993b): Monitoring of large mining induced seismic events -CANMET/MRL's contribution. Rockbursts and Seismicity in Mines, Young (ed.), Balkema, 399-403.

Prager, W., Synge, J.L. (1947): Approximation in elasticity based on the concept of function space. Q. J. Appl. Math., 5, 241-269.

Priest, S.D. (1993): Discontinuity Analysis for Rock Engineering. Chapman & Hall.

Qiu, X., Plesha, M.E., Huang, X., Haimson, B.C. (1993): An investigation of the mechanics of rock joints - Part II. Analytical investigation. Int. J. Rock. Mech. Min. Sci. & Geomech. Abstr., 30, 271-287.

Lord Rayleigh (J. W. Strutt), (1870): On the theory of resonance. Trans. Roy. Soc. (London), A161, 77-118.

Reddy, J.N. (1993): An Introduction to the Finite Element Method. McGraw-Hill.

Rice, J.R., (1983): Constitutive relations for fault slip and earthquake instabilities. Pageoph., 121, 443-475.

Rice, J.R., Tse, S.T. (1986): Dynamic motion of a single degree of freedom system following a rate and state dependent friction law. J. Geophys. Res., 91, 521-530.

Richards, L.R. (1975): The shear strength of joint in weathered rock. Ph.D. Thesis, Univ. of London, Imperial College.

Richardson, L.F. (1910): The approximate arithmetical solution by finite difference of physical problems. Trans. Roy. Soc. (London), A210, 307-357.

Rizt, W. (1909): Über eine neue methode zur lösung gewissen variations - Probleme der mathematischen physik. J. Reine Angew. Math., 135, 1-61.

Rizzo, F.J. (1967): An integral equation approach to boundary value problems of classical elastostatics. Q. Appl. Math., 25, 83-95.

Rizzo, F.J., Shippy, D.J. (1977): An advance boundary integral equation method for three-dimensional thermo-elasticity. Int. J. Num. Meth. in Engng, 11, 1753.

Rizzo, F.J., Shippy, D.J. (1979): Recent advances to the boundary element method in thermoelasticity. Developments in Boundary Element Methods, Banerjee & Butterfield (eds), Applied Science Pub., vol. I, chapter VI.

ROCTEST (1980): Étude sur les coups de charge dans les mines. Rapport final de Roctest Limitée soumis au Gouvernement du Québec, Ministère de l'Énergie et des Ressources, avril 1980.

Ryder, J.A. (1987): Excess shear stress (ESS): An engineering criterion for assessing unstable slip and associated rockburst hazards. Proc. 6th Int. Cong. Rock Mech., IRSM, Montréal, Vol. 2, 1211-1215.

Ryder, J.A. (1988): Excess shear stress in the assessment of geologically hazardous situations. J. S. Afr. Inst. Min. Metall., 88, 1, 27-39.

Ryman-Lipinsky, W.K., Bakker, D. (1997): The development of government rockburst and rockfall hazard monitoring system for South African mines. Rockburst and Seismicity in Mines, Gibowicz and Lasocki (eds), Balkema, 371-376.

Saeb, S. (1989): Effect of Boundary Conditions on the Behavior of a Dilatant Rock Joint. Ph.D. Dissertation, University of Colorado at Boulder.

Saeb, S. (1990): A variance on the Ladanyi and Archambault's shear strength criterion. Rock Joints, Barton & Stephansson (eds), Balkema, 701-705.

Saeb, S., Amadei, B. (1989): Effect of boundary conditions on the shear behaviour of a dilatant rock joint. Proc. 30th U.S. Symp. Rock Mech., 107-114.

Saeb, S., Amadei, B. (1990): Modelling joint response under constant or variable normal stiffness boundary conditions. Int. J. Rock Mech. Min. Sci. & Geomech. Abstr., 27, 213-217.

Saeb, S., Amadei, B. (1992): Modelling rock joint under shear and normal loading. Int. J. Rock Mech. Min. Sci. & Geomech. Abstr., 29, 267-278.

Salamon, M.D.G. (1970): Pillar stability/instability and design of pillar workings. Int. J. Rock Mech. Min. Sci., 7, 613-631.

Salamon, M.D.G. (1974): Rock mechanics of underground excavations. Advances in Rock Mechanics, Proc. 3rd Cong. Int. Soc. Rock. Mech., Vol. 1-B, 951-1099.

Salamon, M.D.G. (1983): Rockburst hazard and the fight for its alleviation in South African gold mines. Proc. Rockbursts Prediction and Control, IMM, London, 11-36.

Salamon, M.D.G. (1983b): The role of pillars in mining. Rock Mechanics in Mining Practice, Budavari (ed.), S. Afr. Inst. Min. and Metall., Monograph Series, 5, 173-200.

Salamon, M.D.G. (1984): Energy considerations in rock mechanics: fundamental results. J. S. Afr. Inst. Min. and Metall., 84, 233-246.

Särkkä, P.S. (1984): The interactive dimensioning of pillars in Finnish mines. Proc. 2nd Int. Conf. Stability in Underground Mining, Lexington, 71-84.

Schneider, H.J. (1976): The friction and deformation behavior of rock joint. Rock Mech., 8, 169-184.

Scholz, C.H., Molnar, P., Johnson, T. (1972): Detailed studies of frictional sliding in granite and implications for earthquake mechanism. J. Geophys. Res., 77, 6392-6406.

Scoble, M.J., Cullen, M., Makuch, A. (1987): Experimental studies of factors relating to destress blasting. Proc. 28th US Symp. Rock Mech., Balkema, 901-908.

Shaw, R.P. (1966): Diffraction of acoustic pulses by obstacles of arbitrary shape with a robin boundary condition - Part A. J. Acoust. Soc. Am., 41, 855-859.

Shaw, R.P. (1969): Diffraction of pulses by obstacles of arbitrary shape with an impedance boundary condition. J. Acoust. Soc. Am., 44, 1962-1968.

Shi, G-H. (1988): Discontinuous deformation analysis: a new numerical model for the statics and dynamics of block systems. Ph.D. Thesis, University of California, Berkeley.

Shi, G-H., Goodman, R.E. (1989): Generalization of two-dimensional continuous deformation analysis for forward modeling. Int. J. Num. & Anal. Methods in Geomech., 13, 359-380.

Simon, R. (1992): Validation d'une méthodologie d'évaluation du potentiel de coups de terrain dans les mines. Mémoire de maîtrise (M.Sc.A.), École Polytechnique, Montréal.

Simon, R., Aubertin, M., Gill, D.E. (1993): Numerical modelling for the evaluation of rockburst potential of an underground excavation. Proc. First Can. Symp. on Numerical Modelling Applications in Min. and Geomech., Montréal, 217-227.

Simon, R., Aubertin, M., Mitri, H.S. (1995): Evaluation of rockburst potential in hard rock mines. 97th Annual General Meeting of C.I.M., Rock Mechanics and Strata Control Session, Halifax.

Simon, R., Aubertin, M., Gill, D.E. (1998): Guide d'évaluation du potentiel de coups de terrain dans les mines à l'aide de la méthode ERP. Rapport final présenté à l'Institut de Recherche en Santé et Sécurité au Travail (IRSST), IRSST Rapport R-182.

Singh, S.P. (1986): Assessment of the rockburst proneness in hard rock mines. Proc. 5th Conf. Ground Control in Mining, 242-248.

Singh, S.P. (1987): The influence of rock properties on the occurrence and control of rockburst. Mining Science and Technology, 5, 11-18.

Singh, S.P. (1988a): Technical note: Burst energy release index. Rock Mechanics and Rock Engng., 21, 149-155.

Singh, S.P. (1988b): The Significance of the knowledge of the burst proneness of rocks in underground mine planning. Mine Planning and Equipment Selection, Singhal (ed.), Balkema, 191-198.

Singh, S.P. (1989): Classification of mine workings according to their rockburst proneness. Mining Science and Technology, 8, 253-262.

Skinas, C.A., Bandis, S.C., Demiris, C.A. (1990): Experimental investigations and modelling of rock joint behaviour under constant stiffness. Rock Joints, Barton & Stephansson (eds), Balkema, 301-308.

Souley, M., Homand, F., Amadei, B. (1995): An extension to the Saeb and Amadei constitutive model for rock joints to include cyclic loading paths. Int. J. Rock. Mech. Min. Sci. & Geomech. Abstr., 32, 101-109.

Southwell, R.V. (1946): Relaxation Methods in Theoretical Physics. Clarendon Press.

Spottiswoode, S.M. (1990): Volume excess shear stress and cumulative seismic moments. Rockbursts and Seismicity in Mines, Fairhurst (ed.), Balkema, 39-43.

Stacey, T.R., Page, C.H. (1986): Practical Handbook for Underground Rock Mechanics. Trans-Tech Publ.

Starfield, A.M., Fairhurst, C. (1968): How high-speed computers advance design of practical mine pillar systems. Engng. Min. J., 169, 78-84.

Starfield, A.M., Wawersik, W.R. (1968): Pillars as structural components in room-and-pillar mine design. Proc. 10th US Symp. on Rock Mech., Austin, 793-809.

Stewarski, E. (1987): Energetic indicator of liability of rocks to burst during shock loading with Hopkin's bar. Stanislaw Staszic Acad. Min. Metall., Cracow, Min. Bul., 129, 263-269.

Stopinski, W., Dmowska, R. (1984): Rock resistivity in the Lubin (Poland) Copper Mine and its relation to variations of strain field and occurrence of rockbursts. Proc. 1st Int. Cong. Rockbursts and Seismicity in Mines, Johannesburg, S. Afr. Inst. Min. Metall., 297-307.

Sun, Z., Gerrard, C., Stephanson, O. (1985): Rock joint compliance tests for compression and shear load. Int. J. Rock Mech. Min. Sci. & Geomech. Abstr., 22, 197-213.

Tajdus, A, Flisiak, J., Cala, M. (1997): Estimation of rockburst hazard basing on 3D stress field analysis. Rockbursts and Seismicity in Mines, Gibowick and Lasocki (eds), Balkema, 273-277.

Tan, T.K. (1986): Hypothesis on rockbursts. Proc. Int. Symp. on Rock Stress and Stress Measurements, 515-520.

Tao, Z.Y. (1988): Support design of tunnels subjected to rockbursting. Rock Mech. and Power Plants, Romana (ed.), Balkema, 407-411.

Telles, J.C.F. (1983): The Boundary Element Method Applied to Inelastic Problems. Lecture Notes in Engineering, Brebbia & Orszag (eds), Springer-Verlag.

Timoshenko, S.P., Goodier, J.N. (1970): Theory of Elasticity, 3rd edn, McGraw-Hill.

Tomlin, G.R., (1973): Numerical Analysis of Continuum Problems in Zoned Anisotropic Media. Ph.D. thesis, Southampton University.

Tomlin, G.R., Butterfield, R. (1974): Elastic analysis of zoned orthotropic continua. Proc. ASCE Eng. Mech. Div., EM3, 511-529.

Turner, M.J., Clough, R.W., Martin, H.C., Topp, L.J. (1956): Stiffness and deflection analysis of complex structures. J. Aero. Sci., 23, 805-823.

Udd, J.E., Hedley, D.G.F. (1985): Recherches sur la mécanique des roches aux laboratoires de recherche minière du CANMET, 1964-1984. Énergie, Mines et Ressources, Canada.

Vandamme, L., Wawrzynek, P.A. (1988): Displacement discontinuities and interactive graphics for three-dimensional hydraulic fracturing simulators. Num. Meth. in Geomech., Balkema, 265-271.

Varga, R.S. (1962): Matrix Iterative Analysis. Prentice-Hall.

Vasak, P. Kaiser, P.K. (1995): Tunnel stability assessment during rockbursts. Proc. 3rd Can. Conf. on Computer Applications in the Mineral Industry, CAMI'95, McGill University, 238-247.

Voegele, M., Fairhurst, C., Cundall, P. (1978): Analysis of tunnel support load using a large displacement, distinct block model. Storage in Excavated Rock Caverns, proc. First Int. Symp., Rockstore 77, Bergman (ed.), Pergamon Press, vol. 2, 247-252.

Walsh, J.B. (1977): Energy changes due to mining. Int. J. Rock Mech. Min. Sci., 14, 25-33.

Watson, J.O. (1973): Analysis of thick shells with holes by using integral equation method. Ph.D. Thesis, Southampton University.

Wawersik, W.R., Rudnicki, J.W., Olsson, W.A., Holcomb, D.J., Chau, K.T. (1990): Localization of deformation in brittle rocks: Theoretical and laboratory investigations. Micromechanics of Failure of Quasi-Brittle Materials, Elsevier Appl. Sci., 115-124.

Whiteway, P. (1985): $4.2 Millions sought for rock burst work. The Northern Miner, April 4th, A1-A6.

Wiles, T.D. Nicholls, D. (1993): Modelling discontinuous rockmasses in three dimensions using MAP3D. Proc. First Can. Symp. on Num. Modell. Applications in Min. and Geomech., 4-49.

Wilson, A.H. (1972): A hypothesis concerning pillar stability. Min. Eng., 131, 407-419.

Wittke, W. (1990): Rock Mechanics - Theory and Applications with Case Histories. Springer-Verlag.

Wood, (1976): On the finite element solution of an exterior boundary value problem. Int. J. Num. Meth. Engng, 10, 885-891.

Wu, Y., Zhang, W. (1997): Evaluation of the bursting proneness of coal by means of its failure duration. Rockburst and Seismicity in Mines, Gibowicz and Lasocki (eds), Balkema, 285-288.

Yoshinaka, R., Yamabe, T. (1986): Joint stiffness and the deformation behaviour of discontinuous rock. Int. J. Rock Mech. Min. Sci., 23, 19-28.

Young, R.P., Talebi, S., Hutchins, D.A., Urbanic, T.I. (1989): Source mechanism studies of mining-induced microseismic events at Strathcona Mine, Sudbury, Canada. Special Issue of Pure and Appl. Geophys. on Mining Induced Seismicity, 129, 455-474.

Young, R.P., Hutchins, D.A., McGaughey, W.J. (1990): Seismic imaging ahead of mining in rockburst prone ground. Rockburst and Seismicity in Mines, Fairhurst (ed.), Balkema, 231-236.

Zienkiewicz, O.C. (1971): The Finite Element Method. 3rd ed., McGraw-Hill.

Zienkiewicz, O.C., Taylor, R.L. (1977): The Finite Element Method - Vol. 1: Basic Formulation and Linear Problems. Third edition, McGraw-Hill.

Zienkiewicz, O.C., Taylor, R.L. (1989): The Finite Element Method - Vol. 1: Basic Formulation and Linear Problems. Fourth edition, McGraw-Hill.

Zienkiewicz, O.C., Kelly, D.W., Bettess, P. (1977): The coupling of the finite element method and boundary solution procedure. Int. J. for Num. Meth. Engng, 11, 335-375.

Zipf, R.K.jr. (1993): New developments in MULSIM/NL - A boundary element method program for stress analysis of coal mines. Proc. First Can. Symp. on Num. Modell. Applications in Min. and Geomech., 119-128.

Zipf, R.K.jr. (1996): Simulation of cascading pillar failure in room-and-pillar mines using boundary-element-method. Rock Mechanics, Tools and Techniques, Aubertin, Hassani & Mitri (eds), vol. 2, 1887-1892.

APPENDIX A
TEST RESULTS ON JOINTS

As it was mentioned in Chapter 5, several test results on rock joints (or similar materials) were compiled to validate the proposed model. These test results were taken from literature and included direct shear tests under constant normal stress. These tests are presented in the following figures. In these figures, the test data are represented by symbols, the Saeb-Amadei model is represented by a straight line and the proposed model is represented by a dashed line. Finally, a correlation table for both models is presented at the end.

TEST RESULTS FROM LEICHNITZ (1985)

Material: Artificial fracture on a sandstone rock split by brazilian test

Figure: A1

Model parameters:

i_0 °	u_p mm	u_r mm	V_m mm	k_{ni} MPa/mm	B_0	ϕ_o °	S_o MPa	ϕ_u °	σ_T MPa
11	0.4	20	10	1000	0.53	40	2.8	40	15

TEST RESULTS FROM FLAMAND ET AL. (1994)

Material: Rock joint replica of cement mortar

Figure: A2

Model parameters:

i_0 °	u_p mm	u_r mm	V_m mm	k_{ni} MPa/mm	B_0	ϕ_o °	S_o MPa	ϕ_u °	σ_T MPa
12	0.55	4	10	1000	0.55	40	23	40	100

TEST RESULTS FROM SKINAS ET AL. (1990)

Material: Artificial joint replica of sand-barytes cement mixture

Figure: A3

Model parameters:

i_0 °	u_p mm	u_r mm	V_m mm	k_{ni} MPa/mm	B_0	ϕ_o °	S_o MPa	ϕ_u °	σ_T MPa
3	1.2	20	0.1	100	0.74	40	4	38	20

TEST RESULTS FROM BERTRAND (1989)

Material: Artificial joint replica of limestone

Figure: A4

Model parameters:

i_0 °	u_p mm	u_r mm	V_m mm	k_{ni} MPa/mm	B_0	ϕ_o °	S_o MPa	ϕ_u °	σ_T MPa
18	0.375	2.5	2	9.8	0.32	40	7	38	12

TEST RESULTS FROM BANDIS ET AL. (1981)

Material: Artificial rock joint replica of plaster

Figure: A5

Model parameters:

i_0 °	u_p mm	u_r mm	V_m mm	k_{ni} MPa/mm	B_0	ϕ_o °	S_o MPa	ϕ_u °	σ_T MPa
5.5	1	4	2	10	0.75	40	1.4	30	2

TEST RESULTS FROM SCHNEIDER (1976)

Material: Artificial plaster joint replica of smooth granite

Figure: A6

Model parameters:

i_0 °	u_p mm	u_r mm	V_m mm	k_{ni} MPa/mm	B_0	ϕ_o °	S_o MPa	ϕ_u °	σ_T MPa
4	5	55	2	10	0.88	46	1.1	28	5

Material: Artificial plaster joint replica of rough and indented granite joint

Figure: A7

Model parameters:

i_0 °	u_p mm	u_r mm	V_m mm	k_{ni} MPa/mm	B_0	ϕ_o °	S_o MPa	ϕ_u °	σ_T MPa
7	2	30	2	1000	0.74	38	1.2	38	5

Material: Artificial plaster joint replica of rough sandstone with large asperities

Figure: A8

Model parameters:

i_0 °	u_p mm	u_r mm	V_m mm	k_{ni} MPa/mm	B_0	ϕ_o °	S_o MPa	ϕ_u °	σ_T MPa
7	5	50	2	100	0.65	38	1.5	40	5

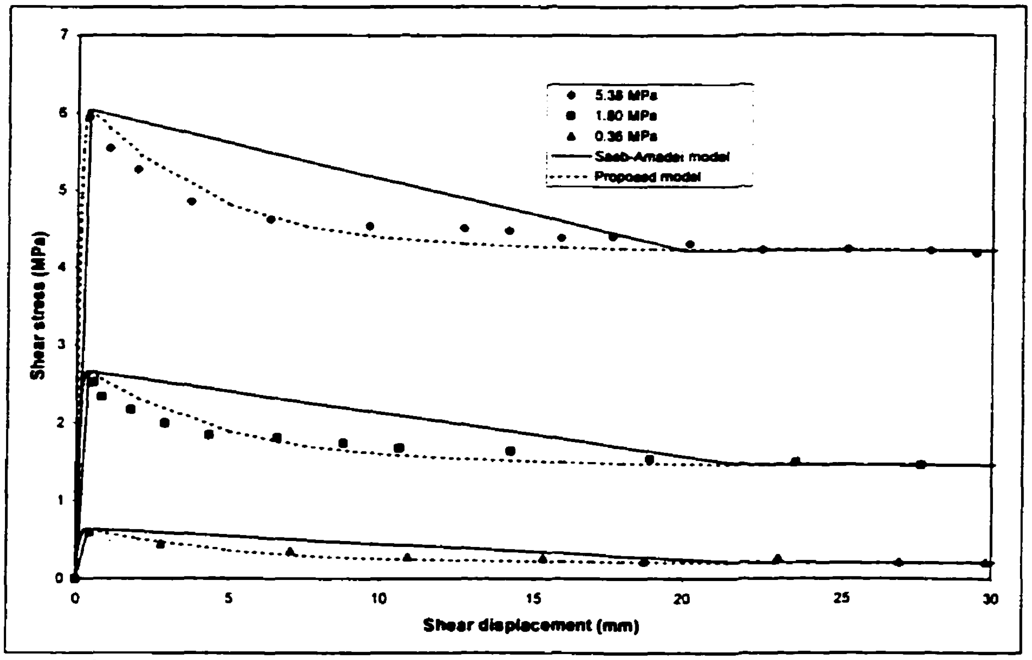

Figure A1a: Shear stress -shear displacement curve for direct shear tests under different normal constant stresses (data from Leichnitz, 1985).

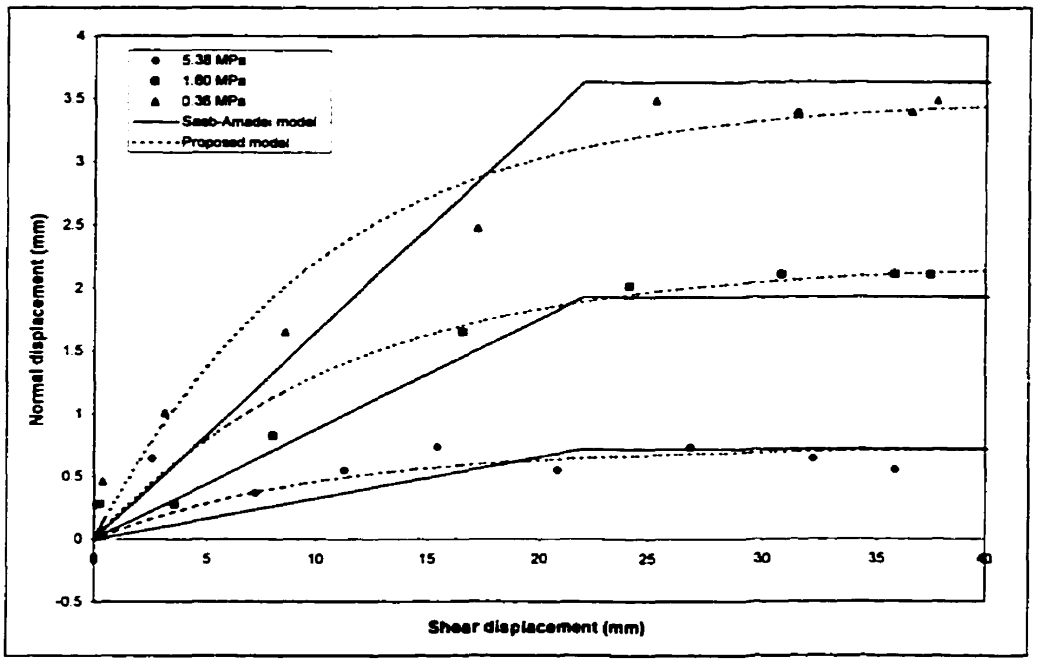

Figure A1b: Normal displacement -shear displacement curve for direct shear tests under different normal constant stresses (data from Leichnitz, 1985).

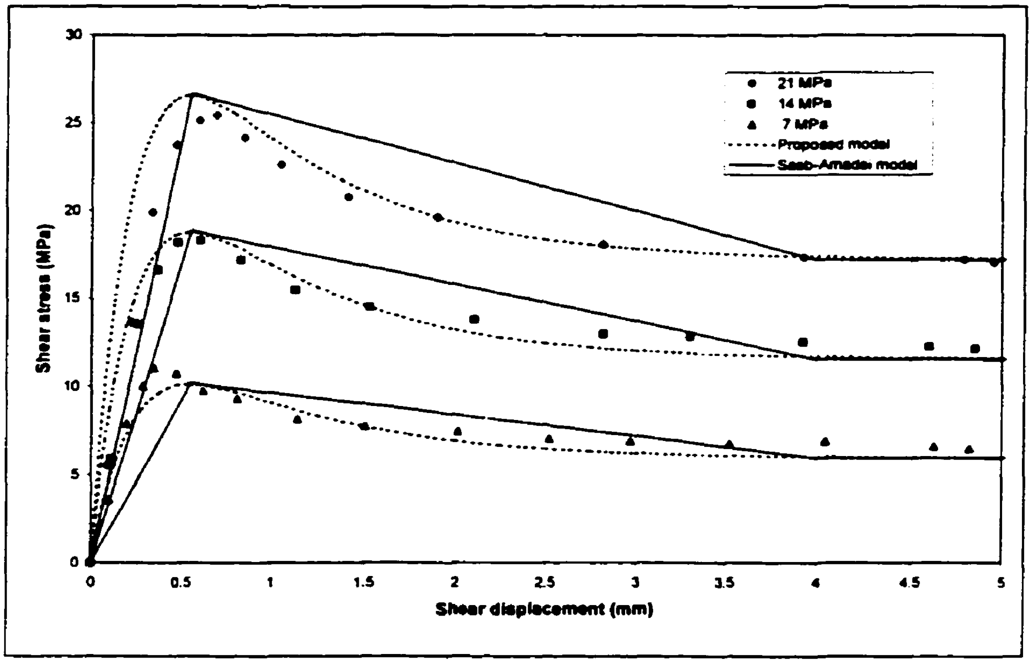

Figure A2a: Shear stress -shear displacement curve for direct shear tests under different normal constant stresses (data from Flamand et al., 1994).

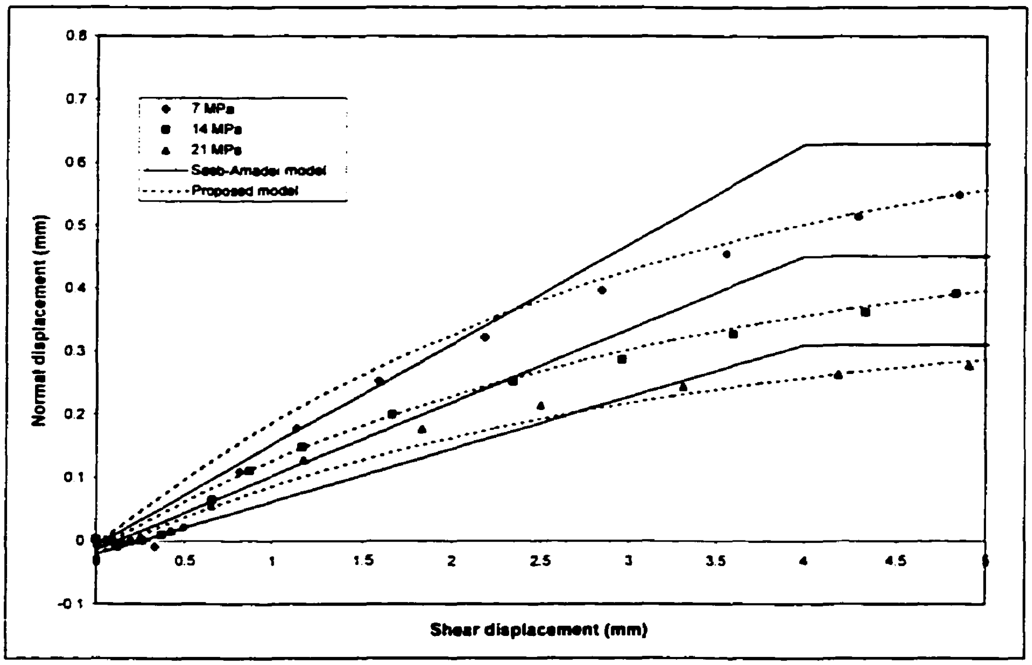

Figure A2b: Normal displacement -shear displacement curve for direct shear tests under different normal constant stresses (data from Flamand et al., 1994).

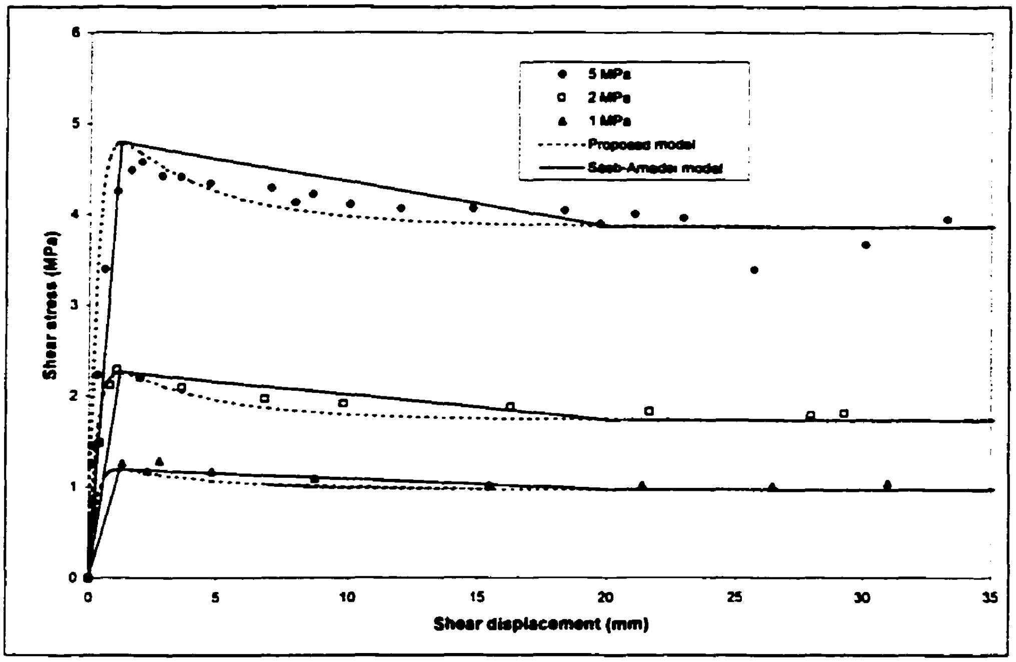

Figure A3a: Shear stress -shear displacement curve for direct shear tests under different normal constant stresses (data from Skinas et al., 1990).

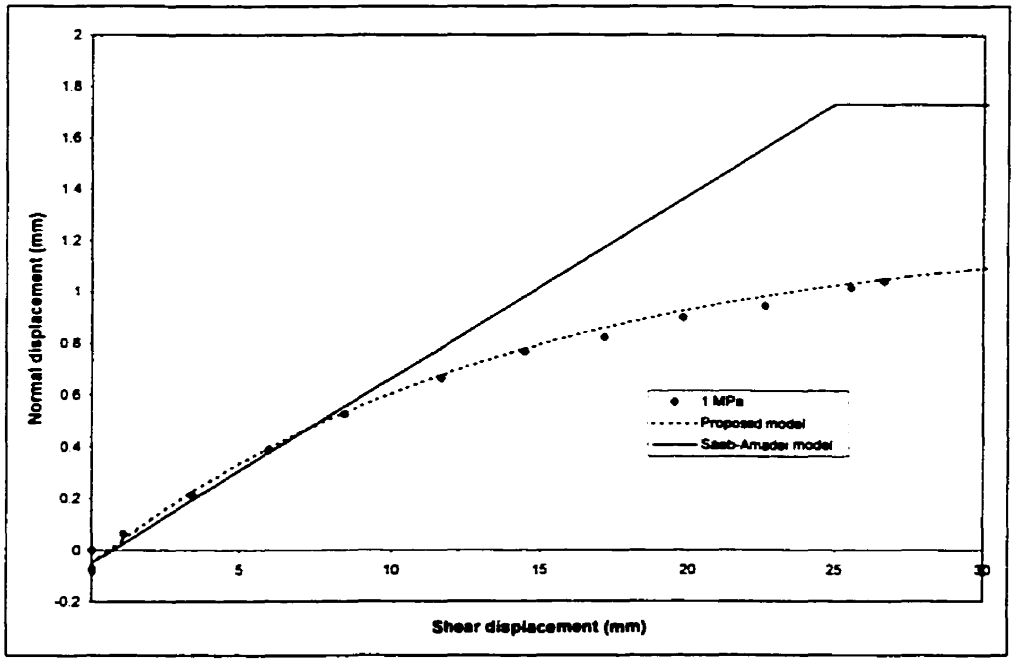

Figure A3b: Normal displacement -shear displacement curve for direct shear test under normal constant stress (data from Skinas et al., 1990).

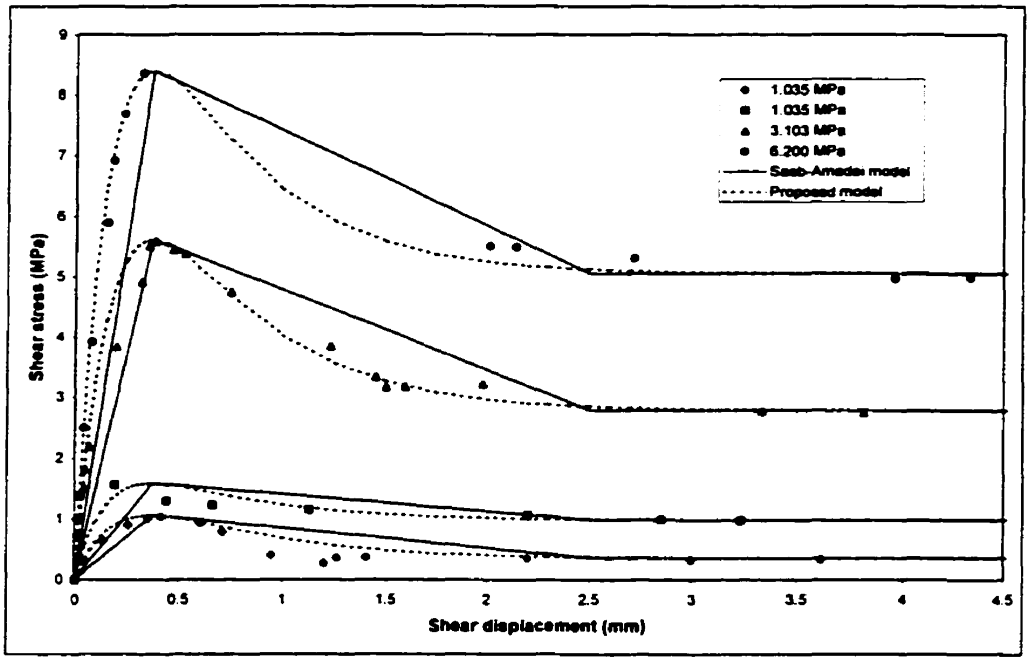

Figure A4a: Shear stress -shear displacement curve for direct shear tests under different normal constant stresses (data from Bertrand, 1989).

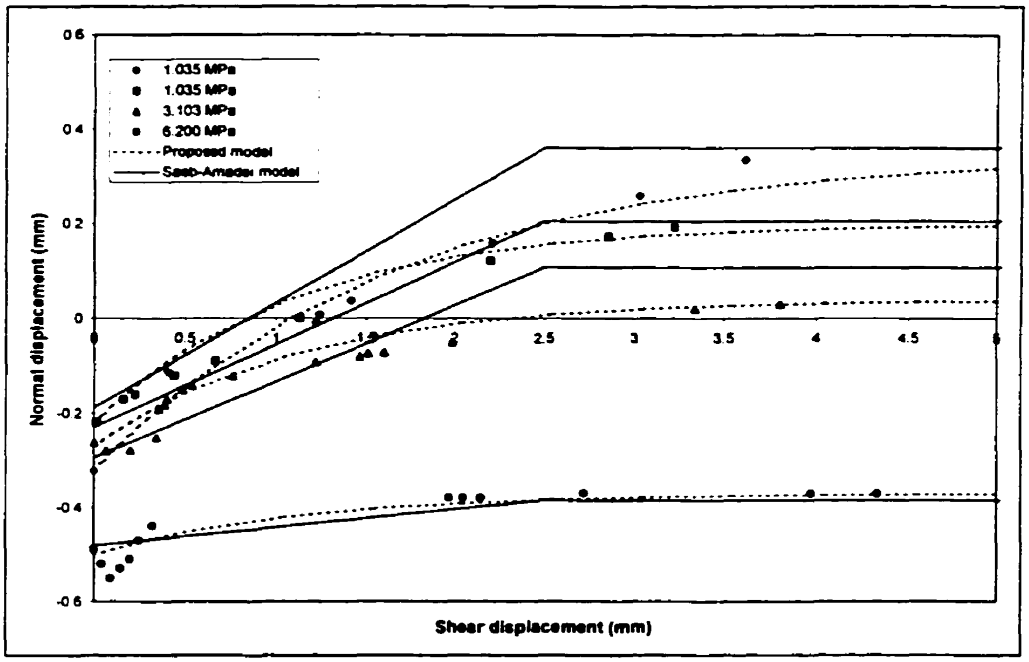

Figure A4b: Normal displacement -shear displacement curve for direct shear tests under different normal constant stresses (data from Bertrand, 1989).

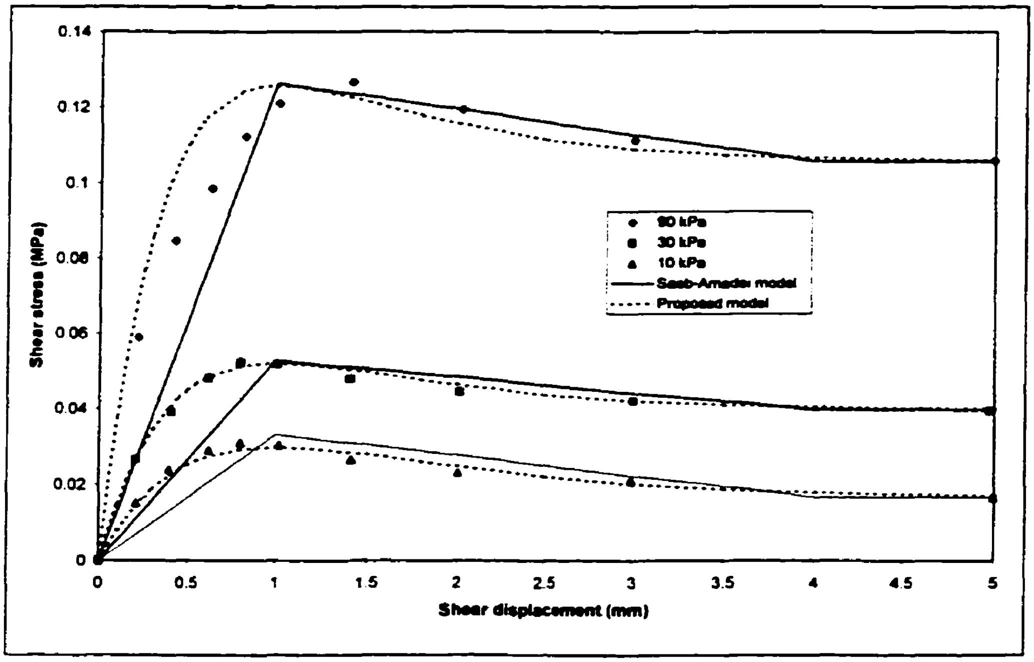

Figure A5a: Shear stress -shear displacement curve for direct shear tests under different normal constant stresses (data from Bandis et al., 1981).

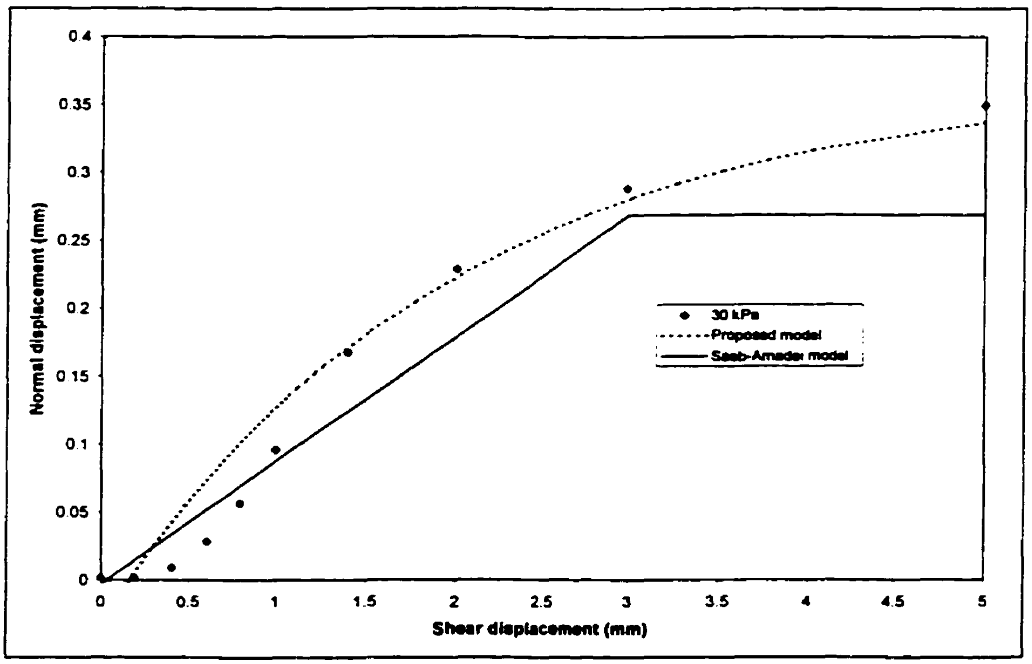

Figure A5b: Normal displacement -shear displacement curve for direct shear test under normal constant stress (data from Bandis et al., 1981).

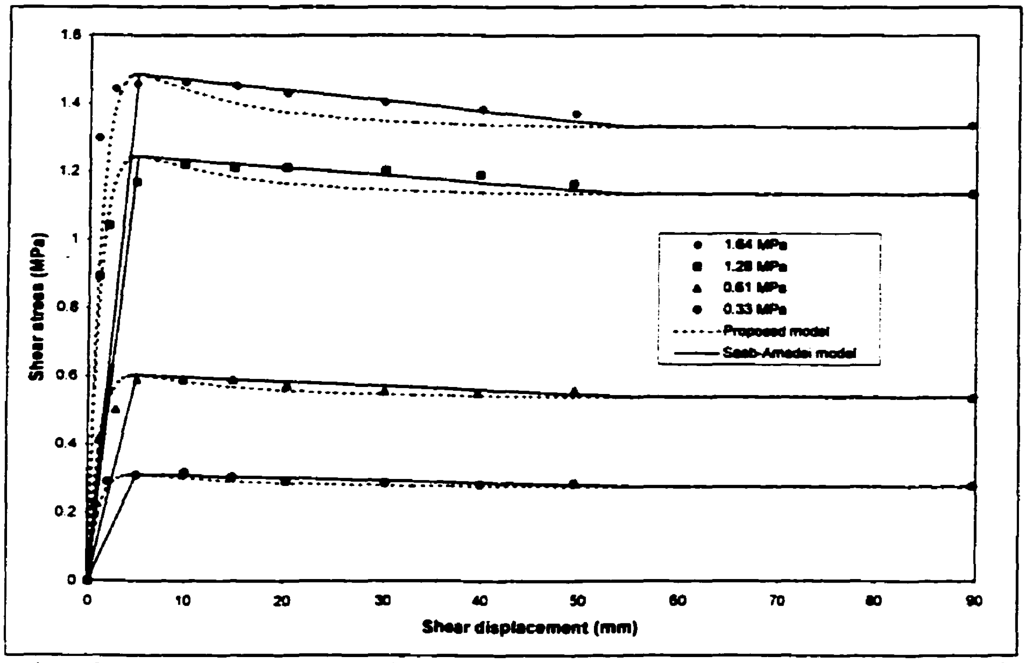

Figure A6a: Shear stress -shear displacement curve for direct shear tests under different normal constant stresses (data from Schneider, 1976).

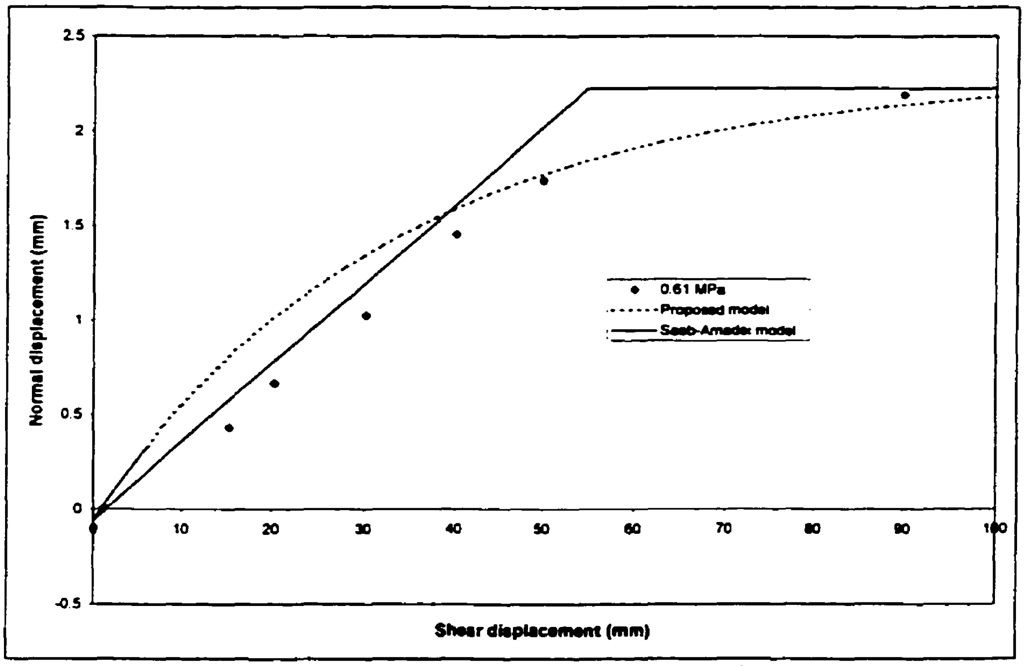

Figure A6b: Normal displacement -shear displacement curve for direct shear test under normal constant stress (data from Schneider, 1976).

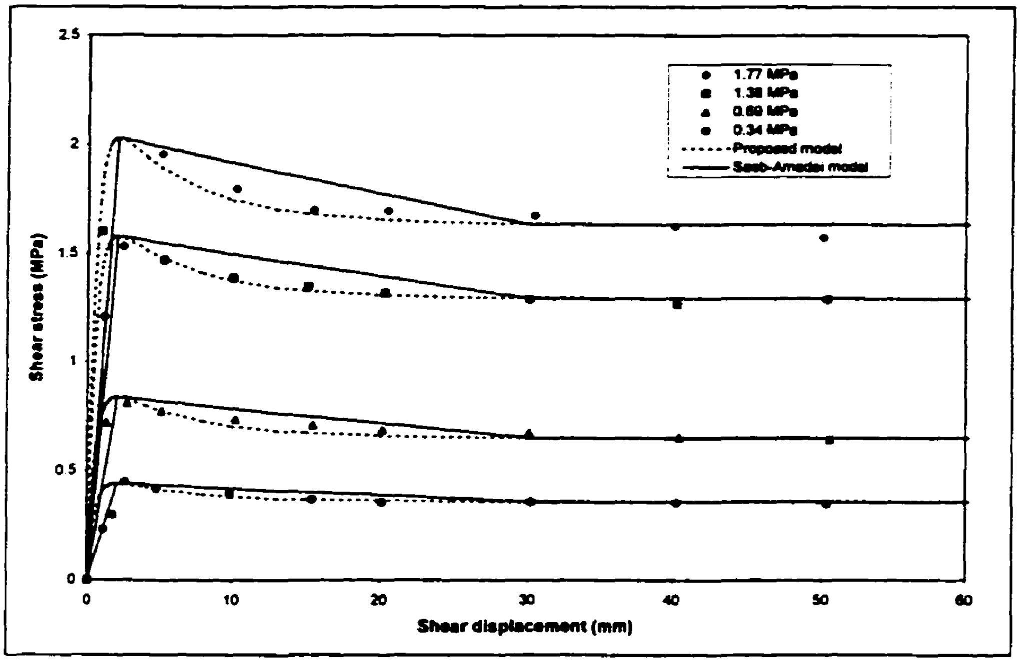

Figure A7a: Shear stress -shear displacement curve for direct shear tests under different normal constant stresses (data from Schneider, 1976).

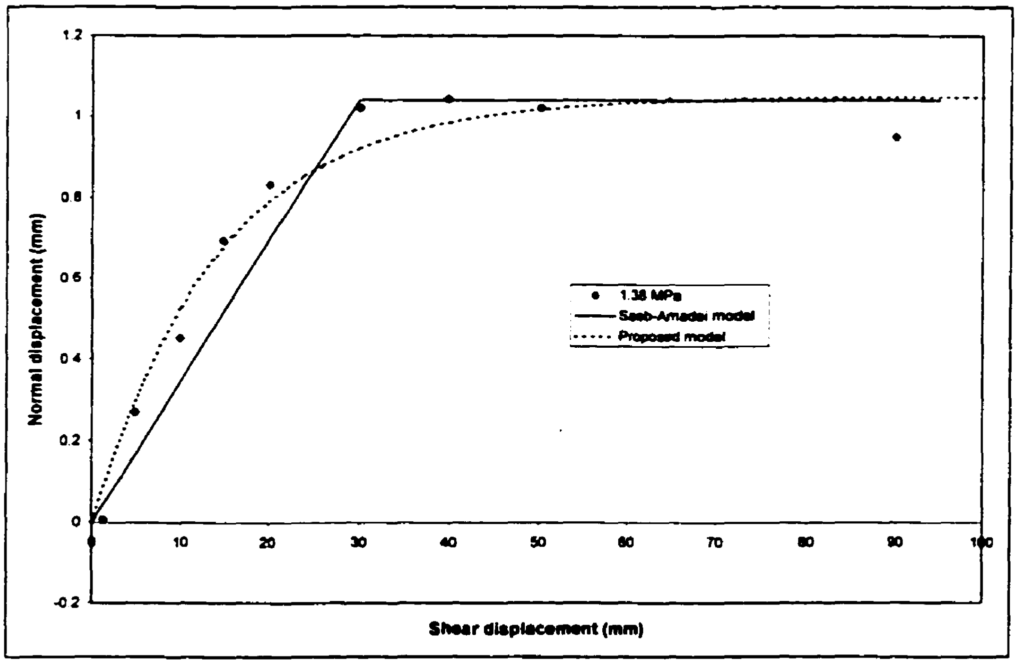

Figure A7b: Normal displacement -shear displacement curve for direct shear test under normal constant stress (data from Schneider, 1976).

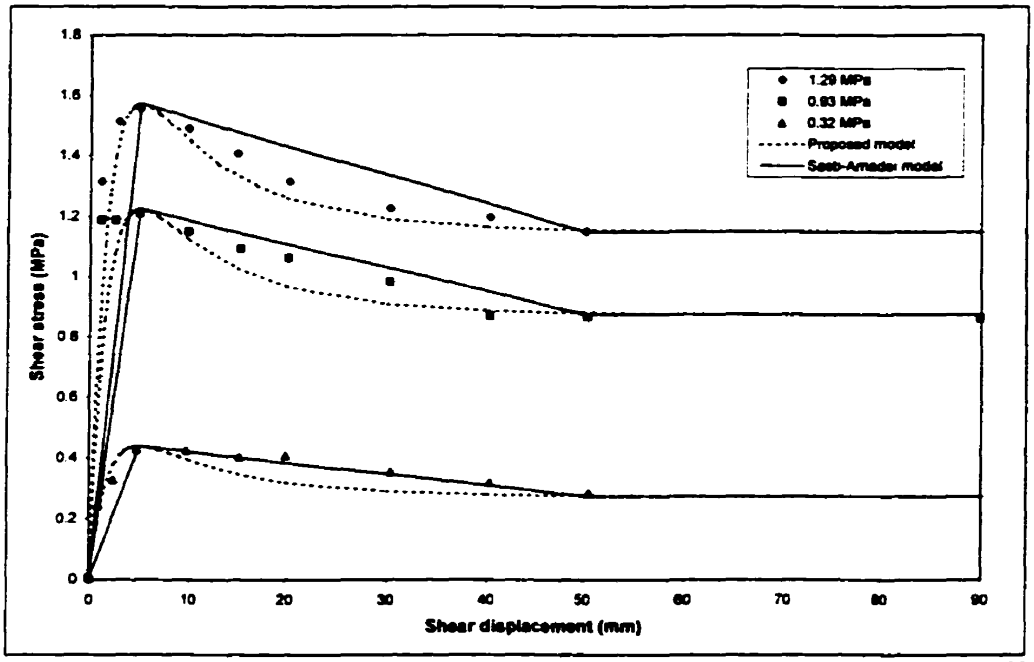

Figure A8a: Shear stress -shear displacement curve for direct shear tests under different normal constant stresses (data from Schneider, 1976).

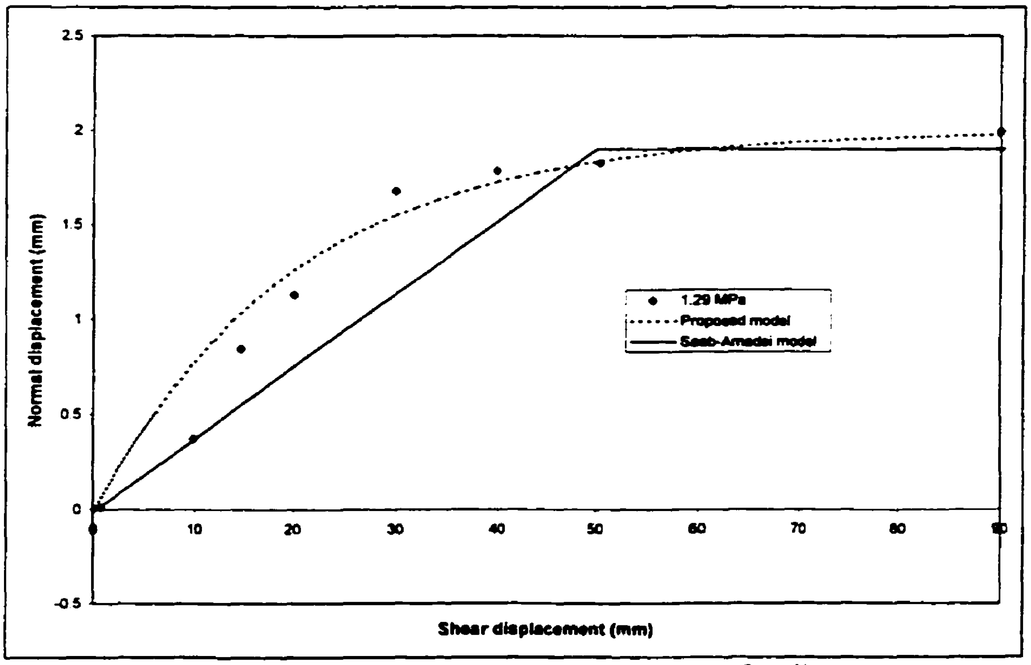

Figure A8b: Normal displacement -shear displacement curve for direct shear test under normal constant stress (data from Schneider, 1976).

Table A1: Comparison of correlation factors between the Saeb-Amadei and the proposed model for shear stress - shear displacement curves

Figure	Normal stress (MPa)	Correlation factor R^2 Saeb-Amadei	Proposed model
A1	5.38	0.939	0.990
	1.8	0.926	0.975
	0.36	0.880	0.977
	Mean value	**0.915**	**0.981**
A2	7	0.529	0.942
	14	0.837	0.932
	21	0.934	0.893
	Mean value	**0.767**	**0.922**
A3	5	0.931	0.861
	2	0.833	0.944
	1	0.191	0.610
	Mean value	**0.652**	**0.805**
A4	1.035	0.546	0.901
	1.035	0.192	0.430
	3.103	0.904	0.968
	6.2	0.719	0.985
	Mean value	**0.590**	**0.821**
A5	0.09	0.911	0.944
	0.03	0.889	0.978
	0.01	0.861	0.974
	Mean value	**0.887**	**0.965**
A6	1.64	0.514	0.925
	1.28	0.731	0.984
	0.61	0.797	0.977
	0.33	0.634	0.965
	Mean value	**0.669**	**0.963**
A7	1.77	0.932	0.789
	1.38	0.665	0.985
	0.69	0.914	0.978
	0.34	0.965	0.724
	Mean value	**0.869**	**0.869**
A8	1.29	0.532	0.929
	0.93	0.383	0.829
	0.32	0.855	0.903
	Mean value	**0.590**	**0.887**
All curves	**Mean value**	**0.739**	**0.900**